THE MICROSTRUCTURE, BIOGEOCHEMISTRY AND AGGREGATION OF ARCTIC CRYOCONITE GRANULES

The University Of Sheffield.

A thesis submitted for the degree of Doctor of Philosophy in the Faculty of Engineering at the University of Sheffield

by

Harry Langford

(MPhil, BSc)

Cell–Mineral Research Centre

Kroto Research Institute

Department of Civil and Structural Engineering

University of Sheffield

September 2012

ABSTRACT

Cryoconite granules are hydrous microaggregates, principally composed of microorganisms, organic matter and mineral particles, that reside upon glacier surfaces. Whilst recent research has highlighted the diverse microbial community within cryoconite granules and their role as biogeochemical reactors, little is known about their microstructure, the cell–mineral interaction within them, or their aggregation mechanisms. Knowledge of these is crucial for the understanding of autotrophic organic matter production and cycling, the entrainment of particulate matter and its consequential effect on glacier melt, and the life cycle of cryoconite granules and its impact on proglacial soil development.

These studies find that cryoconite granules are heterogeneous, demonstrating spatially variable microorganism and organic matter contents, containing significant quantities of filamentous cyanobacteria and exhibiting a fine groundmass of clay-sized particles enmeshed within various extracellular polymeric substances (EPS). The importance of photoautotrophy, EPS production and cation-bridged EPS–mineral interactions as biological 'forming factors' is demonstrated. The cyanobacterial filament and carbohydrate contents of cryoconite material explain 83% of the measured variability in aggregate size and stability upon Longyearbreen glacier. Geospatial investigations of these 'forming factors' reveal spatial patterns, with a zone of excess EPS production evident towards the snowline and increased pigment production evident in stable, down-glacier locations. A variety of mineral particles can co-aggregate with EPS-producing cyanobacteria, with ionic strength, temperature and growth phase all affecting efficiency. Spectroscopic studies reveal evidence for chiefly polymer-based modes of attachment within cyanobacteria–EPS–mineral aggregates, with complex EPS able to overcome surface charge and interact with mineral surfaces in a variety of ways.

This thesis presents the first detailed study of cryoconite granule microstructure and aggregation, finding that photoautotrophy and EPS production are vital to the development of stable aggregates, providing a matrix that attracts aeolian particulates, stabilises granules and promotes biogeochemical interaction and the development of microenvironments.

ACKNOWLEDGEMENTS

Firstly, I must thank my supervisors Prof. Steven Banwart and Prof. Andy Hodson for their guidance and support during these last three and a half years. From stairwell chats to productive meetings to comments on my manuscripts, your advice has been invaluable.

Thank you also to all those who provided advice and assistance in the field and laboratory, as well as with data analysis. Particular mentions must go out to Claire, Tris, Jakub and Johnny for help in the field, to Andy F, Achim, Joh, Jesús and Emma for help in the lab, and to Emma and Tris for help with data analysis. To esteemed colleagues, I am much obliged to you for providing me with samples to study and with cyanobacterial isolates to use.

Thanks also Andy for sorting out some great fieldwork for me in Svalbard with the MSc crew. You guys were all great. The science, camping on the beach, sleeping at the dog pound, drinking Scotch at midnight in the light, dining at the world's northernmost kebab van – altogether, some great times were had with some great people and I have a lot of fond memories.

To all in Kroto, be it in GPRG, CMRC or CSC, thanks for the camaraderie. In our weekly science meetings, I've learnt a lot. Never would I have thought that my mind would entertain such diverse subjects as the synthetic biology of photosynthesis, the recycling of CRT television screens and the management of weirs. Thanks in particular must go to Michael. We started our research at the same time and have sat next to each other ever since. It has been a pleasure being able to bounce ideas off of you, chat about the Chinese economy and drag you out for the occasional pint.

Thank you to my family, friends and fiancée for your support and, from time to time, necessary distractions from the rigours of PhD work. Finally, thank you also to those not directly mentioned above. I've had a very enjoyable time researching for this PhD and you have all played some part in this.

As they say in Norway, tusen takk!

TABLE OF CONTENTS

List of Figures

ABBREVIATIONS

APC	Autofluorescent pixel count
CCD	Charge-coupled device
CHAPS	3-[(3-cholamidopropyl)dimethylammonio]-1-propanesulfonate
CLSM	Confocal laser scanning microscopy
DAPI	4'-6-diamidino-2-phenylindole
EDTA	Ethylenediaminetetraacetic acid
EDX	Energy-dispersive X-ray
EPS	Extracellular polymeric substances
ESEM	Environmental scanning electron microscopy
FPA	Focal plane array
FTIR	Fourier transform infrared spectroscopy
GIS	Geographic information system
GPS	Global positioning system
ICP-MS	Inductively-coupled plasma mass spectrometry
IR	Infrared
LIFE	Laser-induced fluorescence emission
LV	Low-vacuum
NEXAFS	Near edge X-ray absorption fine structure spectroscopy
NMR	Nuclear magnetic resonance
OTU	Operational Taxonomic Unit
PCA	Principal component analysis
qPCR	Quantitative polymerase chain reaction
SEM	Scanning electron microscopy
SIMS	Secondary ion mass spectrometry
SIMSISH	Secondary ion mass spectrometry in-situ hybridisation
SIP	Stable isotope probing
SPRF	Self-pressurised rapid freezing
STXM	Scanning transmission X-ray microscopy
TDIC	Transmission differential interference contrast
TEM	Transmission electron microscopy
TOC	Total organic carbon
UHQ	Ultra-high quality
UV	Ultraviolet
XRD	X-ray diffraction

CHAPTER ONE: THESIS SUMMARY

1.1 Introduction

1.1.1 Supraglacial ecosystems

Recent studies have revealed that glaciers support a high biodiversity considering the extreme environments in which they form. As noted in a recent *Science* paper, there is 'no place too cold' (Laybourn-Parry 2009). Water in the liquid phase, be it within interstitial spaces between ice crystals or as pools on the ice surface, sustains life, whilst environmental pressures promote endemism. Two key glacial ecosystems dominate (Fig. 1). The subglacial ecosystem can be characterised by aerobic and/or anaerobic heterotrophy, with a prevalence of viral activity noted in some ecosystems (Laybourn-Parry & Pearce 2007). The supraglacial ecosystem (Figs. 1 & 2) is relatively complex, often containing various autotrophic and heterotrophic microorganisms, as well as eukaryotic micro-fauna. In addition, an englacial ecosystem is present. This system can be characterised by low metabolic rates, given the more extreme temperature, light and pressure regimes experienced, with chemoautotrophy likely dominating activity (Price 2007, Hodson et al. 2008).

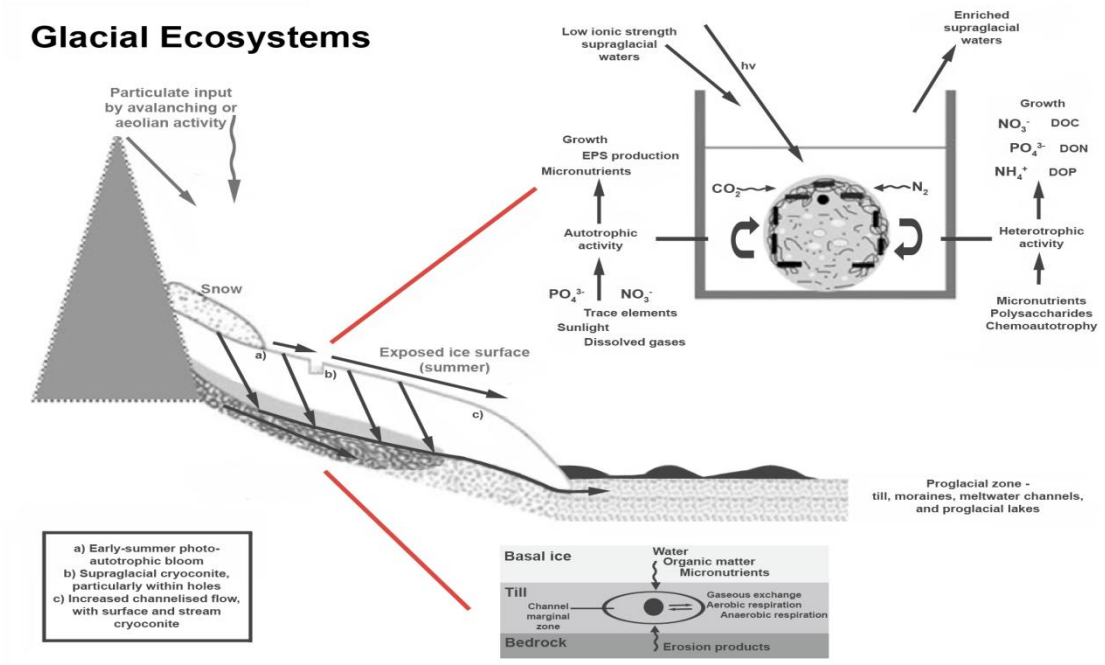

Figure 1: A conceptual model of a glacial ecosystem, detailing the principal supraglacial habitats, supraglacial biogeochemical interactions, and subglacial biogeochemical interactions.

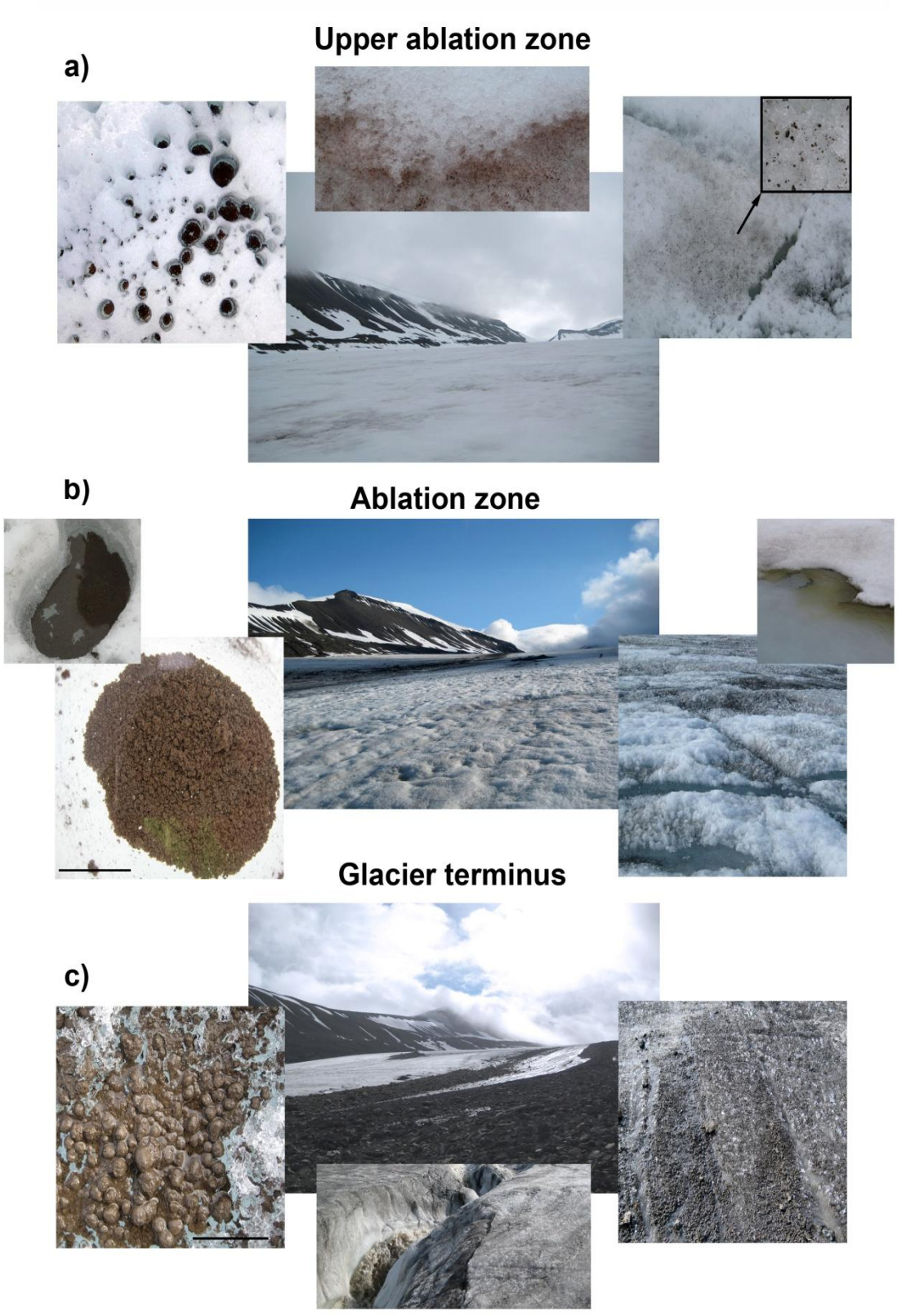

Figure 2: The supraglacial ecosystem – a pictorial representation of a typical Arctic supraglacial ecosystem, in this case Longyearbreen glacier, detailing the principal ecological zones and their characteristic biogeochemical features.

Within the supraglacial ecosystem, several important habitats can be identified, including the snowpack and ice surface, shallow pools and cryoconite holes, supraglacial streams, and features such as moraines and kames (Yoshimura et al. 1997, Battin et al. 2001, Takeuchi et al. 2001b, Stibal et al. 2006, Hodson et al. 2008, Anesio et al. 2009, Larose et al. 2010). These habitats show genuine seasonality, with winter temperatures restricting energy flows and nutrient cycling, and summer sun producing an ablating ecosystem with liquid water. Inputs into the system, chiefly aeolian particulate matter and precipitation (i.e. the melting snowpack), provide microbiological inocula and nutrients, as well as lowering the albedo and modifying the surface heat budget (Takeuchi et al. 2000, Hodson et al. 2008). Furthermore, glacier surface conditions, in particular the presence of a 'weathering crust' (Irvine-Fynn et al. 2011), promote nutrient sequestration and transport biota between habitats. Under these conditions, fruitful periods of microbial activity can be sustained (Anesio et al. 2009). Bacterial abundance and primary production are considered to be principally limited by both temperature and the supply of bio-available phosphorus (Mindl et al. 2007), with both allochthonous and autochthonous carbon considered important for microbial activity in low carbon glacial environments (Hopkins et al. 2006). Of the aforementioned supraglacial environments, cryoconite holes are considered to be microcosms of, and hotspots for, biogeochemical cycling (Hodson et al. 2005, 2008, Anesio et al. 2009). As such, they can be considered to be important habitats within the supraglacial ecosystem.

1.1.2 Cryoconite

Cryoconite granules can be described as being aqueous microaggregates, c. 0.1–10 mm in size and approximately 50% water, consisting largely of mineral grains, organic matter and microorganisms. Organic matter can range from microbial carbohydrates to black carbon, with biological content equally diverse and including photoautotrophic filamentous cyanobacteria, heterotrophic bacteria, snow algae and fungi; as such, cryoconite granules can be considered heterogeneous. Cryoconite literally means 'cold dust', and these granules are typically found both within the weathering crust and within small melt pools – cryoconite holes (Hodson et al. 2010, Irvine-Fynn et al. 2010). Anesio et al. (2009) state that between 0.1–10 % of glacier surfaces are typically covered by cryoconite. Regarding the formation and growth of cryoconite holes, sediments on the ice surface absorb greater solar radiation than the surrounding ice,

warming up and melting the underlying ice, forming generally cylindrical holes. Radiative and convective heating, as well as heat from biological processes, can then further enlarge these holes (Gerdel & Drouet 1960, Gribbon 1979, McIntyre 1984, Wharton et al. 1985), both vertically and laterally, in order to maintain thermal equilibrium (Cook et al. 2010).

A schematic representation of a cryoconite hole is presented in Figure 1, and indicates the complex interaction between microorganisms, abiotic particulate matter and solution chemistry. Furthermore, Figure 2 shows images of cryoconite granules in various supraglacial settings, upon a temperate Svalbard valley glacier – Longyearbreen. Microbiological studies have identified that bacteria within cryoconite sediment comprise chiefly *Proteobacteria*, *Cytophagales*, *Verrucomicrobia*, *Acidobacteria* and *Cyanobacteria* (Christner et al. 2003, Edwards et al. 2011). Operational Taxonomic Unit (OTU) classification reveals that cryoconite holes are generally colonised from terrestrial and freshwater ecosystems (Segawa & Takeuchi 2010, Edwards et al. 2011). Indeed cryoconite food webs show marked similarities to those of glacial lakes. Considering cyanobacteria, the genera of *Phormidium*, *Nostoc*, *Leptolyngbya* and *Oscillatoriales* dominate (Porazinska et al. 2004, Stibal et al. 2006, Namsaraev et al. 2010). When considered with nanoflagellates, particularly snow algae, and diatoms, these photosynthetic biota dominate the supraglacial ecosystem, including cryoconite sediment. Given the prevalence of photoautotrophic biota, rates of photosynthesis are significant (e.g. Säwström et al. 2002, Stibal et al. 2008a, Anesio et al. 2009), although the contribution of autochthonous versus allochthonous carbon to the cryoconite ecosystem is still hotly debated, and in fact likely varies both spatially and seasonally. Recent evidence suggests that significant autotrophy is generally restricted to grains of < 2 mm in diameter, with light levels approximating 100 μmol photons m^{-2} s^{-1} proving most efficient in promoting photosynthesis (Telling et al. 2012). Consummate with this autotrophy is the production of extracellular polymeric substances (EPS). These polymers, dominated by polysaccharides, can condition surfaces and promote adhesion, allowing bacteria to overcome substratum effects or medium characteristics (e.g. pH and hydrophobicity) when necessary, and attach to nutritive surfaces (Donlan 2002, Pereira et al. 2009). Thus, it is likely that photoautotrophy plays a significant role in organic carbon production and promotes the development of cryoconite granules through aggregation of adhering primary mineral particles, cells and organic matter.

Studies of biogeochemical cycling have focused upon the key macronutrients of carbon, nitrogen and phosphorus. Given the net autotrophy in smaller granules, potential for allochthonous input and suggested long residence times for cryoconite granules on glacier surfaces (Hodson et al. 2010, Telling et al. 2012), it is perhaps unsurprising that total organic carbon figures for cryoconite sediment are significant (Takeuchi 2002, Stibal et al. 2008a). Microbially derived products dominate this organic carbon, with some allochthonous input from lower order plants (Xu et al. 2010). Nitrogenase activity has been recorded upon Arctic glaciers (Telling et al. 2011) and, when combined with atmospheric inputs from snowmelt and rain (Hodson et al. 2005), provides the cryoconite ecosystem with a labile source of nitrogen throughout the melt season. Phosphorus can be said to be largely sediment bound, with potentially bio-available phosphorus being found to be in excess of that needed for primary production, again pointing to allochthonous input (Hodson et al. 2004, Stibal et al. 2008b). The availability of key macronutrients, abiotic particulate matter and a biodiverse suite of microorganisms accounts for the prevalence of cryoconite in the Arctic, whilst localised physico-chemical conditions lead to the heterogeneity exhibited.

1.1.3 Cryoconite microstructure and the role of cell–mineral interaction in cryoconite aggregation

A limited foray into cryoconite microstructure has revealed that photoautotrophic microorganisms generally dominate the surface layer of the aggregate, that some cryoconite aggregates exhibit laminations and that predominantly silicate grains sit within a primarily carbon-rich matrix (Takeuchi et al. 2001b, Stibal et al. 2008a, Hodson et al. 2010). As such, similarities exist with cyanobacterial mats, which show mineral-rich layers, cyanobacteria-rich layers, bio-accumulation and bio-alteration at depth, and a tendency for cyanobacteria to orient themselves parallel to the surface when near to it (de los Ríos et al. 2004). Further, it is now clear that cryoconite aggregates contain comparatively high cellular abundances of both photoautotrophic and heterotrophic bacteria (Stibal et al. 2008a, 2012, Anesio et al. 2009, Hodson et al. 2010). This being said, the part that cell–mineral interaction plays in the formation of cryoconite granules is uncertain. In a similar environment, Kapitulçinova et al. (2008) proved that cyanobacteria readily colonise biotite surfaces, whilst the ability of cyanobacteria to form ligand–metal complexes, principally via carboxyl, phosphoryl and amine functional groups, has been shown previously (Phoenix et al. 2002, Yee et al.

2004). These ligand–metal attachment processes can bind cells and EPS to mineral metal oxide surfaces.

Analogous areas of research, namely into photosynthetic biofilms and soil microaggregates, can provide complementary information on the microstructure of and cell–mineral interaction within cryoconite aggregates, given the sparseness of direct research. A biofilm can be defined as a 'simple to complex community of microbial cells, associated with an interface and enclosed in a polymer matrix, and containing varying quantities of non-cellular material' (Davey & O'Toole 2000, Donlan 2002). Research into biofilms highlights the importance of EPS as a structural matrix (Decho et al. 2005, Neu et al. 2010). EPS shows considerable spatial and temporal heterogeneity within biofilms and microbial aggregates, with a well-developed biofilm showing EPS-rich and cell-rich areas, non-biological inclusions and spatial chemical differences (Decho & Kawaguchi 1999, Kawaguchi & Decho 2002, Sheng et al. 2005, Chen et al. 2007a). A large proportion of microbes in natural systems produce meaningful quantities of EPS and, as such, EPS-mediated cell–mineral interaction may be significant within cryoconite. Soil microaggregates, like cryoconite, exhibit stability: the ability to resist disruption by hydrodynamic activity (e.g. Six et al. 1998, Puget et al. 1999). Their structure is determined by the interactions between mineral particles, metal (oxy)(hydr)oxide precipitates, organic matter and microorganisms. Organic matter coatings on mineral surfaces generally contain greater quantities of microbially derived carbon, indicating that organo-mineral interactions in soil aggregates and the adsorption of organic molecules onto mineral surfaces are highly important (Lehmann et al. 2007, Kögel-Knabner et al. 2008). Reactive sorption sites on mineral surfaces are dense and thus generally promote multiple surface attachments (Kaiser & Guggenberger 2003). As such, microbially controlled organo-mineral interaction is likely to be of importance within cryoconite granules.

1.1.4 Scope and motivations for research

Whilst the geochemical intricacies of cryoconite have been studied in relation to supraglacial nutrient fluxes (e.g. Hodson et al. 2008; Stibal et al. 2008a), and the microbiology of cryoconite has been studied in various environments (e.g. Margesin et al. 2002, Christner et al. 2003, Cameron et al. 2011), studies of cell–mineral interaction at the microscale have been decidedly sparse, as alluded to above. Further, whilst there has been research into the microstructure of cryoconite, this has been limited to such

things as mineralogical evaluation via electron microscopy, and studying microorganism content by epifluorescence microscopy. Detailed microstructural analysis of cryoconite has the potential to highlight crucial cell–mineral and organo-mineral interactions, identify microenvironments and provide information concerning spatial differences in granule structure.

Recent research has found the microbial food web present within cryoconite (Edwards et al. 2011, Cameron et al. 2011) to be complex and variable, considering the environment in which it is found, and to show considerable inter-glacier variation. Laboratory research by the author, as well as research by others (Takeuchi et al. 2001b, Anesio et al. 2009, Hodson et al. 2010), has indicated that filamentous microorganisms are often prevalent within cryoconite and show adherence to, and cementation of, inorganic particulate matter, suggesting that these microorganisms may play a crucial role in the formation of cryoconite. However, a detailed study of the aggregation mechanisms of cryoconite has not yet been achieved, and its formation certainly requires further thought, with biological and chemical processes likely playing a key role in entraining and retaining particulate matter that would otherwise be removed by melt. As mentioned by Hodson et al. (2010), the mass evolution of cryoconite is poorly understood, and this evolution is likely to be strongly linked to the carbon balance of individual granules. Further, given the net ablation of many Svalbard glaciers (Moholdt et al. 2010), the aggregation and evolution of cryoconite aggregates and their impact on soil development in recently deglaciated forefield areas need to be given attention. The rate of transfer of cryoconite debris into the glacial forefield and its impact on soil development is, at present, an unknown parameter.

When compared with studies of soil microaggregates, there is a lack of detailed understanding of glacial sediments in general, particularly the biotic component and particularly supraglacial sediments. Arctic cryoconite displays a spherical form, markedly different to other microbial-rich sediments in cold environments, which generally display a laminar mat or biofilm form. The reason for this spherical form is, as yet, unclear. In addition, whilst it is clear that conditions for growth (sunlight, liquid surface water and aeolian deposition) are relatively favourable, it is unclear exactly how cryoconite develops and why its composition varies. Furthermore, combustion activities have provided a strong input of black carbon into the Arctic throughout the past century, whilst mining activities have provided a strong input of sedimentary elemental carbon

to Svalbard glaciers (Forsström et al. 2009, Aamaas et al. 2011). It is clear that the albedo of these particulates is low, and that they aggregate together on the ice, enhancing melt. However, the part that they play in cryoconite aggregate formation is also unclear. Finally, the spatial distribution of biochemical parameters important for aggregate formation is understudied. Recent molecular investigations have revealed distinct biogeography between regions and glaciers (Edwards et al. 2011, Cameron et al. 2011), and recent biogeochemical investigations have improved our knowledge of the spatial distribution of chlorophyll and carbohydrates on the Greenland ice sheet (Stibal et al. 2012), but quantitative data concerning the spatial relationships between biochemical parameters and both cryoconite aggregate size and stability are still lacking.

1.1.5 Literature review

Key literature is reviewed within the above introduction, whilst further literature reviews are presented at the beginning of each individual results chapter. In addition, a detailed literature review, outlining the physical and structural aspects, biology and ecosystem biogeochemistry of cryoconite, and reviewing two other areas broadly analogous to cryoconite ecosystems – the biogeochemistry of biofilms and microbial mats, and the biogeochemistry of soil and organic matter within microaggregates – , is appended as Appendix I.

1.2 Aims and objectives

1.2.1 Research hypothesis

A central research hypothesis was constructed, based upon recent research and preliminary investigations by the author:

‘Cryoconite aggregate formation is a biologically mediated process, whereby phototrophic and filamentous microorganisms provide the matrix for the development of a spherical aggregate, trapping both abiotic particulates and heterotrophic bacteria as they photosynthesise, grow and produce extracellular polymeric substances (EPS); as the aggregate develops, environmental niches develop within it, leading to a heterogeneous microstructure with areas of humification, weathering and mineralisation’.

1.2.2 Aims and objectives

The work presented here was undertaken in order to develop a suite of methods to characterise the microstructure and biogeochemistry of cryoconite, combining laboratory-based research and the spatial field study of biogeochemical parameters, to enable insights to be gained, and to provide a locus for a simple laboratory experiment, into the aggregation and development of cryoconite granules. To fulfil this aim and the aforementioned central research hypothesis, three main research objectives were constructed:

(a) To quantify the heterogeneity of the cryoconite granule, with the aid of bulk, surficial and cross-sectional analytical and microscopy techniques.

(b) To investigate the spatial variability in biochemical parameters on a representative glacier and relate these to physical parameters associated with the cryoconite aggregates present.

(c) To assess the role of ongoing microbial activity, and associated EPS production, in aggregate formation in a model laboratory system.

1.2.3 Experimental design

The overarching experimental design has been concerned with testing analytical methods with which to analyse cryoconite aggregate microstructure and biogeochemistry, allowing a conceptual model for their formation to be developed. Subsequently, this conceptual model acted as a driving force for field research concerning the spatial variability of biochemical parameters. Finally, the above led to further laboratory experiments designed to provide insights into cryoconite aggregate formation, thus testing the conceptual model.

Objective (a): Prior to assessing aggregate formation experimentally, it was necessary to gain a substantial understanding of the microstructure (biological, physical and chemical), and variation in microstructure, of Arctic cryoconite. Characterisation of the microstructure, composition and heterogeneity of the cryoconite granule was achieved through a variety of microscopic and spectroscopic means in the laboratory, and through the study of biological activity and nutrient fluxes in the field. A variety of cryoconite aggregates from several locations in Svalbard and Greenland were studied. From these data, a conceptual model of cryoconite granule formation was developed.

Objective (b): Spatial mapping of biochemical parameters linked to photoautotrophic EPS production and, as such, suggestions made in the conceptual model were based upon field sampling and measurements on Longyearbreen glacier. Characterisation of biochemical parameters was achieved using spectroscopic methods in the laboratory. These were related to physical characteristics of Longyearbreen cryoconite aggregates, as determined by laboratory methods and field-based imagery.

Objective (c): Known species of cyanobacteria interacted in laboratory incubations with selected mineral particles at a range of pH and ionic strength values, utilising information from the completed microstructural studies in the experimental design. Microscopic and spectroscopic methods were utilised to monitor aggregate formation and study the biochemical signatures of co-aggregated cyanobacteria and mineral particles. Data obtained were used to provide insights into cryoconite aggregation formation.

1.2.4 Thesis structure

This thesis comprises this extended summary, five distinct pieces of research work, a concluding chapter and appendices. Chapter 1, this summary, introduces the research, outlines research objectives and overviews key literature and methods. Chapters 2 to 6 describe in detail the research undertaken, with each chapter representing a self-contained piece of research written as a manuscript for peer-reviewed publication. Results chapters 2, 3 and 4 address objective (a), whilst chapters 5 and 6 address objectives (b) and (c) respectively. Chapter 7 concludes the thesis, synthesising the knowledge, drawing conclusions and recommending further research. In all cases, the author of this thesis conducted the research work and prepared the manuscript, including all figures therein. Named co-authors provided supervisory and advisory roles with respect to manuscript content and structure during preparation for submission. The thesis author is the sole author of this extended summary and the concluding chapter.

1.3 Methods

All of Chapters 2–6 are based upon data acquired during both field sampling and subsequent laboratory experiments. The general methodological approach has employed various types of microscopy and spectroscopy as analytical tools. Microscopy techniques included both optical and electron microscopy, with the use of confocal laser scanning microscopy (CLSM) combined with specific functional stains being particularly significant. Spectroscopy techniques included UV-Vis spectroscopy and Fourier transform infrared spectroscopy (FTIR). Specific methodological approaches are outlined in detail in Chapters 2–6. This Methods section outlines the location of field sites and introduces key analytical techniques used in this thesis.

1.3.1 Location of field sites

The Svalbard archipelago is a collection of islands lying between 74° – 81° N and 10° – 35° E, of which the largest is Spitsbergen. Greenland lies due west of Svalbard, centered at 72° N and 40° W. Both land masses have an Arctic climate with some maritime influence at the coast, and both are heavily glaciated (c. 60% and c. 80% respectively). The geology of Svalbard is dominated by Tertiary to Carboniferous coal measures strata, along with Devonian sandstones and basement strata comprising granites and gabbros (Hjelle 1993, Dallmann 1999). The geology of Greenland is dominated by the crystalline lithologies of the Precambrian shield, gneisses and granites, with Proterozoic to Tertiary sandstones and igneous intrusions providing a significant contribution to the geology in places (Henriksen et al. 2009). Outline maps detailing the locations from which cryoconite has been sampled are shown in Figure 3, whilst the images in Figure 2 highlight the supraglacial setting of Longyearbreen, the principal study site for fieldwork. Within Svalbard, four glaciers were sampled: Vestfonna in western Nordaustlandet, Midtre Lovénbreen in the Kongsfjord region of western Spitsbergen, and Aldegondabreen and Longyearbreen in the Isfjord region of western Spitsbergen; the latter glacier was also used as the field study site for Chapter 5. Within Greenland, two glaciers were sampled: Kronprins Christian Land in northeast Greenland, and Kangerlussuaq in southwest Greenland.

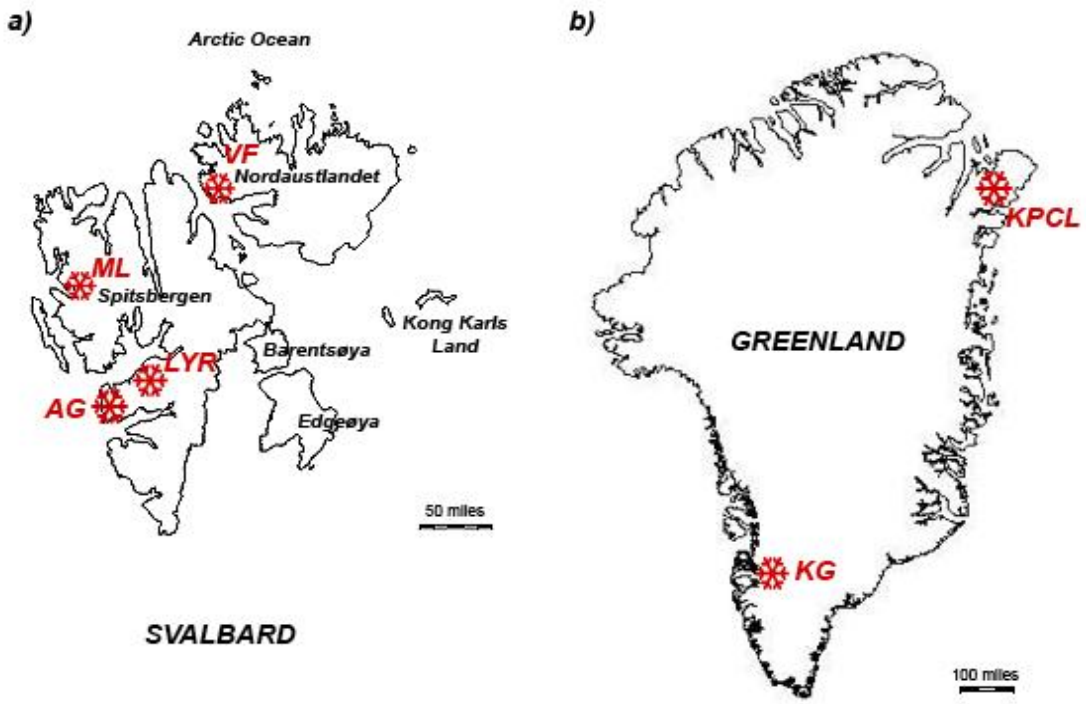

Figure 3: Location maps of (a) Svalbard and (b) Greenland, detailing sampling locations; AG = Aldegondabreen, KG = Kangerlussuaq, KPCL = Kronprins Christian Land, LYR = Longyearbreen, ML = Midtre Lovénbreen and VF = Vestfonna.

Sampling of all glaciers occurred during the summer ablation season. Bulk samples were taken from individual cryoconite holes using pre-sterilised turkey basters that had been rinsed out three times with supraglacial melt water and gently placed into sterile polypropylene bottles or 50 mL centrifuge tubes. Smaller samples were taken using pre-sterilised spatulas and placed into sterile 2.0 mL cryovials or 1.5 mL microcentrifuge tubes. Samples were stored frozen and transferred rapidly by air to the laboratory in Sheffield, wherein they were kept frozen until being defrosted for microscopic and/or spectroscopic analyses.

1.3.2 Confocal laser scanning microscopy

CLSM can be thought of as a more advanced version of conventional epifluorescence microscopy. In epifluorescence microscopy, light of a specific wavelength, as determined by a filter cube, excites fluorophores in the sample, which subsequently emit light at a longer wavelength, which can then be detected and imaged. The condenser is also the objective and a dichromatic beam splitter is used to selectively focus light and improve the signal-to-noise ratio (Bratbak 1985, Herman 1997, Li et al. 2004). CLSM follows a similar principle, except that two pinhole apertures eliminate

out-of-focus light and a laser is used as the light source. As such, CLSM uses 'optical sectioning', which allows it to obtain high-resolution images through the sample, with some depth selectivity (Pawley 2006). Limitations of depth penetration have been addressed more recently with the advent of two-photon laser scanning microscopy, which uses a pulsed laser to excite the sample using two IR photons at half of the normal energy required, resulting in greater depth penetration and resolution (Neu & Lawrence 2005).

Being non-invasive and three-dimensional, CLSM is well suited to biological imaging. When utilised with a combination of fluorescent probes, the structure and composition of complex biological samples can be elucidated (e.g. Lawrence et al. 2003, Chen et al. 2007b, Neu et al. 2010). Chapter 2 employed a combination of 4'-6-diamidino-2-phenylindole (DAPI) (to stain DNA within microbial cells), AlexaFluor 488 concanavalin A (to stain polysaccharides) and autofluorescence (to image photosynthetic microorganisms), staining 60 µm thick sections of individual cryoconite granules, before imaging these on a Zeiss LSM 510 META microscope, using both confocal and two-photon capabilities. Chapter 4 used DAPI staining and autofluorescence in the imaging of ultrathin sections of cryoconite granules, whilst Chapter 6 used autofluorescence and transmission differential interference contrast (TDIC) modes to image laboratory-cultured aggregates throughout their incubation period.

1.3.3 Electron microscopy

Electron microscopes use a series of electromagnetic lenses and apertures to focus an electron beam onto or through a sample. Transmission electron microscopy (TEM) is a stationary or fixed beam method, whereby electrons pass through and interact with an ultrathin sample, producing an image that is subsequently magnified and recorded. Bright field imaging utilises the differential absorption of electrons by thick or electron-dense materials versus thin or electron-poor materials to create an image. Scanning electron microscopy (SEM) is, as the name suggests, a scanning beam method, whereby a narrow electron beam is scanned, in a raster pattern, across the sample surface, whilst the detector, e.g. a secondary electron detector, detects electrons returning from the sample surface and builds up a high-resolution image of the surface, which appears three-dimensional due to the depth-of-field available (Amelinckx et al. 2008).

When imaging biological material using electron microscopy, the principal challenges are that the fragility and poor electron density of the sample often lead to both beam damage and a lack of visualisation; as such, sample preparation is vital. If using SEM or TEM, the use of a heavy metal stain and an embedding resin is highly favoured (e.g. Leppard et al. 1996, de los Ríos et al. 2004, Wrede et al. 2008). Environmental SEM (ESEM), conversely, can allow direct visualisation of electron-poor hydrated biological samples (Muscariello et al. 2005), although resolution and the imaging of EPS may still be problematic (Priester et al. 2007). Chapter 4 uses a ruthenium red heavy metal staining protocol (Priester et al. 2007) and either ESEM imaging or, following embedding in a hydrophilic embedding resin and cutting on an ultra-microtome, TEM imaging to study cryoconite microstructure.

1.3.4 UV-Vis microplate spectroscopy

UV-Vis spectroscopy simply uses either a specific wavelength of light or a spectral range within the UV-Visible region, controlled using a monochromator. This incident light passes through the generally liquid sample, often dissolved in a solvent (e.g. water or ethanol), and the ratio of transmitted light versus incident light allows the user to note absorbance at particular wavelengths, characteristic of certain species (Skoog et al. 2007). This technique is particularly useful for organic and biological macromolecules. Quantitative concentrations of an absorbing analyte can be determined, when conditions are met, by the Beer-Lambert law. This law uses an extinction coefficient value (or calibration curve data) and a known pathlength value to relate absorbance to concentration. More recently, microplate readers have been developed that encompass UV-Vis spectrometers, as well as fluorescence spectrometers. This advancement has allowed the rapid measurement of biochemical concentrations in a large number of samples.

Chapter 5 utilises (a) the phenol–sulphuric acid method for the colorimetric determination of carbohydrate content, scaled down to microplate format (Dubois et al. 1951, Masuko et al. 2005); (b) a 100% methanol extraction and microplate-format absorbance analysis (Warren 2008); and (c) a mechanical and chemical extraction of phycobiliproteins, followed by a microplate-format fluorescence analysis. This combination of analyses allows both photosynthetic and cyanobacterial pigments, as well as labile carbohydrates (a proxy for free EPS) to be determined rapidly in a large

number of samples. This, in turn, enables the rapid geospatial determination and mapping of these sample analytes across the glacier surface.

1.3.5 FTIR spectroscopy

Infrared (IR) spectroscopy utilises IR radiation, of which specific frequencies can be absorbed by molecular species, with the exception of some homonuclear species (e.g. O_2), causing them to undergo a net change in dipole moment and produce a consequent vibration (Skoog et al. 2007). These absorptions, producing either stretching or bending (although several types of both exist) vibrations, can then be detected at specific wavenumbers and can provide characteristic determinations for certain molecular species. The mid-IR range, c. 4000–400 cm^{-1}, is particularly useful for elucidating the structure of organic and biochemical species. Fourier transform is a data processing technique that, when applied to IR spectroscopy, allows a whole sample spectrum to be easily and rapidly measured, with less noise and greater reproducibility. FTIR uses a moving mirror to focus IR light through an interferometer and then, in transmittance mode, through the sample, producing an interferogram. After application of the Fourier transform, a spectrum can be obtained from this interferogram (Smith 1996).

Chapters 2, 3 and 6 report the use of FTIR for a range of applications, from bulk soil mineralogical analyses to spatial chemical mapping of biochemical signatures. FTIR is a useful technique for bulk soil analyses, including organic matter analyses, as it requires a small sample volume and can identify both crystalline and amorphous materials (Ji et al. 2009). Chapters 2 and 3 apply FTIR spectroscopy to bulk powder samples, based upon a KBr pellet sample preparation, and record the characteristic absorbance peaks, enabling mineralogical and geochemical conclusions to be drawn. Briefly, the KBr pellet technique mixes a small amount of powdered sample with KBr powder and presses it into an optically transparent disc (Coleman 1993). When a spatial analysis is advantageous, FTIR microspectroscopy can be a highly useful tool. This technique differs in that a focal plane array (FPA) detector allows rapid, pixel-by-pixel spectra to be taken across a set area, imaged at magnification through a microscope objective lens. This enables chemical maps of spectral peaks to be produced and allows the spatial discrimination of biochemical signatures and microorganisms. Chapter 6 utilises this method to analyse a suite of laboratory-cultured cyanobacterial microaggregates, allowing the scrutiny of variations in biochemistry.

1.3.6 Incubation design

Intimate within the incubation design was the need to monitor the cyanobacterial population in-situ in the reactor, without disturbing aggregate growth, as well as to monitor aggregate size as the cyanobacteria interacted with mineral particles. CLSM allowed the above monitoring, as it has good depth penetration, a narrow focal plane, the ability to stimulate and detect autofluorescence, and a TDIC mode. As such, the overall aggregate would appear as a grey mass, which could be appropriately sized using area or feret diameter measurements, and the autofluorescence could be monitored concurrently. Solé et al. (2007, 2009) utilised CLSM and image analysis to monitor cyanobacteria within phototrophic mats; their analytical techniques provided the inspiration for the ones outlined above. From this starting point, incubation design was driven by the desire to use CLSM to monitor aggregation. Wanting to avoid sub-sampling errors, this led to a design whereby the water-dipping objective of the CLSM could be lowered into the incubation chamber for imaging purposes, before being withdrawn and the incubation re-sealed. Therefore, a design using a series of non-treated 12-well microplates was settled upon (Fig. 4), as it allowed a reasonable volume of liquid (3 mL) to be used and could be lidded and sealed with parafilm when not being imaged, maintaining gaseous exchange and thus an aerobic system.

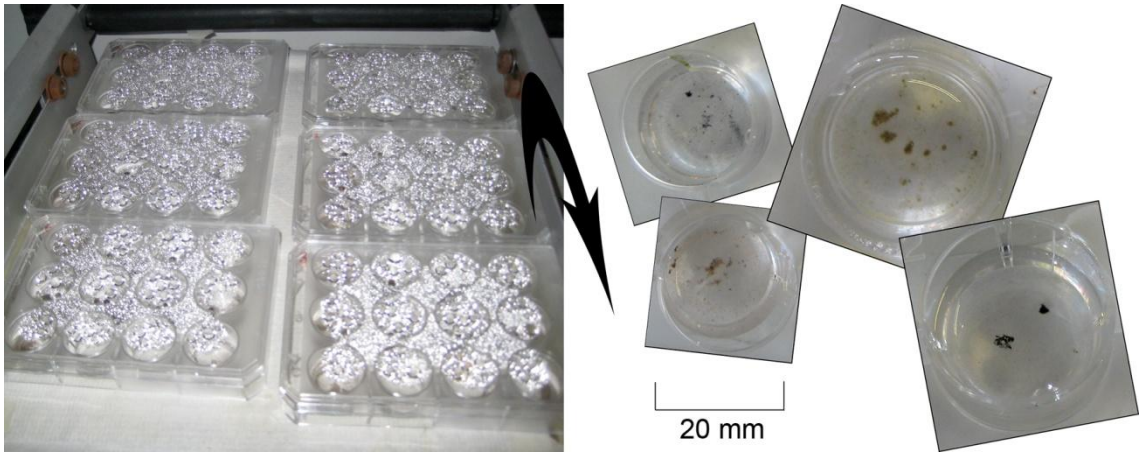

Figure 4: Multi-well plate incubations and bright-field imagery of cyanobacteria–mineral aggregates.

Furthermore, being thin and transparent, effective TDIC imaging could be achieved. The multi-well nature also enabled a suite of mineral particles, ionic strengths and pH values to be tested at the same time. Chapter 6 utilised these incubation chambers to study the co-aggregation of cyanobacteria and mineral particles.

CHAPTER TWO: THE MICROSTRUCTURE AND BIOGEOCHEMISTRY OF ARCTIC CRYOCONITE GRANULES

Published as: Langford, H., A. Hodson, S. Banwart & C. Bøggild, 2010. The microstructure and biogeochemistry of Arctic cryoconite granules. *Annals of Glaciology* 51 (56), 87–94.

2.1 Abstract

A cryoconite granule is a biologically active aggregation of microorganisms, mineral particles and organic matter found upon glacier surfaces, often within shallow pools or cryoconite holes. Observations of the microstructure of a range of cryoconite granules from locations in Svalbard and Greenland reveal their structure and composition. Whereas bulk analyses show that the mineralogy and geochemistry of these granules are broadly similar, analyses of their microstructure, using optical, epifluorescence and confocal microscopy, indicate differences in the location and quantity of photosynthetic microorganisms, heterotrophic bacteria and organic matter. Using these findings, a hypothesis on the aggregation of cryoconite is presented, centered upon multi–level aggregation by bioflocculation and filamentous binding.

2.2 Introduction

Recent studies have revealed a fascinating range of glacier ice ecosystems, with high biodiversity considering the extreme environments in which they form (Hodson et al. 2008). The microbial food web is both complex and variable, comprising a variety of autotrophic and heterotrophic microorganisms, fungi and eukaryotic microfauna (Margesin et al. 2002, Hodson et al, 2008). Cryoconite, meaning ‘cold dust’, is granular organic-rich debris found supra-glacially, particularly within ‘cryoconite holes’, small depressions within the ice. The existence of these holes has been known since the 19th Century (von Drygalski 1897), but only recently have advancements in analytical techniques allowed us to begin to understand the communities of microorganisms living

within them and the interaction between these and inputs into the ecosystem, such as sunlight and inorganic nutrients.

Biogeochemical interactions upon the surface of the glacier play a key role in entraining and retaining aeolian particulate matter upon glaciers, thereby enhancing melt. However, the specific process by which cryoconite aggregates form and sustain themselves has received little research attention. Hodson et al. (2010) suggest that both processes are likely to be strongly linked to carbon balance. Further, given the net ablation of many Svalbard glaciers, the aggregation and evolution of cryoconite aggregates and their impact on soil development in recently deglaciated forefield areas need to be given attention. For example, Sigler and Zeyer (2002) find that forefield successional gradients contain a diverse microbial assemblage, increasing in both biomass and activity with age, yet they note that it is still unclear as to the source(s) of this community and the importance of specific pioneer bacteria.

Although the impact of cryoconite has been studied in relation to supraglacial biogeochemistry (e.g. Hodson et al. 2008, Stibal et al. 2008a), and the microbiology of cryoconite is now well characterised in various environments (e.g. Margesin et al. 2002, Christner et al. 2003), specific studies on the microstructure and biogeochemistry of cryoconite are few (Takeuchi et al. 2001a,b). As noted by Dittrich and Luttge (2008), there is increasing evidence that microorganisms obtain competitive advantage through using their reactive cell surfaces as interfaces to actively control water-solid interactions. Microscopic imaging is becoming an increasingly important tool for investigating hydrated, biologically active structures, due to it being non-invasive, three-dimensional and having the ability to cover many spatial scales (Neu et al. 2010). In recent years, a range of microscopic imaging methods have been employed, with confocal laser scanning microscopy (CLSM) leading the way. By using specific fluorescent probes, the structure, composition and microhabitats of biological samples have now been investigated (Chen et al. 2007b, Neu et al. 2010). For example, CLSM has quantified the spatial distribution and structural form of extracellular polymeric substances (EPS): glue-like substances vital for the formation of aggregates and composed of microbial polysaccharides, proteins, nucleic acids and polymeric lipophilic compounds (e.g. Lawrence et al., 2003). In order to hypothesise on the aggregation and development of cryoconite, it is necessary to gain a comprehensive understanding of its microstructure and the variation of this microstructure across differing biogeochemical

environments. A novel combination of microscopic and spectroscopic techniques are therefore used below to better understand the microstructure and biogeochemistry of cryoconite granules from three glaciers in Svalbard: Vestfonna (VF) in western Nordaustlandet, Midtre Lovénbreen (ML) in the Kongsfjord region of western Spitsbergen, and Longyearbreen (LY) in the Isfjord region of western Spitsbergen; and two areas upon the Greenland Ice Sheet: Kronprins Christian Land (KP) in northeast Greenland, and Kangerlussuaq (KG) in southwest Greenland. It is hypothesised that microstructural evaluation of cryoconite granules will reveal them to be heterogeneous biotic aggregates.

2.3 Methodology

All cryoconite was sampled in the field using sterile implements and sterile containers, and was transferred frozen and stored at −20°C until just prior to analysis. To enable microstructural analyses to be undertaken, a range of thin-section techniques were developed and are outlined below. These thin-section techniques reduced problems associated with the attenuation of light intensity (Barranguet et al. 2004). This cross-sectional approach, combined with bulk and surface analyses, therefore enabled the structure and composition of cryoconite granules to be studied in great detail. The methodological approach can be split into '*mineralogical and geochemical analyses'*, performed principally upon dried cryoconite, and '*biological and biochemical analyses'*, performed principally on defrosted, hydrated cryoconite.

2.3.1 Mineralogical and geochemical analyses

Ten cryoconite granules were dried at low temperature (35°C), infiltrated with an Araldite resin under vacuum, ground and polished until a thin section of approximately 30 µm in thickness was produced. These thin sections were analysed using a brightfield, cross–polarizing microscope with SLR camera attachment. To complement the mineralogical characterisation undertaken upon thin sections, bulk mineralogical investigations using powder X-ray diffraction (XRD) and KBr–pellet Fourier transform infrared (FTIR) spectroscopy were employed. Powder XRD was performed on a Siemens D500 powder diffractometer (Cu-source), with 150 mg of finely powdered

cryoconite, at angles between 5° and 70°, at 1°/min and with a step size of 0.02. KBr–FTIR was performed on a Perkin-Elmer Spectrum One, with 3 mg of finely ground cryoconite and 150 mg of KBr granules (1:50 ratio), pressed into a disc under 10N force in a die press; 100 scans were sequentially recorded and averaged. The absorbance of KBr was accounted for by running blanks consisting of solely KBr powder.

Granule size, constituent particle size and organic matter analyses were also undertaken on dried cryoconite subsamples. Granule size analyses were performed in order to assess the morphology of the whole cryoconite granules and its variability. An 'imaging chamber' was constructed by cutting a well into cellophane tape that had been layered upon a glass slide. Five hundred milligrams of cryoconite granules from each location were deposited into the well and imaged using a dissecting microscope with CCD camera attachment (brightfield reflected light and 1× magnification). The raw images were subsequently adjusted for brightness and contrast and, using ImagePro™, the 'area' function was used to calculate the projected 2D area of the granules; any touching granules were manually separated. The average diameter of each granule was calculated using the formula (length + width)/2.

Particle size analyses of constituent particles followed disaggregation by boiling the aggregates in a 30 % hydrogen peroxide solution for one hour and until effervescence ceased. Analysis was then undertaken in triplicate (following standard operating protocols) on a Horiba LA950 laser diffraction particle sizer.

Bulk organic matter content and composition was determined using step–wise thermogravimetric analysis, based upon the protocol of Kristensen (1990). Five hundred milligrams of each sample was heated in a muffle furnace at 105°C, 200°C, 350°C and 520°C, for 4 hours at each temperature, allowed to cool within a desiccator and weighed. This procedure enables the calculation of total organic carbon (TOC) contents, as well as the differentiation of thermo–labile (200–350°C) and thermo–stable organic matter (350–520°C) (Cuypers et al. 2002).

2.3.2 Microbiological and biochemical analyses

Fully hydrated cryoconite granules were dropped into a small amount of ultra-high quality (UHQ) water and immediately frozen using liquid nitrogen. These blocks of

cryoconite and amorphous ice were then sectioned at −15°C within a Cryostat, to a thickness of 60 µm, and deposited on a Superfrost™ glass microscope slide. Sections were allowed to dry for one hour at room temperature and were then stained with various fluorescent biological stains.

The development of a multiple fluorescent staining protocol to stain thin sections of cryoconite material and image using CLSM requires the consideration of autofluorescence, particularly from photosynthetic microorganisms, which can directly interfere with the fluorochromes used (Neu et al. 2002). Consequently, a three-pronged approach was employed, using 4', 6-diamidino-5-phenylindole (DAPI) to stain cellular material, AlexaFluor 488 (concanavalin A conjugate) to stain the polysaccharides within EPS, and autofluorescent emission to visualise photosynthetic microorganisms. This approach was developed based upon the protocols of Chen et al. (2007a,b) & Neu et al. (2004). The autofluorescence of photosynthetic microorganisms was excited at 543 nm and detected between 650 and 700 nm. Each thin-section was therefore covered with 100 µL of DAPI stain (12.5 µg/mL final concentration) and incubated for 5 minutes in the dark. This stain solution was then removed by pipette and the thin-section was washed with a 100-µL drop of UHQ water, three times for 5-minute durations. Following this, a 100-µL drop of AlexaFluor 488 (concanavalin A conjugate) fluorescent dye was added (at 100 µg/mL final concentration), incubated for 20 minutes in the dark and then washed as described above. Each thin section was subsequently imaged on a Zeiss LSM 510 META microscope with two-photon capabilities.

To characterise the bulk microbial biomass of cryoconite debris, a small amount (10 mg) of thawed cryoconite was re-suspended in 1mL of UHQ water, buffered with phosphate buffered saline (PBS), and incubated with DAPI stain as described above, filtered onto a 0.2 µm black polycarbonate filter paper and mounted onto a glass slide. These slides were analysed and imaged under fluorescent light using a Zeiss Axioplan 2 epifluorescence microscope with a DAPI filter cube. Autofluorescence of both photosynthesising microorganisms and certain inorganic particulates was detected using the FITC broad filter. Due to the attachment of biota to mineral surfaces, a z-section technique was employed, whereby 15 random fields of view were imaged at 0.5 µm z-intervals and cell counts undertaken on these images.

2.4 Results

2.4.1 Geological and geochemical

Figure 5 illustrates some of the typical spectral profiles obtained using powder XRD and KBr-FTIR. XRD analyses indicate a prevalence of silicate minerals and their weathering products (Cullity 1978, Ruffell and Wiltshire 2004). The strongest peaks correspond well to the International Centre for Diffraction Data (ICDD) file 46-1045, indicating an abundance of quartz. Cryoconite from KP shows the simplest diffraction pattern, indicative of a mineralogy dominated by quartz, with contributions from orthoclase and plagioclase feldspar. Cryoconite from VF and ML show similar diffraction patterns, with data suggesting a dominance by quartz, with significant contributions by mica, kaolinite–type clays, and orthoclase feldspar. Silicates and dolomite dominate the diffraction pattern from LY, as outlined by Hodson et al. (2010). Cryoconite from KG shows the most complex signal, suggesting a broader mineralogy with a greater dominance by plagioclase feldspar, and contributions from calcareous minerals and apatite. FTIR spectra complement the XRD data, in that the peak assignments indicate a prevalence of quartz and weathered silicates. The peaks at ~3,430 cm^{-1} and ~1640 cm^{-1} can be attributed to 'free' water within the sample. The labelled groups of peaks can be attributed as follows: (i) stretching of inner hydroxyl groups between tetrahedral and octahedral sheets of phyllosilicates (e.g. kaolinite, illite and smectite), (ii) aliphatic C-H stretching indicative of organic acids and lipids, (iii) calcite and dolomite peaks at ~1430 cm^{-1} and ~1450 cm^{-1} respectively, (iv) Si–O stretching vibrations of phyllosilicates, (v) vibrations that can be largely attributed to quartz, and (vi) Si–O–metal bending bands (Madejova 2003, Madejova et al. 2009). If the phyllosilicate vibrations are studied in more detail, it is clear that all cryoconite samples show a peak at ~1026–1034 cm^{-1}, indicative of biotite, illite and kaolinite (Matteson and Herron 1993). Most cryoconite samples also show a shoulder at ~1016–1000 cm^{-1}, indicative of muscovite and orthoclase feldspar, with KG cryoconite showing a pronounced peak at 1004 cm^{-1}, indicative of glauconite (Matteson and Herron 1993).

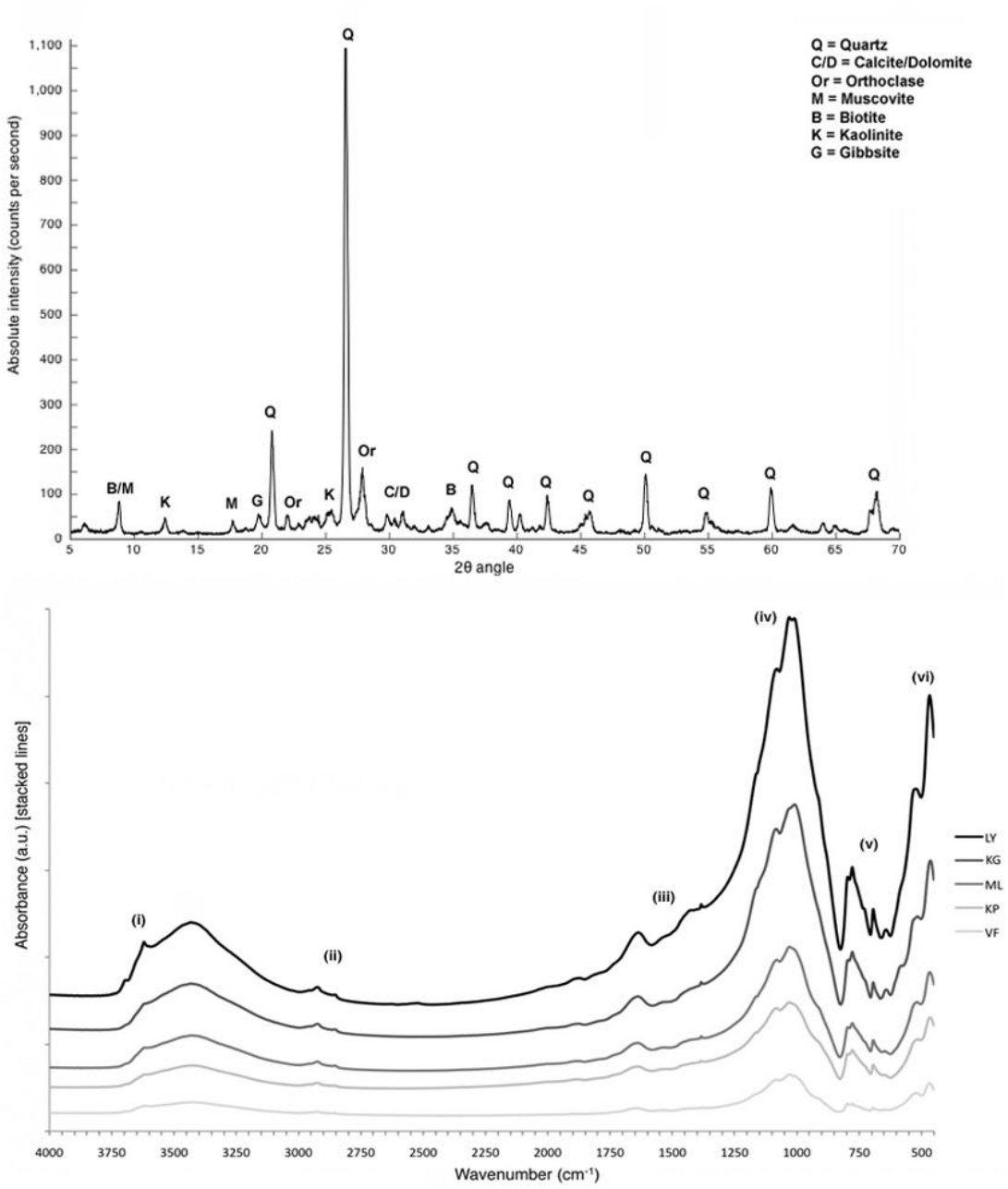

Figure 5: Mean combined powder XRD profile, an example to illustrate interpretation, showing the dominance of silicate minerals and their weathering products. Typical KBr-FTIR profiles for each of the cryoconite samples; features of interest (i–vi) are discussed in the text.

Optical microscopy of geological thin-sections revealed that mineral particles were typically <100 μm in diameter and showed evidence of weathering and organic coatings. The organo-mineral groundmass showed evidence of zoning and clustering, and varying degrees of humification. In agreement with the XRD and FTIR data, it was also found that the three principal mineralogies were quartz, orthoclase feldspar and micas, with calcite, clays, trace minerals and organic matter making up a varying

proportion of the remaining solid material. For example, KP cryoconite in Figure 6 shows an abundance of quartz, low quantities of mica and feldspar, and small regions of organic material (i), some organic coatings on particles and a rich organic layer around one edge (ii). ML cryoconite in Figure 6 shows a heterogeneous distribution of quartz, orthoclase feldspar and mica, with a higher and more variable quantity of clay–sized particles, with larger quantities and regions of organic matter (iii), as well as a dark, organic layer near to the edge of the granule (ii).

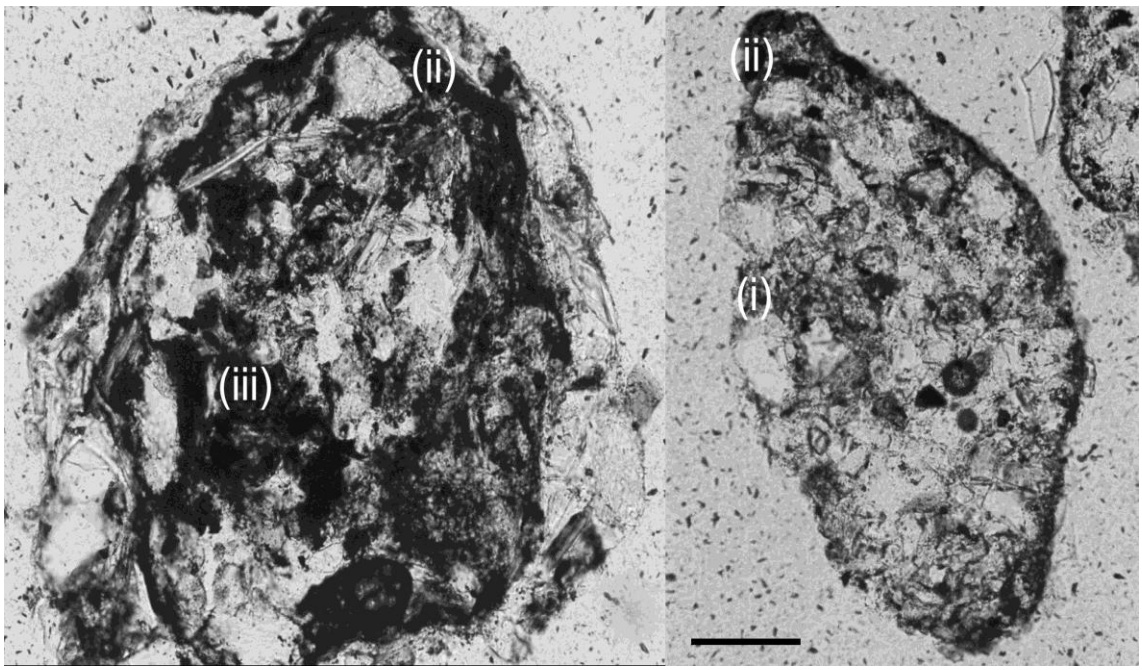

Figure 6: Low magnification (20×) brightfield imagery of, from left, ML cryoconite granule and KP cryoconite granule. Zoning of mineral grains and organic matter is evident, with translucent green–yellow organic matter clustering near the granule edge (i), and opaque near–black organic matter evident both as a layer around/near the granule edge (ii) and clustering within the centre of an organic–rich granule (iii); scale bar = 100 µm.

Differences in granule composition were evident between granules from the same sampling location, especially from KP, where thin sections revealed a continuum between aggregations of minerals with near–transparent organic matter between the mineral particles, and rarer aggregations of minerals surrounded by near–opaque green to black organic matter. The opacity and colour of organic matter within the granule may well be directly influenced by the age of the aggregate, though other factors such as the accumulation of microbial pigments or colloidal black carbon particles may also be significant.

Cryoconite particle size analyses found silt to be the dominant particle size (following Gale and Hoare, 1991) at four out of the five sampling locations. Cryoconite from KG and VF were found to have the highest clay contents (<3 μm), cryoconite from ML showed the highest sand content (>63 μm), and cryoconite from KP and VF showed the highest silt contents (3–63 μm). The median and mean particle sizes varied from 64.754 and 80.492 μm (σ_M = 0.128 μm) at ML, to 16.315 and 28.830 μm (σ_M = 0.604 μm) at VF, respectively. It must be noted, however, that the majority of particle size data was non-normal in form.

When comparing the aggregate size distribution, cryoconite from KG and KP showed the smallest mean aggregate sizes (~400 μm), whilst ML and LY showed mean aggregate sizes of ~500 μm, and cryoconite from VF showed the highest mean aggregate size (~600 μm). A more comprehensive study of aggregate size upon LY using field–based imagery (Hodson et al. 2010) found a considerably larger aggregate size (median 6.74 mm), perhaps indicating that *in situ*, hydrated aggregates are significantly larger in size.

Triplicate thermogravimetric analyses found that organic matter content (as a percentage of dry weight) varied from 1.30% (± 0.166%) for cryoconite from KG, to 6.07% (± 0.118%) for VF. Cryoconite from KP, LY and ML exhibited TOC values of 1.48% (± 0.166%), 2.76% (± 0.224%) and 3.27% (± 0.171%) respectively. These values are in agreement with TOC values determined for cryoconite from other Svalbard glaciers (e.g. Stibal et al. 2008a). The R_p values (Kristensen 1990) for Arctic cryoconite, a ratio of mass loss between 200 and 350°C and mass loss between 350 and 520°C, were all < 0.5, indicating that the majority of organic matter present within these aggregates is thermo–labile, i.e. dominated by carbohydrates (Kristensen 1990, Siewert 2004).

2.4.2 Biological and biochemical

Total counts of DAPI-stained cryoconite indicated between ~ 1.95×10^3 cells/mg for KG cryoconite and 1.05×10^4 cells/mg for VF cryoconite. Cryoconite from KP showed a similar total count to VF (9.07×10^3 cells/mg), with LY and ML cryoconite showing

2.18×10^3 and 2.57×10^3 cells/mg respectively. The majority of DAPI-stained microorganisms were found to be either coccoid in shape or filamentous, with some rod and a few vibrio also present. Autofluorescence imagery indicated the presence of variable quantities and types of photosynthetic microorganisms. Microscopic analysis has identified, based upon the classification system of Rippka et al. (1979), a dominance of filamentous cyanobacteria, particularly thinner *Leptolyngbya sp.* (diameter 0.7-2 µm), and thicker *Phormidium sp.*, *Lyngbya sp.*, and *Oscillatoria sp*. (diameter 4-11 µm). Unicellular cyanobacteria, likely *Synechococcus sp*. or *Gloeocapsa sp.*, various algae and diatoms have also been identified.

Low magnification CLSM images (Figure 7a–d) indicated the heterogeneous distribution of photoautotrophs within cryoconite. KG cryoconite (image not shown) contained a relatively low microbial content. KP cryoconite showed a dominance of heterotrophic bacteria and infrequent clusters of unicellular photoautotrophs (Figure 7a), whereas ML and LY cryoconite (Figure 7b and c respectively) showed a greater prevalence of photoautotrophs and clusters of heterotrophic bacteria, and VF cryoconite (Figure 7d) aggregates showed the highest prevalence of photosynthetic microorganisms, as well as a prevalence of heterotrophic bacteria. Whilst it is appreciated that chemoautotrophic bacteria and archaea may also be present, the differentiation of photoautotrophs and heterotrophs using autofluorescence and nuclear staining has been the traditional approach when studying phototrophic biofilms (e.g. Neu et al. 2004). ML and LY aggregates supported a greater number of thicker filaments (*Phormidium sp*. and *Oscillatoria sp.*), whereas VF aggregates seemed to principally contain a far denser network of thinner filaments (*Leptolyngbya sp*.). Unicellular photosynthetic microorganisms were rarely seen to dominate, and were often found associated with clusters of filamentous microorganisms. Larger single–celled phototrophs, likely green algae, were found sporadically throughout the granule, either singly or as small colonies.

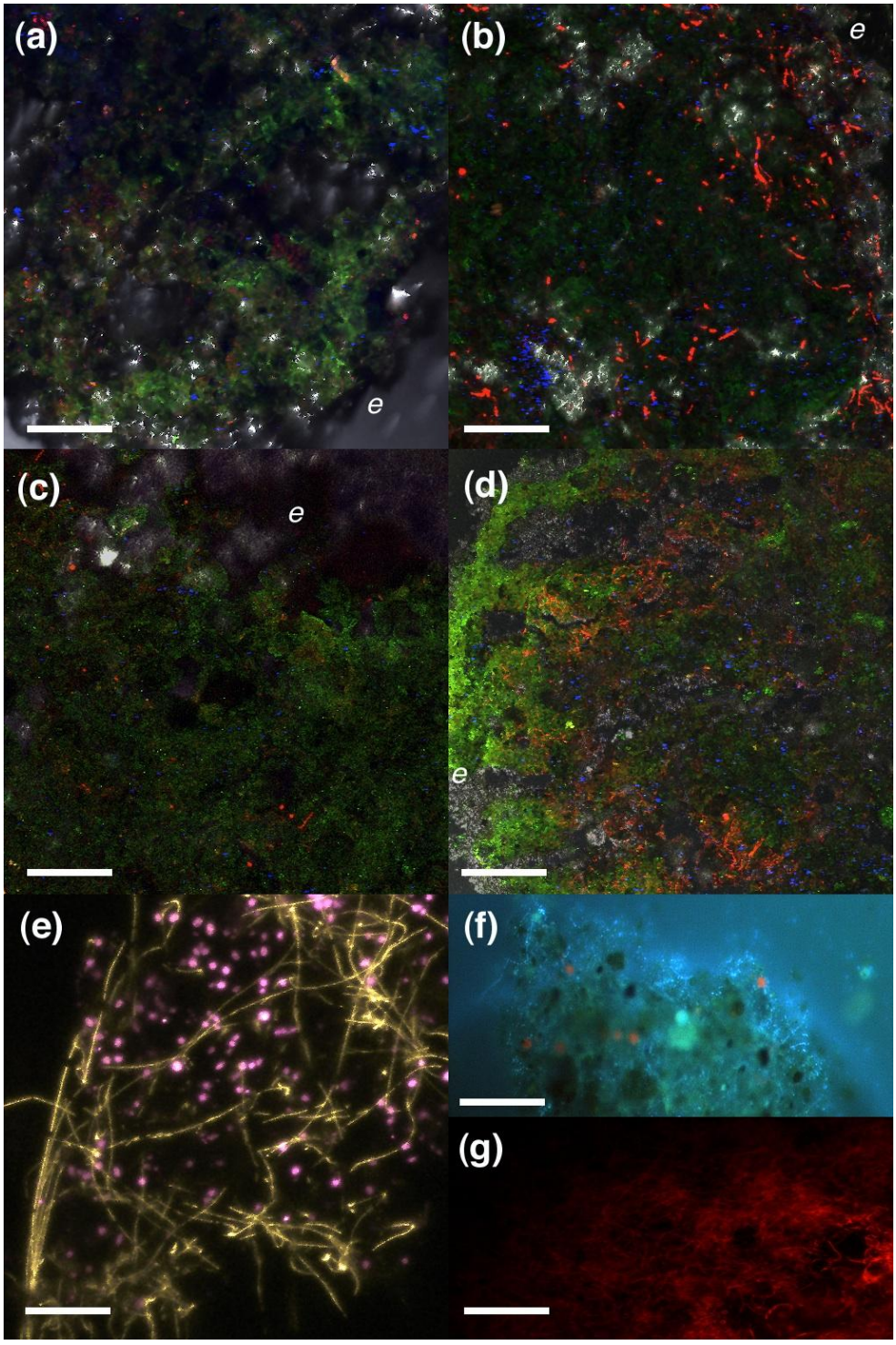

Figure 7: CLSM images showing (a–d) variation in photoautotrophic microorganism (red; autofluorescence), heterotrophic microorganism (blue; DAPI), and polysaccharide contents (green; AlexaFluor 488) of cryoconite aggregates [e = outer edge of aggregate]; (e) differentiation of photosynthetic pigments using their fluorescent emissions; (f and g) epifluorescent images detailing a heterotroph–rich and an autotrophic filament–rich granule respectively; scale bars = 50 µm.

As evidenced in figure 7(d), aggregates enriched with filamentous cyanobacteria tended to exhibit a denser network of filaments at or just below the surface, in this case extending for ~50–70 μm into the granule and providing structural support for the aggregate. Aggregates impoverished in filamentous cyanobacteria, as evidenced in Figure 7(a), showed disruption when cut with a microtome blade, indicative of a more fragile aggregate structure. Within cryoconite aggregates, filament orientation was generally random and encapsulated mineral particles. Aggregates with a dense network near to the surface showed a slightly greater tendency for filaments to orient parallel to the surface of the granule, perhaps to maximise the surface area exposed to sunlight. Figure 7(a–d) also illustrates that polysaccharides could be found covering the surfaces of mineral particles, with greater concentrations of polysaccharides nearly always associated with clusters of photoautotrophs. Furthermore, high concentrations of polysaccharides were most evident at or near the surface of cryoconite granules (Figure 7d). Those aggregates showing a relatively homogeneous distribution of polysaccharides throughout, such as those from LY (Figure 7c), showed a finer fabric, suggestive of strong clay–organic matter interactions.

Figure 7(e) indicates two separate autofluorescent emissions captured using short pass filters covering the wavelength ranges of 650–700 nm (pink) and 590–650 nm (yellow), in this case for a biofilm mechanically removed from the surface of a cryoconite granule from ML. It can be seen that the stronger fluorescent emissions (coloured pink) emanated from the unicellular microorganisms. In fact emission spectra for these unicellular microorganisms, taken from lambda stack images using a 'region of interest' filter, showed a fluorescence peak at ~678 nm, which can be correlated with chlorophyll *a* content (Barranguet et al. 2004). The slightly weaker fluorescent emissions (coloured yellow) emanated from the filamentous microorganisms, with emission spectra indicating a fluorescence peak at ~645 nm, which can be correlated with phycocyanin, a cyanobacterial phycobiliprotein.

Both CLSM– and epifluorescence– based analyses of heterotrophic bacteria confirmed their heterogeneous occurrence throughout cryoconite aggregates. The low magnification CLSM images in figure 3 indicate that they tend to cluster in greatest numbers in areas often associated with photoautotrophic activity and the presence of organic matter. In cryoconite from KP, greater concentrations of heterotrophic bacteria were found at the edge of the granule, clearly visualised in figure 7(f). This is in direct

contrast to the filament–rich surface layer dominating in cryoconite from VF (Figure 7g) for example.

2.5 Discussion

2.5.1 Microstructure and biogeochemistry of Arctic cryoconite

In summary, optical microscopy, XRD and KBr-FTIR analyses found that Arctic cryoconite granules are dominated by phyllosilicate, tectosilicate and quartz minerals, showing a dominance of small particle sizes (< 100 μm) and a varying but significant quantity of organic groundmass, characterised by varying degrees of pigmentation and/or humification. Mineral coatings are also prevalent, with constituent mineral particles showing both organic and metal oxide/hydroxide coatings. These findings are in agreement with other biogeochemical and structural investigations of cryoconite from the Arctic and elsewhere in the world (Hodson et al. 2010, Stibal et al. 2008a, Takeuchi et al. 2001a,b). Clear differences in the mineralogy and geochemical aggregate structure can be seen both when comparing cryoconite from different glaciers and when comparing cryoconite from one sampling location upon a single glacier. This structural heterogeneity allows for the existence of microenvironments exhibiting different physicochemical and structural characteristics (Ranjard and Richaume 2001); indeed Carson et al. (2009) find that mineral heterogeneity directly contributes to the spatial variation in bacterial communities. Fine–textured sediment can be seen to promote microbial abundance, in accord with Stibal et al. (2006). In addition, the data indicate a relationship between mean organic matter content and mean aggregate size, most clearly seen when comparing cryoconite granules from VF and KP. This relationship can also be seen in soil microaggregates, whereby the interaction of microbial biomass within the soil, governed by variations in the microbiology and soil properties (particularly texture, clay mineralogy, pore–size distribution and aggregate dynamics), can culminate in the protection of microbially produced organic matter through aggregation (Six et al. 2006). Arctic cryoconite has been shown by thermogravimetry to be dominated by thermolabile carbohydrates, suggesting that microbial EPS contributes significantly to the stabilisation of these aggregates, both through its own cohesive properties and by moderating the surface chemistry of nearby substrates, promoting

cation exchange and interaction with fine clay and colloid fractions (Kögel–Knabner et al. 2008).

Fluorescence microscopy techniques indicated that cryoconite granules are rich in microorganisms, with total counts comparing favourably with recent literature (Stibal et al. 2008a). CLSM images illustrated a heterogeneous distribution throughout the granule and evidence of clustering and association with organic matter. In agreement with Hodson et al. (2010) and Takeuchi et al. (2001a,b), the majority of aggregates of organic-rich cryoconite, such as upon VF, showed a network of filamentous cyanobacteria on or near to the surface. Cyanobacterial filaments showed a broad range of morphotypes, as evidenced in other glacial environments (de los Rios et al. 2004). This network did not appear to show a dominant orientation, but does entangle mineral particles and support clusters of unicellular photoautotrophs, heterotrophic bacteria, and a prevalence of organic matter within its surround. Not all cryoconite can be said to conform to the above description, however, as cryoconite from KP in particular shows a greater concentration of filamentous and unicellular heterotrophic bacteria, dominating the near surface of the granule, and a sporadic distribution of photoautotrophs, chiefly unicellular cyanobacteria and algae. In contrast to aggregates from VF, which show little change in size upon light agitation, aggregates from KP disaggregate into smaller, microaggregates (or flocs). These are generally composed of a cluster of heterotrophic bacteria surrounding an aggregation of organic matter, with some small mineral particles entrained and occasionally a single cyanobacterial filament. Indeed these microaggregates show a similarity to ‘marine snow’: suspended aggregates rich in microbia, organic matter and trace metals (Simon et al. 2002). Furthermore, fluorescent images of cryoconite aggregates indicate that, in general, there is a positive relationship between the number of photoautotrophic microorganisms and aggregate size. This is likely to be due to filamentous binding and the presence of cyanobacterial EPS. It has been shown that cyanobacterial filaments actively form ligand-metal complexes (Yee et al. 2004) and, as such, can interact and readily bind with clays and organic matter. A long summer without disruption by snowfall has been identified as a key factor in the proliferation of cyanobacteria and algae on the glacier surface (Yoshimura et al. 1997).

EPS plays an important role in the microstructure of aggregates from other environments, since it can assist cell–cell attachment by forming bridging complexes, alter the surface charge of dispersed cells or filaments, allowing coagulation, and also

provide protection from abiotic stress and predation (Adav et al. 2010, Schmidt and Ahring 1994). Further, the trapping of particulate matter and adsorption of nutrients by EPS in aquatic environments enables functional advantages, such as assisting in the formation of sedimentable aggregates and providing diverse microenvironments for nutrient uptake (Leppard et al. 1995). Zulpa de Caire et al. (1997) found that aggregate size and stability both increase when either EPS or cyanobacteria are inoculated into soil, with solely EPS showing only a short–term aggregating influence, as opposed to cyanobacteria, which show a long-term influence. It has been proposed (de Winder et al. 1999) that the exopolymer sheaths of cyanobacteria are, to an extent, recalcitrant to mineralisation, and as such their cohesive binding effect upon sediment can be maintained. Consequently, it may be said that microbial composition can fundamentally affect the microstructure and composition of cryoconite granules. A continuum is evident, between cryoconite aggregates that are dark, dense structures compiled of a large number of cyanobacterial filaments, and cryoconite aggregates that are lighter, gelatinous structures compiled of smaller, microaggregates showing greater dominance by heterotrophic microorganisms. Whilst one end–member is more akin to microbial mats and soil microaggregates, the other is more akin to sludge flocs and marine snow.

2.5.2 Implications for cryoconite aggregate formation

The data reported above, as well as current knowledge within the literature, allow a hypothesis for cryoconite aggregation to be developed. Given the prevalence of photosynthetic microorganisms within cryoconite, it is clear that they are actively involved in the aggregation of cryoconite granules. As such, it is proposed that:

1) Photosynthetic blooms in near-surface suspension (witnessed at sites across Svalbard; A. Hodson, personal communication) result in micro–aggregations of EPS and both filamentous and unicellular photoautotrophs in wet snow and slush. Here aeolian colloidal particulates also aggregate through physico–chemical interaction, such as hydrophobic interaction of black carbon and perikinetic and orthokinetic flocculation (Folkersma et al. 1999), whilst interactions between planktonic bacteria and clay-sized particles result in biofilm development (Zavarzin and Alekseeva 2009). These are all potential precursory steps that could

take place upon glaciers, with the 'straining' of particulates from meltwaters percolating through snow physically promoting interaction.

2) EPS–rich microaggregates will grow further by acting as sticky sieves that trap suspended or settling particulates in transit across the glacier. EPS provides an extensive surface area for binding, with total concentrations of electrostatic binding sites being over 20× higher than for cell surfaces (Liu and Fang 2002), as well as containing both hydrophobic and hydrophilic polymers (Jorand et al. 1998) and having the ability to partially overcome a cell's negative charge (Tsuneda et al. 2003).
3) Increasing aggregation leads to a greater settling ability and, due to dark particulate matter within these micro–aggregates, differential melt into the ice (Wharton et al. 1985). As with other bio–aggregates, it is likely that filamentous binding then takes over as the dominant influence upon aggregate structure and development. Given the CLSM observations discussed above, it is considered that certain aggregates and locations do not support a proliferation of cyanobacterial filaments. These aggregates, as in KG for example, are therefore weakly bound with sporadic cyanobacterial filaments, meaning that they can be disrupted by increases in shear strength. In aggregates and locations where the biogeochemistry is conducive to cyanobacterial proliferation, such as in VF, filaments do indeed proliferate, mechanically and chemically binding the aggregate substrate. Cyanobacteria, being slow growing, should positively influence the density and stability of bio–aggregates (de Kreuk and Loosdrecht 2004).
4) The fate of cryoconite aggregates after the above growth stages is most likely dominated by stochastic transport events that result from glacier ablation during the summer. On gentle sloping ice surfaces the persistence of cryoconite for several years appears possible (Hodson et al 2010), whilst those aggregates that combine to form cryoconite holes in close proximity to migrating supraglacial streams are at greater risk of transfer from the system (Takeuchi et al 2000).

2.6 Conclusions

It is clear that the cryoconite granule is a complex, heterogeneous entity showing broad similarities in structure and composition across the Arctic region, yet showing

variability even between granules within the same cryoconite hole. The dominance of filamentous microorganisms within the strongest granules, particularly cyanobacteria, point towards the pivotal role these bacteria play in the stable aggregation of supraglacial sediments. However, the roles of other photosynthetic microorganisms and heterotrophic bacteria are clearly elevated in some granules. When combined with the fact that polysaccharides were present in all granules studied, this suggests that EPS also has an important role to play in the aggregation of cryoconite. The tight clustering of organic matter, phototrophs and heterotrophs in many granules suggests a relationship between autotrophy and heterotrophy within cryoconite, with implications for carbon cycling within aggregates. Furthermore, it is clear that various geochemical factors can support aggregation, in particular the availability of weathered minerals and colloidal particles. A theory of cryoconite aggregate formation has been hypothesised, centered upon multilevel aggregation, with bioflocculation and filamentous bulking the two key steps. Knowledge of the roles of photosynthetic microorganisms and EPS in aggregation is still, however, in its infancy, and it is thought vital to further this research in order to better understand supraglacial ecosystems.

CHAPTER THREE: USING FTIR SPECTROSCOPY TO CHARACTERISE THE SOIL MINERALOGY AND GEOCHEMISTRY OF CRYOCONITE FROM ALDEGONDABREEN GLACIER, SVALBARD

Published as: Langford, H., A. Hodson & S. Banwart, 2011. Using FTIR spectroscopy to characterise the soil mineralogy and geochemistry of cryoconite from Aldegondabreen glacier, Svalbard. *Applied Geochemistry*, 26 (S1), S206–S209

http://dx.doi.org/10.1016/j.apgeochem.2011.03.105.

3.1 Abstract

Mineralogical and geochemical diversity in cryoconite granules from Aldegondabreen glacier was investigated using FTIR spectroscopy. Results suggest that the technique is an effective tool for investigating mineralogy and identifying spatial differences in geochemistry, based upon characteristic spectral signatures.

3.2 Introduction

Cryoconite granules are biologically active aggregations of microorganisms, mineral particles and organic matter that occur on glaciers, either within shallow melt on the glacier surface or within deeper meltpools, termed cryoconite holes. Recent research has focused primarily on nutrient cycling (e.g. Stibal et al. 2008a,b, Xu et al. 2010) at various scales, and microstructural characterisation (e.g. Takeuchi et al. 2001b, Langford et al. 2010) of granular biogeochemistry. Although cryoconite is organo-sedimentary, unlike research into soil structure and composition, spectroscopy has not been widely employed within the field. FTIR spectroscopy provides the opportunity to identify crystalline, poorly crystalline and amorphous materials based upon characteristic absorbance peaks (Ji et al. 2009). In addition, when combined with an extraction protocol, it can also provide useful information on the composition and origin

of organic matter (Giovanela et al. 2010). This study applies FTIR spectroscopy to the study of cryoconite granules sampled from 12 locations (AG1-12) across Aldegondabreen glacier, Grønfjorden, Svalbard, Norway (Figure 8). It is our hypothesis that there will be spatial variability in the geochemical composition of cryoconite across the glacier surface. All FTIR analyses were performed on a Perkin-Elmer 'Spectrum One' spectrometer, using the KBr pellet technique, with 150 mg of spectroscopy grade KBr, and recording 100 scans at 4 cm^{-1} resolution.

Figure 8: Location map of Aldegondabreen glacier, showing sampling points AG1-12; (a) = bird cliffs.

3.3 Results and discussion

FTIR spectra of bulk cryoconite samples (3 mg subsamples) are characteristic of a soil dominated by clays (Madejova 2003) and show variability between sampling points. Figure 9(a) details the principal absorbance peaks of two characteristic and different FTIR spectra (AG1 & AG2), and their classifications. Briefly, spectra show peaks associated with quartz, feldspar, mica, a range of clays, and organic matter.

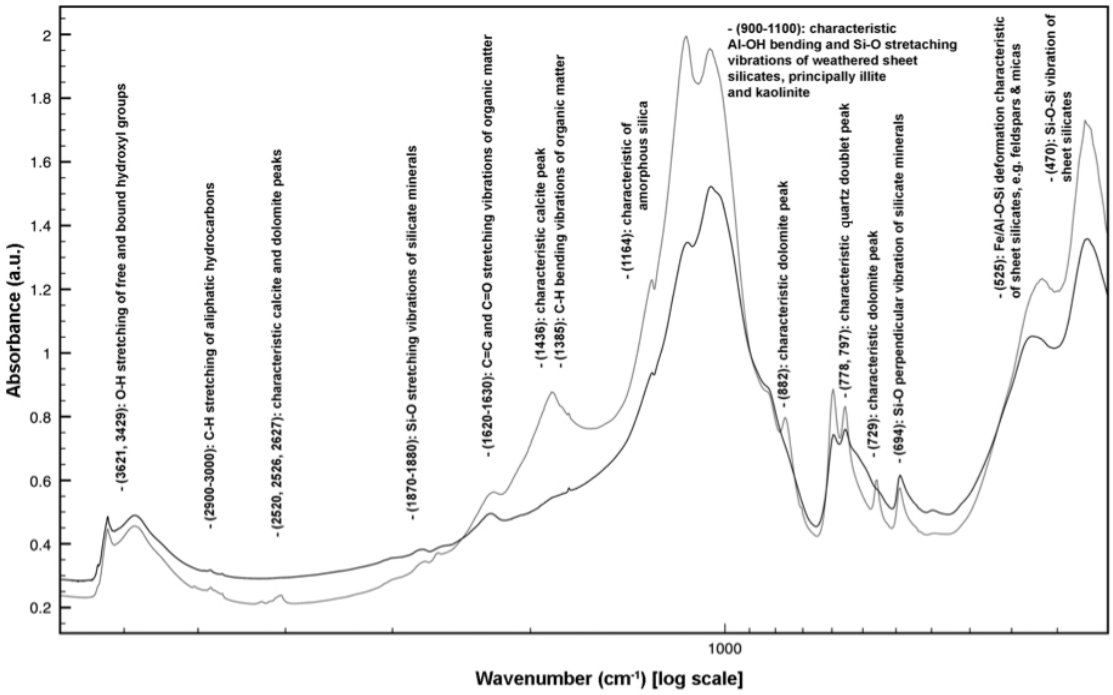

Figure 9(a): Characteristic FTIR spectra from Aldegondabreen cryoconite (grey = AG1, black = AG2), with notable peaks identified. Peak identification is based upon Farmer (1974) and Madejova (2003).

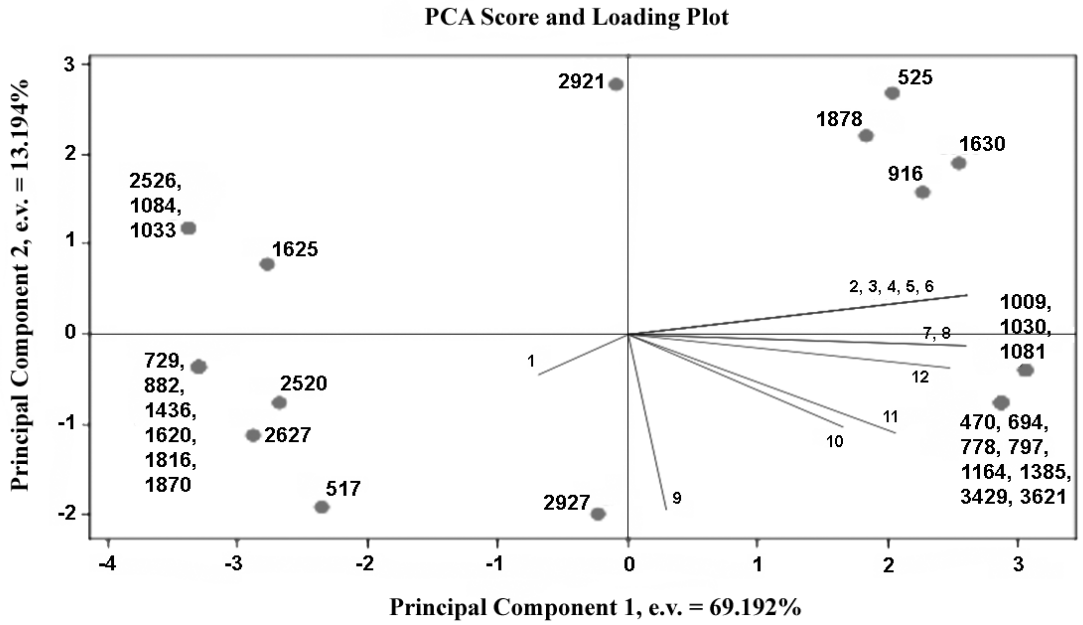

Figure 9(b): Principal Component Analysis (PCA) score and loading plot for peak presence (binary). The larger bold values are wavenumbers of peaks in the spectra, the smaller values are sample numbers; e.v. = explained variance.

In order to assess the change in mineralogy between the different sampling locations, principal component analysis (PCA) was undertaken in Minitab 15. PCA (Jolliffe 1986)

is an orthogonal transformation of data into a set of principal components that attempt to account for as much of the variability in the dataset as possible; each principal component consists of a score vector and a loading vector. Results of the PCA of the binary (presence/absence of peaks) FTIR data are presented in Figure 9(b). This combined 'score' and 'loading' plot of principal components 1 and 2, which cumulatively explain 82.386% of the variance in the data, identifies that the majority of samples share some common peaks, clustered to the bottom-right of the plot, such as the characteristic quartz doublet peak at 778 cm^{-1} and 797 cm^{-1}. However, sample AG1 (and to an extent sample AG9) shows a significantly different spectrum characterised by a number of dissimilar peaks. The principal peaks contributing to this difference are those at 729 cm^{-1} and 882 cm^{-1} – dolomite, one at 1436 cm^{-1} – calcite, and one at 1816 cm^{-1} – a wavenumber suggestive of a carbonyl functional group, likely associated with organic matter. Smaller differences, appearing more centrally on the plot, can account for some of the minor variability between the samples. For example, the peaks at 2921 cm^{-1}, 2927 cm^{-1} (aliphatic hydrocarbons) and between 1620 and 1630 cm^{-1} (carboxylate groups), show minor changes in wavenumber, possibly indicative of compositional differences in organic matter. Kaiser et al. (1997) note that a shift in the carboxylate peak to a lower wavenumber occurs due to increased interaction between organic matter and Fe & Al inorganic compounds. As well as peak presence, peak intensity was also analysed. Samples from locations near to the edge of the glacier show proportionately higher peaks in the main 'silicate' regions of 900–1200 cm^{-1}, 650–800 cm^{-1} and 450–550 cm^{-1}, indicating that they contain proportionally greater concentrations of clays. Sample AG1 shows a particularly strong peak at 1084 cm^{-1}, evidence of higher concentrations of crystalline quartz than elsewhere upon the glacier. These data suggest that the cryoconite mineralogy at the edge of Aldegondabreen has a different composition, signifying differing source rocks. It is considered likely that the centre of the glacier is principally fed by Aeolian input, whilst the sides of the glacier receive characteristically greater quantities of avalanche-fed debris. Regular rockfall from the cliffs at location (a) (Figure 8) was witnessed whilst sampling.

Regarding soil organic matter content, initial evaluation of total organic carbon content revealed some spatial variation, varying from 1.93% (± 0.165%) (AG9) to 3.58% (± 0.357%) of dry weight (AG4). To further assess the organic matter content and composition, the humic substances within each cryoconite sample were extracted

using NaOH, following the protocol of Giovanela et al. (2010). Triplicate UV/Vis spectra of each extract were taken to confirm the presence of humic substances: spectra showed a characteristic featureless slope rising from low absorbance at 700 nm to a peak in absorbance between 260 and 280 nm. FTIR spectra of the humic acid (HA) extract from each cryoconite sample were taken (1mg HA subsamples). Spectra show some small peaks associated with silicates and carbonates, and a range of peaks commonly associated with organic matter. A number of peaks between 2800 and 3000 cm^{-1} are indicative of aliphatic C–H stretching vibrations, whilst small peaks between 1500 and 1650 cm^{-1} are indicative of aromatic C=C stretching vibrations (Bustin & Guo 1999). Other identifiable peaks, such as at 1384 cm^{-1} (C–H bending), and at both 1095 cm^{-1} and 1163 cm^{-1} (C–O–H bending and C–O stretching respectively), are suggestive of less humified material, such as fatty acids and polysaccharides (Kalbitz et al. 1999). The general organic matter signature revealed in the spectra correlates with the findings of Xu et al. (2010), who studied cryoconite organic matter from the Canadian Rocky Mountains using molecular methods. Artz et al. (2008) note that with increasing humification, you get a decline in polysaccharide peaks at c. 3400 cm^{-1} and 1040 cm^{-1}, and an increase in aliphatic structures at c. 2920 cm^{-1} and 2850 cm^{-1}.

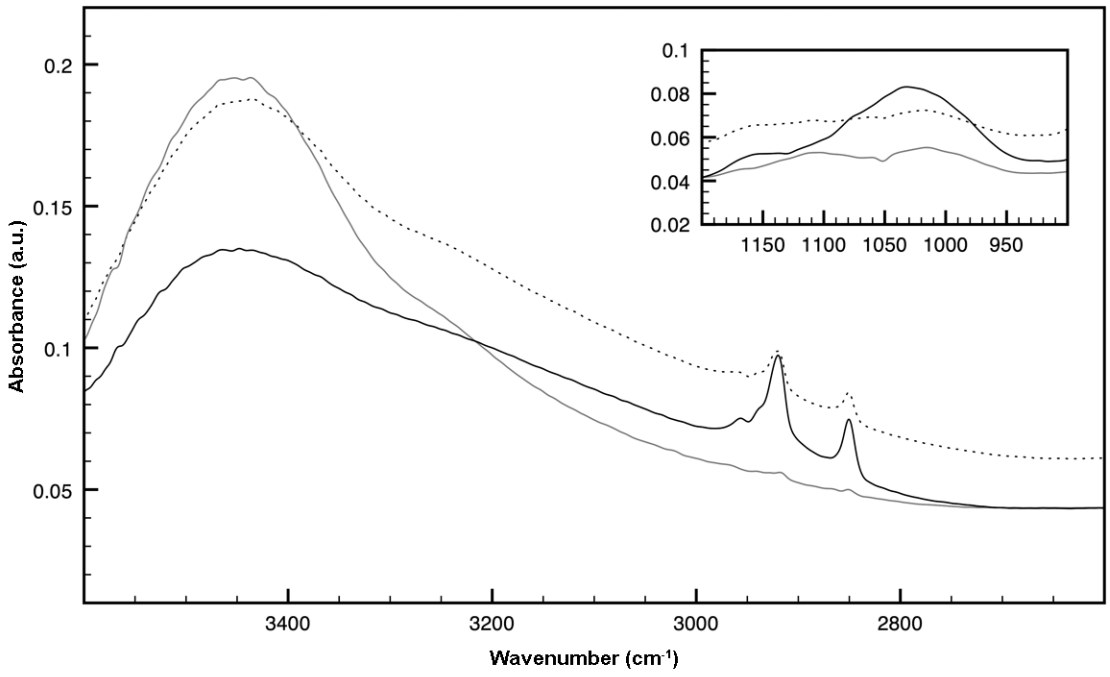

Figure 10: Selected peaks from characteristic FTIR spectra of humic acid extracts from Aldegondabreen cryoconite (grey = AG1, dotted = AG8, black = AG11).

Spatial variability in organic matter composition is clearly visible (Fig. 10), with cryoconite at AG1, for example, showing two relatively small aliphatic C–H peaks between 2850 and 3000 cm^{-1} and a minimal peak at 1040 cm^{-1}. Cryoconite from AG8 shows a three-peak arrangement between 2850 and 3000 cm^{-1} and a minimal peak at 1040 cm^{-1}. Finally, cryoconite from AG11 shows a four-peak arrangement between 2850 and 3000 cm^{-1} and a broad peak centred at 1040 cm^{-1}. These data suggest that cryoconite near to the centre of Aldegondabreen is dominated by carbohydrate-rich organic matter and associated, largely aliphatic, humification products, whereas cryoconite near to the glacier edge tends to contain both a lesser quantity and less diverse composition of organic matter.

3.4 Conclusions

FTIR spectroscopy has proven to be an effective tool for elucidating spatial variations in cryoconite mineralogy. When combined with an organic matter extraction, smaller peaks previously masked by stronger mineral absorbance can be seen and, consequently, used to study spatial variation in organic matter composition. Results indicate that cryoconite across the ablation zone of Aldegondabreen varies in mineralogy and geochemistry, with centrally-located cryoconite showing a greater concentration of aliphatic- and carbohydrate- rich organic matter, and ice-marginal cryoconite showing a less biogenic signature, with a greater diversity in mineralogy.

3.5 Acknowledgements

H. Langford gratefully acknowledges the RGS, NGS and Gilchrist Education Trust awards, which provided the funds for the field expedition to Grønfjorden in summer 2009.

CHAPTER FOUR: USING ELECTRON AND OPTICAL MICROSCOPY TO STUDY SOIL MICROAGGREGATE STRUCTURE IN CRYOCONITE FROM ALPINE AND ARCTIC LOCATIONS

Prepared for submission to Arctic, Antarctic and Alpine Research: Langford, H., S. Banwart & A. Hodson, 2012. Using electron and optical microscopy to study soil microaggregate structure in cryoconite from Alpine and Arctic locations.

4.1 Abstract

The supraglacial environment has traditionally been viewed as extreme. However, within this environment exists a diverse microbial community, particularly within the microbial reservoirs and biogeochemical reactors that are cryoconite granules: microaggregates of microbial cells, organic matter and mineral particles. A combination of electron and optical microscopy allowed us to visualise these aggregates at a hitherto unparalleled spatial resolution. Cryoconite granules showed a dense structure, with a fine groundmass of clay-sized particles and extracellular polymeric substances (EPS), a surface layer dominated by filamentous cyanobacteria, along with significant EPS enmeshing. Various EPS types were identified, as well as significant EPS–mineral interaction in the form of 'clay hutches'. These findings highlight the ubiquitous presence and importance of EPS, both capsular and free, in shaping these aggregates, controlling granule hydraulics and biogeochemical interaction, and providing protection from freezing and UV exposure. Furthermore, they suggest that autochthonous organic matter production, in the form of EPS, is prevalent within supraglacial ecosystems.

4.2 Introduction

Within polar and alpine settings, recent research has revealed a fascinating range of supraglacial, englacial and subglacial microbial communities (Hodson et al. 2004, Priscu & Christner 2004, Price 2007). These communities exhibit a high microbial diversity, with spatial and seasonal changes in the microbial community evident. Within the supraglacial environment, several environmental niches exist, from the snowpack

(Amato et al. 2007, Larose et al. 2010) through to supraglacial streams (Battin et al. 2001). Perhaps the best studied of these communities is the cryoconite ecosystem (e.g. Takeuchi et al. 2001b, Christner et al. 2003, Stibal et al. 2008a, Hodson et al. 2010, Edwards et al. 2011). Cryoconite granules are complex, heterogeneous aggregates of microorganisms, mineral particles and amorphous organic matter; they are found on supraglacial surfaces in cold regions, especially the Arctic and lower latitude alpine environments. It is becoming increasingly apparent that cryoconite shares many similarities with a number of other bio-aggregates, including microbial mats, stromatolites, marine snow and natural biofilms.

Cryoconite granules can be thought of as being both microbial reservoirs and biogeochemical reactors. Investigations have highlighted the diverse microbial community present (Säwström et al. 2002, Christner et al. 2003, Edwards et al. 2011), as well as the importance of cryoconite granules to carbon, nitrogen, phosphorus and sulphur cycling (Stibal et al. 2009, Anesio et al. 2010, Gleeson et al. 2011, Telling et al. 2011). The prevalence of photoautotrophic microorganisms promotes the production of extracellular polymeric substances (EPS), allowing these aggregates to preferentially bind mineral and organic particulates, promoting cell–mineral interaction, growth and the development of microenvironments (Langford et al. 2010). Limited research, however, has attempted to probe the ultrastructure of cryoconite granules in order to better understand their formation, development and role in biogeochemical cycling.

Whilst optical microscopy has proven to be a highly effective tool in studying the photoautotrophic and heterotrophic microbial populations within cryoconite (Takeuchi et al. 2001b, Stibal et al. 2006, Langford et al. 2010), limitations to the optical resolution make it difficult to study the detailed ultrastructure of cryoconite granules, particularly such things as cell–mineral interaction and the nanometre-sized polymer fibrils of EPS. When studying bio-aggregates, many researchers have turned to electron microscopy in order to gain new information regarding such ultrastructural details as stratification, porosity and cell–EPS–mineral interaction (Heissenberger et al. 1996, Sabater et al. 2000, Donlan 2002, Dupraz et al. 2004, Webster-Brown & Webster 2007, Roldan & Hernández Mariné 2009).

With biological material being electron-poor, its imaging using electron microscopy is challenging. When preparing sample material for conventional scanning electron microscopy (SEM), extensive sample manipulation is involved, from fixation and dehydration through to embedding and/or coating (Little et al. 1991). This sample manipulation is harsh and can both interfere with the sample matrix and cause such issues as cellular collapse. Modern variations of sample preparation techniques and modifications to conventional SEM have attempted to address these issues.

Environmental scanning electron microscopy (ESEM) uses pressure-limiting apertures to allow low-vacuum operation (Muscariello et al. 2005) and water vapour as the chamber gas, which has good amplifying efficiency and thermodynamic properties (Fletcher et al. 1997), thus allowing direct observation of uncoated, electron-poor, hydrated specimens. However, ESEM still presents some challenges, with the presence of a condensed water layer, as well as sample tilt, shape and uniformity, affecting contrast, resolution and visualisation (Mestres et al. 2003, Muscariello et al. 2005). Furthermore, without a cationic heavy metal stain, such as ruthenium red, high-resolution imaging of EPS can still be problematic (Priester et al. 2007). Cryo- and low temperature (LT-) SEM have also proven popular for imaging biological structure, as sample preservation is again better than for conventional SEM, with good density site–reactivity correlation observed (Beveridge 2006). For sub-micron ultrastructure, transmission electron microscopy (TEM) provides better resolution and, with 'inordinate attention to sample handling and stabilisation' (Leppard et al. 1996), fibrillar EPS with a diameter of < 10 nm can be visualised. Advances in sample preparation, such as high-pressure freeze substitution, low-temperature resin embedding and focused ion beam milling, have improved the preservation of cellular material and, as such, its imaging using both SEM and TEM has improved.

Correlative microscopy is receiving increasing research attention within the biological sciences. A combination of various optical and electron microscopy techniques undertaken on the same sample, correlative microscopy allows functional cellular and molecular staining to be combined with high-resolution electron microscopy in order to provide greater insights into the structure and function of biological materials, such as biofilms and biological aggregates. Working with microbial mats, de los Ríos et al. (2004) used a combination of optical and electron microscopy to image their vertical stratification, identify characteristic cyanobacteria within these strata, study the porosity of the sample, and look at bio-accumulation and bio-alteration products within the mat, such as silica and carbonates. Wrede et al. (2008) performed correlative microscopy on the same sample, using a multi-purpose hydrophilic embedding resin to cut an ultrathin section for TEM and a semi-thin section for confocal laser scanning microscopy (CLSM). They noted that good antigenic preservation meant that samples could be stained post-section.

In order to develop the understanding of the microstructure of cryoconite initiated by Langford et al. (2010), electron microscopy, in combination with CLSM, is used to probe the ultrastructure of cryoconite aggregates from one glacier in alpine Austria and three glaciers in Svalbard: Vestfonna in western Nordaustlandet, Midtre Lovénbreen in the Kongsfjord region of western Spitsbergen, and Longyearbreen in the Isfjord region of western Spitsbergen. In particular, this research addresses cell–mineral and EPS–

mineral interaction within cryoconite granules in an attempt to ascertain preferential interactions for the development of stable aggregates. It is hypothesised that ultrastructural analyses of cryoconite will reveal that EPS is a key constituent of the groundmass of cryoconite, acting as the principal adhesive force within the aggregate.

4.3 Methodological approach

Sampling was conducted in bulk from randomly chosen individual cryoconite holes on each glacier surface. All cryoconite samples were collected from their respective glacier surfaces using pre-sterilised implements rinsed with supraglacial water, placed into polyethylene centrifuge tubes, along with supraglacial water, and frozen for transit back to the UK. In the laboratory, each sample was defrosted in a refridgerator before being processed for microscopy as detailed below.

4.3.1 ESEM and low-vacuum scanning electron microscopy

Whole cryoconite granules and cryo-sectioned granules were examined using ESEM and low-vacuum scanning electron microscopy (LV-SEM). Samples were prepared according to Treatment 4 of Priester et al. (2007). Briefly, individual granules were pre-fixed with 0.075% ruthenium red, 2.5% glutaraldehyde and 50 mM L-lysine for 30 minutes. Fixation was for 2 hours in 0.075% ruthenium red and 2.5% glutaraldehyde. The granules were then washed three times in 0.1 M HEPES buffer and post-fixed for 2 hours in 2% osmium tetroxide, before being washed again, as above, for 10 minutes. Some granules were then sectioned to a thickness of 60 µm using a cryostat, as described in Langford et al. (2010). These granules and sections were then deposited onto double-sided carbon tape and attached to a standard EM stub. Samples for ESEM were imaged in secondary electron mode on an FEI Quanta™ 200 3D at 20 kV, with a spot size of 3.0, at 1.4 Torr and at a working distance of 6.1 mm. Samples for LV-SEM were imaged on an FEI Nova™ NanoSEM in low-vacuum mode, using a Helix detector at 10 kV, with a spot size of 3.5 and at a working distance of 5.2 mm.

4.3.2 Correlative TEM and CLSM

Whole cryoconite granules were subjected to two different preparation techniques. For the first technique, a suspension of small granules was drawn up into a copper capillary tube and a modified version of the self-pressurised rapid freezing (SPRF) method was followed, as in Leunissen & Yi (2009). Briefly, the Leica copper capillary tube (0.35 mm internal diameter) was sealed at both ends using a pair of needle-nosed pliers and plunged horizontally into liquid nitrogen for 30 seconds. Following this, the tubes were cut in a shallow liquid nitrogen bath using pre-cooled capillary tube cutters and transferred into cryovials, pre-cooled to −80°C (with dry ice) and containing the freeze

substitution medium (96% acetone). The cryovials were freeze substituted in a −80°C freezer for 3 days, before being slowly warmed to -20°C and kept in a standard freezer at −20°C for 2 hours. Working on ice, the capillary tube contents were emptied into pre-cooled microcentrifuge tubes using gentle pipetting and an eyelash probe. Whilst keeping the samples in an ice bath, they were then exchanged with ethanol as follows: 3:1, 2:1, 1:1, 1:2 and 1:3 acetone–ethanol for 30 minutes each; and two changes of 96% ethanol for 1 hour. Resin infiltration with Unicryl resin then proceeded as follows: 2:1 and 1:2 ethanol–resin for 30 minutes each; and overnight in pure resin. The next day, following a final resin change for 2 hours, the samples were polymerised at low temperature (−20°C) with UV light for 3 days. Finally, the polymerised blocks were cut on a Reichert-Jung Ultracut E ultra-microtome, to 50 nm for TEM and 500 nm for optical microscopy, and transferred to copper grids and glass microscope slides. All manipulation was done using a pair of sterilised and appropriately cooled tweezers.

For the second technique, a suspension (10 µL) of small granules was set in a small amount of 2% low-temperature gelling agar (30 µL) at 37°C, as in Stradalova et al. (2008). These gel blocks were picked up using a pair of sterile tweezers and plunged into liquid nitrogen for 30 seconds. They were then placed into pre-cooled freeze substitution medium, as above, and processed in the same way as for the above samples. Ultrathin sections were post-contrasted with aqueous uranyl acetate and analysed on an FEI Tecnai™ G^2 Spirit TEM, at 5–12 kV.

Directly after each ultrathin section was cut, a 1-µm thin section was cut from the same sample block. These sections were not post-contrasted, but instead were stained using the fluorescent nuclear stain DAPI and the fluorescent carbohydrate stain AlexaFluor 488 concanavalin-A, following the protocol detailed by Langford et al. (2010). Consequently, they were analysed on a Zeiss LSM 510 META confocal microscope at 630× magnification, using a multi-photon tunable laser to excite DAPI, a 488 nm Ar laser to excite the AlexaFluor dye, and both a 532 nm and a 633 nm He/Ne laser to excite phototrophic autofluorescence. Images were recorded at 1024 × 1024 pixels. For biovolume calculations, images were processed in ImageJ™. The autofluorescent channel was thresholded using an above and below threshold and, using the resulting binary image, a 5 × 5 µm polygon was moved manually along 12 transects on each image, recording the percentage area covered with red pixels, denoting autofluorescence. These results were averaged to obtain mean biovolume data from the surface of cryoconite aggregates inwards.

4.3.3 Self-pressurised rapid freezing

Whilst this technique has been shown to work with dense cellular suspensions (Leunissen & Yi 2009), both sample heterogeneity and size affected its reproducibility

when applied to cryoconite aggregates. Ultimately, insufficient cryoconite aggregate material could be taken up and effectively rapidly frozen to enable the TEM study of cell–organo–mineral interaction. As such, the data presented below relate to specimens obtained using the second TEM preparation technique (Stradalova et al. 2008).

4.4 Results and Discussion

Whole cryoconite granules showed a dense aggregate structure (Fig. 11a), with evidence for the co-aggregation of smaller microaggregates and the adhesion of larger mineral particles to the aggregate surface. These larger mineral particles were loosely held to the aggregate surface (Fig. 11b) when compared with the smooth, EPS-covered particulate matter below them and in other areas of the granule surface (Fig. 11c). Whilst ESEM (Fig. 11a–c) provided excellent detail of the hydrated granule ultrastructure, including clear imagery of hydrated EPS enmeshing the granule surface, the resolution of cellular features at higher magnifications proved problematic. This may have been due to the density and coverage of the EPS at the surface. Given the heterogeneity of the substrate, EPS development is likely to hinder the visualisation of structural details and biogenic components, as it acts to smooth the surface (Priester et al. 2007). As noted by Joubert and Pillay (2008), this is a particular problem when attempting to visualise smaller bacteria, as an accumulation of EPS can turn a sandy biofilm into an undulating film. Conversely, working with a drier sample and LV-SEM with Helix detection, greater resolution and contrast was achievable at higher magnifications, enabling various biogenic components to be visualised (Fig. 11d–i). Figures 11d and 11e, cryoconite from Longyearbreen, highlight a surface biofilm consisting principally of filamentous microorganisms. Their size (c. 0.7–1 μm in width) and association with copious EPS suggest that these are filamentous cyanobacteria. Furthermore, lambda-scanning CLSM of the thin section pictured in Figure 12 (data not shown) and by Langford et al. (2010) indicate an autofluorescent peak at c. 645–650 nm associated with these filaments, representing the presence of cyanobacterial phycocyanin. This surface biofilm feature is akin to the ‘slime nets’ reported by Esch and Nehrkorn (1988) as being associated with attachment of planktonic bacteria to a biofilm surface, albeit on a slightly larger scale. The EPS associated with these cyanobacteria displays a striated, sponge-like form (Fig. 11e; marked with a *). In this way, it is similar to alginic acid structures as visualised by Andrade et al. (2004). The effect of the development of surface biofilms on cryoconite granules is unclear, although they do function to protect sediment particles from erosion (e.g. Paterson 1997). Cyanobacterial and algal soil surface crusts in other environments have been

found to increase water repellency initially, before extensive EPS production decreased this repellency, whilst increasing pore-clogging (Fischer et al. 2010).

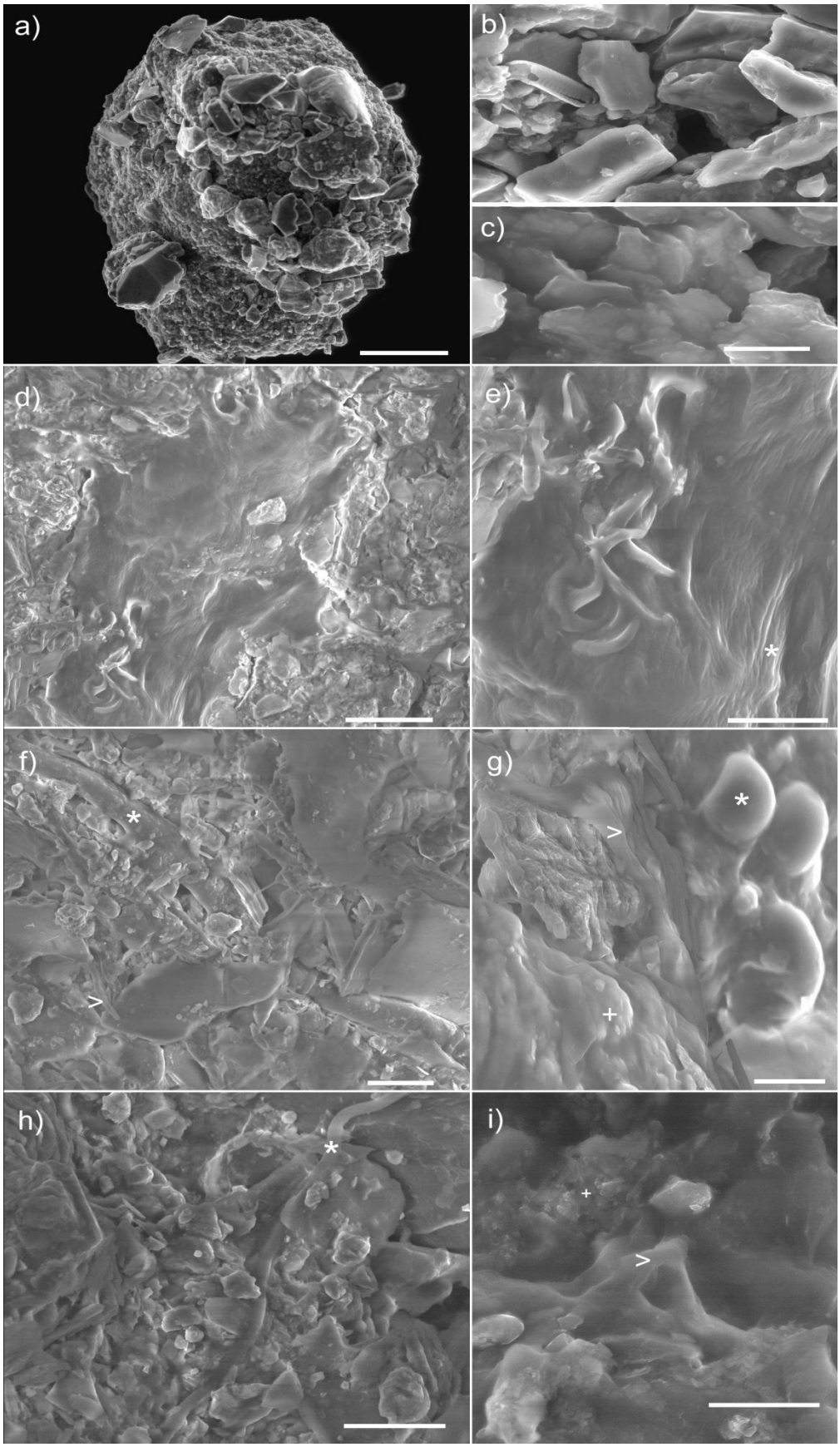

Figure 11: (a) Electron micrograph of a whole cryoconite granule, scale bar = 100 µm; (b) & (c) Details of particulate and EPS-rich portions of the granule surface, scale bar = 5 µm; (d) & (e) A surface biofilm on Longyearbreen cryoconite, scale bars = 20 µm & 5 µm; (f) & (g) Autotrophic communities present within Midtre Lóvenbreen cryoconite, scale bars = 10 µm & 2 µm; (h) & (i) Granule structure and cell–EPS–mineral interaction within Vestfonna cryoconite, scale bars = 20 µm & 5 µm.

Figures 11f and 11g, cryoconite from Midtre Lóvenbreen, highlight a complex community at the granule surface. In Figure 11f, a large filament (annotated with a *) is visible, which, given its size (c. 5 µm in width and > 100 µm in length), lack of observable surface banding and debris-encrusted surface, is most likely to be a fungal hypha. In addition, several smaller, filamentous cyanobacteria (marked with a $^{>}$) are also present. The fungal hypha has clay-sized to colloidal particles attached to its surface and EPS can be seen to enmesh it within an organo-mineral matrix. In Figure 11g, a cluster of unicellular cyanobacteria (annotated with a *) and associated EPS are visible. As is often the case, these unicellular cyanobacteria are present as a small cluster and are associated with filamentous cyanobacteria (marked with a *). A biofilm containing c. 0.3 µm bacterial cells (annotated with a $^{+}$) is also visible. Figures 11h and 11i, cryoconite from Vestfonna, also highlight filamentous cyanobacteria (*), EPS ($^{>}$) and associated clusters of heterotrophic bacteria ($^{+}$). These images serve to highlight the diverse microenvironments created by photoautotrophs on and within cryoconite aggregates, where physicochemical variability can drive proliferation of a diverse range of species (Decho 2000). Also highlighted is the structured association of microorganisms, an effective survival strategy in extreme environments (de los Ríos et al. 2003, 2004).

Thin sections, analysed by CLSM, highlight the surface and near-surface microstructure (Fig. 12a). Unfortunately, as is often the case when preparing heterogeneous sediment samples for microscopic analysis, the presence of larger mineral particles within the granule core caused fracture and ejection of parts of each thin section when cut on the microtome. However, as emphasised in the inset of Figure 12a (red = autofluorescence, blue = DAPI-stained bacteria, green = polysaccharides), the outermost portion of the cryoconite granule often exhibits a comparatively greater concentration of biota (Takeuchi et al. 2001b, Hodson et al. 2010, Langford et al. 2010), particularly photoautotrophic microorganisms, and is useful in understanding how cell–mineral interaction shapes these granules.

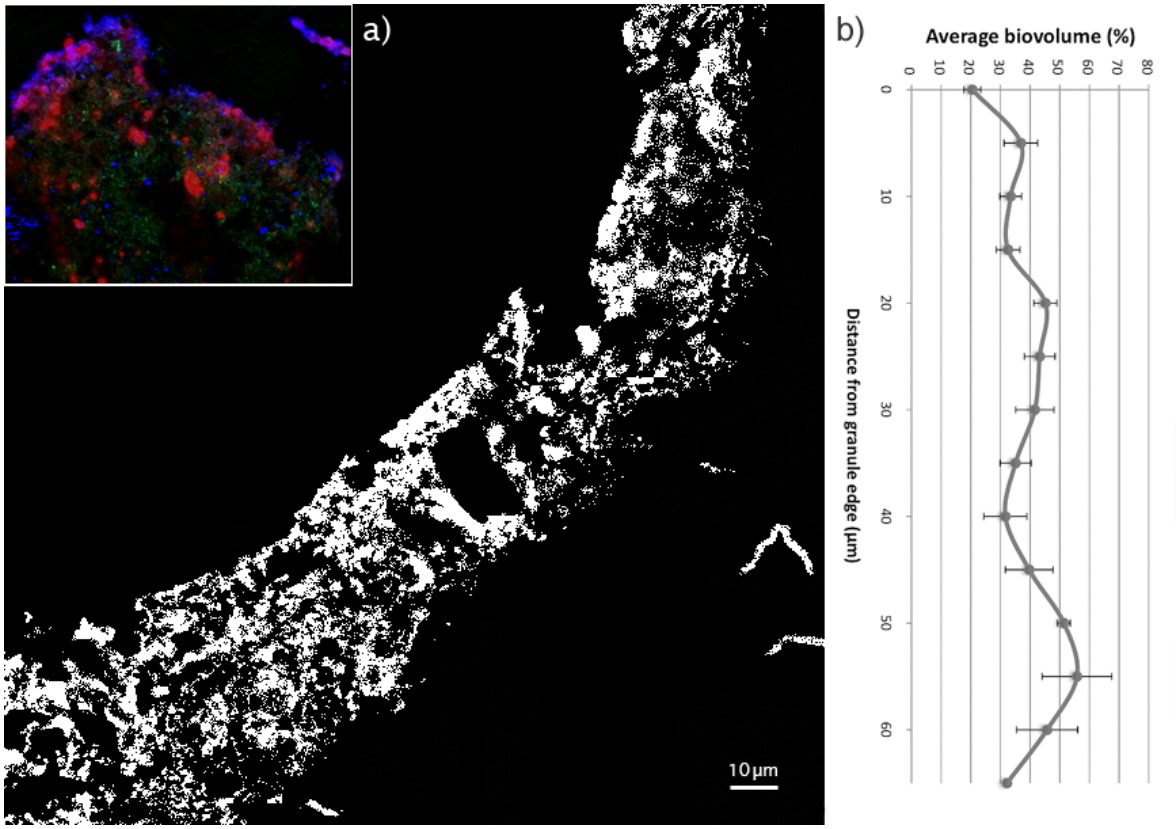

Figure 12: (a) Binary image, post-threshold, of the autofluorescence within the outer layers of a typical cryoconite granule, taken at 630× magnification; inset = low magnification cryosection, taken at 100× magnification, detailing the spatial distribution of photoautotrophs (red), DAPI-stained bacteria (blue) and EPS (green) within a typical cryoconite granule. (b) Graph indicating variance in average biovolume (%) with distance from granule edge (µm) for the outer surface layer in Figure 2a; error bars represent standard error values.

Figure 12a shows a binary image of the autofluorescent surface layer of a cryoconite granule from an Alpine glacier. As has been noted previously (Stibal et al. 2006, Langford et al. 2010, Segawa & Takeuchi 2010), this dense surface network, extending to c. 70 µm depth in places, contains principally filamentous cyanobacteria (generally from the order Oscillatoriales) and some unicellular cyanobacteria (e.g. from the order Chroococcales) and algal cells, as well as high polysaccharide concentrations due to the presence of copious EPS. From this binary image, we can study the variability in average biovolume (%) with distance from the granule surface (Fig. 12b). It can be seen that, in general, the biovolume increases towards the interior of this surface layer. This is likely due to the production of excess EPS at the very outer surface in order to capture mineral particles that would otherwise be swept away by water or wind (Golubic et al. 2000) and to protect the cells from UV exposure. Within this general trend, three peaks in the biovolume can be seen to occur. This may indicate a laminar development of this surface layer, showing similarities to the findings of Takeuchi et al. (2010), and may either be the result of different cyanobacterial species occupying slightly different

photo-physical and/or physico-chemical niches, or be evidence for annual laminations. It has been noted that radially spreading cyanobacteria can initiate domal sedimentary structures with concentric internal textures (Golubic et al. 2000).

To enable high-resolution imaging of ultrastructural details without the ubiquitous presence of EPS and such analytical issues as edge effects affecting resolution, TEM proved to be a useful tool. Ultrathin sections, analysed by TEM, again show a dense organo-mineral structure (Fig. 13a). Between small mineral particles, fibrillar EPS can be clearly visualised, binding these particles together (Fig. 13b). These fibrils are <10 nm in diameter and form a dense cloud that encapsulates and adheres to mineral grains. These fibrillar networks have been found in other natural aggregates, such as marine snow (Leppard 1992, Heissenberger et al. 1996), and are highly likely to be acidic polysaccharides, e.g. alginic acid (Lünsdorf et al. 2000, Andrade et al. 2004). Research indicates that these EPS fibrils connect predominantly via cationic bridging (Theng 1982, van Boekel 1992, Decho & Herndl 1995, Leppard et al. 1996, Sanin & Vesilind 1996). Also present within the ultrathin sections is a globular EPS (e.g. Toda et al. 1987), which can be seen on the left-hand side of Figures 13c and 13d. Also in Figure 13c (annotated with a *), and in greater detail in Figure 13d, is a single bacterial cell in contact with an elongate mineral grain. Figures 13e and 13f detail a photoautotrophic community within the outer layer of an Alpine cryoconite aggregate (Fig. 12a). Figure 13e shows a transverse section through a cluster of filamentous cyanobacteria, with some empty sheaths evident (highlighted with a $^{+}$), as well as the presence of nanometre-sized mineral particles, most likely clays and/or aluminium/iron (oxy)hydroxides. At a higher degree of magnification, the capsular sheath, composed principally of extracellular polysaccharides, is clearly visible (Fig. 13f). The hydrated, amorphous EPS in this picture shows few gaps. Around the edges of the EPS-bound flocs, further detail of these nanometre-sized mineral particles (annotated with a $^{<}$) indicates that they are almost a monolayer, surrounding the edge of a pore space. Clay–polysaccharide interaction at the surface of microorganisms has been documented by a number of authors (e.g. Kilbertus et al. 1979, Kilbertus 1980, Foster 1981, Chenu 1993), with Lünsdorf et al. (2000) noting the presence of what they term ‘clay hutches’ in a soil biofilm: phyllosilicate and iron oxide mineral particles forming a layer around one or more bacterial cells, held in place by EPS. Clay–polysaccharide interaction has been found to increase water retention upon desiccation (Chenu 1993) and, as such, is considered likely to be an important aspect of microbial protection against psychrophilic freeze–thaw conditions. In addition, given that many polar photoautotrophs are low light adapted, consequential protection from potentially damaging levels of solar insolation is an added advantage.

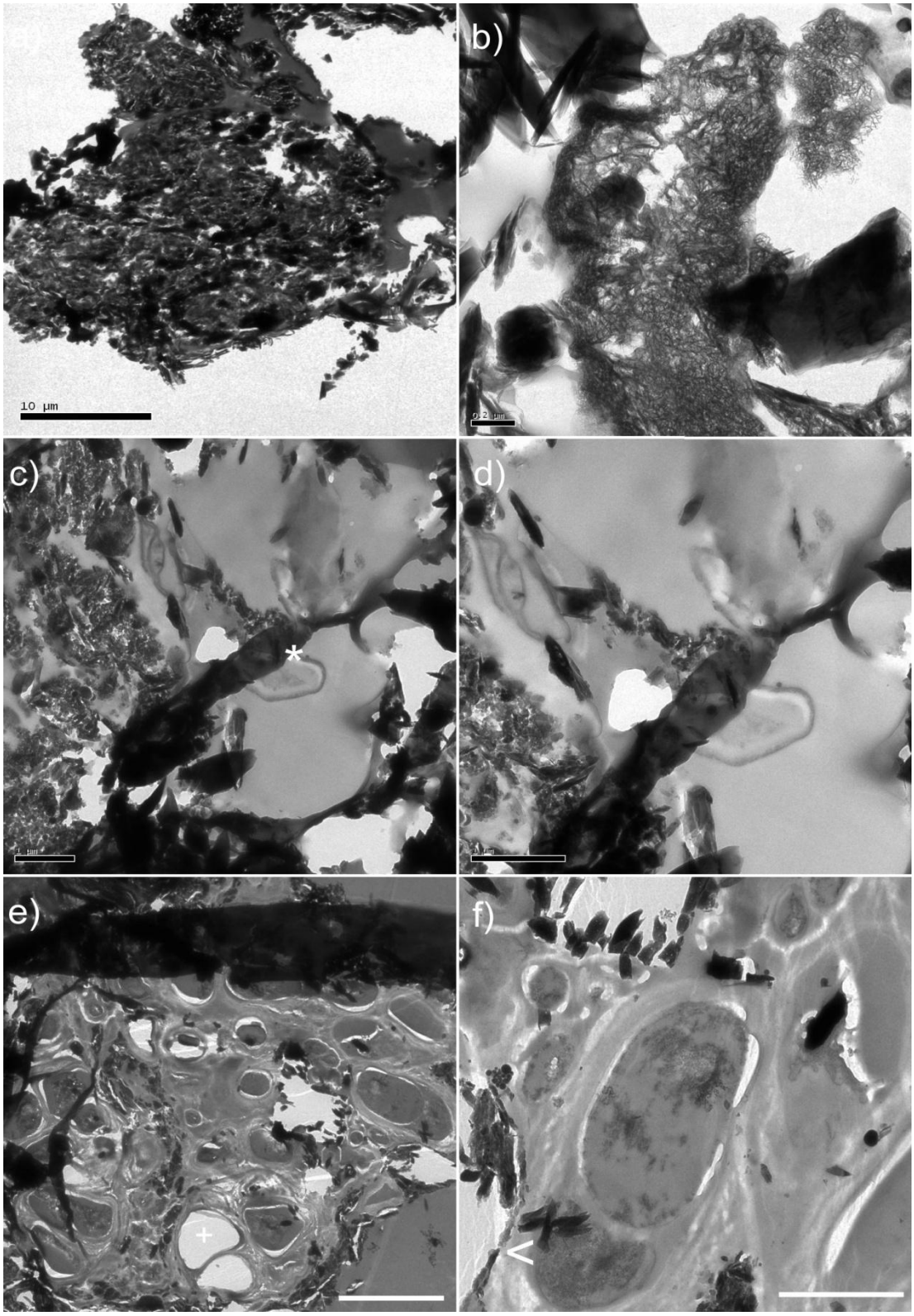

Figure 13: (a) Dense organo-mineral microaggregate, scale bar = 10 µm; (b) Ultrastructural detail showing EPS binding clay-sized mineral particles, scale bar = 0.2 µm; (c) & (d) Cell–EPS–mineral interaction within cryoconite material, scale bar = 1 µm; (e) & (f) Photoautotrophic community within cryoconite material, detailing cyanobacteria and empty sheath material, scale bars = 2 µm & 1 µm.

Whilst the particle size distribution is, on the whole, relatively random and disordered, a greater number of small, clay-sized particles are often seen to be associated directly with flocs of photoautotrophic microorganisms, an observation often noted (e.g. Tiessen & Stewart 1988). This both suggests their affinity for one another, as well as suggesting that photoautotrophic bloom activity could act as a sieve for Aeolian fines, whether within a melting snowpack or within a glacial weathering crust. Even small amounts of EPS can reduce hydraulic conductivity by several orders of magnitude (Or et al. 2007). The presence of filamentous microorganisms throughout the cryoconite granules studied, principally cyanobacteria and often in flocs, reinforces their importance as stabilisers of both the granule as a whole and its surface, similarly noted by Paterson et al. (2008) and Zheng et al. (2011). Interactions between the capsular sheath and abiotic particulates appear to be particularly important. In similar environments, nearly half of all bacteria were found to exhibit a capsular sheath larger than their cell diameter, with this capsular EPS mediating associations between microorganisms and abiotic particulates (Heissenberger et al. 1996). Combined with the ubiquitous presence of both globular and fibrillar EPS varieties, these polysaccharides, glycoproteins and lipopolysaccharides act as anchors for mineral particles and organic matter. Paterson et al. (2008) find that light deprivation significantly encourages EPS production in cyanobacteria-rich sediments. As such, albedo-induced melt of cryoconite debris, forming cryoconite holes on the glacier surface, as well as accumulation of abiotic particulates on the surface of microbial capsules, may induce further production of EPS.

Cyanobacteria are known to actively participate in the production of sedimentary structures via growth, movement and behavioural response (Golubic et al. 2000). In the case of cryoconite granules, organo-mineral interactions within a matrix of filamentous cyanobacteria were shown, via electron microscopy, to bind particulate matter and create a hydrated structure, less open and more sedimentary than similar microbial mats (de los Ríos et al. 2004). This matrix showed heterogeneity and the presence of copious and varied EPS, within which diverse microenvironments are suggested to exist, created by physicochemical variability and autotrophic activity. The interaction between EPS and mineral surfaces is well documented, as previously noted, and thus allows for a conceptual diagram to be created for cryoconite (Fig. 14), based upon electron microscopy findings and scientific literature.

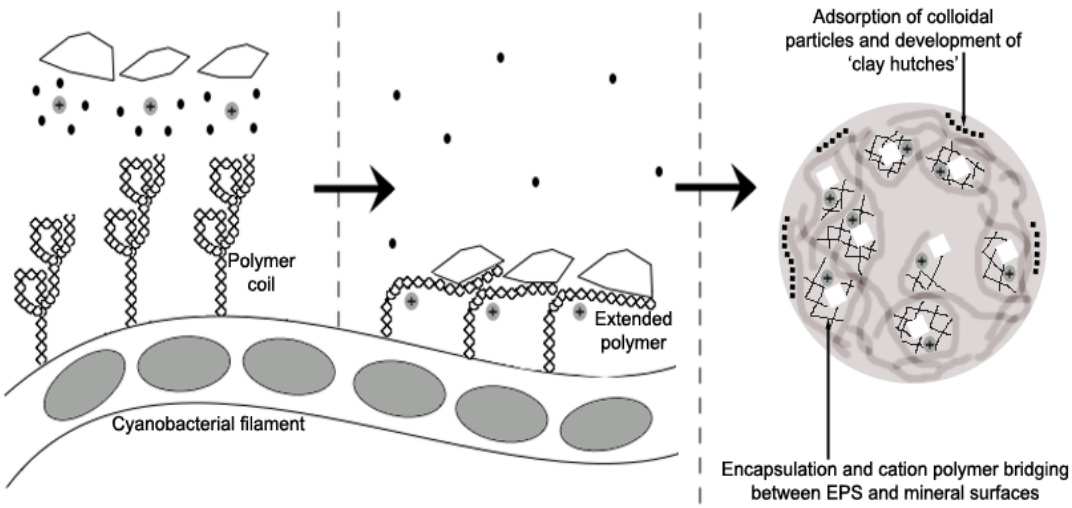

Figure 14: Conceptual diagram of cell–EPS–mineral interaction within cryoconite granules, detailing cation polymer bridging between polysaccharide chains and mineral particles and the development of 'clay hutches'; modified from Theng (1982) and Sanin & Vesilind (1996).

The polysaccharides within EPS can be uncharged, positively charged or negatively charged. As such, they can interact with mineral surfaces through both electrostatic attraction and cation polymer bridging (Theng 1982). With the enthalpy change of adsorption being typically low, and divalent cations being known to maintain polymer tertiary structure and promote interaction, interaction between a large number of functional groups and the mineral surface allows whole segments of polymer to be adsorbed (Theng 1982, Sanin & Vesilind 1996). Though weak individually, these interactions are strong en masse, leading to resistance to desorption on dilution (Theng 1982). These interactions are suggested to be of primary importance to the development of cryoconite granules.

4.5 Conclusions

Electron microscopy, particularly a combination of either ESEM or LV-SEM and TEM, allows for good ultrastructural characterisation of cryoconite aggregates if care in specimen preparation is taken. When combined with optical microscopy, this complementary suite allows structure to be deduced and spatial relationships to be studied. This study used the above techniques to provide the highest resolution imagery of cryoconite ultrastructure yet achieved. In doing so, we have shown that the capsular EPS of photoautotrophs significantly attracts sub-micron-sized particulate matter, and have visualised the dense organo-mineral groundmass, dominated by polysaccharidic EPS, that has only recently been suggested to exist. Cryoconite can be seen to have a

dense aggregate structure with significant EPS enmeshing and surface biofilms/layers showing evidence for laminations. Various EPS types have been deduced visually, with cell–EPS–mineral interaction contributing to aggregate shape and controlling granule hydraulics. Diverse microenvironments are visible, with clay–polysaccharide interaction, in a similar vein to ‘clay hutches’, showing potential significance for the biogeochemistry of these aggregates.

4.6 Acknowledgements

H. Langford acknowledges Chris Hill at the Electron Microscopy Unit for assistance in preparing and imaging the TEM specimens, and both A. J. Hodson and B. Sattler for provision of samples. H. Langford also acknowledges the Confocal Imaging Facility at the Kroto Research Institute for the necessary analytical time. A. J. Hodson acknowledges the RGS, NGS and Gilchrist Education Trust awards, as well as B. Sattler’s award, GLAC.LIFE from the Alpine Research Station Obergurgl, which facilitated Arctic and Alpine field trips and necessary sample collection.

CHAPTER FIVE: GEOSPATIAL INVESTIGATION OF PHOTOSYNTHETIC PIGMENTS AND CARBOHYDRATES WITHIN CRYOCONITE ON LONGYEARBREEN GLACIER, SVALBARD

Prepared for submission to Polar Biology: Langford, H., S. Banwart & A. Hodson, 2012. Geospatial investigation of photosynthetic pigments and carbohydrates within cryoconite on Longyearbreen glacier, Svalbard.

5.1 Abstract

A cryoconite granule is a spherical aggregation of biota and abiotic particles. Recently, microstructural studies have revealed that photosynthetic microorganisms and extracellular polymeric substances (EPS) are omnipresent within cryoconite and have suggested their importance as biological 'forming factors'. To assess these forming factors, and their biological control over aggregate size and stability, across a typical Arctic valley glacier surface, a suite of rapid, spectrophotometric, microplate methods were utilised. Subsequent geospatial mapping of these data revealed distinct patterns. Labile carbohydrates were found to increase up-glacier, suggestive of EPS production for cryoprotection and nutrient assimilation. Conversely, pigment concentrations were found to increase down-glacier, with the exception of a zone of hydraulic erosion, suggestive of a general reduction in physical disturbance and of the build-up of photosynthetic pigments and less labile cyanobacterial sheath material. Aggregate size was found to increase towards the glacier edges, linked to the input of particulate matter from the valley sides, and to broadly increase down-glacier, in the same way as pigment concentrations. Statistical analyses of transect data revealed that the photoautotrophic count and carbohydrate–chlorophyll ratio of the cryoconite sampled could explain 83% of the measured variation in aggregate size and stability. Considering solely aggregate size, the number and length of photoautrophic filaments could explain 92% of the variation in this parameter. These findings demonstrate the two-dimensional distribution of key biological controls upon cryoconite aggregation for the first time, and highlight the importance of filamentous cyanobacteria and EPS production to the development of stable cryoconite granules.

5.2 Introduction

Cryoconite granules are biologically active aggregations of microorganisms, mineral particles and organic matter. Located on the surface of glaciers and ice sheets, cryoconite material harbours a complex and variable microbial community (Margesin et al. 2002, Hodson et al. 2008), sourced largely from aeolian input (Pearce et al. 2009). The physical and chemical characteristics of cryoconite material are also variable, both between granules and between cryoconite holes, the quasi-cylindrical holes formed as they preferentially melt into the ice (Fountain et al. 2008). Microstructural evaluation of cryoconite granules from across the Arctic reveals this variability well, indicating that the location and quantity of photosynthetic microorganisms, heterotrophic microorganisms and labile organic matter is highly variable between glaciers, resulting in differing aggregate size and stability (Langford et al. 2010). Langford et al. (2010) proposed a hypothesis for the formation of cryoconite granules, which highlighted the importance of photosynthetic microorganisms and labile organic matter (polysaccharides) in the development of stable cryoconite granules. Indeed, Takeuchi et al. (2010) showed that environments rich in filamentous cyanobacteria promote the development of highly stable, large granules with visible quasi-annual growth layers.

The study of the concentration and composition of both carbohydrate and pigment concentrations within cryoconite has received limited research attention (e.g. Stibal et al. 2008a, 2010). However, within the fields of soil science and microbial ecology, the quantity of related research has been far greater. Carbohydrates, along with other low molecular weight organic molecules, play an important role in nutrient cycling (Fischer et al. 2007) and are instrumental in the formation and stabilisation of soil microaggregates (Cheshire et al. 1979, Oades 1984, Puget et al. 1999). Indeed, it has been shown that there is a strong correlation between labile carbohydrates and aggregate stability in agricultural soils (Tisdall 1994; Puget et al. 1999). In certain sediments, a significant proportion of carbohydrates are microbially-sourced extracellular polymeric substances (EPS). EPS is a labile and absorptive matrix, the production and composition of which depends upon the nutrient status and growth phase of the biota involved (Decho 1990, Decho & Lopez 1993). Cyanobacterial EPS has been found to be particularly complex (De Phillipis & Vincenzini 1998, Pereira et al. 2009). In low nutrient environments, EPS production can, perhaps surprisingly, be stimulated (Myklestad & Haug 1972), particularly in phototrophic microorganisms (Ortega-Calvo & Stal 1994). Furthermore, EPS has been found to actively promote flocculation and aggregation (Bar-Or & Shilo 1988, Zulpa de Caire et al. 1997). Considering these factors, it is important to identify glacier-wide variability in

carbohydrate production, as carbohydrates may control the formation of aggregates upon glaciers and ice sheets (e.g. Hodson et al. 2010, Stibal et al. 2010).

When carbohydrate contents and pigment contents (as a proxy for the number of photosynthetic microorganisms present) co-exist in substantial amounts, they are found to significantly increase the threshold of shear stress required for sediment erosion by flowing water (Underwood & Paterson 1993, Sutherland et al. 1998a). Pigment contents, principally chlorophyll *a*, have long been utilised as biomarkers for phototrophic activity in soils and sediments (e.g. Swain 1985, Downing & Rath 1988). Pigment analyses have been performed in a variety of ways, using: HPLC (Barranguet et al. 1997), Raman spectroscopy (Edwards et al. 2004), fluorescence spectroscopy (Gregor & Marsalek 2005) and spectrophotometry (Pinckney et al. 1994). The usefulness of chlorophyll *a* comes from its prevalence amongst photosynthetic microorganisms, from algae and diatoms to cyanobacteria. Whilst chlorophyll *a* is a good general biomarker, the importance of additional biomarkers, in order to measure the abundance and distribution of particular photoautotrophs, should not be underestimated (Stewart & Farmer 1984). Photosynthetic microorganisms have been found to be present in a range of glacial locations, with cyanobacteria in particular producing a suite of photosynthetic pigments, for both protection and light-harvesting, some of which have motility within the cell (Vincent 2007). Those motile pigments are termed phycobiliproteins (Wildman & Bowen 1974) – a group of water-soluble pigments chiefly comprising phycoerythrin, phycocyanin and allophycocyanin. The usefulness of pigment biomarker analyses within glacial studies has been highlighted recently (Stibal et al. 2010; Morato et al. 2011), although research often fails to consider phycobiliproteins as biomarkers.

Recent research into the biogeochemistry of cryoconite has focused on the concentration and composition of organic carbon (Stibal et al. 2010, Xu et al. 2010), and the concentration of chlorophyll *a* (Foreman et al. 2007). Phycobiliprotein concentrations have been under-studied, with only Sattler et al. (2010) exploring this avenue, utilising laser-induced fluorescence imagery (LIFE) to study cyanobacterial autofluorescence within ice core debris. Whilst this research has highlighted the sparse application of some techniques such as ion chromatography and nuclear magnetic resonance (NMR) spectroscopy, research has focused on isolated samples or transects. Given the lack of two-dimensional coverage, little can be understood regarding the supraglacial biogeography of these key environmental biomarkers. Furthermore, whilst research has provided good estimates of photosynthesis within cryoconite (e.g. Säwström et al. 2002, Anesio et al. 2009, Hodson et al. 2010, Telling et al. 2010), more reliable values for non-degraded chlorophyll concentrations could enable photosynthesis to be normalised for chlorophyll. This would allow us to gain a greater

insight into the efficiency of photosynthesis. The objective of this paper is therefore to investigate the geospatial variations in key biochemical aggregate-forming factors across an entire ablation zone. It is hypothesised that spatial variability in these aggregate-forming factors will be seen, driving consequent variability in both aggregate size and stability. This research employs a spectrophotometric approach, using 96-well plates and performing a variety of assays, to allow rapid, glacier-wide determination of specific biochemical parameters – in this case carbohydrate, chlorophyll *a* and phycobiliprotein concentrations.

5.3 Field site and methods

5.3.1 Field site

Fieldwork was undertaken on Longyearbreen glacier, Svalbard (78° 10' 49" N, 15° 30' 21" E), in July 2010. The glacier is almost entirely at melting point, except for a cold surface layer that exists during summer (Etzelmüller et al. 2000), and has an active and ablating ice surface comprising large amounts of cryoconite debris (Hodson et al. 2010; Irvine-Fynn et al. 2010). It is set within a geology of coal-bearing shales, siltstones and sandstones (Yde et al. 2008). A sample grid was devised, spanning broadly 2 km from the snout of the glacier to the snow line, at time of sampling. The grid had a spacing of 100 m between points and was as regular as possible, given surface topographical constraints (Fig. 15). This grid was pre-programmed into a GPS and followed, with cryoconite debris being sampled from the nearest patch or hole to each point, in order to maintain a regular sampling grid and negate bias.

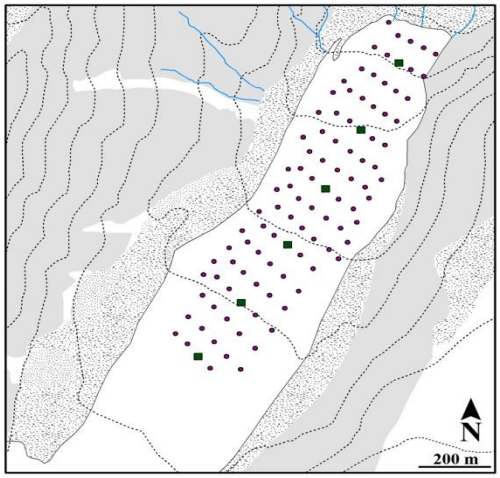

Figure 15: Longyearbreen glacier showing sample grid (circles) and centre-line transect location (squares).

From each grid point, four samples of cryoconite were taken. Samples were collected in 1.8mL cryovials, using pre-sterilised implements, kept frozen and transported back to

the UK on ice, in a cool bag. Within each 1.8 mL cryovial, 0.2 mL of cryoconite granules were collected. In addition, pictures of the cryoconite debris were taken at each grid point, for subsequent granule size analysis. In the laboratory, the frozen cryoconite samples were defrosted and the following procedures conducted.

5.3.2 Carbohydrate extraction and analysis

The phenol–sulphuric acid method for the colorimetric determination of carbohydrate content (Dubois et al. 1951) has proven to be a simple yet reliable method for measuring the amount of neutral sugars present in a solution. Recently, this procedure has been successfully scaled down to microplate format (Masuko et al. 2005).

In order to extract the carbohydrates from the cryoconite, a dilute hot acid extraction was employed. To the cryovials containing 0.2 mL of cryoconite, 1.0 mL of 0.5M sulphuric acid (H_2SO_4) was added. These vials were then briefly vortexed to mix and shaken at 400 rpm, in a water bath at 80°C, for 2 hours. Following this, the vials were centrifuged at maximum speed for 10 minutes and 50 µL of supernatant was removed from each vial and transferred into a well of a 96-well microplate (NB: two microplates were used for each set of assays). Following the protocol of Masuko et al. (2005), 150 µL of concentrated (18M) H_2SO_4 and 30 µL of 5% phenol (aq.) were added to each well in quick succession. The microplate was then incubated on a shallow tray of quartz sand, on a hot plate in a standard laboratory fume cupboard, at 90°C for 5 minutes, before being cooled on an ice pack for 5 minutes. The base of the microplate was dried and the absorbance measured at 490 nm on a Synergy 2 microplate reader. Triplicate readings were taken. Average values were calculated for each sampling point. Blanks of solely ultra-high quality (UHQ) water, and of UHQ water with phenol and sulphuric acid, were run to determine the baseline for absorbance measurements.

5.3.3 Chlorophyll extraction and analysis

Spectrophotometric determination of chlorophyll concentrations, after extraction in a common solvent such as methanol, ethanol or acetone, is commonplace within the life sciences. Several authors note the strengths of using methanol as an extractant, namely the high extraction efficiency and shorter processing time (Holm-Hansen & Riemann 1978; Sartory & Grobbelaar 1984; Thompson et al. 1999). Most recently, Warren (2008) provides a methodology for the rapid extraction of chlorophyll from ground plant tissue using methanol, and subsequent analysis on a microplate reader.

To the cryovials containing 0.2 mL of cryoconite, 1.0 mL of methanol and 0.1 g of 0.5-mm glass bead-beating beads were added. The vials were then shaken in a bead

beater for 1 minute, in order to disrupt the cellular component. Afterwards, the vials were shaken on a vortex mixer (with cryovial attachment) for a further 2 minutes. Following this, the vials were centrifuged at maximum speed for 10 minutes and 200 µL of each supernatant removed to a well of a 96-well microplate. Absorbance spectra were measured, between 300 nm and 750 nm, on a Synergy 2 microplate reader. Triplicate readings were taken. Average values were calculated for each sampling point. Blanks consisting solely of methanol were run to determine the baseline for absorbance measurements.

5.3.4 Phycobiliprotein extraction and analysis

The general approach to phycobiliprotein extraction has been to disrupt the cellular material (physically and/or chemically) and extract the phycobiliproteins into a buffered aqueous solution, such as a Trizma–EDTA solution or phosphate buffer (Stewart & Farmer 1984; Beer & Eshel 1985). Recently, Viskari and Colyer (2003) developed a rapid method for extraction showing high efficiencies. This method was modified for the present study so that it could be completed in microplate format.

Initially, the method of Viskari and Colyer (2003) was followed, modified principally by replacing the nitrogen cavitation step with a bead-beating homogenisation step. The 0.3% asolectin and 3% CHAPS solution was prepared as in Viskari & Colyer (2003). To each cryovial, 0.1 g of 0.5-mm glass bead-beating beads was added, along with 1 mL of asolectin–CHAPS solution. The vials were vortexed and incubated, in the dark, for 2 hours at 37°C. Following this, the vials were subjected to 1 minute of bead beating, to disrupt the cells, and centrifuged for 30 minutes at maximum speed. From each vial, 200 µL of supernatant was pipetted into a well of a 96-well microplate. Absorbance spectra were measured, between 300 nm and 750 nm, on a Synergy 2 microplate reader. Triplicate readings were taken. Fluorescence spectra were measured on a Synergy 2 microplate reader using the 590/35 emission filter.

Extraction of the phycobiliproteins proved to be highly challenging and, using the above method, no significant phycobiliprotein absorbance or fluorescence peaks were detected. A single small peak was detected at abs. 670 nm, which most likely correlates with aqueous chlorophyll *a*, a potential side-effect of using asolectin in the buffer solution (Murata & Sato 1978). Furthermore, epifluorescence microscopy found intact cyanobacterial and algal cells within the cryoconite slurry, similar to Lawrenz et al. (2011). The lack of efficient extraction may be down to a variety of reasons, although it is considered that the complexity of the substrate, copious exopolysaccharides and low cell numbers, when compared to a cultured sample, all play a part. Whilst nitrogen cavitation was not an option open to us, two further disruption methods were trialled:

lysozyme–EDTA extraction and freeze–thaw extraction; combinations of these techniques, as well as with bead beating, were also trialled. Similarly to Lawrenz et al. (2011), it was found that the greatest cell disruption was achieved with a combination of techniques and that an extraction time of up to 96 hours was indeed necessary. As such, each cryovial, containing 0.2 mL of cryoconite and 0.5 mL of phosphate buffer, was subjected to three freeze–thaw cycles in liquid nitrogen for 30 seconds and then on dry ice for 15 minutes, followed by ice for 15 minutes. Following this, 0.5 mL of a 2× lysozyme–EDTA solution was added to achieve a working concentration of 1 mg/mL lysozyme and 50 mM Na-EDTA. The cryovials were then incubated at 37°C for 30 minutes, before being cooled to 4°C. Finally, the cryovials were homogenised in a bead beater for 60 seconds, before being left to stand for 96 hours, with one change of supernatant after 48 hours. Of the resultant 2 mL of supernatant, 200 µL of each sample was added to a 96-well microplate and fluorescence measured on a Synergy 2 microplate reader using the 590/35 emission filter. Blanks of phosphate-buffered UHQ water were also run, to provide a baseline for fluorescence measurements.

5.3.5 Image analysis to determine granule size

The analysis of field-based imagery for Longyearbreen was performed using ImageJ™, based upon the protocol of Irvine-Fynn et al. (2010). Each image was first scaled to determine the pixel resolution. Consequently, images with sufficient contrast between ice and cryoconite were 'thresholded' using an above/below threshold and converted into binary areas. Average diameter was subsequently calculated. For images with low contrast, manual assignment of area was conducted and again average diameter was calculated. For each grid point, a minimum of 50 granules were sized, and mean average values were calculated for each grid point.

5.3.6 Mapping of biochemical parameters and granule size

For each parameter (carbohydrate, chlorophyll *a* and phycobiliprotein concentrations, and granule size), mean average values were taken. The mean standard error values of these raw data, expressed as percentages of their range, were as follows – carbohydrates = 12.16%, chlorophyll *a* = 16.77%, phycobiliproteins = 20.00%, and granule size = 4.04%. Concentration values for total carbohydrates and chlorophyll a were determined using standard curves of concentration versus absorbance for two standards: mannose and chlorophyll *a* from spinach (Sigma-Aldrich). Phycobiliproteins were mapped as relative abundance (ratio).

Mean concentration data and mean granule size data were plotted as contour maps, using ESRI ArcGIS. GPS co-ordinates for each grid point were converted from decimal

degrees to UTM co-ordinates and a base map image was geo-referenced using 20 GPS data points and projected using the WGS84 Zone 33 co-ordinate system and a spline transformation. The sampling grid was uploaded as x,y point data. Each dataset was uploaded as x,y,z point data and interpolated using the geostatistical wizard function. Various interpolation routines were investigated and multiquadratic was chosen, using nine neighbours, as it produced the lowest root mean square (RMS) errors. The RMS errors (and normalised RMS errors) for each dataset were as follows – carbohydrates = 0.057 (1.77%), chlorophyll *a* = 0.021 (17.88%), phycobiliproteins = 0.012 (15.19%), and granule size = 154.4 (9.72%). The spatial data outputs from the geostatistical wizard function were then transformed to raster layers and contour plots drawn using the spatial analyst toolset. Following this, the contour plot was limited to the extent of the sampling grid by using the clip function based upon a manually drawn polygon.

5.3.7 Environmental predictors for granule size and stability

Using six of the grid points (marked with squares on Fig. 15), a centre-line transect was devised. Average carbohydrate, chlorophyll *a* and phycobiliprotein data were taken from the above spatial mapping dataset and plotted alongside further biochemical data – namely cryoconite organic matter content, granule size and stability, and both the number and characteristics of photoautotrophs within samples from these six data points. In the laboratory, the organic matter content of the cryoconite debris was measured, in triplicate, using a Shimadzu Total Organic Carbon (TOC) analyser following an overnight 0.1M NaOH extraction at a 1:5 solid–liquid ratio. Aggregate size and stability were measured photographically using image analysis. For each sample, a 100-mg sub-sample was imaged and average granule diameter was measured using ImageJ™, as detailed previously. Following this, each sample was agitated by vortexing for 30 seconds and re-imaged, with average granule diameter once again measured. Considering the fraction > 250 µm to be the stable macroaggregate fraction (Tisdall & Oades 1982; Puget et al. 1999), the percentage of aggregates > 250 µm after agitation versus before agitation was calculated and used as a simple indicator of aggregate stability. Photoautotroph total counts were performed on 10 mg of disaggregated cryoconite, at 400× magnification, on a Zeiss Axioplan 2 epifluorescence microscope using autofluorescent emission and a Cy5 filter cube; images were recorded with a colour CCD camera. The numbers of filamentous and unicellular photoautotrophs were counted separately across five fields of view, in triplicate, for each of the six samples. In addition, within ImageJ™, fifty measurements of filament length were made from the above images for each sample. From these data, average filament length values for each sample could then be multiplied by the filamentous photoautotroph count to obtain an estimate of filament length per gram of cryoconite.

Using this small dataset, multivariate linear regression models were run in SPSS v. 19, using granule size and granule stability as dependent variables, and all aforementioned biochemical parameters as predictors. Multivariate linear regression, using a single dependent variable, was conducted in both stepwise and backwards formats, using $P < 0.05$ as the selector for the stepwise format. Multivariate linear regression, using two dependent variables, was run as a full factorial model, with Type III sums of squares.

5.4 Results

5.4.1 Spatial mapping of biogeochemical parameters

Figure 16 shows how mean carbohydrate concentrations varied across the ablation zone of Longyearbreen. The general trend shows a greater concentration of carbohydrates up-glacier, near to the snow line (at the time of sampling). Up to 3.50 µg/mL of monosaccharide carbohydrates were detected in this region closest to the snow line.

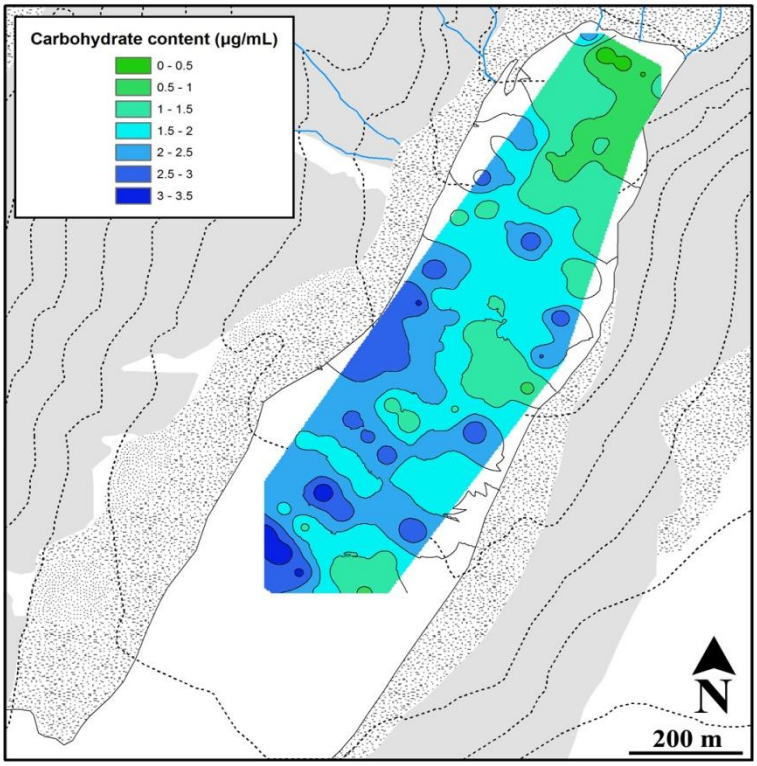

Figure 16: Variation in carbohydrate concentration (µg/mL) across Longyearbreen glacier ablation zone.

Using a mean cryoconite density value of 1.49 g/mL (A.J. Hodson, unpublished data), on a dry weight basis, this value equates to approximately 5.215 µg/g. In addition, some 'hotspots' of high carbohydrate concentration were evident, particularly towards the northwestern edge of the glacier. Finally, a central region closest to the glacier terminus showed particularly low carbohydrate concentrations, with values dipping below 0.5 µg/mL.

The variability in mean chlorophyll *a* concentrations across the glacier surface is contour-plotted in figure 17. The general trend, clearer in this case, indicates that greater concentrations of chlorophyll *a* were present nearer to the glacier terminus. A maximum chlorophyll *a* concentration of 0.1825 µg/mL (0.273 µg/g) was found at the edge of the glacier terminus. Again, there were slightly elevated concentrations along the glacier edges, particularly the northwestern edge. Additionally, a greater level of localised variability is visible on Figure 3 than was measured for mean carbohydrate content (Fig. 2). Figure 18 shows the carbohydrate–Chlorophyll ratio (CCR) as measured across the glacier surface. This figure serves to highlight the significant excess of carbohydrates up-glacier, when compared with the glacier terminus. At the up-glacier edge of the ablation zone, at the time of sampling, up to 40× more carbohydrates were present than chlorophyll *a*.

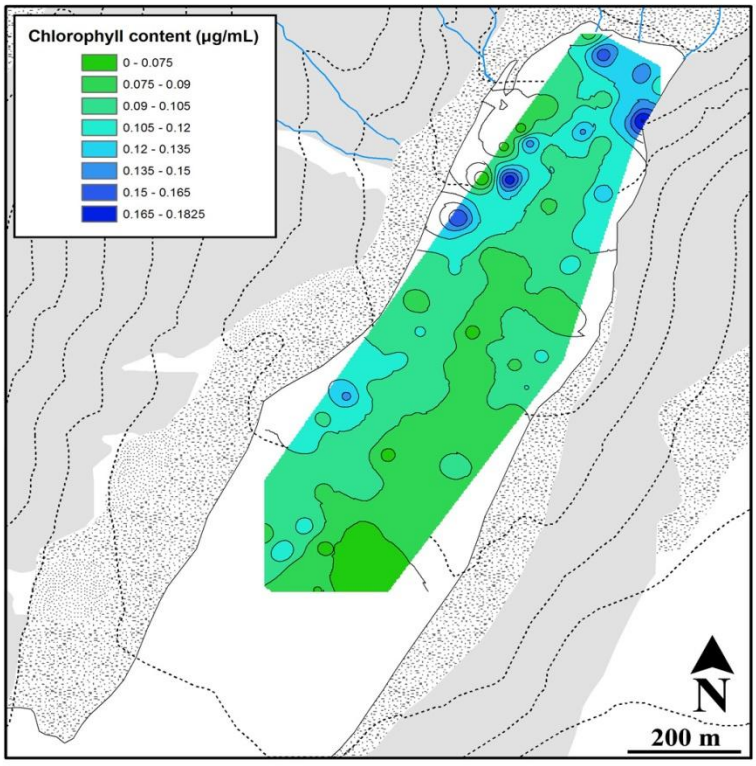

Figure 17: Variation in chlorophyll a concentration (µg/mL) across Longyearbreen glacier ablation zone.

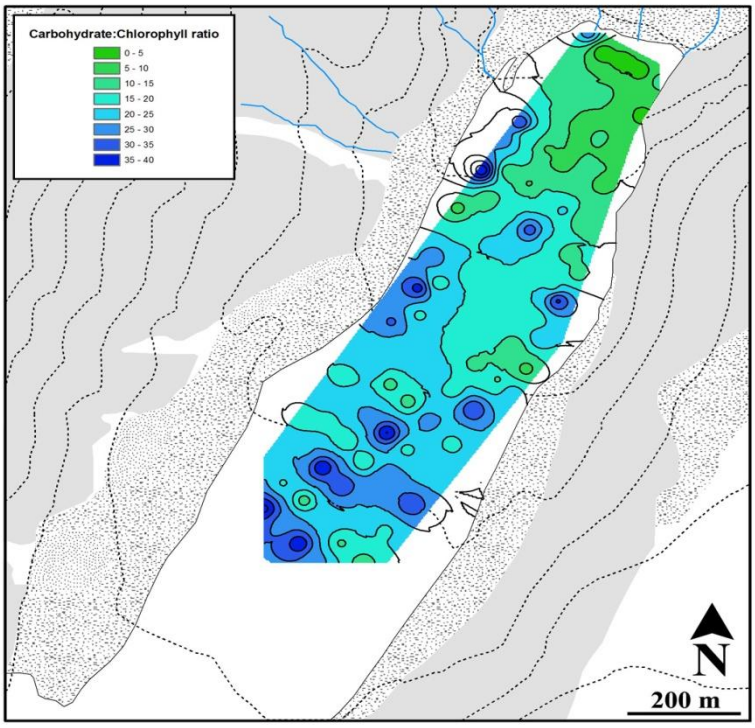

Figure 18: Variation in the carbohydrate/chlorophyll ratio (%) across Longyearbreen glacier ablation zone.

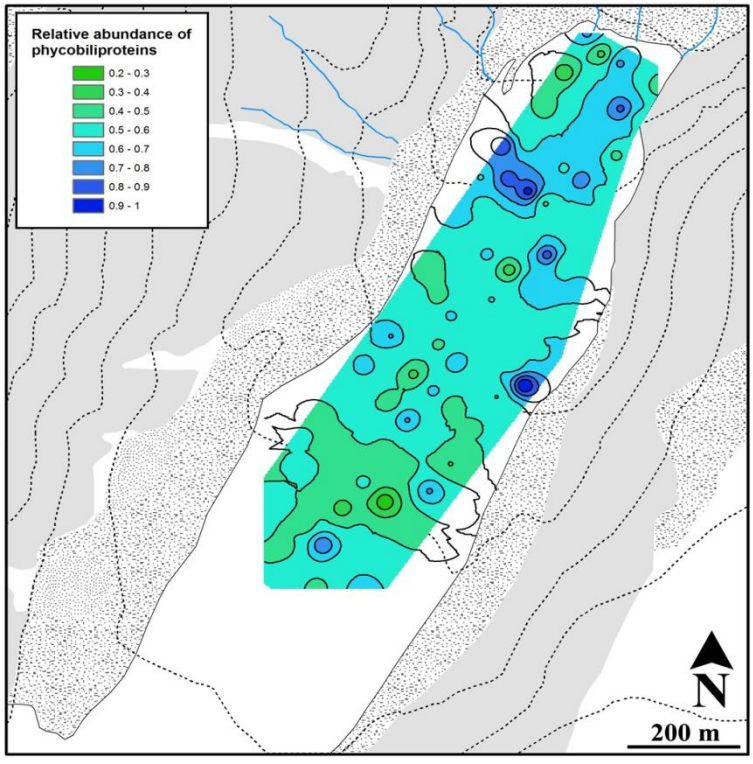

Figure 19: Variation in phycobiliprotein concentration (relative abundance; fraction) across Longyearbreen glacier ablation zone.

Figure 19 shows the variability in phycobiliproteins across the glacier surface, plotted as relative abundance values. When compared with the other geospatial maps, a lower localised variability is observable. The data show that, in general, concentrations were elevated near to the glacier terminus, and in places along the glacier edges, in a similar manner to mean chlorophyll *a* concentrations. There were also some 'hotspots' towards the top of the ablation zone, in contrast to findings with regard chlorophyll. The greatest phycobiliprotein concentrations measured were extracted from cryoconite sampled near to the northeastern valley side, although this value seemed to be geospatially isolated.

The variability in granule size across the glacier surface is mapped in Figure 20. Granule size shows perhaps the greatest variability between locations, varying between <300 µm and c. 1.5 mm. Granule size can be seen to increase, in general, towards the edges of the glacier and, to a smaller extent, towards the glacier terminus. Furthermore, to a greater extent than the other three parameters mapped, a central zone of lower values is visible. This relates to the lower average granule size that was present in that region at the time of sampling, whereby the average granule size did not exceed 600 µm.

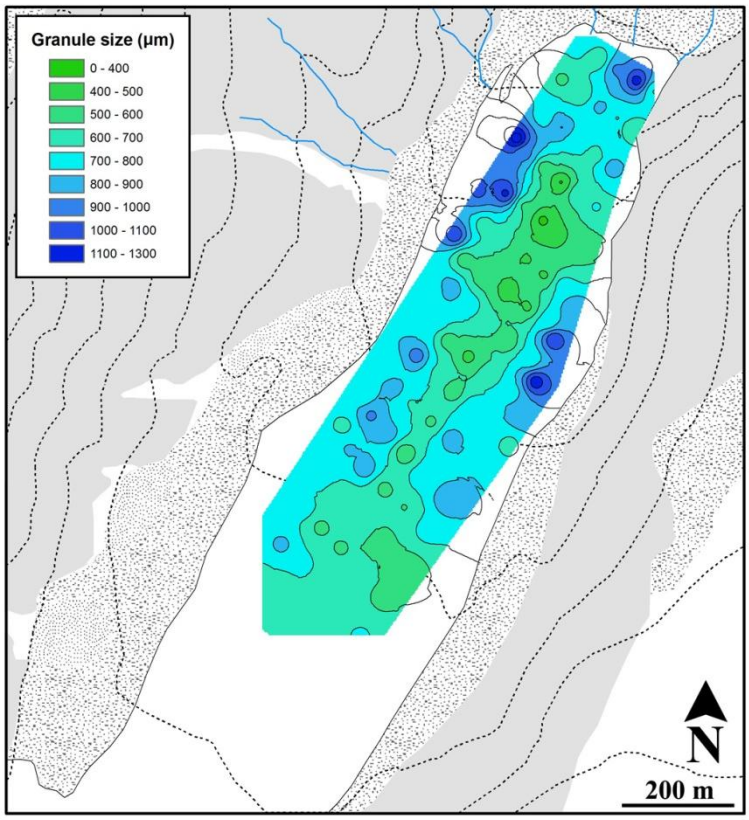

Figure 20: Variation in cryoconite granule size (µm) across Longyearbreen glacier ablation zone.

5.4.2 Comparison of geospatial data

When comparing chlorophyll *a* and granule size (Figs. 17 & 20), a very similar spatial pattern is clear. Both maps show a general down-glacier increase consummate with an increase towards the glacier sides, as well as 'hotspots' of concentration and size respectively. Conversely, free carbohydrate content and granule size (Figs. 16 & 20) did not show such a strong spatial relationship. In certain areas along the glacier sides, higher carbohydrate concentrations can be related to larger granule sizes. However, the opposite was the case near to the glacier terminus. The spatial pattern of phycobiliprotein abundance shows some similarity to granule size data (Figs. 19 & 20) towards the glacier edges, and overall in that phycobiliprotein abundance generally increased towards the glacier terminus. However, the patterns of 'hotspots' were dissimilar, particularly towards the glacier terminus.

As demonstrated by the CCR (Fig. 18), an inverse spatial relationship between chlorophyll *a* and carbohydrate concentration (Figs. 16 & 17) can be seen, in general, in that comparative excesses of carbohydrates were found up-glacier and comparative excesses of chlorophyll *a* were found down-glacier. When the geospatial distributions of both pigments are compared (Figs. 17 & 19), a positive relationship can be seen. However, the phycobiliprotein concentrations showed less spatial variability, with fewer 'hotspots', than chlorophyll *a* concentrations. Finally, as with chlorophyll *a* concentrations, an inverse spatial relationship between phycobiliproteins and carbohydrates (Figs. 16 & 19) is evident, in general. However, towards the glacier sides, this relationship becomes less clear.

5.4.3 Environmental influences over aggregate size and stability

Figure 21 shows the principal biogeochemical data for the centre-line transect through the grid area (ablation zone) of Longyearbreen glacier. This small dataset was intended to provide both a summary of the glacier biogeochemistry and a dataset for multivariate linear regression, in order to statistically deduce the principal factor(s) affecting cryoconite granule size and stability. Along the glacier transect, aggregate size and stability (Fig. 21a) were well correlated (Pearson's correlation coefficient = 0.765; P = 0.077). Near to both the glacier terminus (GT) and the snow line (SL), aggregate size and stability were at their greatest, with a generally stable average aggregate size evident otherwise. The organic matter content of the cryoconite granules (Fig. 21b) shows a negative linear trend with distance up-glacier, falling from 176.50 mg/g to 127.85 mg/g. This is in complete contrast with carbohydrate content (Fig. 21c), which increases up-glacier from 0.816 µg/g to 2.662 µg/g.

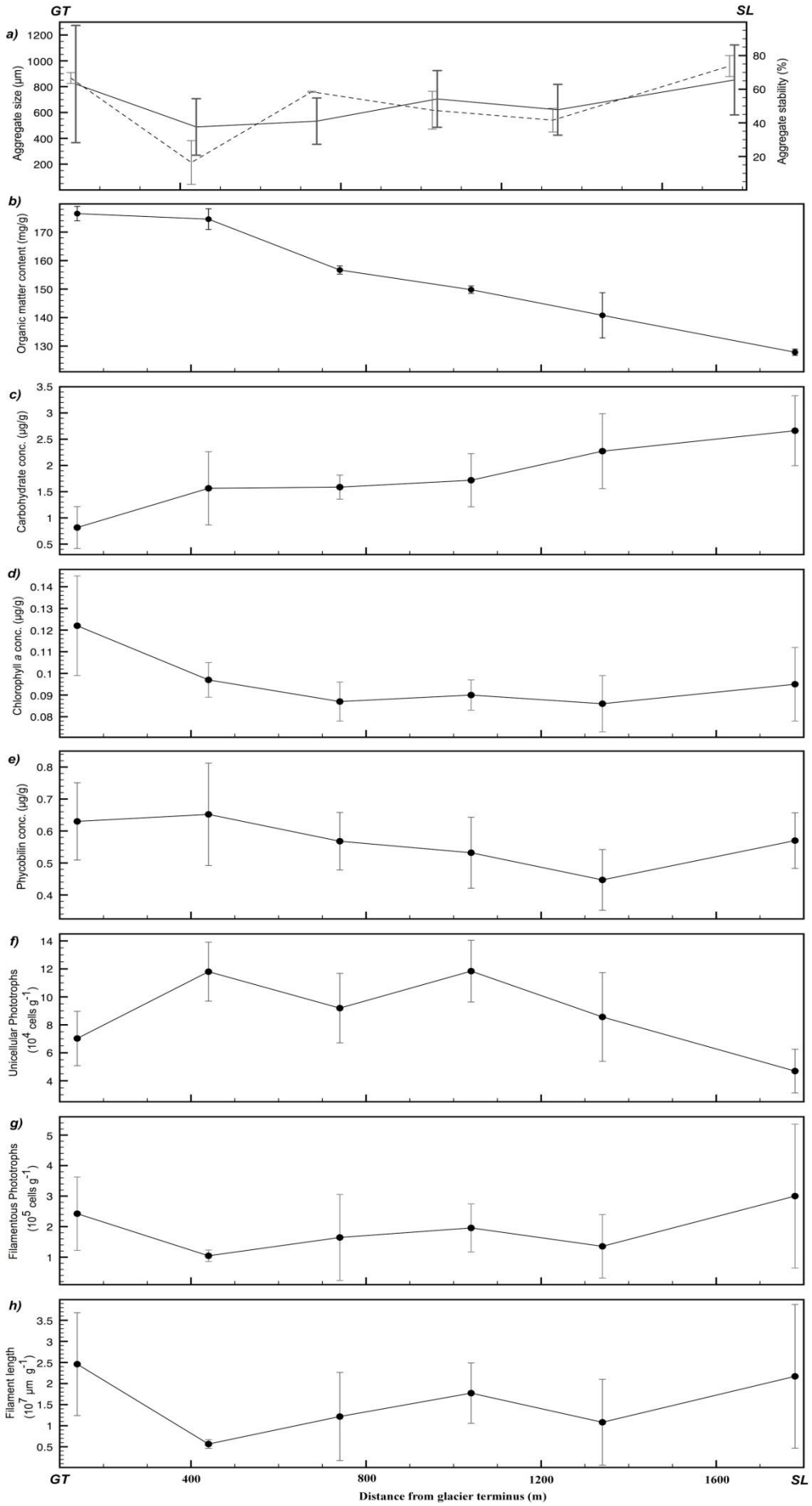
GT
SL
a)
Aggregate size (µm)
Aggregate stability (%)
b)
Organic matter content (mg/g)
c)
Carbohydrate conc. (µg/g)
d)
Chlorophyll a conc. (µg/g)
e)
Phycobilin conc. (µg/g)
f)
Unicellular Phototrophs (10^4 cells g^{-1})
g)
Filamentous Phototrophs (10^5 cells g^{-1})
h)
Filament length (10^7 µm g^{-1})
GT
400
800
1200
1600
SL
Distance from glacier terminus (m)

Figure 21: Glacier centre-line transect data, summarising biogeochemical data between glacier terminus (GT) and snow line (SL), detailing variation in: (a) aggregate size (μm; solid line) and stability (%; dashed line); (b) organic matter content (mg/g); (c) labile carbohydrate content (μg/g); (d) chlorophyll a concentration (μg/g); (e) phycobiliprotein (phycobilin) concentration (μg/g); (f) unicellular photoautotroph count (10^4 cells g^{-1}); (g) filamentous photoautotroph count (10^5 cells g^{-1}); and (h) filament length (10^7 μm g^{-1}).

Chlorophyll *a* concentrations (Fig. 21d) were generally similar, with greater variability and slightly greater concentrations towards the GT and at the SL. Averaged phycobiliprotein concentrations (Fig. 21e) were relatively constant along the glacier transect, with coefficients of variation of c. 10–20% signifying some variability. As such, these data serve only to illustrate the ubiquitous presence of cyanobacteria across the glacier. The phototrophic content of cryoconite (Figs. 21f–h), when broken down into unicellular and filamentous photoautotroph counts and filament length parameters, varies considerably more than the phycobiliprotein concentrations. The filamentous photoautotroph count (Fig. 21g) shows some variability, with greater numbers present near to the GT, as well as greater numbers (but greater variability) near to the SL (averaging c. 3.0×10^5 cells g^{-1}). Conversely, the unicellular photoautotroph count (Fig. 21f) is nearly the inverse of the filamentous count. The filament length data (Fig. 21h) are, as expected, similar in trend to the filament count data. The main difference is that the greatest mean filament length was found in cryoconite closest to the GT (2.46×10^7 μm g^{-1}).

In order to explore the above patterns, multivariate linear regression analysis was applied to the above-described centre-line transect data. Considering granule size as the dependent variable, the only single parameter/combination of parameters that showed statistically significant relationships ($P < 0.05$; and therefore included in the model) were (i) filament length and (ii) filament length combined with filament area. Filament length was found to explain 89.5% of the variation in granule size ($P = 0.004$), whilst filament length and area could explain 92.0% of the measured variation in granule size ($P = 0.022$). Considering both granule size and granule stability as correlating dependent variables, the greatest R^2 value was found when (i) unicellular photoautotroph count ($P = 0.036$), (ii) filamentous photoautotroph count ($P = 0.007$) and (iii) carbohydrate–chlorophyll ratio ($P = 0.028$) remained in the model (the rest being removed due to high *P* and/or *F* values). These three parameters could explain 83.0% of the variation in granule size and stability.

5.5 Discussion

5.5.1 Spatial mapping of biogeochemical parameters

As visualised in Figure 16, average carbohydrate concentrations were found to generally increase up-glacier, with some 'hotspot' variability evident. With thinner deposits and smaller granule sizes, net primary production and the concentration of labile carbohydrates have been found to be greater in the upper ablation zone of the Greenland ice sheet (Cook et al. 2010, Stibal et al. 2010, Telling et al. 2012). Furthermore, microbial EPS production has been shown to be advantageous to survival in cold-temperature environments (Vincent 2007). When subjected to freezing, polysaccharides can hold larger quantities of unfrozen water than smaller carbohydrates (Biswas et al. 1975), and the hexose monosaccharides – glucose, mannose and galactose – have been found to be better at maintaining liquid water (Furuki 2000). Both cyanobacterial EPS and cryoconite have been found to contain proportionally greater concentrations of certain hexose monosaccharides, particularly glucose and galactose (Pereira et al. 2009, Stibal et al. 2010). With this in mind, it may be that a proliferation of EPS occurs at the onset of freezing, as a cryoprotection mechanism. Recently thawed cryoconite material, near to the snow line, would thus be expected to contain proportionally more carbohydrates.

As mentioned above, carbohydrate concentration data did show localised variability around the general trend, with concentration 'hotspots' evident. In the late spring or early summer, supraglacial phototrophic blooms, e.g. those of the red snow alga *Chlamydomonas nivalis*, can be readily witnessed on both snow and superimposed ice surfaces (Newton 1982, Müller et al. 1998, Stibal et al. 2006). As such, and given the 'patchy' nature of phototrophic bloom activity, this activity is likely to preferentially raise carbohydrate concentrations in 'hotspots' associated with earlier bloom activity. Furthermore, in locations near to the glacier edge, and thus valley side, slightly higher concentrations are evident, particularly along the northwestern edge. This might indicate allochthonous input of carbohydrates from the valley sides, or greater allochthonous nutrient inputs and thus higher productivity. Finally, it is considered that the input of larger mineral particles from moraine debris goes some way to explaining the reduced carbohydrate concentrations measured in cryoconite near to the glacier terminus. Indeed spatial studies using Fourier-transform infrared (FTIR) spectroscopy (Langford et al. 2011) provide evidence for localised mineral- and clay-rich cryoconite near to the glacier terminus on Aldegondabreen, another Svalbard glacier.

With regard to chlorophyll *a* concentrations, a broad down-glacier increase is evident in Figure 17, reaching a maximum value of 0.1825 µg/mL (c. 0.27 µg/g). In similar

polar environments, between c. 0.3 and c. 15 µg/g of chlorophyll *a* have been reported (Stibal et al. 2008a, Stibal et al. 2010, Hodson et al. in review). In glacial river and polar lacustrine and fjord environments, between c. 0.2 and c. 65 g/L have been detected (Owrid et al. 2000, Battin et al. 2001, Laybourn-Parry & Marshall 2003). Assuming a cryoconite density of 1.49 g/mL, as discussed earlier (A.J. Hodson, unpublished data), maximum chlorophyll concentrations upon Longyearbreen glacier, at the time of sampling, were approximately 0.2 g/L. As such, they are comparable with values from alternative, aqueous environments.

The down-glacier increase in chlorophyll *a* can be attributed, in part, to a reduction in physical disturbance, a trend also seen in glacial streams (Battin et al. 2001). In addition, exposure time since snowmelt likely plays a part. Towards the top of the ablation zone, at the time of sampling, a thick layer of refrozen snowmelt (superimposed ice) was present, which had been heavily weathered by solar radiation. Distributed pore water flow, combined with the presence of cryoconite material in pores within the superimposed ice, likely created increased hydraulic disturbance of cryoconite sediment, with this lack of stability reducing the opportunity to photosynthesise and perhaps even eroding smaller and weaker cryoconite aggregates. Secondly, this up-glacier superimposed ice environment, being only partially ablated, contained biomass only recently exposed to liquid water. Additionally, being a porous and ablating weathering crust, this environment provides increased shading of the newly ablated cryoconite material within and below it. As such, the level of biological activity at the time of sampling could well have been lower than for fully exposed, down-glacier cryoconite.

Towards the glacier terminus, larger interstitial flow paths created regions of the glacier with reduced water flow (Irvine-Fynn et al. in press) and thus greater stability. Indeed, the superimposed ice layer could be considered an ephemeral habitat, within which the cyanobacterial strategy of slow growth is likely to be less successful (Vincent 2007). The main supraglacial stream in 2010 ran down the centre of Longyearbreen glacier, incising deeper in the lower 200 m. This region is concomitant with reduced chlorophyll *a* content in Figure 17, a fact that further supports the claim that stability promotes photosynthesis. Other factors that must be considered are that chlorophyll produced at low light levels can avoid photo-degradation and persist (Carpenter et al. 1986), and that chlorophyll degrades more slowly at cold temperatures (Vincent & Howard-Williams 1989). It may be, therefore, that, as cryoconite granules melt down into the ice, shading, combined with the prevalent cold temperature, allows older cryoconite granules to accumulate chlorophyll. Given these facts, it is expected that stable cryoconite at the terminus of the glacier, the area that ablated first and has thus

been exposed to solar radiation for the longest, should contain greater concentrations of chlorophyll.

Regarding the excesses of carbohydrates present up-glacier, as revealed by the CCR, this is likely to be both a cryoprotection mechanism and a result of phototrophic bloom activity. As mentioned previously, phototrophic bloom activity has been documented on glacier surfaces (e.g. Newton 1982); the authors have also observed this activity upon Longyearbreen glacier. Furthermore, given the 'stickiness' of carbohydrates, it is likely a mechanism for particulate nutrient scavenging following the onset of melt, in order to obtain the necessary nutrients for photosynthesis, e.g. iron for the construction of phycobiliprotein molecules. Nutrient scavenging has been postulated as important within glacial biological communities (e.g. Battin et al. 2001, Hodson et al. 2008), and recently it has been determined that Arctic microbial mat communities are 'designed' for nutrient scavenging (Varin et al. 2010).

Concerning phycobiliproteins, geospatial mapping determined a lower localised variability, as well as elevated concentrations towards the glacier terminus and sides, similar to data for chlorophyll *a*. Taking phycobiliprotein concentration as a proxy for cyanobacterial biomass, the lower localised variability suggests a relatively constant cyanobacterial biomass, in agreement with the findings of Segawa and Takeuchi (2010). Regarding the broad increase in phycobiliproteins towards the glacier edges, this again suggests that stability promotes photosynthesis and growth, as well as suggesting the potential for 'hotspots' of cyanobacterial and nutrient influx from the valley sides. Midway through the ablation season one would expect, given the long doubling times of cyanobacteria (potentially on the order of 8–13 days; Nadeau & Castenholz 2000), elevated concentrations near the glacier terminus. Other photo-physical factors, such as slope, may also have an effect upon both the influx of solar radiation and the stability of the surface. Radar surveys have revealed that the strata beneath Longyearbreen glacier dip towards the glacier centre-line (Etzelmüller et al. 2000), and personal observations noted that the margins of the glacier were slightly flatter. Therefore, a stable ice surface is more likely to be present towards the glacier sides.

As noted in the Results section, 'hotspots' of phycobiliprotein abundance were also found up-glacier, arguably to a greater degree than for chlorophyll *a*. These 'hotspots' were not as strong as those towards the glacier terminus and are possibly due to random variation associated with a tendency for cyanobacteria to cluster (Stibal et al. 2010). Research into the variability of phycobiliproteins has found that a range of photo-physical and physico-chemical factors can affect the quantity and quality of phycobiliproteins, including intensity and energy distribution of incident radiation (Glazer 1977, Korbee et al. 2005), position within the photic zone (Jørgensen et al.

1987), number of motile cyanobacteria (Kruschel & Castenholz 1998) and macronutrient concentrations (Liotenberg et al. 1996). All of these factors could be expected to contribute to spatial variability in phycobiliprotein concentrations.

Geospatial analyses of granule size revealed a high variability, with granule size, in general, increasing towards the glacier edges. This potentially indicates a significant source of avalanched and/or water-borne debris from the valley sides. In addition, this is also an indicator of stability, promoting organic matter production, cell–mineral interaction and amalgamation (Takeuchi et al. 2010; Telling et al. 2012). The central corridor of the ablation zone can be characterised by relatively smaller granule sizes, indicative of hydraulic erosion by the flowpaths entering the principal supraglacial stream.

5.5.2 Comparison of geospatial data

Geospatial data indicate significant similarities between elevated average chlorophyll *a* concentrations and larger mean aggregate sizes. Even without statistical analysis, this similarity is evidence of a linkage between the two. A positive correlation between chlorophyll *a* concentration and aggregate size has been found many times when studying microaggregates in a variety of systems (e.g. Maxwell & Neuman 1994, Lunau et al. 2006, Bowker et al. 2008). In addition, a positive correlation between chlorophyll *a* content and soil aggregate stability has been shown in biological soil crust systems (Belnap et al. 2008). Indeed, aggregate stability has been shown to positively correlate with both chlorophyll *a* content and observations of cyanobacterial sheaths in these soil crust environments (Herrick et al. 2010).

In some contrast to the geospatial similarities between chlorophyll *a* concentrations and granule size, carbohydrate concentrations do not show such a strong positive influence upon aggregate size. Although this is contrary to findings with regard temperate soil microaggregates (e.g. Puget et al. 1999), this finding is not unexpected. Firstly, net ecosystem productivity reduces with sediment thickness (Telling et al. 2012) and, as granule size increases, heterotrophic consumption exceeds autotrophic accretion of free carbohydrates (Stibal et al. 2010). Secondly, the carbohydrate extraction method utilised was a gentle, dilute-acid hydrolysis designed to extract labile carbohydrates from the sediment. The majority of cyanobacteria have capsular, bound carbohydrates surrounding them as a sheath. As such, these findings suggest that bound carbohydrates, as inferred by sediment chlorophyll and phycobiliproteins (Figs. 17 & 19), exert a greater control over granule size than free carbohydrates, in agreement with others (Cook et al. 2010, Stibal et al. 2010).

5.5.3 Environmental influences over aggregate size and stability

Biogeochemical data for the centre-line transect indicated that whilst the organic matter content of Longyearbreen cryoconite is greatest towards the terminus, and decreases up-glacier, the labile carbohydrate content is greatest near to the snow line and decreases down-glacier. When considered together, these data are in contrast with the findings of Stibal et al. (2010, 2012) in Greenland, who found that both TOC and carbohydrate contents increased up-glacier; however the scales at which these datasets were taken are vastly different. Furthermore, relating this negative correlation between carbohydrate content and organic matter content to granule size, it may be suggested that autotrophic production of carbohydrates and the adhesion of allochthonous material up-glacier give way to clay–organic matter interaction and the amalgamation of individual grains down-glacier as controls upon granule size (Takeuchi et al. 2010, Telling et al. 2012). As such, these organic carbon data may represent younger granules rich in labile, autochthonous carbohydrates ageing and becoming enriched in both: (i) allochthonous organic matter from the valley sidewalls and (ii) more humified forms of carbon.

Considering the down-transect variation in pigment concentrations, chlorophyll *a* was found to decrease up-glacier, in general, save for a slight increase near to the snow line. This up-glacier decrease is likely due to a combination of factors, including stability and persistence – discussed earlier. Phycobiliproteins showed relatively constant average values, with relatively large error bars, meaning that a significant trend could not be determined. Direct counting of filamentous and unicellular photoautotrophs provided further data to compare with granule size and stability data, in order to understand the biological controls over aggregation. As mentioned in the Results, the photoautotrophic content of Longyearbreen cryoconite varied considerably along the transect of study. Anesio et al. (2010) found little evidence of a correlation between bacterial abundance and bacterial production. This, combined with the fact that the quantity and quality of phycobiliproteins have been shown to be highly variable (e.g. Korbee et al. 2005), and the fact that cyanobacterial sheaths may be preserved in the centre of aggregates, away from solar radiation, goes some way to explaining this greater variability.

Along the glacier centre-line transect, filamentous photoautotroph counts, and the measured length of filaments, showed increases at the glacier terminus and the snow line, whilst unicellular photoautotroph counts showed an inverse trend. This may suggest that proliferation of filaments restricts space within the aggregates, reducing growth in unicellular photoautotrophs. It may well also be that cryoconite age and stability (as alluded to earlier) contribute to the higher average filament count and length, particularly to the greater average filament length, which was found closest to

the glacier terminus. When the photoautotroph data are compared with granule size and stability data, it is clear that they show similar trends. This suggests that the presence of filamentous cyanobacteria has a significant control over the size and stability of cryoconite granules, a suggestion that warranted statistical investigation.

Statistical analyses showed that the number of photoautotrophic filaments, and their length, could explain 92.0% of the variation in cryoconite granule size along the transect. Furthermore, when the number of unicellular photoautotrophs and the carbohydrate–chlorophyll ratio were also considered, 83.0% of the variation in granule size and stability could be accounted for. These results suggest that photoautotrophic activity, along with the production of carbohydrates (EPS), contributes significantly to the variation in granule size and stability seen on Longyearbreen glacier. These results agree with findings from terrestrial environments, where algal inoculation has been shown to improve soil stability by reducing the damaging effect of erosion by water (Falchini et al. 1996) and retaining silt and clay size fractions (Starks et al. 1981). There is also agreement with findings from marine environments, where substantial research into the stabilisation of sediments by photoautotrophs has been conducted (e.g. Yallop et al. 1994, Sutherland et al. 1998a,b, Noffke et al. 2001, 2003, Tolhurst et al. 2002). As covered in detail by Stibal et al. (2012), the interplay of various physical and chemical factors, from altitude and slope to nitrogen and phosphorus limitation, all contribute to the variability in microbial productivity, when considering microbial abundance and activity as dependent variables. This study instead uses granule size and stability together as dependent variables, in an attempt to improve our current understanding of cryoconite aggregate formation, finding good correlation between cyanobacterial proliferation, associated EPS production, and granule size and stability, as suggested previously by a number of authors (e.g. Takeuchi et al. 2001b, Hodson et al. 2010, Langford et al. 2010). These findings have important implications for the distribution of aeolian debris and its residence time upon the ice, both of which exert a crucial control over albedo (Bøggild et al. 2010). Thus, photoautotrophy and the interaction of microorganisms with atmospheric impurities clearly make a significant contribution towards supraglacial melt.

5.6 Conclusions

The spatial variability in both pigment and carbohydrate concentrations across a glacier ablation zone can be rapidly ascertained and quantitatively mapped using a combination of spectrophotometric microplate methods and GIS techniques. Free carbohydrates were found to increase up-glacier, likely where newer, thinner deposits and EPS production

for cryoprotection and nutrient scavenging are prevalent. Chlorophyll *a* concentrations were highest near the glacier terminus, likely evidencing both a reduction in physical disturbance and potentially its persistence within cryoconite granules. Phycobiliproteins showed relative homogeneity, with slight excesses near the glacier terminus, evidence of both the ubiquitous presence of cyanobacteria and their controlling contribution towards chlorophyll concentrations; difficulties experienced in extraction prevent further conclusions from being drawn. Granule size showed greatest variability, with a general increase towards the edges of the glacier. In all cases, a zone of hydraulic erosion was evident down some of the central tract of the ablation zone, whilst allochthonous input and/or stability contribute to higher values of biogeochemical parameters near the glacier edges.

Granule size and stability were well correlated along the centre-line transect, with organic matter and carbohydrate concentrations showing negative correlation, indicative of a shift in organic matter composition and perhaps evidence of increasing age (i.e. humification) down-glacier. The numbers and lengths of filamentous photoautotrophs correlate well with, and can statistically explain, variability in cryoconite aggregate size. Combined with the carbohydrate–chlorophyll ratio, variability in both the aggregate size and stability of cryoconite is explainable. Thus, these data emphasise the strong link between filamentous cyanobacterial proliferation (and associated EPS production) and the development of stable cryoconite macroaggregates, and highlight the importance of both hydraulic erosion and humification to the variability in aggregate size and stability. Furthermore, they outline useful procedures for the rapid determination of biochemical parameters on glacier surfaces. The application and development of these methods has the potential to provide two-dimensional temporal mapping of supraglacial biochemistry and to further our understanding of cryoconite granule development. When combined with other data, this could enable the albedo evolution of the glacier surface, the cryoconite mass balance and the associated nutrient balance to be monitored during a photic period or ablation season.

5.7 Acknowledgements

H. Langford acknowledges R. Smith for assistance with sample collection and T. Irvine-Fynn for assistance with GIS mapping. A.J. Hodson acknowledges the RGS, NGS and Gilchrist Education Trust awards.

CHAPTER SIX: THE AGGREGATION OF CYANOBACTERIA AND MINERAL PARTICLES: INSIGHTS INTO THE DEVELOPMENT OF CRYOCONITE GRANULES

Prepared for submission to Geobiology: Langford, H., E. Wharfe, R. Goodacre, A. Hodson & S. Banwart, 2012. The aggregation of cyanobacteria and mineral particles: Insights into the development of cryoconite granules.

6.1 Abstract

Cryoconite granules – supraglacial bioaggregates dominated by photoautotrophic microorganisms – are phylodiverse and biogeochemically active micro-environments. The development of these granules is also fundamental to the entrainment of particulate matter upon ice surfaces and consequently to albedo-driven melt. However, little is known about the aggregation mechanisms operating upon glacier surfaces, driving granule development. This study combines microscopy and spectroscopy to study the co-aggregation of cyanobacteria and mineral particles, finding that a variety of mineral powders are readily incorporated into bioaggregates. Various physicochemical conditions, including ionic strength, temperature and growth phase, were shown to affect both the success of attachment and the survival of the cyanobacteria. Fourier transform infrared (FTIR) imaging suggested that capsular and free extracellular polymeric substance (EPS) interactions with mineral particles dominated cell–mineral attachment. Elemental carbon showed greater evidence for hydrophobic and cationic protein interactions, whilst quartz showed greater evidence for polysaccharide and carboxyl group interactions, suggesting that a variety of attachment mechanisms can exist. The above suggests that the aggregation of aeolian particulate matter on glacier surfaces is strongly biologically mediated.

6.2 Introduction

Cryoconite granules – quasi-spherical aggregations of microorganisms, organic matter and particulate mineral matter – are found on the surfaces of glaciers in many regions of the world. Molecular sequencing and microscopic observation of the microbial communities within these granules have highlighted their phylodiversity (Christner et al. 2003, Stibal et al. 2006), whilst microstructural evaluation has suggested the importance of phototrophs, particularly cyanobacteria, in the formation and

development of cryoconite granules (Takeuchi et al. 2001b, Langford et al. 2010). Aggregation of microorganisms and particulate matter retains material on the ice surface that would otherwise be removed by melt, darkening the surface and enabling further melt via the albedo feedback loop (Takeuchi et al. 2001a, Takeuchi 2002, Hodson et al. 2008, 2010). The aggregation and development of a sediment-based microbial ecosystem is also considered important in the seeding of the glacial forefield, glacial carbon balance, and in the cycling of other key nutrients such as nitrogen and phosphorus (Mindl et al. 2007, Stibal et al. 2008b, Anesio et al. 2009, Hodson et al. 2010). As such, research into the aggregation of photoautotrophic microorganisms and mineral particles can be considered to be highly relevant in achieving a greater understanding of supraglacial ecosystems.

The attachment of microorganisms to abiotic surfaces has received a great deal of recent research attention. Initially focusing on gram-positive bacteria due to their simpler cell wall structure, research now encompasses gram-negative bacteria, cyanobacteria and eukaryotic algae in a whole host of differing natural and anthropogenic environments. Cell–substratum attachment is a net result of attractive and repulsive forces (Geoghegan et al. 2008), with factors such as surface charge, surface site densities and hydrophobicity highly influential in attachment efficacy (Dittrich & Sibler 2005, Andrews et al. 2010). When considering aggregates such as marine snow, sludge flocs and cryoconite granules, both cell–cell interaction and the prevalence of extracellular polymeric substances (EPS), to condition surfaces and promote adhesion, are also very important (Sutherland 2001, Brehm et al. 2004, Eboigbodin et al. 2007). Alongside this, shear and settling velocity gradients affect the induction of collision, which subsequently affects the probability of attachment (Simon et al. 2002, Bouyer et al. 2005). Finally, cell density has been shown to be important in attachment, with the number of attached/aggregated cells being shown to be proportional to the cell density in various experimental environments (Chaignon et al. 2002, Simon et al. 2002, Sekar et al. 2004, Kim et al. 2010).

Cyanobacteria are gram-negative prokaryotes, containing a photosynthetic apparatus involving both chlorophylls and phycobiliproteins, and noted for their thick peptidoglycan layer, production of polysaccharidic EPS, high concentrations of unsaturated fatty acids and membrane lipids, and ability to form trichomes (filament structures) and heterocysts (nitrogen-fixing cells) (Stanier & Cohen-Bazire 1977, Chintalapati et al. 2004, Vincent 2007). Filamentous cyanobacteria, such as *Nostoc* and *Phormidium* species, have been shown to co-flocculate with clay and iron oxide minerals under various conditions (Leslie et al. 1984, Bar-Or & Shilo 1988, Pan et al. 2006), with flocculation correlated with the production of EPS, the presence of macronutrients and hydrophobic interaction (Bar-or & Shilo 1988, Pan et al. 2006, Silva

& Silva 2007). Investigations into the binding of both unicellular and filamentous cyanobacteria to metal ions have determined the importance of carboxyl, phosphoryl and amine functional groups, on both the cell wall and exopolymer sheath, to attachment (Phoenix et al. 2002, Yee et al. 2004, Omoike & Chorover 2004, Dittrich & Sibler 2005).

Investigations specifically relating to polar isolates are sparse. Kapitulçinova et al. (2008) find that a *Leptolyngbya* species isolated from a Svalbard tundra soil shows surface and interlayer attachment to flakes of biotite in nutrient-deficient conditions. As such, interaction between biota and abiotic particulate matter in cryoconite is still poorly understood, particularly at a cell–mineral scale. To provide insights into the development of cryoconite granules and explore cell–mineral interaction between cyanobacteria and mineral particles, laboratory experiments have been conducted to monitor the aggregation of cyanobacteria and a suite of mineral particles, under varying pH and ionic strength conditions. High-resolution measurements of aggregate size, quantity and quality of cyanobacteria, and aggregate organo-mineral chemistry, have been recorded using confocal laser scanning microscopy (CLSM) and Fourier transform infrared (FTIR) microspectroscopy.

CLSM has been used to study both natural and synthetic flocs/aggregates (Neu et al. 2002, Barranguet et al. 2004, Chen et al. 2007a,b, Neu et al. 2010), using a variety of fluorescent probes to study aggregate architecture, namely the distribution and type of microorganisms, the distribution of proteins and polysaccharides, and the pore spacing (Kawaguchi & Decho 2002, de los R*í*os et al. 2004, Chen et al. 2007a,b, Solé et al. 2007, 2009). FTIR microspectroscopy (FTIR imaging), having a spatial parameter and resolution, enables the non-destructive spatial analysis of functional groups across a sample (Naumann et al. 1991, Lewis et al. 1995). Modern FTIR imaging is achieved using a focal plane array (FPA) detector, which, using a step-scanning approach, allows rapid measurement of spectra across an array of pixels, enabling the construction of high-density chemical maps at a resolution of typically 4–10 μm (Lewis et al. 1995). FTIR imaging has rapidly developed as a tool in both the biochemical and geochemical sciences (e.g. Petibois et al. 2009, Della Ventura et al. 2010). Relating specifically to cyanobacteria, FTIR imaging has the ability to discriminate cyanobacteria (Kansiz et al. 1999) as well as to study the biochemical composition of their biomass, and how this changes with nutrient supply and/or stress (Heraud et al. 2005, Stehfest et al. 2005, Pistorius et al. 2009). As such, CLSM and FTIR microspectroscopy are considered suitable techniques with which to probe the architecture of photoautotrophic aggregates.

This study utilises a simple laboratory incubation to study the entrainment, attachment and aggregation of mineral particles by cyanobacteria. As such, it aims to help

understand how aeolian particulates, from mineral particles to pollutants, are entrained upon glacier surfaces, the specific attachment mechanisms involved and the variance of this attachment with different particulate types. Furthermore, it aims to understand how the rate of attachment and aggregation is affected by physicochemical conditions, and finally the effect of cell–mineral aggregation on the subsequent growth of cyanobacteria. It is hypothesised that cyanobacterial filaments will show an affinity for a range of mineral powders and that EPS will be involved in the cell–mineral attachment.

6.3 Methodological approach

6.3.1 Incubation of cyanobacteria and mineral particles

Incubations of cyanobacteria and mineral particles were conducted in Nunc™ 12-well, untreated, polystyrene microplates. To each well, 2.5 mL of BG-11 medium, of varying pH (pH 4, 7 and 9) and ionic strength (64 mM, 6.4 mM and 640 μM), was added. BG-11 medium is a mineral medium, composed principally of sodium nitrate and containing sodium carbonate (Na_2CO_3) as the carbon source (Stanier et al. 1971). To these wells, 1 mg of various mineral powders was added; minerals used were quartz, orthoclase, mica, haematite, kaolinite, elemental carbon and a mixed mineral powder. These minerals were chosen based on their prevalence in previous X-ray diffraction and FTIR spectroscopic analyses of disaggregated cryoconite material by the authors (Langford et al. 2010). Each mineral was milled in a TEMA laboratory disc mill, washed, dried and sieved to 25–63 μM. This particle size range has been shown to be representative of mean and median cryoconite particle sizes (Langford et al. 2010). Following this, 10 μL of either a *Leptolyngbya* S-47 or a *Phormidium* S-34 cyanobacterial suspension was added. These cyanobacteria were from the Polar Cyanobacteria Collection of the Belgian Coordinated Collections of Microorganisms (BCCM), where they are denoted as ANT.ACEV6.1 and ANT.PENDANT.1 respectively; these strains have been described in detail previously (Taton et al. 2006). The cyanobacteria were, with the exception of one 12-well plate, at early exponential growth phase at the time of addition. With regard to *Leptolyngbya* S-47, all combinations of mineral type, ionic strength and pH were incubated in triplicate, along with true, cyanobacteria-only and mineral-only blanks. *Phormidium* S-34 cyanobacteria were interacted with the mixed mineral powder under various ionic strength and pH conditions.

These plates were incubated on an orbital shaker under an Eye ColorArc® photosynthetically active radiation (PAR) bulb, with 16 hours of light per day, at an illumination of 100 μmol photons m^2 s^{-1}. Experiments were conducted at two

temperatures – room temperature (21°C) and refridgerated temperature (4°C). Microplates were sealed with parafilm to help prevent evaporative losses. Aggregation was studied over an 18-day period via CLSM on a Zeiss LSM 510-META upright confocal microscope. Autofluorescent images were excited with a 633 nm HeNe laser and autofluorescent emission between 650–700 nm was captured and imaged. Transmitted differential interference contrast (TDIC) images, illuminated with a 532 nm HeNe laser, were collected concurrently with the autofluorescent images. To allow comparison of images taken on different days, all autofluorescent images were captured using the same pinhole size, pass and gain settings.

Following completion of the incubations, end-point aqueous chemistry and carbohydrate analyses were completed using ion chromatography, inductively coupled plasma mass spectrometry (ICP-MS) and UV–Vis spectrophotometry, with the aggregates also studied via FTIR microspectroscopy. Dominant ions were analysed using ion chromatography, which was carried out on 0.45 μm filtered samples of the various incubation media, using a Dionex ICS 3000 ion chromatograph. Using a 10-μL sample loop, all detection limits were < 1 mg/L. For the specific ions discussed in this paper, detection limits were as follows: sodium, potassium, chloride and magnesium = 0.25 mg/L, calcium = 0.35 mg/L, nitrate = 0.50 mg/L and phosphate = 1.00 mg/L. A set of external calibration standards were analysed at the beginning and end of the sample run, and a 1 mg/L reference was analysed after every 10 samples had completed. Changes in trace metals were monitored using a Perkin-Elmer ELAN ICP-MS. Detection limits were all 5 μg/L except for As, Be, Fe, Se and Zn (50 μg/L). UV–Vis spectrophotometry was carried out in microplate format using the phenol–sulphuric acid method, as outlined by Langford et al. (in prep. 2012b).

6.3.2 FTIR microspectroscopy

Aliquots (20 μL) of each incubated sample were taken, containing micro-aggregations of cyanobacteria and mineral particles. These aliquots were applied onto CaF_2 disks (Crystran Ltd, Dorset, UK) and air-dried to remove water, which can mask spectral peaks. The spectra were collected in transmission mode using an Equinox 55 FTIR spectrometer coupled to a Hyperion 3000 microscope (Bruker Optics Ltd, Billerica, MA, USA). The microscope was equipped with a 64 × 64, liquid nitrogen cooled, mercury cadmium telluride focal plane array (MCT FPA) detector, which allows the simultaneous acquisition of spectral data from a 267 μm × 267 μm area, using a 15× objective lens. The FTIR spectral maps were collected between 4000–900 cm^{-1}, at a spectral resolution of 4.2 cm^{-1}. Spectral data were collected using routines within the OPUS 4.0 IR imaging software (Bruker Optics). The sample/background ratio was used to generate transmittance images of each sample. Finally, all spectral images were

converted to absorbance and exported into Matlab version 7.12.0 (The MathWorks, Inc., Natick, MA, USA) as ASCII files.

6.3.3 Image processing

CLSM images were processed in ImageJ™. To determine the autofluorescent pixel count (APC), images containing the 650–700 nm output were thresholded, using an above/below threshold, converted to binary and the pixels counted using the pixel counter tool; this process was automated using a macro. Aggregate size was measured from the TDIC output images. Starting with the raw image, an above/below threshold was again applied. Following this, the 'area' function was used to calculate the two-dimensional area of the granules. Any touching granules were manually separated into separate 'areas'; the average diameter of each granule was subsequently calculated.

FTIR spectral images were explored in Matlab, using a number of in-house algorithms. Firstly, a deterministic threshold was set and each image was automatically thresholded, defining each pixel as either 'containing spectral information' or 'background'; each threshold was checked against its corresponding optical image to make sure that only those pixels of biological relevance were selected. All background pixels were then set to zero so that they did not interfere with subsequent analyses. Following this, functional group mapping was performed on the spectral images, in order to investigate the spatial distribution of selected functional groups and their variation between different aggregation scenarios.

Functional group mapping can focus in on specific absorption bands (peaks), using integrated peak area, intensity and position to plot them spatially, thus allowing the chemical mapping of single peaks, or the ratio of two peaks of interest. Peaks mapped were as follows: amide I and II, lipid, carbohydrate, carboxylate, lipid/amide and carbohydrate/amide. For each of the chemical maps, the IR spectral intensity was presented on a colour scale, from blue (low IR absorbance) to red (high IR absorbance). Gouraud shading (Gouraud 1971) – an interpolated shading function – was applied to the maps in order to reduce the appearance of pixelation. Composite spectra were created in CytoSpec.

6.4 Results

6.4.1 Co-aggregation of cyanobacteria and mineral particles

In the case of quartz (Fig. 22a), and for all three ionic strengths, the APC was found to rise initially, before slowly falling with incubation time. Data showed a moderate linear fit (0.64 mM, $R^2 = 0.858$). Orthoclase feldspar showed a similar trend (not shown). The

deviation within the data (average absolute deviation [AAD]) was high in places, most notably on day 2. This was due to the large range of aggregate sizes, from small single flocs to aggregates composed of conjoined multiple flocs. When compared to aggregate size data for the quartz incubations (Fig. 22a, inset), presented as a moving average ± AAD, the two show a degree of inverse correlation. For all incubations undertaken, aggregates had formed between day 0 (inoculation) and day 1. For quartz, a slight increase in average aggregate size was exhibited over the course of the incubation, although aggregate size clearly fluctuated as larger aggregates broke up and smaller aggregates adhered together. For the case of elemental carbon (Fig. 22b), APC rose in all cases, irrespective of ionic strength, but achieved the greatest rise with time in the 64 mM set of incubations, showing a good linear fit (R^2 = 0.894). Again, similarly high ranges contribute to a relatively high deviation in the data. Initially, when compared with aggregate size (Fig. 22b, inset), the data show a positive linear correlation until day 10. Following this, a levelling off and slight decrease in average aggregate size was observed. When a mixed rock powder was used, a positive linear trend (R^2 = 0.978) was exhibited for the high ionic strength wells (Fig. 22c), whilst the lower ionic strength incubations showed slight reductions in average APC. As with the elemental carbon data, aggregate size for the mixed powder incubations increased linearly with time initially, before falling. However, in this instance, a greater fall in average aggregate size was seen, returning to similar values as for day 1. Figure 22d shows the change in the APC plotted against the change in aggregate size, for all incubation wells. When all data points are considered, the data do not show a strong trend. This suggests that further parameters affect one or both variables, contributing to the variance observed and the weak linear regression model fit (R^2 = 0.217). If the two principal outliers are excluded, a moderate fit can be achieved (R^2 = 0.575).

When considering pH, no significant differences were evident between incubations conducted at acid, neutral and alkali starting pH values. For the mixed rock powder (Fig. 22e), pH 9 incubations exhibited the greatest increase in the average APC, with the data again showing a positive linear trend over time (R^2 = 0.933). However, all pH data for the mixed powders showed a similar trend initially, with error bars overlapping. It was only towards the end of the incubation period that these data diverged slightly and differences in these trends emerged. A similar trend was clear for all other rock powders studied. Figure 22f shows the variation of aggregate size over time with pH. Data indicated that average aggregate size showed considerable variation over time, irrespective of pH. As such, in these incubations, pH did not significantly affect the growth of cyanobacteria or the adhesion of these cyanobacteria together and to mineral particles.

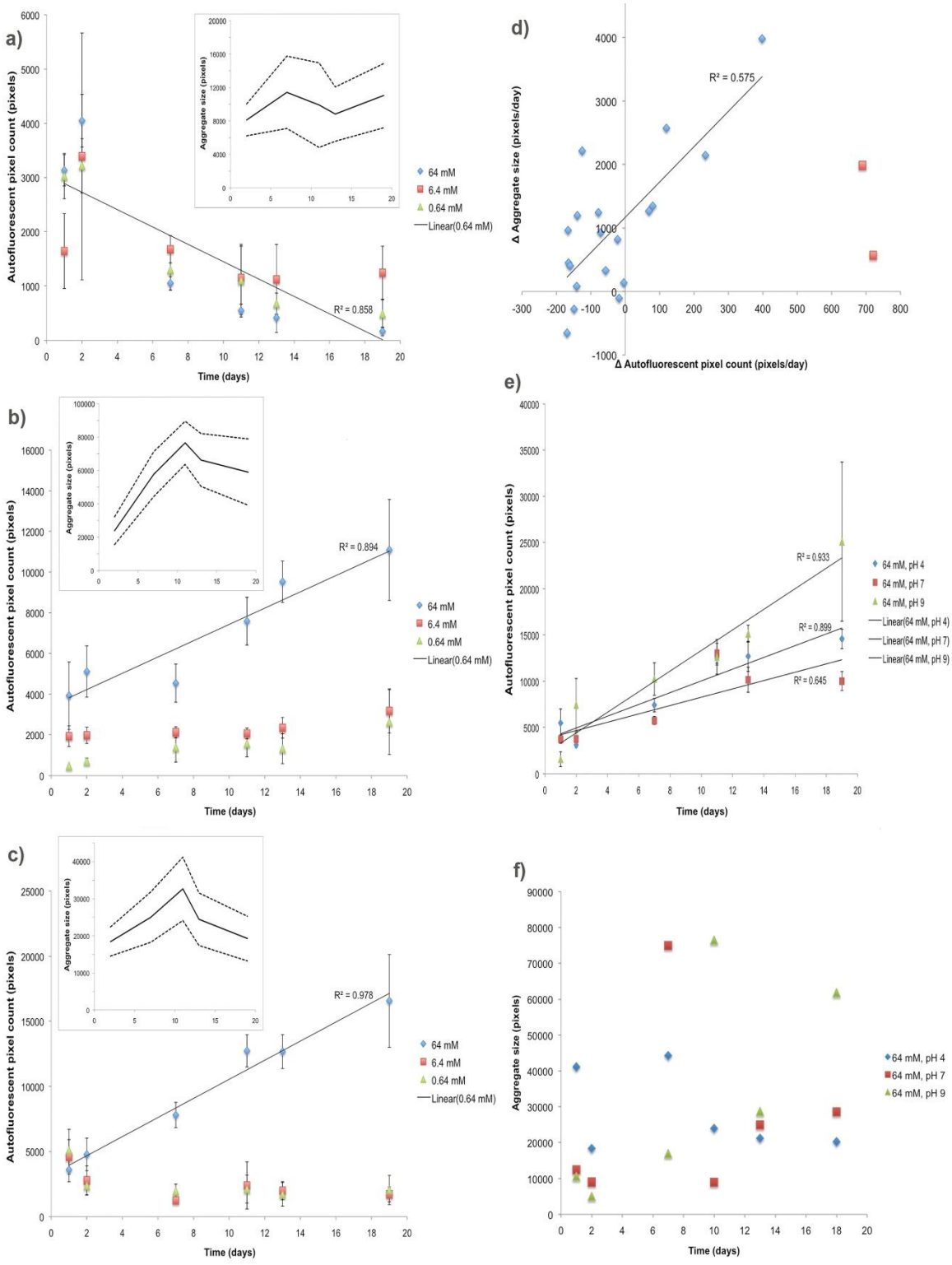

Figure 22: Results of cyanobacteria and mineral particle incubations, highlighting the variations in APC and aggregate size with ionic strength for (a) quartz, (b) elemental carbon and (c) a mixed mineral powder, (d) the change in APC versus the change in aggregate size, and the variation of (e) APC and (f) aggregate size with pH.

Figure 23 shows averaged data for both APC and aggregate size, presented as a ratio of the initial count or size (adjusted so that the initial pixel count equals zero). Although each well was inoculated with the same volume of cyanobacterial suspension, random variation in filament concentrations, combined with the tendency of these cyanobacteria to flocculate, led to some variation in the initial 'load' of cyanobacteria. Transforming the data to ratio values negates this initial variation.

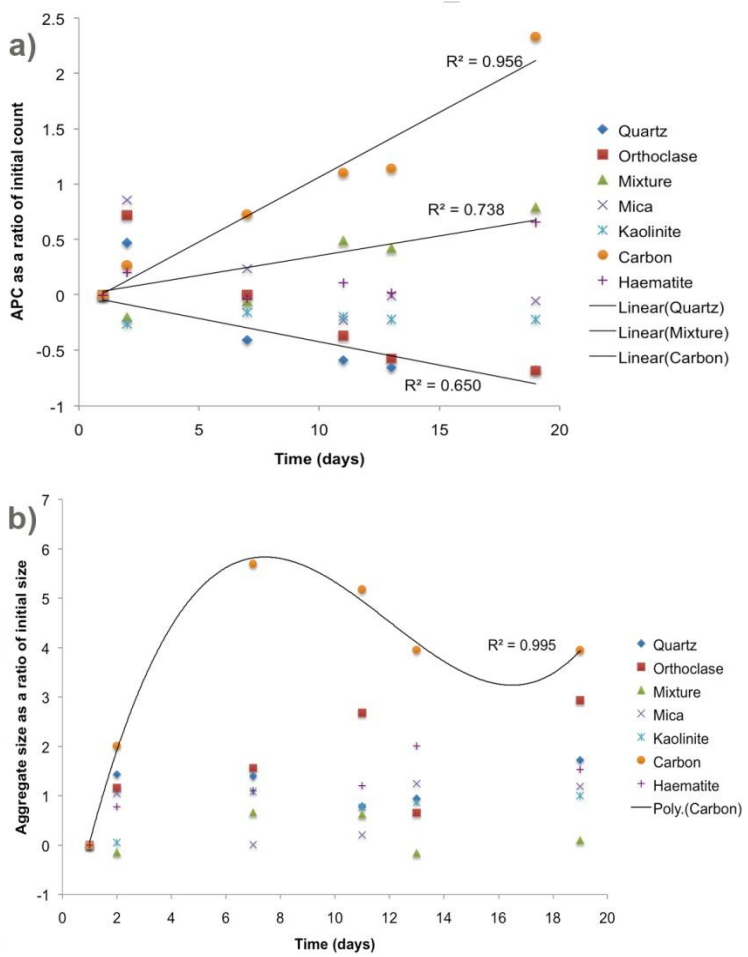

Figure 23: Averaged (a) APC values and (b) aggregate sizes, expressed as a ratio of their values on day 1, for all mineral types.

An initial increase in APC (Fig. 23a) on day 2 was evident in the majority of cases, most likely due to both the growth of cyanobacteria and, more importantly, the flocculation of planktonic filaments and the adhesion of these filaments onto existing aggregates, increasing the number of filaments per aggregate. As in Figure 22, linear lines of regression have been added to quartz, elemental carbon and mixed powder data, given that these show the greatest difference. To summarise, Figure 23a shows that elemental carbon aggregates showed the greatest increase in APC (R^2 = 0.956), followed by the mixed powder (R^2 = 0.738) and haematite, both exhibiting relative growth. Kaolinite and mica showed a similar APC to the initial value, whilst orthoclase

and quartz showed slightly declining APC values (quartz R^2 = 0.650). The trend in aggregate size with time was less clear. As with APC, aggregate size increased the most in the elemental carbon wells (Fig. 23b); at the end of the incubation period, a five-fold increase in average aggregate size was recorded. The data show an initial sharp rise in average aggregate size, followed by a slight fall, as noted in Figure 22b (inset). Orthoclase feldspar in fact showed the second greatest increase in average aggregate size (four-fold), with the remaining mineral types exhibiting a two- to three-fold increase in average aggregate size over the incubation period, with the exception of the mixed powder, which showed a stable average aggregate size across the incubation period.

Figure 24 shows examples of the aggregates formed during these incubation experiments. The aggregates formed were floc-like and quasi-spherical, exhibiting varying densities of mineral particles, from the dense aggregations of either elemental carbon or kaolinite and cyanobacteria (Figs. 24a & b) to the relatively mineral-poor aggregations of quartz and cyanobacteria (Fig. 24e). EPS can be seen as 'clouds' of light grey material between both mineral particles and cyanobacterial filaments (e.g. Fig. 24f). Clusters of cyanobacteria or single filament lengths were often found to extend from the exterior of the aggregate into the surrounding supernatant (e.g. Fig. 24c), presumably in order to facilitate the adhesion of further cyanobacteria and/or mineral particles. Indeed, particularly in the high ionic strength wells, multiple flocs were increasingly conjoined to form larger aggregates (e.g. Fig. 24d). Over the course of the incubations and within certain wells, particularly those associated with quartz and orthoclase, cellular autofluorescence (signifying live, autofluorescing cells) diminished in certain cells along the filament lengths. This is likely indicative of stress-induced cell death or senescence.

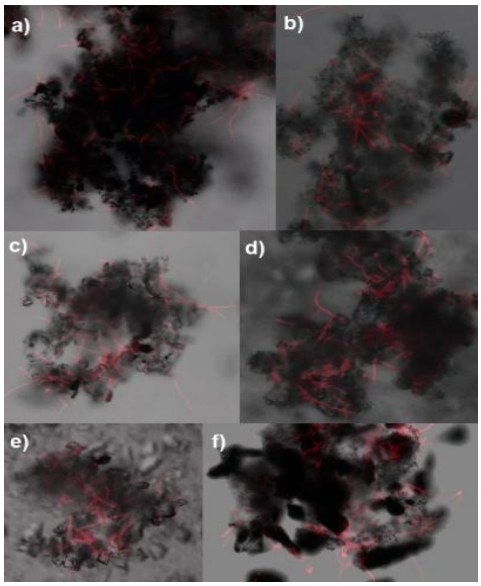

Figure 24: TDIC and autofluorescent channel CLSM images of cyanobacteria and mineral aggregates, specifically (a) elemental carbon, (b) kaolinite, (c) mixed mineral powder, (d) orthoclase, (e) quartz and (f) haematite.

6.4.2 Temperature, species and growth-phase effects

In addition to the above data, detailing the interaction of *Leptolyngbya* sp. with mineral particles at room temperature, incubations were also conducted using *Phormidium* sp. cyanobacteria and a mixed mineral powder, and at a refridgerated temperature; Figure 25a summarises these results, detailing the change in both APC and aggregate size over the incubation period for various temperatures and biological parameters. Average trends indicate that, at 4°C, *Leptolyngbya* sp. cyanobacteria show a slight reduction in APC, combined with a c. 80% increase in aggregate size. Conversely, *Phormidium* sp. cyanobacteria show an increase in APC, but a far smaller increase in aggregate size, c. 10%. When compared to data collected at 21°C, the APC preservation can be seen to be much better for *Leptolyngbya* sp. at this higher temperature, and slightly better for *Phormidium* sp. cyanobacteria. As expected, associated with greater APC values, aggregate size is also slightly greater for both species at higher temperatures, but *Phormidium* sp. once again show smaller aggregate sizes. When a late exponential growth phase inoculum of *Leptolyngbya* sp. was used, preservation of APC was greater still, but average aggregate size was lower than for an early exponential growth phase inoculum.

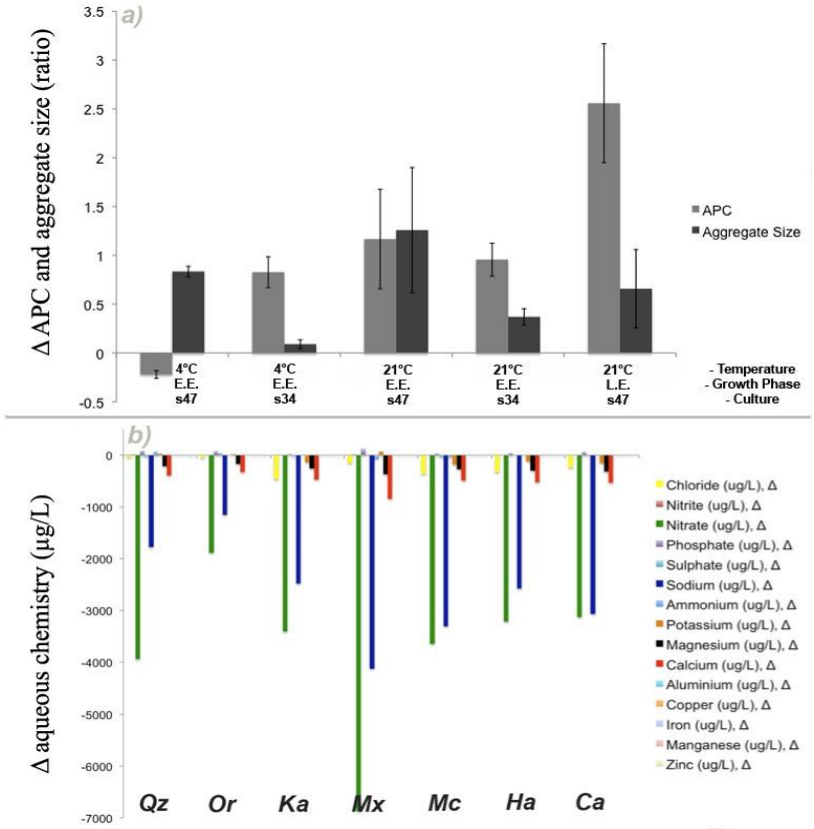

Figure 25: (a) Variation of APC and aggregate size with temperature and cyanobacteria species; error bars = standard error. (b) Average changes in the aqueous chemistry of incubation supernatant and their variation with mineral type; Qz = quartz, Or = orthoclase, Ka = kaolinite, Mx = mixed powder, Mc = mica, Ha = haematite, Ca = elemental carbon.

6.4.3 Aqueous chemistry analyses

Regarding aqueous chemistry changes in the incubation media over the course of the incubations (Fig. 25b), the majority of ions and trace metals were found to exhibit very small losses or gains (< ±10 μg/L, e.g. nitrite, copper, manganese and zinc). Calcium, magnesium and chloride showed average reductions of between 237 and 513 μg/L, whilst potassium showed average reductions in most incubations but average increases in quartz, orthoclase and mica incubations. Phosphate also showed a slight increase on average, although only the 64 mM ionic strength media showed this increase. Overall, increases and reductions in major ions and trace metals were < 1 mg/L, with those incubations conducted at 64 mM ionic strength showing far more change in aqueous chemistry than those conducted at lower ionic strengths. The two exceptions to this were sodium and nitrate. In all wells, and particularly in the 64 mM wells, significant decreases in sodium and nitrate were observed, averaging c. 2.6 and 3.7 mg/L respectively. All pH measurements were slightly alkaline (pH 7–8). End-point carbohydrate concentrations, analogous to free EPS concentrations, averaged 31.5 μg/mL in the 64 mM incubations, varying between c. 22 μg/mL (quartz, orthoclase and mica) and c. 70 μg/mL (mixed powder). In the 6.4 mM incubations, carbohydrate concentrations were approximately half of 64 mM incubation concentrations, whilst those in the 0.64 mM incubations were at or near the detection limit.

6.4.4 FTIR imaging of cyanobacterial aggregates

The spectra obtained from the FTIR imaging of cyanobacterial aggregates were typical of cyanobacteria, consisting of characteristic amide I and II peaks at c. 1650 cm^{-1} and c. 1570 cm^{-1} respectively, alongside lipid peaks between c. 2850–2960 cm^{-1}, carboxylic acid and protein peaks at c. 1380–1420 cm^{-1}, and carbohydrate peaks between c. 900–1200 cm^{-1}, as noted by several authors (Kansiz et al. 1999, Benning et al. 2004, Omoike & Chorover 2004, Dittrich & Sibler 2005, Pokrovsky et al. 2009, Fischer et al. 2010).

The transmitted light image of a sub-sample of the cyanobacteria from one of the control wells (Fig. 26a) details a thin layer, punctuated by some denser flocs. These dense clusters are highlighted well in chemical maps of the amide I region (Fig. 26a, i); often being the largest peak, the amide I data correlate well with the full spectrum intensity when mapped. Chemical maps of the lipid, carbohydrate and carboxylate regions (Fig. 26a, ii–iv) showed very similar patterns, with denser flocs showing greater quantities of these compounds, and an even spread overall, with little variance when compared against one another. These results show the ‘standard’ growth of these

cyanobacteria. Chemical mapping and visible imaging of a mixed powder aggregate (Fig. 26b) again showed clustering and dense regions of cyanobacteria, with total amide I (Fig. 26b, i), lipid (Fig. 26b, ii) and carboxylate (Fig. 26b, iv) intensity patterns showing relatively good correlation. The lipid chemical maps, in particular, showed mineral particles as regions of low intensity, with evidence for the encasement of these particles by bundles of cyanobacterial filaments. When quartz is the substrate of choice (Fig. 26c), the chemical mapping results are very similar. In both cases, high intensity carbohydrates showed a larger spread (Figs. 26b & 26c, iii), evidence of EPS production and the carbohydrate infilling of spaces between filaments and between filaments and mineral particles. Carbon (Fig. 26d) shows a similar story, but the spread of carbohydrates within the aggregate appeared to be at a lower intensity. Whilst it is acknowledged that silicate minerals do produce spectral peaks within the carbohydrate region, the frequently observed peak positions within the data (c. 1030, 1050, 1130, 1150 and 1165 cm^{-1}), modal maximum intensity peak (1050 cm^{-1}), lack of strong Si–O vibrations at c. 950 cm^{-1} and c. 800 cm^{-1}, and use of transmission mode all allow us to be confident that this carbohydrate 'region' is indeed representative of polysaccharides.

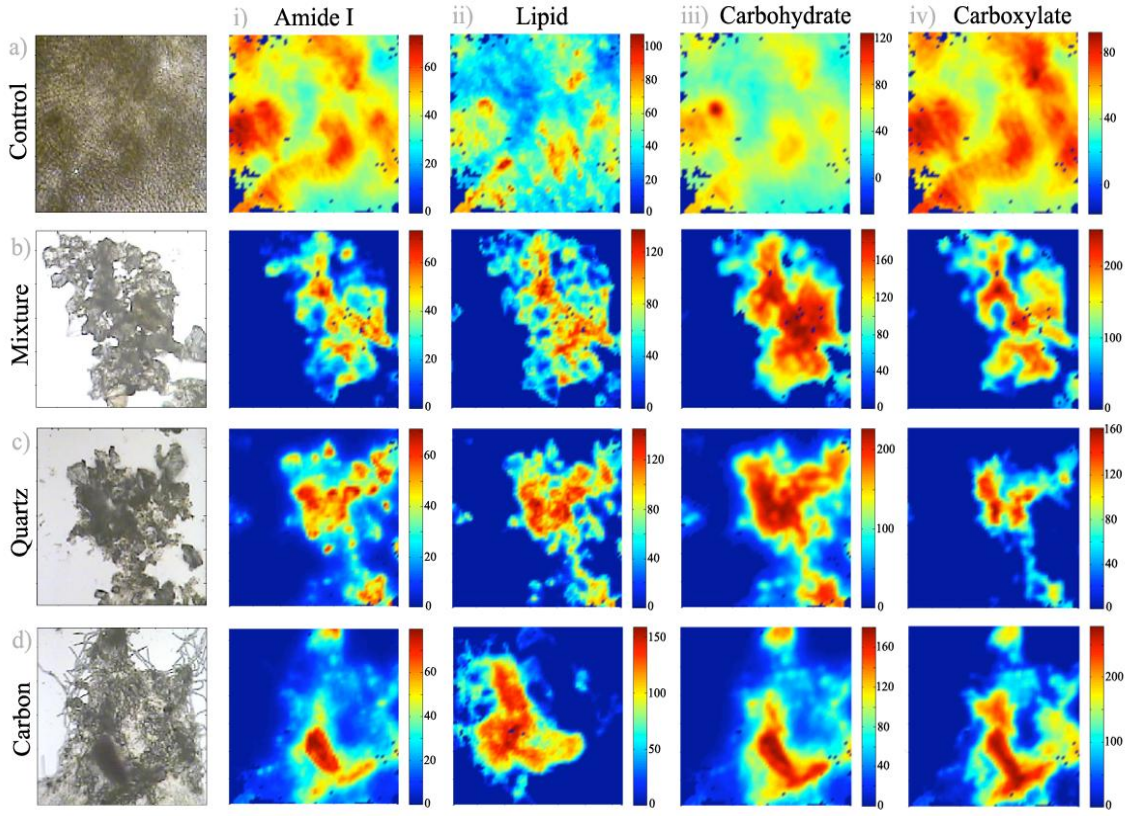

Figure 26: Chemical maps created from FTIR imaging spectra, detailing spatial variability in (i) amide I, (ii) lipid, (iii) carbohydrate and (iv) carboxylic acid/protein concentrations for (a) a Leptolyngbya sp. cyanobacteria control, (b) a mixed mineral powder, (c) quartz and (d) elemental carbon incubations; field of view = 256 μm square.

When comparing maximum relative intensity values (arbitrary units), amide I intensity was found to be relatively similar between all of the quartz (max. = 70), carbon (max. = 80) and mixed powder (max. = 70) aggregates, and when compared with the control (max. = 75). Maximum intensity values for the carboxylic acid region varied from 180 in the quartz aggregates to 270 in the black carbon aggregates, with the control and the mixed powder aggregates showing maximum values of 220 and 250 respectively. Both lipid and carbohydrate intensities were significantly greater in the aggregates than in the control, with lipid intensities being greatest in the black carbon aggregates (max. = 160, control = 110) and carbohydrate intensities being greatest in the quartz aggregates (max. = 220, control = 120). Both the black carbon and mixed aggregate data exhibited equally elevated maximum intensities (black carbon = 180, mixed = 190).

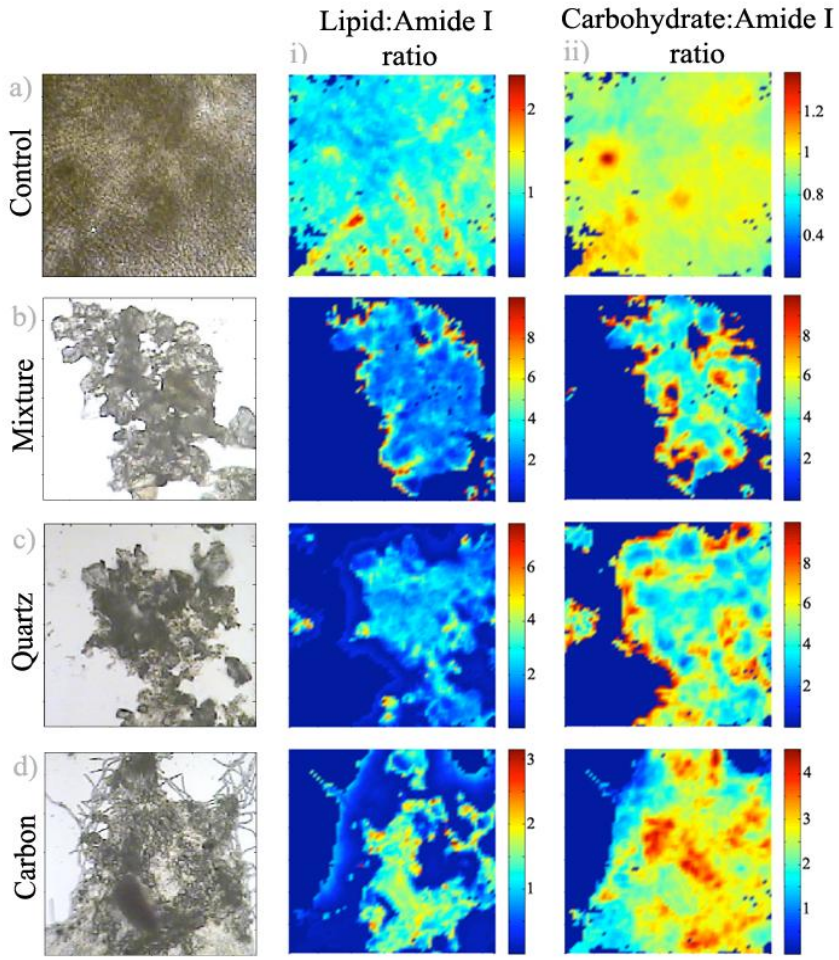

Figure 27: Chemical maps detailing the spatial variation in (i) lipid/amide I and (ii) carbohydrate/amide I concentrations for (a) a Leptolyngbya sp. cyanobacteria control, (b) a mixed mineral powder, (c) quartz and (d) elemental carbon incubations; field of view = 256 μm square.

Both lipid and carbohydrate peak regions were ratioed against the amide I peak (representing the cellular backbone), so that any relative excesses of lipids and/or carbohydrates could be visualised (Fig. 27). The resultant chemical maps for the control (Fig. 27a) showed large quantities of green and blue colours, indicating that carbohydrate intensities were relatively similar to amide I intensities across the images. Some small hotspots were visible though, where intensities were approximately twice that of amide I intensities. Both the mixed powder (Fig. 27b) and quartz (Fig. 27c) aggregates showed lipid intensities approximately 2–3 times greater than amide I intensities across the aggregates, with localised hotspots exhibiting ratios far higher than found in the control sample. In the case of the mixed powder, significant excesses of both lipids (Fig. 27b, i) and carbohydrates (Fig. 27b, ii) could be seen around the edge of the aggregate, with intensities up to 10 times greater than amide I intensities. Similarly, quartz showed relative carbohydrate enrichment (Fig. 27c, i) at the aggregate edge (max. = 10×), but less lipid enrichment (max. = 8×) and certainly lower lipid ratio values (Fig. 27c, ii) across the interior of the aggregate. Carbon aggregates showed a different relative pattern. As noted in the transmitted light image in Figure 4d, the carbon aggregate was slightly more floc-like, with a greater number of individual visible filaments. Chemical mapping data showed that a central cluster of cyanobacterial filaments is lipid enriched (Fig. 27d, i), by a ratio of 2:1 over the amide I region, but that the majority of the outer granule showed a lipid/amide I ratio of < 1. Conversely, a large area of the chemical map for the carbohydrate/amide I ratio (Fig. 27d, ii) indicated a three- or four-fold relative enrichment of carbohydrate compared with the amide I intensity peak.

Composite spectra (Fig. 28) highlighted the differences between aggregates formed with *Leptolyngbya* sp. and either carbon or quartz, and contrasted these with the control well, containing flocculated *Leptolyngbya* sp. cyanobacteria. Peak assignments for these spectra are detailed in Table 1.

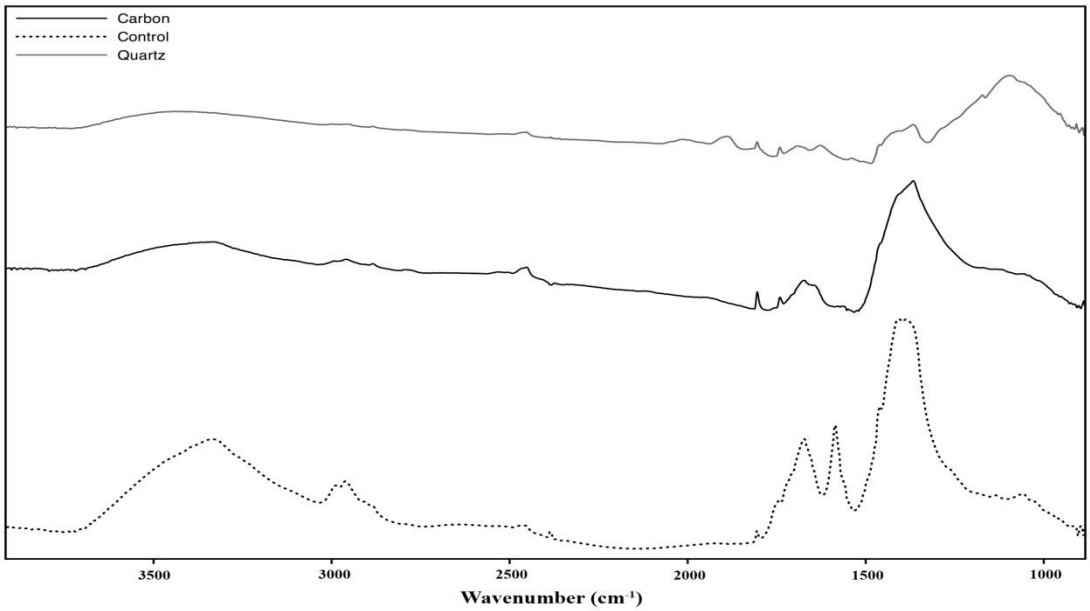

Figure 28: Composite spectra for cyanobacteria control (dotted), elemental carbon (black) and quartz (grey) incubations (stacked lines).

Allocation	**Carbon Aggregate**	**Cyanobacteria Control**	**Quartz Aggregate**
C–O–C & C–O of polysaccharides, Si–O bonds	883, 897, 909, 919, 947, 1029, 1049, 1059, 1114, 1126, 1134, 1163	889, 906, 916, 955, 1024, **1053**, 1071, 1081, 1095, 1109, **1130**, 1167	888, 903, 914, 924, 950, **1089**, **1164**
C–O & C–H stretch of amino acids & proteins, C–O stretch of carboxylic acids	**1355**, 1397, 1448	**1377**, **1396**, 1447	**1355**, 1395, 1449, 1495
C–H asymmetric stretch of proteins (Amine III)	1510, 1535, **1553**, 1563		**1526**, 1542
C–H & N–H stretch of proteins (Amide II)	**1631**	**1572**	**1613**
C=O stretch of proteins (Amide I)	**1657**	**1658**	**1676**
C=O stretch of lipids and fatty acids, O–acetylated carbohydrates	**1725**	**1726**	**1725**, 1741
C=O stretch of carboxylic acids	**1788**	**1788**	**1788**
Si–O–Si skeleton overtone vibrations			**1870, 1998**
Various N–H stretch vibrations of amino acids and proteins	2349, **2427**, 2480, 2507	**2362**, **2430**, **2443**, 2507	**2428**, 2481, 2497
Alkyl and aldehyde C–H stretch and asymmetric stretch of lipids and fatty acids	2764, **2853**, 2876, **2927**, **2959**, 3026, 3091	2769, **2855**, **2873**, **2929**, **2956**, 3027	2764, **2851**, 2876, **2925**, **2967**, 2992
O–H of water, N–H stretch of proteins	**3292**	**3298**	**3404**

Table 1: Peak identification table for FTIR composite spectra of cyanobacteria control, carbon aggregate and quartz aggregate incubations. Peak assignments are based upon Benning et al. (2004), Omoike & Chorover (2004), Heraud et al. (2005), Ojeda et al. (2009), Badireddy et al. (2010), and Fischer et al. (2010).

These composite spectra indicated that: (a) greater relative peak intensities of carboxylic acids and proteins were recorded in the control and elemental carbon incubations, (b) a substantially greater response in the carbohydrate region was clear for the quartz incubations, with variation in composition evident, and (c) amide peaks varied in both intensity and wavenumber across the samples. When comparing the carboxylate region, a reduction in the comparative intensity of the c. 1400 cm^{-1} band was evident in the mineral–cyanobacteria aggregates. This suggests a comparative increase in the amount of carboxylic acid groups, versus proteins, within the samples. When considering the amide I and II region, the amide I peak position remained relatively constant, shifting from c. 1658 cm^{-1} in both the control and elemental carbon incubations to c. 1676 cm^{-1} in the quartz incubation. The amide II position, however, varied significantly, from c. 1572 cm^{-1} in the control incubation to c. 1613 cm^{-1} in the quartz and c. 1631 cm^{-1} in the elemental carbon incubations. This has been previously noted when bacteria adsorb iron (oxy)hydroxide groups (Omoike & Chorover 2004). Within the polysaccharide fingerprint region, the peaks present can be said to, in general, correspond well with those for a mixed polysaccharide sample containing the six principal hexose sugars (Kaçurakova et al. 2000). When considering the elemental carbon aggregate, this polysaccharide functionality appeared to diminish, with no significant peaks being evident. Conversely, polysaccharide functionality was far higher when considering the quartz aggregate, potentially evidencing the formation of organo-silicon compounds (Kovac et al. 2002). Regarding lipid functionality, these composite spectra indicate characteristic lipid vibrations at c. 1725 cm^{-1} and between c. 2750–3000 cm^{-1}. An additional C=O peak was visible at 1788 cm^{-1}, indicative of carboxyl-rich amino acids, such as glutamic acid (Barth 2000), and found to be an important constituent of certain EPS types (Kawaguchi & Decho 2002).

6.5 Discussion

6.5.1 Co-aggregation of cyanobacteria and mineral particles

To summarise, the data from the incubation experiments indicated that the number of live and photosynthetically active cyanobacterial cells incorporated into aggregates, as measured by the APC, was dependent upon the ionic strength of the media, and thus upon the nutritional state. Low ionic strengths led to, in general, a plateau or slight fall in APC values, whilst high ionic strengths promoted growth to a varying degree. This is

in agreement with other studies of cyanobacterial flocculation and attachment (Kiørboe et al. 1990, Sekar et al. 2004, Silva & Silva 2007, Kim et al. 2010). Furthermore, nutrient limitation, such as iron limitation (Silva & Silva 2007), can alter the chance of and capacity for aggregation (Kiørboe et al. 1990). In a similar vein to the APC, aggregate size showed dependence upon ionic strength, although multi-aggregation and break up contributed to a large AAD in these data values. Considering this deviation and when two outliers were removed, APC and aggregate size showed a linear trend with moderate fit (R^2 = 0.575). These simplified laboratory experiments thus do not show as good a fit, between filament count and aggregate size/stability, as for data from natural systems (Langford et al. in prep. 2012b). Given the deviation of these data from the trend line, it can be seen to support the fact that other parameters are affecting aggregate size and stability in these simplified systems. As with all natural microbial aggregates, both the abundance of EPS and the surface properties of the mineral particles are considered likely to contribute to this variation, as noted in similar experiments (Guenther & Bozelli 2004, Sekar et al. 2004, Bhaskar et al. 2005). In these experiments, pH was not found to significantly affect aggregation. In fact, in all experiments, pH values were found to trend towards pH 7–8. This pH range is well known as being the most favourable for cyanobacterial growth, and indeed the uptake of calcium in most of the wells points to the homeostatic maintenance of a circum-neutral pH by the cyanobacteria (Giraldez-Ruiz et al. 1999). As such, nutrient supply, and its subsequent control over cyanobacterial growth, motility and EPS production, was found to be important in the co-aggregation of cyanobacteria and mineral particles.

Previous studies into the co-flocculation or co-aggregation of cyanobacteria and mineral particles have largely focused on clays (e.g. Bar-Or & Shilo 1988, Guenther & Bozelli 2004, Kim et al. 2010), whilst occasionally focusing on other minerals, such as iron oxides (e.g. Pan et al. 2006). This study utilised a broader suite of prevalent natural minerals, finding that aggregation does indeed vary with mineral type. When APC and aggregate size are considered together, distinct differences in aggregation can be noted, from continued proliferation and incorporation in elemental carbon incubations to initial proliferation and incorporation, followed by cellular senescence, inactivity and/or death, as exhibited in quartz incubations. Between these two end-points, the mixed mineral powder incubations showed a tailing off of the APC, combined with a reduction in aggregate size, but to a lesser degree than for quartz. Furthermore, ratioed values indicated a spike in APC on day 2, signifying rapid initial co-flocculation. The release of excess EPS, which increases the stickiness of colliding cyanobacteria, modifies mineral surfaces and enhances co-flocculation, is often invoked to explain this rapid attachment (Avnimelech et al. 1982, O'Melia & Tiller 1993, Kovac et al. 2002, Bhaskar et al. 2005). Elemental carbon exhibited the greatest co-aggregation and this can be attributed, in part, to hydrophobic interaction, which is known to be highly important

for cyanobacterial attachment to mineral surfaces (Bar-Or & Shilo 1988, Liu et al. 2004, Sekar et al. 2004, Ivanova et al. 2006). Suspensions of coal dust have been effectively flocculated using cationic polysaccharides (Pal et al. 2008), with similar high-molecular-weight polysaccharides being characteristic of cyanobacterial EPS (Klock et al. 2007, Pereira et al. 2009). It has also been shown that greater proportions of acetyl groups, peptides and/or de-oxy sugars confer hydrophobicity in some types of EPS (de Phillipis & Vincenzini 1998, Dignac et al. 1998, Jorand et al. 1998, Richert et al. 2005). In contrast to elemental carbon, mineral particles with greater resistance to weathering, such as quartz, did not sustain an increasing APC, suggesting that these cyanobacteria may be experiencing nutrient limitation in the system and/or that certain lithologies are more conducive to growth. Whilst the quartz APC declined, the mean aggregate size grew initially and then remained relatively constant. This suggests that EPS production and physical enmeshing by the filament sheaths play a part in aggregate stability, regardless of the fraction of living biomass, in agreement with others (Fenchel & Kühl 2000, Chaignon et al. 2002); the fact that the aggregates in this study were not found to disperse upon dilution adds further support to this.

Further differences in aggregation were witnessed with temperature, with *Leptolyngbya* sp. cyanobacteria in particular showing increased proliferation and incorporation at higher temperatures, as well as showing better aggregation when an early exponential growth phase inoculum was used, as seen in other investigations (Sekar et al. 2004). Conversely, *Phormidium* sp. cyanobacteria appeared to show a degree of cold adaptation, showing slower growth, maintaining cell numbers and producing stable aggregates at lower temperatures. The importance of slow-growing organisms to the stability of biofilms has been demonstrated previously (Zippel & Neu 2005). As noted in experiments by Davey and O'Toole (2000), there was evidence in aqueous chemistry data for trace metal enrichment of cyanobacterial aggregates, indicating their usefulness in cyanobacterial growth and aggregation. Uptake of calcium and magnesium, as noted in this study, was expected, as they are required for the synthesis of chlorophyll and photosystem II activity in cyanobacteria, with calcium also being involved in phosphate uptake (England & Evans 1983, Baker & Brand 1985, Keurson et al. 1984). Nitrate and sodium concentrations showed the most dramatic fall, which is evidence of the nitrogen demands of cyanobacteria and of sodium-dependent nitrate transport (Lara et al. 1993). Glacier hydrochemistry studies have previously revealed an excess of nitrate anions in glacier ice, and have suggested that cyanobacterial mats cause down-stream reductions in nitrate concentrations (McKnight et al. 1999, Fortner et al. 2005) Overall, the aqueous chemistry data are representative of nutrient uptake by cyanobacteria, offset by small dissolution inputs, such as rubidium from the mica.

6.5.2 Biogeochemistry of aggregate formation

FTIR imaging data showed a larger spatial spread of relatively abundant carbohydrates in all mineral–cyanobacteria aggregates studied, indicating that the production of carbohydrate-rich EPS occurs concurrently with co-aggregation. This has been shown in a variety of bioaggregates (Kovac et al. 2002, Omoike & Chorover 2004, Geoghegan et al. 2008, Sartoni et al. 2008, Badireddy et al. 2010) and is indicative of the release of free EPS. Indeed organic matter extracted from natural phototrophic mats shows good spectral correlation with high-molecular-weight polysaccharides (Fischer et al. 2010), indicating their importance in cell–mineral interaction in natural aggregates.

Imaging data and composite spectra also indicated that (a) lipid and carboxylate/protein intensities were greatest in elemental carbon incubations, whilst (b) carbohydrate intensities were greatest in quartz incubations. Omoike and Chorover (2004) note that a high relative abundance of C=O moieties is indicative of the dominance of bound (or capsular) EPS. In fact, further C=O moieties, suggestive of carboxyl-rich amino acids (Barth 2000), are highlighted on the composite spectra. Furthermore, shifts in both the amide I and II peaks are associated with modifications to the protein structure and/or absorption of minerals onto these proteins (Omoike & Chorover 2004, Badireddy et al. 2010). An increase in the relative concentration of antiparallel β-sheets (1680–1695 cm^{-1}) may well account for the shift in the amide I peak (Badireddy et al. 2010). In addition, an increase in the relative concentration of such structures as β-sheets, random coils and aggregated strands (1610–1645 cm^{-1}) may account for the shift in the amide II peak. This high proportion of carboxylic acids, when combined with modifications in secondary protein structures and the presence of O-acetylated carbohydrates (1725 cm^{-1}), is said to be indicative of the presence of copious and acidic EPS (Nivens et al. 2001, Badireddy et al. 2010); all of these groups have been shown to be important in bioflocculation. *Leptolyngbya* species of cyanobacteria have been shown to possess both capsular and free EPS (De Philippis et al. 2005).

High carbohydrate intensities and an increase in functionality point towards increased polysaccharide–cation interaction and the formation of organo-silicon compounds (Kovac et al. 2002, Mecozzi & Pietrantonio 2006). As noted earlier, the polysaccharide fingerprint shows marked similarity to that of a mixed polysaccharide sample composed of the glucose, mannose, galactose, xylose, arabinose and glucoronic acid (Kaçurakova et al. 2000). Whilst the Si–O vibrations and C–O/C–O–C vibrations in this area are likely to overlap (Benning et al. 2004, Stehfest et al. 2005), the strong ionic quartz responses (Benning et al. 2004, Nakamoto 2009) are not visible in the composite

spectra. As such, in the case of the quartz incubations, the region as a whole can be said to be (a) representative of free EPS carbohydrates and (b) responding to increased interaction between polysaccharide functional groups and silica functional groups. In marine aggregates, carbohydrate–cation interaction has been shown to be important in aggregation (Leppard 1995).

When the ratios of both lipids and carbohydrates to the amide I peak were mapped, an excess of lipids and carbohydrates at the edge of the aggregate was apparent. It is considered that this is both evidence of the tight clustering of cyanobacterial filaments towards the centre of the aggregate and evidence for the production of excess EPS at the aggregate edges, in order to attract and encapsulate fresh mineral particles and/or further cyanobacterial filaments. To summarise, differences in the biogeochemistry of aggregation between *Leptolyngbya* sp. cyanobacteria and mineral particles are clear. In one instance (the case of elemental carbon), free EPS is comparatively diminished and bound EPS can be seen to dominate. Spectra indicate that interaction between cyanobacteria and mineral particles is likely dominated by protein–cation aggregation, with both the cationic mechanism (acidic regions dominated by carboxylic acids) and hydrophobic interaction valid (Mecozzi & Pietrantonio 2006). In another instance (the case of quartz), less bound EPS functionality is visible, whilst free EPS is either comparatively enriched or its functionality and interaction is enriched. Spectra indicate that interaction between cyanobacteria and carbohydrates is likely dominated by polysaccharidic components and organo-silicon interaction. These differences in attachment may well be down to the hydrophobicity of the material, with carbohydrate-based attachment dominant in hydrophilic conditions but proteins contributing more in hydrophobic circumstances (Jorand et al. 1998). Unfortunately, end-point FTIR analyses meant that any changes in the biogeochemistry of aggregation over time could not be elucidated.

6.5.3 Insights into the development of cryoconite granules

Investigations into the microstructure of cryoconite have revealed that these aggregates contain large numbers of photoautotrophic microorganisms, particularly cyanobacteria, and that carbohydrates, specifically EPS, are important for their aggregation (Takeuchi et al. 2001b, Langford et al. 2010, Stibal et al. 2010). Cryoconite granules have been found to be heterogeneous, showing evidence of the clustering of both photoautotrophic and heterotrophic microorganisms (Langford et al. 2010), whilst one or several laminar growth layers have been evidenced by some authors (Hodson et al. 2010, Takeuchi et al. 2010). It has therefore been suggested that the mechanisms central to their formation are those of bioflocculation, associated EPS production and filamentous binding (Langford

et al. 2010). The importance of EPS in producing a heterogeneous matrix, with a large surface area for both physical encapsulation and chemical adsorption, has been highlighted for a number of natural aggregates, mats and biofilms (e.g. Leppard et al. 1996, Kawaguchi & Decho 2000, Sutherland 2001, Donlan 2002, Simon et al. 2002, Brehm et al. 2004, Sekar et al. 2004, Mecozzi & Pietrantonio 2006, Fischer et al. 2010). Organic matter analyses of cryoconite have found a dominance of aliphatic and polysaccharidic components (Langford et al. 2011), showing similarities with other studies (Kovac et al. 2002, Fischer et al. 2010).

Microstructural investigations of cryoconite granules have evidenced the binding of cyanobacteria to silicate minerals (Stibal et al. 2008a). More detailed ultra-structural investigations have determined the presence of various types of EPS, from striated alginate structures to fibrillar and globular EPS (Langford et al. in prep, 2012a). Along with photoautotrophic filaments, EPS is fundamentally involved in the binding of cryoconite aggregates. Furthermore, the interactions of clay and colloidal iron (oxy)hydroxide particles with polysaccharides are seen to be important within the aggregate structure.

Field studies have not only highlighted the spatial variability in carbohydrate and chlorophyll concentrations across glaciers and ice sheets (Langford et al. 2010, Stibal et al. 2010, 2012), but also found that filament length correlates well with aggregate size and stability (Langford et al. in prep, 2012b). This study finds that both mineral type and ionic strength affect photoautotrophic aggregate development in a simplified system, with elemental carbon in particular supporting continued growth and aggregate development. In addition, this study highlights the complex and variable interactions between both the bound and free EPS of cyanobacteria and mineral particles (conceptualised in Figure 29), from aggregation dominated by hydrophobic and cationic protein interactions to aggregation dominated by hydrophilic polysaccharidic carboxylic interactions and the formation of organo-silicon compounds.

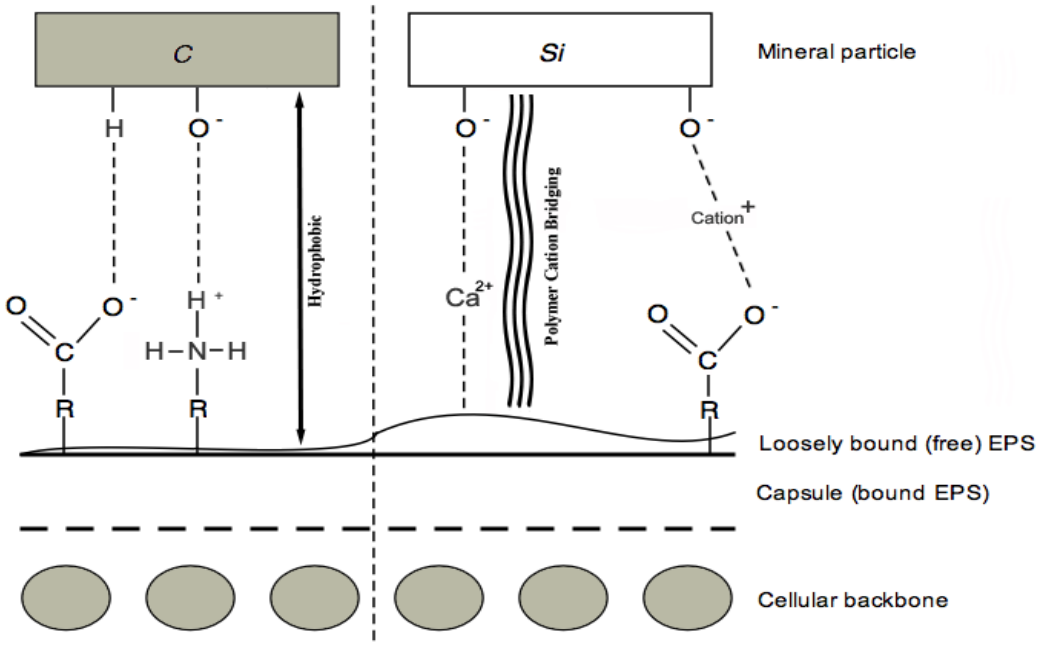

Figure 29: A conceptual diagram highlighting the principle mechanisms of cell–EPS–mineral interaction involved in cryoconite granule formation, based upon the findings of this study and upon previously reported literature.

6.6 Conclusions

This study represents the first laboratory examination of the relationship between ice surface biota and atmospheric impurities. Filamentous cyanobacteria were found to readily flocculate and co-aggregate with a variety of minerals, utilising bound and free EPS to bind minerals within an organic matrix that is dominated by a network of filaments. Binding mechanisms were found to vary between mineral types, with direct binding of elemental carbon to the cyanobacterial capsule allowing continued growth and aggregation, and organo-silicon interactions between bound and free EPS contributing to aggregation in quartz. The long-term stability of aggregates dominated by resistant lithologies such as quartz seems unlikely, as these laboratory experiments indicated that growth-limitation and cellular senescence were occurring, likely due to nutrient limitation and/or radiation damage. With regard to nutrient limitation, nitrate was identified as potentially nutrient-limiting in this artificial environment. Conversely, elemental carbon, an abundant component of aeolian debris in Arctic ecosystems, can be said to both enhance aggregation and promote growth. Finally, these data support the suggestion that bioflocculation, EPS production and filamentous binding are dominant in the formation of cryoconite granules.

6.7 Acknowledgements

H. Langford acknowledges Z. Namsaraev for the cyanobacterial isolates used in this study. Confocal microscopy was undertaken in the Confocal Imaging Facility at the Kroto Research Institute, and FTIR imaging was undertaken at the Manchester Interdisciplinary Biocentre.

CHAPTER SEVEN: SUMMARY OF RESULTS AND CONCLUSIONS

7.1 Summary of results

7.1.1 The microstructure and biogeochemistry of Arctic cryoconite granules

A suite of complementary techniques, namely optical microscopy of mineralogical thin sections, powder X-ray diffraction (XRD) and KBr pellet FTIR analyses (chapter 2), determined that Arctic cryoconite is dominated by phyllosilicate, tectosilicate and quartz minerals. A composite XRD profile highlighted the prevalence of quartz, whilst smaller peaks evidenced the presence of weathered feldspars, micas and clays in smaller quantities. This mineralogical profile agrees with both FTIR data and the mineralogical assessments of others (Takeuchi et al. 2001b, Stibal et al. 2008a, Hodson et al. 2010). Optical microscopy provided additional data concerning intra-granule spatial structure. These data indicated that surrounding the mineral particles there is, to a greater or lesser degree, a fine and poorly crystalline to amorphous, largely organic groundmass. This groundmass showed varying degrees of humification and pigmentation, with zones of darker, opaque organic matter and lighter, translucent regions, likely dominated by EPS. These data, when considered alone, provide insight into the heterogeneity of cryoconite, with the presence of a fine organic groundmass suggesting an associated abundance of microorganisms, forming microenvironments, interacting with mineral particles and promoting adhesion and aggregation. Furthermore, the significant quantities in which this organic material is present suggests that microorganisms may be producing either an excess of organic matter or, alternatively, recalcitrant organic matter with aggregation further acting as a protection mechanism for this (Six et al. 1998, Stibal et al. 2006, Carson et al. 2009).

Considering specifically the organic matter within cryoconite, Chapter 2 demonstrated that the total organic carbon content of Arctic cryoconite varied between 1.30% and 6.07%, with this organic carbon dominated by the thermo-labile fraction (Kristensen 1990), i.e. carbohydrates. These organic carbon values are comparable with others determined (e.g. Stibal et al. 2008a) and are also significant, considering that conditions for the growth of microorganisms and accumulation of organic carbon are not conducive for a sizeable proportion of the year. Chapter 3 evidences that, when

combined with a simple extraction protocol (Giovanela et al. 2010), the geochemistry of cryoconite organic matter can be effectively studied using FTIR spectroscopy. When combined with principal component analysis (PCA), differences in both mineralogy and geochemistry can thus be elucidated. For cryoconite from Aldegondabreen glacier, Chapter 3 demonstrated that the larger 'centimetre-size' granules at location AG1 contain calcite and dolomite. Furthermore, a comparatively larger compound peak at c. 900–1100 cm^{-1} can also be taken as evidence for greater quantities of clay within this sample (e.g. Madejova 2003). These data are useful in that they support the notion that clay–organic matter interactions may be particularly important in certain cryoconite granules, allowing them to become larger than they otherwise would. FTIR spectra of organic matter extracts revealed that the fraction was dominated by fatty acid and polysaccharide signatures, whilst PCA analyses of organic matter extracts revealed that cryoconite closer to the glacier edge showed a less diverse composition of organic matter and a more mineralogical signature. Recent investigations (Stibal et al. 2012) find that distance from the margin is the most significant factor in explaining variance in organic carbon accumulation upon the Greenland ice sheet. This suggests that spatial variations in both supraglacial physico-chemical parameters and in the mode of particulate input can affect cryoconite debris biogeochemistry.

In addition to the above mineralogical and geochemical data, Chapter 2 also provides data on the biology and biochemistry of Arctic cryoconite. In agreement with recent research (Takeuchi et al. 2001b, Stibal et al. 2006, 2008a, Hodson et al. 2010), Chapter 2 indicated that cryoconite granules harbour significant numbers of both photoautotrophic and heterotrophic microorganisms, with heterogeneous clustering, association with both mineral and organic matter and a near-surface network of filamentous cyanobacteria all evident. A range of cyanobacterial morphotypes, analogous to those of other glacial environments (e.g. de los Ríos et al. 2004), were identified: i.e. *Leptolyngbya*, *Phormidium*, *Oscillatoria* and *Synechococcus* species. With the exception of the near surface, where parallel orientation was exhibited to an extent, cyanobacterial filaments were found to be randomly oriented, unlike in laminar mat ecosystems (de los Ríos et al. 2004, Wrede et al. 2008). Noticeable also was the fact that aggregates impoverished in filamentous microorganisms exhibited greater fragility upon agitation, suggesting that filaments play an active role in stabilising cryoconite aggregates.

It is known that EPS plays an important role in aggregate formation and stability in other environments, such as in marine snow, stromatolite microspheres and aerobic granular sludge (Simon et al. 2002, Brehm et al. 2004, Chen et al. 2007a). The FTIR analyses in Chapter 3 and investigations into the organic matter within cryoconite (Xu et al. 2010) reveal a dominance of microbial fatty acids and polysaccharides, pointing to autochthonous carbon production as significant. Chapter 2 indicated that, in the Arctic cryoconite granules studied, polysaccharides, as stained by AlexaFluor 488 concanavalin A, were widespread throughout the granules, as well as being intimately associated with clusters of photoautotrophs. The capsular EPS of cyanobacteria has been proposed to be, to an extent, recalcitrant to mineralisation (de Winder et al. 1999). Further studies highlight the importance of EPS in promoting coagulation by altering surface charge, in trapping particulate matter, aiding nutrient absorption, and in providing protection from abiotic stresses, such as over-winter freezing (Leppard 1995, Adav et al. 2010). Chapter 2 also indicates that the darker and denser aggregates dominated by cyanobacterial filaments tended to be less fragile, indicating that microbial composition, particularly the presence of filamentous cyanobacteria and associated EPS, fundamentally affects cryoconite aggregate structure.

Whilst Chapters 2 and 3 further our knowledge of cryoconite microstructure and biogeochemistry, Chapter 4 provides ultrastructural detail, allowing cell–mineral interaction within cryoconite to be probed. Chapter 4 utilised techniques and sample preparations, namely ESEM, low-vacuum SEM, heavy metal staining and hydrophilic embedding, designed to provide improved preservation and resolution of biological material. SEM techniques, whilst not reaching the higher magnifications of TEM, provided excellent detail of hydrated EPS enmeshing the granule surface, as well as of the variety of unicellular and filamentous microorganisms present, from fungal hyphae to algae and cyanobacteria. Also clear were both the attachment of mineral particles to filaments and the clustering of heterotrophic bacteria next to visible EPS, noted as being striated and similar to alginic acid structures (Andrade et al. 2004). Chapter 4 also highlighted the principal drawback of SEM-type techniques when examining heterogeneous biological samples – the fact that EPS acts to smooth out features of interest (Priester et al. 2007). To address this, and to enable useful high-resolution correlative microscopy (de los Ríos et al. 2004, Wrede et al. 2008), cryoconite granules were embedded in a hydrophilic embedding resin (to preserve antigens and hydrated

structures) and ultrathin sectioned on a microtome, for subsequent analysis by both CLSM and TEM.

The CLSM results in Chapter 4 highlighted a dense surface network, to c. 70 µm depth, dominated by cyanobacteria. Within this, a variability in biomass distribution suggested laminar development, and a reduction in biomass volume at the surface indicated that periodical and significant EPS production here might be the chief strategy for growth. In other bioaggregates, a greater proportion of carbohydrate-rich EPS has been found in the outer layer of the aggregate (de Beer et al. 1996, Liu et al. 2004, Li et al. 2011). An EPS-rich surface layer has been associated with: higher nutrient availability at biofilm surfaces (Zhang & Bishop 2001), greater shear strength of aggregates (Batstone & Keller 2001), cryoprotection (Marx et al. 2009) and UV protection (Gao & Garcia-Pichel 2011). Containing a density of functional groups and exhibiting stickiness (Adav et al. 2010), EPS can also capture particulate matter and nutrients from the water column (Golubic et al. 2000). TEM micrographs confirmed the dense organo-mineral structure suggested by SEM and glimpsed by analyses within Chapters 2 and 3.

In particular, nanometre-sized strands of fibrillar EPS were clearly visualised, adhering to mineral grains, potentially via cationic bridging as postulated previously (Decho & Herndl 1995, Leppard et al. 1996), and filling void spaces. Furthermore, Chapter 4 evidences the association of the capsular EPS of filamentous cyanobacteria with nanometre-sized mineral particles, likely clays and/or metal (oxy)hydroxides. Previous research has identified analogous features, termed ‘clay hutches’ (Lünsdorf et al. 2000), which have been proposed to improve water retention (Chenu 1993) and solar protection. It is clear that cryoconite ultrastructure is permeated with significant quantities of EPS, and that many of the microorganisms within the granule exhibit a large capsular sheath, readily incorporating particulate matter. This is consistent with the cyanobacterial filament and EPS matrix acting as a sieve for aeolian fines that are surficially deposited at the site of cryoconite granule formation.

Chapters 2, 3 and 4 thus provide a substantial investigation of cryoconite microstructure and biogeochemistry. They highlight the ubiquitous presence of photosynthetic microorganisms within cryoconite aggregates, the existence of significant quantities of both capsular and free EPS within these granules, and the

significant interaction between organisms, EPS and mineral particles, particularly smaller aeolian fines, such as clays. These results have several important implications. Regarding particulate transport, the presence of significant quantities of cyanobacterial capsular and free EPS, associated with cryoconite and within the weathering crust, likely strongly limits the supraglacial and englacial transport of aeolian particulates, by instigating biologically-mediated aggregation and differential melt. Given the previously characterised stickiness and polymeric bridging abilities of EPS, an important question to ask is: to what degree is particle incorporation selective? Regarding heterogeneity, EPS plugging of pore spaces (Fischer et al. 2010) can modify the biogeochemical environment by slowing down the flow of water. Cell–mineral interaction must also produce heterogeneity. It has been suggested that abiotic factors are more important than geographical location in determining microbial diversity and abundance (Wieland et al. 2001). Further, primary production and bacterial oxidation likely maintain steep redox gradients within aggregate systems (Golubic et al. 2000). As such, it is likely that grain-scale differences in cryoconite granule aggregation and biogeochemistry are ubiquitous within the supraglacial ecosystem. Regarding aggregate microstructure, the interaction between weathered phyllosilicates and the carbohydrate-rich groundmass, with clay minerals being impregnated with EPS (Kilbertus et al. 1979) and organo-silicon compounds likely forming (Kovac et al. 2002), provides conducive conditions for the bio-alteration of minerals. The importance of bio-alteration and bio-accumulation within cryoconite granules is, at present, unknown. Finally, regarding aggregate stability, the presence of sheathed and motile species of cyanobacteria (e.g. *Oscillatoria*), combined with the suggestion that capsular EPS can show recalcitrance (de Winder et al. 1999), implicates accumulated sheath material in having a significant role in aggregate development and stability, as has been determined in cyanobacterial mats (e.g. Fenchel & Kühl 2000). Furthermore, if aggregate stability is intimately linked to the photoautotrophy and associated EPS production, a degree of spatial variability, associated with solar radiation receipt, should be observed on glacier surfaces.

As discussed in detail in Chapter 2, these data and current knowledge enable a hypothesis for cryoconite aggregation to be developed. Chapter 2 proposes that aggregation begins in the wet snow, within which physical ‘straining’, photosynthetic bloom activity (and associated EPS production) and self-flocculation of aeolian particulates (e.g. via hydrophobic or orthokinetic means) lead to microaggregate

formation. Recent investigations into the metagenomics of snow upon Arctic glaciers have determined that snow chemistry drives microbial community structure, and that genes for EPS and pigment production dominate the early ablating snowpack (Larose et al. 2010). Adhesion of further particulate matter, due to the presence of copious EPS, enlarges these microaggregates and, combined with the presence of dark particulates (e.g. elemental carbon and soot), creates sinking and differential melting of these aggregates into the ice. Further to this initial bioflocculation, filamentous binding of certain aggregates increases their density and stability (Jorand et al. 1998, Folkersma et al. 1999, Liu & Fang 2002, Tsuneda et al. 2003, de Kreuk & van Loosdrecht 2004, Hodson et al. 2010). With this hypothesis emphasising the importance of photosynthetic microorganisms and labile organic matter in the formation of cryoconite granules, it was concluded to be important to further study these biological controls on aggregation, both experimentally in the laboratory and in the field.

7.1.2 Geospatial mapping of the biological controls on cryoconite granule physical characteristics

The microstructural evaluation of cryoconite granules revealed that photosynthetic microorganisms and carbohydrates, in the form of EPS, were vital to their cohesion. Indeed previous research finds that carbohydrate contents and pigment concentrations (as a proxy for photoautotroph abundance) significantly increase the threshold for sediment erosion (Underwood & Paterson 1993, Sutherland et al. 1998). Chapter 5 provides a geospatial study of these key biological controls upon cryoconite aggregation and stability. Whilst recent investigations have studied biogeochemical parameters along a Greenland ice sheet transect, including carbohydrate and chlorophyll contents (Stibal et al. 2010, 2012), Chapter 5 maps carbohydrate and pigment concentrations, as well as mean aggregate size, across the entire ablation area of an Arctic valley glacier, Longyearbreen – something that had not yet been achieved.

Contour mapping of carbohydrate concentrations determined that a greater average carbohydrate concentration was present up-glacier at the time of sampling. As noted within Chapter 5, recent work upon the Greenland ice sheet indicated that the thinner, autotrophic sediments up-glacier showed a dominance of labile carbohydrates (Cook et al. 2010, Stibal et al. 2010, 2012). In fact, carbohydrate-rich EPS, as is produced by cyanobacteria (Pereira et al. 2009), is often produced as a precursor to freezing by cold-tolerant microorganisms (Vincent 2007), and is also promoted in nutrient- (particularly

phosphorus) limited environments (Obernosterer & Herndl 1995). As such, recently ablated cryoconite and young, recently formed aggregates could be expected to contain proportionally higher concentrations of labile carbohydrates. Furthermore, carbohydrate concentrations showed evidence of 'hotspots' of high concentration; this was noted as evidence for phototrophic bloom activity. These blooms are known to take place particularly upon the ablating snow surface (Newton 1982, Müller et al. 1998, Stibal and Tranter 2007). More recently, research has indicated that hydraulic dilution plays an important role in terminating these blooms (Schwiertzke-Wade et al. 2011), which, upon a sloped glacier and within a weathering crust (Irvine-Fynn et al. 2011), would result in accumulations of 'bloom' material in certain depressions, or hotspots. Finally, carbohydrate concentrations showed raised values towards the edge of the glacier, suggesting allochthonous input of microorganisms and/or organic matter from the glacier sidewalls. Overall, the geospatial distribution of carbohydrates can be said to be indicative, therefore, of both autochthonous input (and associated cryoprotection and nutrient scavenging) and allochthonous input.

Chlorophyll *a*, being the principal photosynthetic pigment, is present in all photoautotrophic microorganisms and, as such, is a useful proxy for photoautotroph abundance within sediments. The chlorophyll *a* concentrations mapped in Chapter 5 indicated less localised variability, when compared to carbohydrate concentrations, and a general increase in average concentrations towards the glacier terminus. As noted, there is analogous evidence within the literature that a down-glacier reduction in physical disturbance, a trend seen in biofilms within glacial streams (Battin et al. 2001), can explain changing chlorophyll concentrations. Upon the glacier surface (illustrated pictorially in Figure 2, Chapter 1), a down-glacier transformation from a distributed 'weathering crust' network to an ablated surface truncated by major supraglacial flow paths (Irvine-Fynn et al. 2011) could provide this reduction. Indeed the region of the main supraglacial stream is concomitant with reduced chlorophyll *a* concentrations in the centre of the ablation zone. Secondly, the sampling regime undertaken at Longyearbreen glacier was discrete and, as such, both the period of exposure following melt and the solar radiation receipt have to be considered as potentially significant variables. With the melt of the winter snowpack and superimposed ice proceeding up-glacier, with altitude, the terminus of a glacier is exposed first and may possess suitable conditions for photosynthesis for several days to weeks longer in each summer ablation

season. As such, a slightly elevated average chlorophyll *a* concentration at the glacier terminus is entirely reasonable. However, as with the carbohydrate data, some hotspots are also evident, particularly along the northwestern edge. Although allochthonous input of pigment-rich material, e.g. from lichens, may explain some of the variance, the aspect and comparative lack of shading of this portion of the glacier is considered likely to enhance solar radiation receipt and thus photoautotrophy. Finally, species-specific variation in chlorophyll concentration, as well as in response to key growth parameters, namely temperature and phosphorus supply, have been determined in other environments (Chen et al. 2011). Although the temperature difference will be negligible, up-glacier nutrient limitation or variations in the number of low-light adapted photoautotrophs, for example, could well affect chlorophyll *a* concentrations. Whilst this is undoubtedly significant at aggregate scale, it is considered to be insignificant at glacier scale.

Chapter 5 highlighted the difficulties in extracting phycobiliproteins, due to the robustness of cyanobacterial cells, the complex and EPS-rich substrate, and the lower cell numbers present within natural samples. Indeed a combination of physical and chemical techniques was necessary, as noted by Lawrenz et al. (2011). Spatial mapping showed low variability, indicating a relatively constant cyanobacterial biomass, in agreement with findings on Himalayan glaciers (Segawa & Takeuchi 2010). In agreement with chlorophyll *a* data, phycobiliprotein concentrations were found to increase towards the glacier terminus. Not only does this act to validate the accuracy of the chlorophyll measurements, but it again suggests that a combination of hydraulic stability, solar radiation receipt and exposure time likely controls cryoconite granule pigment concentrations. Once more, concentration hotspots were evident, noted as suggestive of the cyanobacterial tendency for clustering (Stibal et al. 2010) and/or of allochthonous input. Furthermore, photo-physical factors, such as the motility of the cyanobacteria (Kruschel & Castenholz 1998) and the position of aggregates within ice (analogous to the photic zone; Jørgensen et al. 1987), could also be expected to contribute to the spatial variability observed.

Chapter 5 determined that granule size showed the greatest spatial variance, with generally larger average granule sizes towards the glacier edges, away from the principal supraglacial stream, and slightly larger granules down-glacier. It has previously been noted that stability allows extended microbial growth and organic

matter production (Takeuchi et al. 2010, Telling et al. 2012). As such, greater cell–mineral interaction and amalgamation can also be expected when stability prevails. Furthermore, avalanched debris could be expected to provide increased load, as well as larger particle sizes, towards the valley sides, explaining this noted increase. A similar spatial pattern can be seen when comparing chlorophyll *a* and granule size, indicating their inter-relationship; this relationship has been found in other aggregate systems (e.g. Lunau et al. 2006, Bowker et al. 2008). Conversely, labile carbohydrate content and granule size show an inverse trend. This finding alludes to the importance of bound or 'capsular' carbohydrates, present as cyanobacterial sheath material and in cryoconite granule aggregation. In addition, net ecosystem productivity decreases as granule size increases (Telling et al. 2012) as heterotrophic consumption of labile carbohydrates exceeds autotrophic production (Stibal et al. 2010). Finally, younger cryoconite, which could be expected to reside near to the snow line, may well exhibit the EPS-rich signature of a phototrophic bloom and associated microbial conditioning films, again explaining the comparative excesses of labile carbohydrates up-glacier.

A centre-line transect dataset, incorporating further data – including total organic carbon (TOC), aggregate stability and filament count plus length measurements was used in Chapter 5 to statistically probe the principal biological factors affecting cryoconite aggregate size and stability. Summarising these further data, TOC was found to decrease up-glacier, in contrast to labile carbohydrate content. This represents a shift from a dominance of young, autochthonous carbon up-glacier to more humified and/or allochthonous carbon down-glacier (Takeuchi et al. 2010, Telling et al. 2012), suggesting a shift in the control of aggregation from autotrophy to clay–organic matter interaction. Aggregate stability was found to correlate well with aggregate size (Pearson's r = 0.765), as expected. Along the centre-line transect, filamentous phototroph abundance (and length) was found to be highest in samples near to the snow line and to the glacier terminus, whilst unicellular phototroph abundance was found to be highest in the centre of the glacier – coincidentally the area in which the principal supraglacial stream ran in 2010. Again, this suggests the importance of photoautotrophic bloom activity, stability and period of exposure to cryoconite aggregate stability and size.

Statistical data indicated that filamentous photoautotroph length and count best explained aggregate size (R^2 = 92.0%, P = 0.022), whilst a combination of filamentous

photoautotroph count, unicellular photoautotroph count and carbohydrate–chlorophyll ratio best explained both aggregate size and stability as correlating variables (R^2 = 83.0%, P = < 0.037). These data indicated a statistically significant role for photoautotrophy and associated EPS production in the aggregation of cryoconite and in spatial variations in both granule size and stability. These results agree with many in the fields of terrestrial and marine sediment stabilisation (e.g. Yallop et al. 1994, Falchini et al. 1996, Tolhurst et al. 2002). Paterson et al. (2010) note that filamentous cyanobacteria can effectively stabilise marine sedimentary material, including ooids (laminar, spherical, calcium carbonate concretions), within a period of 'days'. Interestingly, light deprivation was found to reduce the amount of organic exudates (EPS) produced, lessening the effectiveness of this stabilisation. Geesey et al. (1978) emphasise the strong functional links between algae, cyanobacteria, EPS and heterotrophs in sediment biofilms, whilst Decho and Kawaguchi (1999) stress the importance of EPS as a structural matrix within marine stromatolites. As such, it is clear from geospatial investigations of the biological controls over cryoconite granule aggregation, namely photoautotrophy and EPS production, that considerable variation can be seen. This variation is likely a result of a combination of photo-physical and geochemical factors, such as nutrient availability, position within the ice and solar radiation receipt; in turn, this variation leads to heterogeneity in granule size and stability. However, biologically mediated attachment is a complex phenomenon, with various factors affecting it, including: effects of the substratum, the presence of conditioning films, hydrodynamics, characteristics of the fluid medium and properties of the cell surface (Donlan 2002). In order to attempt to understand these biological controls over aggregation, within cryoconite, it was considered useful to develop a laboratory incubation procedure in which the experimental aggregation of cyanobacteria and mineral particles could be undertaken.

7.1.3 The experimental aggregation of cyanobacteria and mineral particles, and insights into the development of cryoconite granules

The aggregation of microorganisms and particulate matter retains material on the ice surface, enhancing surface melt and, via outwash or erosion, seeding the glacial forefield (Takeuchi 2002, Hodson et al. 2008, Mindl et al. 2007). Research by the authors, as noted in Chapters 2–5, indicate the fundamental role of photoautotrophy and EPS production in cryoconite aggregation. As mentioned in the preceding section,

however, mechanisms of adhesion, rates of attachment and the initial development of the cryoconite granule remained unstudied. Chapter 6 addresses the aggregation of cyanobacteria and mineral particles experimentally, in order to gain insights into cell–mineral interaction and cryoconite granule development.

CLSM was used in Chapter 6 to monitor two variables throughout the c. 3-week incubation period: autofluorescent pixel count (APC), which was used as a measure of the abundance of actively photosynthesising cyanobacterial cells, and aggregate size. The aggregates formed during the incubation period were floc-like and quasi-spherical. EPS was ubiquitous, although varying densities of both mineral particles and cyanobacterial filaments were evident, as well as the presence of filament lengths protruding from the aggregate surface, which may facilitate further attachment. Different minerals showed differing responses; Chapter 6 highlights three of these – quartz, a mixed mineral powder, and elemental carbon. Briefly, quartz showed an initial rise in APC, but overall a fall, concurrently with a fluctuating but slight increase in average aggregate size. These data indicate that, even when APC falls, EPS production and physical enmeshing can sustain aggregation. In a natural system, the importance of heterotrophic modification of autotrophic EPS and organo-mineral interactions may take over as the driving force when cyanobacterial growth is rate-limited (Battin et al. 2001). Regarding the measurement of aggregate size, both amalgamation and break-up of aggregates are occurring throughout the incubation period, which accounts for the large fluctuations and thus large error bars present. As mentioned previously, cell–mineral interaction is complex and various other factors, including the abundance and surface-active properties of EPS, are clearly affecting aggregation (Guenther & Bozelli 2004, Sekar et al. 2004).

Elemental carbon showed a rise in APC in all ionic strength solutions, although, as with all incubations, the high ionic strength solution promoted a significantly greater APC rise. Aggregate size data for elemental carbon incubations also showed significant rises, particularly between days 1 and 10, after which plateauing occurred. Chapter 6 postulates that this strong positive interaction between *Leptolyngbya* sp. cyanobacteria and elemental carbon is evidence for the importance of hydrophobic interaction within these aggregates, noted as important by others (e.g. Bar-Or & Shilo 1988, Ivanova et al. 2006, Pal et al. 2008). In fact the average aggregate size increased five-fold over the course of the incubation. The mixed mineral powder data in Chapter 6 showed a similar

rise in APC for the high ionic strength incubations, with the two lower ionic strength solutions sustaining APC values, but not increasing them. Data from other aggregation or flocculation studies indicate that high ionic strength solutions are far better at promoting attachment (e.g. Sekar et al. 2004, Silva & Silva 2007, Kim et al. 2010), so these results are not unexpected. Aggregate size data for the mixed powder mirrored those of elemental carbon until day 10, although after this a drop in average aggregate size was experienced. This suggests that the incubations became rate-limited after day 10, exposing the autotrophic EPS to heterotrophic consumption, leading to more rapid break-up of certain aggregates than the rate of formation of new aggregates.

Whilst the growth in the high ionic strength solutions was moderately to strongly linear (R^2 = 0.858 to 0.978), and variations were clear between different ionic strengths, pH data showed no significant trends. The addition of mineral powders and cyanobacterial homeostasis (Giraldez-Ruiz et al. 1999) likely contributed to this, as all incubations trended towards a neutral pH. When considering the ratio data presented in Chapter 6, a useful summary of the incubation results, a spike is clearly visible on day 2. This is indicative of rapid co-aggregation of cyanobacterial filaments and mineral particles, associated with the release of excess EPS to condition surfaces and promote adhesion (Avnimelech et al. 1982, Kovac et al. 2002, Bhaskar et al. 2005). Excluding two outliers, the linear trend between APC and aggregate size has an R^2 value of 0.575, and as such is not as strong as the trend between filament count and granule size in Chapter 5. This suggests the presence of further controls over aggregation, in addition to those addressed in this simplified experimental system.

Chapter 6 also addressed temperature by conducting incubations at both room temperature and 4ºC. Temperature was found to affect aggregation, with APC preservation significantly better at 21ºC, and average aggregate size slightly greater also. The notable differences between the different cyanobacterial species used, *Leptolyngbya* and *Phormidium*, point to species-specific optimum growth conditions. Zippel and Neu (2005) find that slow-growing cyanobacteria produce more stable phototrophic mats; Chapter 6 determined that *Phormidium* cyanobacteria exhibited slower growth, greater adaptation to cold and more stable aggregate structures. Finally, fluid chemistry data showed calcium and magnesium uptake over the course of the incubations, which is as expected given their need within the photosystem (e.g. England & Evans 1983) and their role in cell–mineral attachment by polymer bridging (e.g.

Theng 1982). In addition, nitrate and sodium uptake was also significant, which is best explained by sodium-dependent nitrate transport (Lara et al. 1993). To summarise, experimental studies of aggregation indicate that cyanobacteria can adhere to a variety of mineral particles and form stable aggregates when key macronutrients and a source of visible light are available.

In addition to the studies of aggregation summarised above, Chapter 6 utilises FTIR microspectroscopy, or FTIR imaging, to probe the biochemical signatures within these aggregates, to aid our knowledge regarding their formation. FTIR imaging showed an abundance of spectral peaks diagnostic of carbohydrates, indicating that EPS is produced to aid aggregation and is omnipresent, a result seen in a variety of bioaggregates (e.g. Kovac et al. 2002, Sartoni et al. 2008). Organic matter and carbohydrate signatures within analogous photoautotrophic mats show good spectral correlation with long-chain polysaccharides (Kaçurakova et al. 2000, Fischer et al. 2010), indicating that polysaccharide-rich EPS is a principal component of bioaggregates.

Some variability in composite spectra was noticed, whereby elemental carbon aggregates showed greater lipid and carboxylic acid/protein intensities than quartz aggregates. A high relative abundance of C=O moieties has been suggested to indicate the relative abundance of bound EPS (Omoike & Chorover 2004). Conversely, quartz and, to an extent, the mixed mineral powder showed a greater spread of high-intensity carbohydrate spectral peaks, with carbohydrate intensities up to 10 times greater than amide I region intensities. This, along with the fact that carbon aggregates displayed a greater number of discrete, visible cyanobacterial filaments, suggests infilling of quartz and mixed powder bioaggregates by polysaccharides. It has been shown that free EPS exhibits a different sulphur content and monosaccharide composition (Micheletti et al. 2008, Pereira et al. 2009) to capsular EPS. As such, it is suggested that the spectral signature of the quartz bioaggregates is indicative of an increased incidence of free EPS. Within the elemental carbon aggregates, shifts in position of the amide I and II peaks, indicative of alterations to the protein structure (Badireddy et al. 2010), may well indicate both the deprotonation of amino acids (Braiman et al. 1999) and the presence of acidic EPS (Nivens et al. 2001). This is potentially important for EPS charge, as the acidic EPS of certain cyanobacteria have been shown to be anionic (e.g. Pereira et al.

2009). Thus, the EPS can attract cations and chelate metal ions (Decho 1990, 2000, Pereira et al. 2009) and is therefore important for attachment to mineral surfaces.

From the data presented in Chapter 6, it can be said that the spectral signatures of cyanobacteria and mineral co-aggregates show a variability that is suggestive of differing compositions. Furthermore, it can be inferred that both capsular (bound) and free EPS are important in the aggregation of *Leptolyngbya* sp. cyanobacteria with mineral particles. Where a decline in APC and a reduction in aggregate stability were observed, e.g. the quartz aggregates, both high carbohydrate intensities and an increased functionality suggest that polysaccharide–mineral interactions are significantly contributing to aggregation. The formation of organo-silicon compounds may also occur, as postulated by Kovac et al. (2002). Conversely, greater carboxylic acid and protein intensities, combined with 'amide shifts', indicate that, for certain minerals, capsular EPS, and presumably a more direct contact, plays the more significant part in aggregation. This is particularly true for elemental carbon, where large peaks within both the carboxylic acid and protein regions of the spectra suggest that both a cationic and a hydrophobic method of cell–mineral interaction are plausible (De Phillipis & Vincenzini 1998, Jorand et al. 1998). Furthermore, the data also suggest that those cyanobacteria within the incubations that maintain or improve their APC utilise their capsules for aggregation, and that significant free EPS release may be a response to stress.

As detailed in Chapter 6, insights into the development of cryoconite granules can be drawn from the data obtained via these experimental studies of aggregation. The cyanobacteria used in the study both produce capsules and secrete EPS, and both are polar isolates common within cryoconite (Porazinska et al. 2004, De Phillipis et al. 2005, Stibal et al. 2006, Namsaraev et al. 2010). As such, EPS was ubiquitous within the resultant aggregates. Both mineral type and ionic strength were found to affect the development of bioaggregates. Data suggest that elemental carbon was particularly good at supporting cyanobacterial proliferation and aggregation, with mica, kaolinite and a mixed mineral powder moderately good, and quartz particularly weak. As such, local mineralogy will have a degree of influence over the development and subsequent stability of cryoconite granules, a fact noted in the development of polar soils (Cannone et al. 2008, Schaefer et al. 2008). In addition, it was clear that high ionic strength incubations performed noticeably better than lower ones. This suggests that the

presence of an easily weathered mineralogy, such as the sedimentary strata in Svalbard, is conducive to granule development, as the liberation of solutes will be higher (Schaefer et al. 2008). Combined with significant quantities of EPS, aiding adhesion and limiting hydraulic conductivity, a high ionic strength could easily be maintained within cryoconite granules in the vicinity of photoautotrophic cells. Fluid chemistry data suggested that nitrate uptake, facilitated by sodium (Lara et al. 1993), was particularly important in maintaining an abundance of healthy cyanobacteria within the aggregates.

FTIR spectral data provided an insight into the complex interactions between cyanobacteria and mineral particles in bioaggregates. In particular, spectra suggested that aggregation is dominated by polymer cation bridging, with capsular EPS utilising protein and carboxylic acid interactions, suggestive of acidic EPS, and free EPS utilising carboxylic acid and polysaccharide organo-silicon interactions. In addition, interaction with elemental carbon and black carbon, as well as the noticeable and comparative dominance of protein-based interactions in these aggregates, suggests a role for hydrophobic interaction (Jorand et al. 1998) in aggregation. A conceptual diagram highlighting the above proposed attachment mechanisms is presented in Figure 29 in Chapter 6. Thus, experimental studies in Chapter 6 concur with hypotheses created in Chapter 2, namely that bioflocculation and EPS–mineral interactions, combined with filamentous binding, are the major creative forces within cryoconite granules.

7.1.4 Cryoconite granule aggregation, microstructure and biogeochemistry: a synthesis of knowledge

Photosynthesis oxygenated the earth, fixed carbon and allowed life to flourish; as the primary producer on glacier surfaces, photosynthetic microorganisms can be said to have an analogous and equally important role. Anesio et al. (2009) estimated that phototrophs within cryoconite worldwide could fix 64 Gg of carbon per year, and recent incubation experiments have found net ecosystem productivity to be either autotrophic or balanced (Anesio et al. 2009, 2010, Hodson et al. 2010, Telling et al. 2010). Whilst net heterotrophy undoubtedly exists, caused principally by changes in sediment thickness and shading (Cook et al. 2010, Telling et al. 2012), recent research suggests

that autotrophy dominates until a thickness of c. 3 mm is reached. Furthermore, recent molecular and microbiological investigations have highlighted the genetic and physiological diversity of photosynthetic microorganisms on the glacier surface, particularly cyanobacteria, but also algae and diatoms (Comte et al. 2007, Edwards et al. 2011, Segawa & Takeuchi 2010, Yallop & Anesio 2010). Recent trends in polar warming have the potential to further boost ecological activity, given that greater water absorption at higher temperatures leads to greater rates of photosynthesis (Zhao et al. 2008). Finally, the importance of photosynthetic microorganisms and associated EPS to the development, structure and stability of cryoconite granules is now clear (Hodson et al. 2010, Langford et al. 2010, Takeuchi et al. 2001b, 2010). With this in mind, it is considered prudent to return to the hypothesis outlined in Chapter 2 and update it, accounting for and synthesising recent knowledge. Figure 30 summarises the hypothesis below as a conceptual model.

The onset of summer melt creates photosynthetic oxygen and dissolves salts precipitated during freezing conditions (Tranter et al. 2004), creating high ionic solute concentrations of up to c. 1000 µS cm^{-1} (Fountain et al. 2008). In Arctic locations, high quantities of nitrogen, a key macronutrient for photoautotrophs, are precipitated within snow (Hodson et al. 2005) and dissolve out upon ablation. Photosynthesis can occur as soon as liquid water is present (Stibal & Tranter 2007), and photoautotrophs take advantage of these high nutrient conditions and bloom upon the snow surface. In particular, snow algae such as *Chlamydomonas nivalis* form watermelon snow (Newton 1982). Photosynthetic bloom activity results in micro-aggregations of photoautotrophs and associated EPS in wet snow and slush upon the glacier surface. In lacustrine environments, analogous microaggregates >60 µm in size were found to be principally composed of photosynthetic microorganisms and associated decomposition products (Brachvogel et al. 2001). As such, the primary microaggregates that 'seed' cryoconite granule development are likely to be directly related to bloom activity. Physical straining of aeolian particulate matter, largely clays, minerals and elemental carbon, between ice crystals promotes adhesion onto these EPS-rich microaggregates.

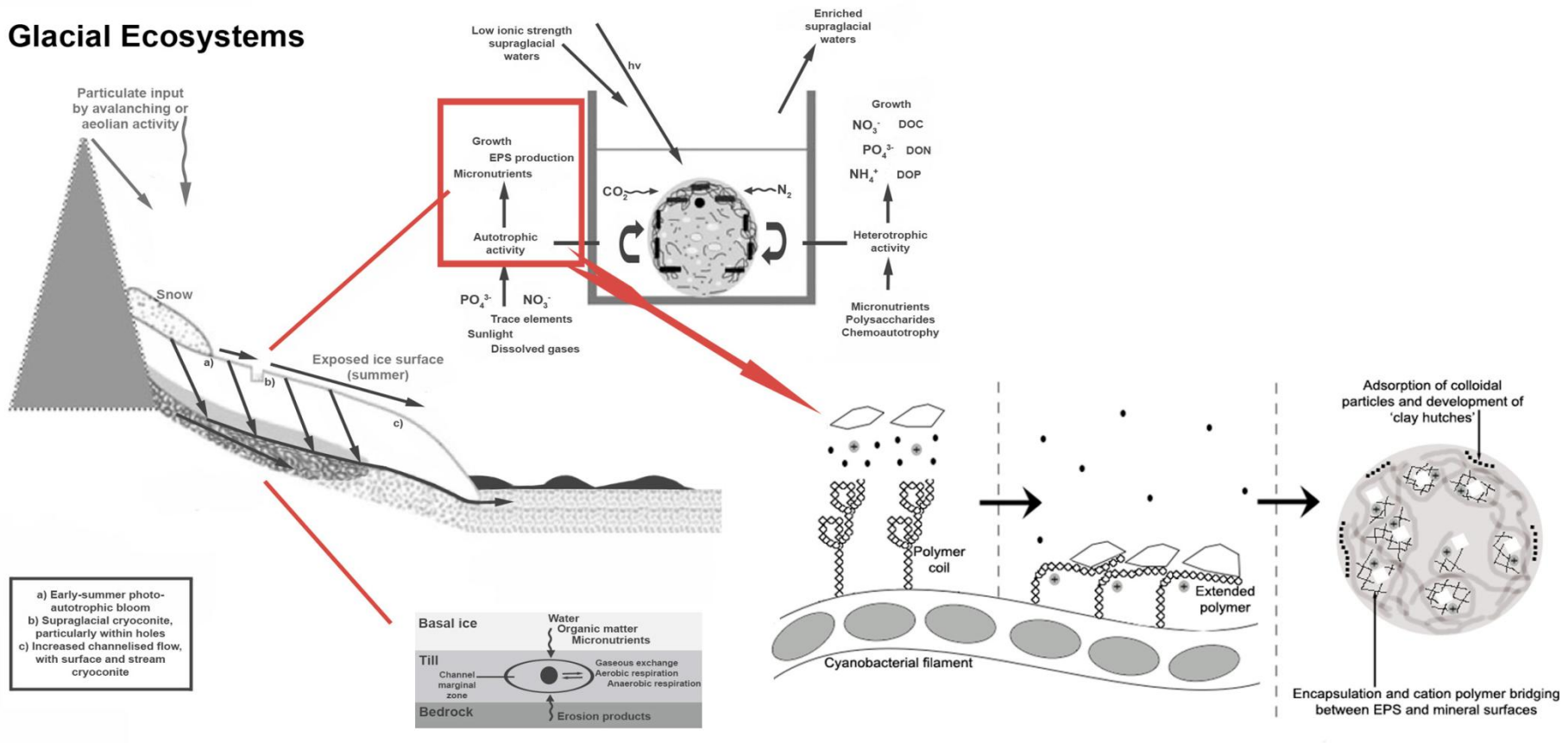

Figure 30: A conceptual diagram of the glacial ecosystem, modified from Figure 1, detailing the role of autotrophic activity and associated EPS production in the development of cryoconite granules.

As noted in Chapter 2, hydrophobic attraction in certain cases and, more usually, orthokinetic and perikinetic flocculation can then occur between cells and particulate matter (Folkersma et al. 1999). Perikinetic flocculation is simply aggregation caused by collisions due to Brownian motion. Orthokinetic flocculation is aggregation caused by collisions due to bulk fluid motion, e.g. supraglacial flow through a distributed 'weathering crust' network. A bloom in heterotrophic bacteria is likely to occur after the initial photoautotroph bloom, as shown when experimentally studying ooid formation (Plee et al. 2008).

In Chapter 5, carbohydrate concentrations were found to be greatest close to the snow line, supporting the above. Furthermore, Chapters 2–4 determined the presence of various types of EPS as a matrix material within sectioned cryoconite granules, closely associated with photoautotrophs in many cases, and exhibiting signs of 'early decomposition', not only in the colours seen in thin section in Chapter 2 but also in the organic matter spectra presented in Chapter 3. Chapter 5 also determined hotspots of chlorophyll *a* and thus of photosynthetic activity, suggestive of bloom activity and clustering of photoautotrophs, mediated by their EPS secretions. As mentioned in Chapter 2, EPS provides an extensive capacity for binding (Liu & Fang 2002), contains both hydrophobic and hydrophilic polymers (Jorand et al. 1998), and can partially overcome surface charge of substrata, facilitating adhesion (Tsuneda et al. 2003). As such, the production of copious EPS to aid attachment is clear, and this bioflocculation allows cryoconite granules to begin to develop. In analogous lacustrine environments, the abundance of aggregates is directly affected by plankton dynamics and wind conditions (Grossart et al. 1997). As such, stability should be highly important to successful photosynthesis and bioflocculation; in fact, Chapter 5 suggests a positive relationship between stability and the presence of stable cryoconite granules. Additionally, Stibal et al. (2012) find a statistical relationship between slope and ecological activity. Thus, photo-physical and physico-chemical conditions need to be considered when attempting to explain geospatial variation in ecological activity and cryoconite granule size.

As noted in Chapter 2, increasing aggregation leads to greater sedimentation in melt holes, and a reduced albedo, due to the presence of darkening particulate matter, causes differential melt into the ice. Bøggild et al. (2010) find that cryoconite albedo (a ratio of reflected to incident electromagnetic radiation) averages c. 0.09, significantly lower

than the surrounding ice, at c. 0.57–0.65. This albedo change increases the amount of shortwave energy available for melt. The lower solar radiation receipt in polar regions induces a slower melt, with comparatively low hydrodynamic agitation leading to higher settling rates (MacDonnell & Fitzsimons 2008). Localised melt causes accumulations of cryoconite across the weathering crust, with certain accumulations transforming into cryoconite holes, whereby the equilibrium depth and width are functions of the radiation reaching the sediment and the quantity of sediment within the melt hole (Gribbon 1979, Cook et al. 2010).

Cyanobacteria thrive in the supraglacial environment, not least due to their cryoprotection mechanisms (Vincent 2007), but also due to their adaptability. Cyanobacterial photosynthetic rates are species-specific (Garcia-Pichel & Belnap 1996), but cyanobacteria can metabolically control their surface charge to electrostatically attract carbonate anions (Martinez et al. 2008) and can excrete hydroxyl ions to raise pH (Plee et al. 2008), promoting photosynthesis. As noted in Chapters 2 and 4 and by others (Stibal et al. 2006, Comte et al. 2007), filamentous cyanobacteria are highly prevalent within cryoconite and can be characterised as having both significant capsular sheaths and the ability to produce free EPS. As in other bioaggregates, such as ooids and aerobic granular sludge (e.g. Brehm et al. 2004, Chen et al. 2007a), filamentous binding takes over as the dominant influence on aggregate structure, increasing the strength and stability of cryoconite granules. Chapter 2 finds that the distribution of cyanobacterial filaments is ubiquitous, yet random in terms of numbers. Physical forces were found to more easily disrupt filament-poor aggregates. Indeed, Chapter 5 finds that a positive trend exists between the number and length of filaments and both aggregate size and stability. As mentioned previously, slow-growing cyanobacteria have been found to positively affect sediment stability in other environmental systems (de Kreuk & van Loosdrecht 2004).

It is now clear that a surface to near-surface layer of cyanobacteria exists in many cryoconite granules, as noted in Chapter 2 and by others (Hodson et al. 2010, Takeuchi et al. 2001b, 2010). Chapter 4 details the ultrastructure of this surface layer, determining that it is around 70 μm thick and dominated by filamentous cyanobacteria and EPS, exhibiting a degree of laminar profiling. In certain environments, this laminar development is far more significant (Takeuchi et al. 2010), with up to seven laminar ‘growth’ layers visible. Within the EPS matrix, small aeolian fines, likely clays and iron

oxides, are attached to cyanobacterial sheath material – potentially evidence of nutrient scavenging and UV protection. A significant heterotrophic population is associated with this phototrophic layer, attached to, and thus likely consuming, organic matter secreted by the photoautotrophs present. Similar surface layers exist at the top of benthic microbial mats or soil crusts, whereby a layer of photoautotrophs in favourable conditions for productivity undertake photosynthesis, below which phototrophic cells are dispersed downwards into the sediment (Herlory et al. 2004), providing carbon for heterotrophic metabolism. Photosynthetically active radiation diminishes to a negligible amount beyond 1 mm in sandy minerals and less in opaque minerals (Stal et al. 1985), meaning that the centre of larger cryoconite granules must be heterotrophic. Both chemoorganoheterotrophy and chemolithoheterotrophy may occur, given the prevalence of both mineral particles and organic matter within cryoconite granules.

The attachment of cyanobacteria to a variety of mineral particles has now been demonstrated, as outlined in Chapter 6. As noted in Chapter 6, co-aggregation was readily observed in all cases, with subsequent 'survival' of cyanobacterial cells seemingly dependent upon mineral type and ionic strength, and thus upon nutrient availability. Similar sheathed and EPS-producing cyanobacteria have been found to successfully attach to surfaces, with morphology and extent of mucilage (EPS) production deemed most important (Davey et al. 1991). FTIR investigation of the attachment mechanisms identified that the biochemical signatures of chemical bond formation within the aggregates varied, indicating that interactions of bound and free EPS were utilised, to a greater or lesser degree, to facilitate attachment. Cyanobacterial EPS has a variable composition showing, in addition to the principal polysaccharide component (deoxy-sugars), an excess of sulphate groups and a high uronic acid content, which confers an anionic nature (Decho 1990, Pereira et al. 2009), as well as the presence of ester-linked acetyl groups, which confer hydrophobicity (Neu et al. 1992). In addition, the composition of EPS produced by a single species can vary depending on its growth conditions (Brüll et al. 2000). Chapter 6 finds evidence of cationic attachment, particularly using carboxylic groups, as well as both hydrophobic attachment mechanisms, to elemental carbon, and polysaccharide-dominated organo-silicon interactions, to quartz and similar silica-rich minerals.

As has been proven upon the Greenland ice sheet (Stibal et al. 2012), the abundance of photoautotrophic microorganisms exerts a significant control over carbon cycling,

capturing inocula and nutrients, transforming carbon in-situ and releasing carbon via supraglacial hydraulic activity. Organic carbon clearly accumulates on ice surfaces; Anesio et al. (2010) suggest that only 7% of organic carbon within cryoconite undergoes heterotrophic metabolism and alteration. Alongside respiration, debris erosion keeps accumulation of organic carbon in check (Stibal et al. 2008a, Hodson et al. 2010). Recent investigations have clarified that cryoconite material remains on glacier surfaces for 'years' (Hodson et al. 2010, Takeuchi et al. 2010), with larger granules showing potential for exhaustion of organic matter at the core, as well as for diffusion limitation and consequent anoxia. Indeed, clay-rich cryoconite granules on Longyearbreen occasionally show blackened centres, suggesting anoxia (R. Smith, unpublished data). These larger granules typically occur down-glacier or near to the glacier edge, as demonstrated in Chapter 5, where shading effects and increased input of mineral material from glacier edges help to explain this phenomenon.

With respect to supraglacial erosion, hydraulic activity and albedo-driven melt within the weathering crust connect patches of cryoconite and cryoconite holes, forming networks and eventually supraglacial streams (MacDonnell & Fitzsimons 2008). Within the weathering crust, the bulk movement of cryoconite is slow, at c. 0.2 mm per hour (Irvine-Fynn et al. 2011). Nonetheless, both down-glacier transport of whole granules and erosion of granules undoubtedly occur. Erosion, as well as melt, can liberate 8.69×10^{11} cells per hour in a typical supraglacial stream (Irvine-Fynn et al. in press), indicating the importance of atmospheric deposition and cryoconite granule formation for determining sediment and cellular fluxes into the glacial forefield.

Recent advancements in glaciology have changed the way that we view supraglacial biogeochemistry and, in particular, cryoconite granules. Detailed grain-scale studies of the microstructure and aggregation of cryoconite have been completed, as reported in Chapters 2–6, for the first time. These Chapters demonstrate the granule-to-granule heterogeneity of cryoconite, as well as confirming the importance of cyanobacteria within these granules, and contributing to the understanding of cell–mineral interaction within cryoconite, an area previously untouched within the field. The resulting conceptual model provides a basis upon which to scale up and accurately comment on glacier-scale and global biogeochemistry. Furthermore, these Chapters provide data on granule-scale organic carbon distribution and composition, and thus insights into carbon cycling. Recent advancements, namely those by the authors and by Stibal et al. (2012),

demonstrate the photosynthetic control over organic carbon cycling, whereby photo-physical and geochemical factors control photosynthesis, which ultimately controls the amount of labile carbohydrates present for heterotrophic metabolism, as well as the structural integrity of the cryoconite granule. In addition, data have been obtained that can contribute to our understanding of nutrient cycling in glacial environments, particularly the discovery of sodium-dependent nitrate transport in cyanobacterial bioaggregates. Recently, the presence and activity of nitrogen fixing bacteria has been proven in Svalbard glaciers for the first time (Telling et al. 2011): further evidence that sustained photosynthetic activity can be achieved across the entire ablation season.

Chapters 2–6 also shed light on the EPS-based attachment mechanisms within cryoconite, as well as highlighting the abundance of these polymers within granules. As such, we can now view cryoconite granules as bioaggregates, within which polymeric adhesion facilitates the capture of mineral particles and useful nutrients. Indeed data show, for the first time, the presence of 'clay hutches' surrounding cyanobacterial filaments. This information is important when attempting to understand albedo-driven supraglacial melt, a hugely relevant and important area of glaciology presently, given the significant rise in average temperatures recently. Indeed, our data, as well as research by others (Zhao et al. 2008), suggest that cyanobacterial proliferation and co-aggregation, and thus cryoconite granule formation, is significantly greater at higher temperatures. Mineralogical and geochemical data show the presence of weathered silicates and humified organic matter, indicating that 'pedogenesis' does occur within these cryoconite granules. As such, well-developed cryoconite granules can be considered analogous to soil microaggregates. The molecular profile of cryoconite has now been determined (Edwards et al. 2011, Cameron et al. 2011), detailing a complex community, with work now underway to probe the functional genes within these communities to further understand their ecology. As such, this work can be considered highly important when attempting to understand how cryoconite granule formation affects global climate change, global carbon cycling and soil development in cold regions.

7.2 Conclusions and future work

In summary, this thesis arrives at the following major results:

1. Cryoconite granules are heterogeneous microaggregates, formed by photoautotrophic bloom activity and bioflocculation, and strengthened by filamentous binding. These granules are dominated by weathered silicate minerals, with particle sizes suggesting a largely aeolian source, set within an organic groundmass. This groundmass is composed of aliphatic- and carbohydrate-rich organic matter, as well as elemental and black carbon, and microorganisms, of which filamentous cyanobacteria dominate the photoautotrophic community. Ultrastructural analyses highlight the significant role played by microorganisms and EPS in enmeshing the aggregate structure, attracting mineral particles and creating distinct microenvironments.

2. Geospatial analyses on glacier surfaces highlight the ubiquitous presence of cyanobacteria and, via proxy measurements (chlorophyll *a* and carbohydrate concentrations), the spatial variability in photoautotroph and EPS abundance, the two principal biological controls over cryoconite granule formation and stability. Spatial data indicate a supraglacial 'snapshot', whereby newer, freshly ablated and thinner deposits near to the snow line contain high carbohydrate concentrations, and older, stable deposits near to the glacier terminus contain greater chlorophyll *a* concentrations. A zone of hydraulic erosion is clearly evident, with granule size and stability correlating well with the abundance and length of photoautotrophic filaments, as well as with the chlorophyll–carbohydrate ratio, emphasising their importance in cryoconite granule aggregation.

3. The experimental co-aggregation of cyanobacteria and mineral particles demonstrates the adaptability of cyanobacteria characteristic of cryoconite granules, in that they can co-aggregate with a variety of mineral particles under a variety of pH and ionic strength conditions. Interactions between both bound and free EPS and mineral particles are vital in cell–mineral interaction, with hydrophobic, polysaccharide cationic, protein-based and organo-silicon interactions all suggested. Nitrate is identified as potentially nutrient limiting, and more inert minerals such as quartz are noted for their potential inability to support cryoconite ecosystems in the

long term, whilst elemental carbon is demonstrated to promote aggregation and cyanobacterial proliferation.

The present thesis provides the first, detailed, granule-scale study of the microstructure and aggregation of cryoconite, utilising a novel combination of microscopic and spectroscopic techniques to further knowledge regarding these microaggregates. As alluded to in the 'synthesis' section, the work substantiates the concept that net autotrophy drives cryoconite aggregation and biogeochemistry, acting as a control over the supraglacial carbon cycle. Furthermore, this thesis provides evidence for pedogenesis within cryoconite, and aids understanding with relation to albedo-driven glacier melt.

However, gaps in the knowledge of cryoconite microstructure and biogeochemistry still exist. Future research should focus on scaling down from granule to cell–mineral scale, improving our understanding of the complex relationship between the microbial community and the abiotic surfaces and nutrients within the cryoconite ecosystem. In particular, Chapter 4 could only suggest the details of cell–mineral interaction between clay-sized particles and cyanobacterial sheaths, and Chapter 2 could only discriminate between cyanobacteria, algae and heterotrophs based upon fluorescence information. Scanning transmission electron microscopy and electron energy loss spectroscopy could provide nanometre-scale elemental analysis (e.g. Leapman & Aronova 2008), allowing clay-sized particles in thin sections to be formally identified and the attachment between them and organic molecules on the cyanobacterial capsule elucidated. Furthermore, the application of fluorescent in-situ hybridisation techniques could allow the spatial distribution of particular functional types of bacteria, with particular metabolic roles, within cryoconite aggregates to be probed (e.g. Pernthaler & Amann 2004).

In addition, our understanding of organic matter dynamics within individual cryoconite granules is still in its infancy. FTIR techniques, applied in Chapters 3 and 6, have allowed us to begin to understand the carbohydrate EPS component of cryoconite granules, but further compositional detail is necessary in order to understand carbon cycling in supraglacial environments. Techniques such as Raman spectroscopy, combined with stable isotope probing (SIP-Raman), and spatially resolved nano-secondary ion mass spectrometry (nano-SIMS) would be particularly useful in addressing this. Indeed, a combined approach using nano-SIMS, scanning transmission

X-ray microscopy (STXM) and near edge X-ray absorption fine structure spectroscopy (NEXAFS) may prove highly useful in locating and characterizing mineral-associated organic matter (e.g. Mueller et al. 2012, Remusat et al. 2012). Utilising labelled nutrients and/or probes, carbon cycling within an individual granule, from photosynthesis to EPS production to humification, could be effectively studied. Similarly, Li et al. (2008) highlight the usefulness of in-situ hybridisation probes combined with SIMS, for investigating microbial identity and function concurrently, a technique that they call SIMSISH. Regarding 'function', little work has been completed investigating the function of the now-characterised microbial communities within cryoconite. As such, further work should also incorporate the use of quantitative real-time polymerase chain reaction (qPCR) and metabolomics (e.g. Fierer et al. 2007, Bundy et al. 2009) to study organism functions within cryoconite at the molecular level.

Finally, the results of Chapter 6 highlight the hydrophobic interaction between elemental and black carbon and cyanobacteria. With combustion and mining activities contributing to atmospheric deposition of elemental and black carbon onto Arctic glaciers (e.g. Forsström et al. 2009, Aamaas et al. 2011) in surprisingly high quantities, and considering the very low albedo of these particles, it is vital that we try to understand more about how they interact with microorganisms on the surface of the ice. As such, future work should also address the biological aggregation of albedo-reducing carbonaceous particles, both experimentally and in the field, to understand how this aggregation occurs and its affect upon glacier albedo.

REFERENCES

AAMAAS, B., BØGGILD, C. E., STORDAL, F., BERNTSEN, T., HOLMEN, K. & STROM, J. 2011. Elemental carbon deposition to Svalbard snow from Norwegian settlements and long-range transport. *Tellus Series B – Chemical and Physical Meteorology,* **63,** 340–351.

ADAV, S. S., LIN, J. C. T., YANG, Z., WHITELEY, C. G., LEE, D. J., PENG, X. F. & ZHANG, Z. P. 2010. Stereological assessment of extracellular polymeric substances, exo-enzymes, and specific bacterial strains in bioaggregates using fluorescence experiments. *Biotechnology Advances,* **28**(2)**,** 255–280.

AMATO, P., HENNEBELLE, R., MAGAND, O., SANCELME, M., DELORT, A. M., BARBANTE, C., BOUTRON, C. & FERRARI, C. 2007. Bacterial characterization of the snow cover at Spitzberg, Svalbard. *FEMS Microbiology Ecology,* **59,** 255–264.

AMELINCKX, A., VAN DYCK, D., VAN LANDUYT, J. & VAN TENDELOO, G. (eds.) 2008. *Electron Microscopy: Principles and Fundamentals,* Weinheim: VCH.

ANDRADE, L. R., SALGADO, L. T., FARINA, M., PEREIRA, M. S., MOURAO, P. A. S. & FILHO, G. M. A. 2004. Ultrastructure of acidic polysaccharides from the cell walls of brown algae. *Journal of Structural Biology,* **145,** 216–225.

ANDREWS, J. S., ROLFE, S. A., HUANG, W. E., SCHOLES, J. D. & BANWART, S. A. 2010. Biofilm formation in environmental bacteria is influenced by different macromolecules depending on genus and species. *Environmental Microbiology,* **12,** 2496–2507.

ANESIO, A. M., HODSON, A. J., FRITZ, A., PSENNER, R. & SATTLER, B. 2009. High microbial activity on glaciers: importance to the global carbon cycle. *Global Change Biology*, **15**, 955–960.

ANESIO, A. M., SATTLER, B., FOREMAN, C., TELLING, J., HODSON, A., TRANTER, M. & PSENNER, R. 2010. Carbon fluxes through bacterial communities on glacier surfaces. *Annals of Glaciology,* **51,** 32–40.

ARTZ, R. R. E., CHAPMAN, S. J., ROBERTSON, A. H. J., POTTS, J. M., LAGGOUN-DEFARGE, F., GOGO, S., COMONT, L., DISNAR, J. R. & FRANCEZ, A. J. 2008. FTIR spectroscopy can be used as a screening tool for organic matter quality in regenerating cutover peatlands. *Soil Biology & Biochemistry,* **40**(2)**,** 515-527.

AVNIMELECH, Y., TROEGER, B. W. & REED, L. W. 1982. Mutual flocculation of algae and clay – evidence and implications. *Science,* **216,** 63–65.

BADIREDDY, A. R., CHELLAM, S., GASSMAN, P. L., ENGELHARD, M. H., LEA, A. S. & ROSSO, K. M. 2010. Role of extracellular polymeric substances in bioflocculation of activated sludge microorganisms under glucose-controlled conditions. *Water Research,* **44,** 4505–4516.

BAKER, D. W. & BRAND, J. J. 1985. *Anacystis nidulans* demonstrates a photosystem II cation requirement satisfied only by Ca^{21} or Na^{21}. *Plant Physiology***, 79**, pp. 552–558.

BAR OR, Y. & SHILO, M. 1988. The role of cell-bound flocculants in coflocculation of benthic cyanobacteria with clay particles. *FEMS Microbiology Ecology,* **53,** 169–174.

BARRANGUET, C., HERMAN, P. M. J. & SINKE, J. J. 1997. Microphytobenthos biomass and community composition studied by pigment biomarkers: importance and fate in the carbon cycle of a tidal flat. *Journal of Sea Research,* **38,** 59–70.

BARRANGUET, C., VAN BEUSEKOM, S. A. M., VEUGER, B., NEU, T. R., MANDERS, E. M. M., SINKE, J. J. & ADMIRAAL, W. 2004. Studying undisturbed autotrophic biofilms: still a technical challenge. *Aquatic Microbial Ecology,* **34,** 1–9.

BARTH, A. 2000. The infrared absorption of amino acid side chains. *Progress in Biophysics*

& Molecular Biology, **74,** 141–173.

BATSTONE, D. J. & KELLER, J. 2001. Variation of bulk properties of anaerobic granules with wastewater type. *Water Research,* **35,** 1723–1729.

BATTIN, T. J., WILLE, A., SATTLER, B. & PSENNER, R. 2001. Phylogenetic and functional heterogeneity of sediment biofilms along environmental gradients in a glacial stream. *Applied and Environmental Microbiology,* **67,** 799–807.

BEER, S. & ESHEL, A. 1985. Determining phycoerythrin and phycocyanin concentrations in aqueous crude extracts of red algae. *Australian Journal of Marine and Freshwater Research,* **36,** 785–792.

BELNAP, J., PHILLIPS, S. L., WITWICKI, D. L. & MILLER, M. E. 2008. Visually assessing the level of development and soil surface stability of cyanobacterially dominated biological soil crusts. *Journal of Arid Environments*, **72**, 1257–1264.

BENNING, L. G., PHOENIX, V. R., YEE, N. & TOBIN, M. J. 2004. Molecular characterization of cyanobacterial silification using synchrotron infrared micro-spectroscopy. *Geochimica et Cosmochimica Acta***, 68**, pp. 729–741.

BEVERIDGE, T. J. 2006. Understanding the shapes of bacteria just got more complicated. *Molecular Microbiology,* **62,** 1–4.

BHASKAR, P. V., GROSSART, H. P., BHOSLE, N. B. & SIMON, M. 2005. Production of macroaggregates from dissolved exopolymeric substances (EPS) of bacterial and diatom origin. *FEMS Microbiology Ecology,* **53,** 255–264.

BISWAS, A. B., KUMSAH, C. A., PASS, G. & PHILLIPS, G. O. 1975. Effect of carbohydrates on heat of fusion of water. *Journal of Solution Chemistry,* **4,** 581–590.

BØGGILD, C. E., BRANDT, R. E., BROWN, K. J. & WARREN, S. G. 2010. The ablation zone in northeast Greenland: ice types, albedos and impurities. *Journal of Glaciology,* **56,** 101–113.

BOUYER, D., COUFORT, C., LINE, A. & DO-QUANG, Z. 2005. Experimental analysis of floc size distributions in a 1-L jar under different hydrodynamics and physicochemical conditions. *Journal of Colloid and Interface Science,* **292,** 413–428.

BOWKER, M. A., BELNAP, J., CHAUDHARY, V. B. & JOHNSON, N. C. 2008. Revisiting classic water erosion models in drylands: The strong impact of biological soil crusts. *Soil Biology & Biochemistry,* **40,** 2309–2316.

BRACHVOGEL, T., SCHWEITZER, B. & SIMON, M. 2001. Dynamics and bacterial colonization of microaggregates in a large mesotrophic lake. *Aquatic Microbial Ecology,* **26,** 23–35.

BRAIMAN, M. S., BRIERCHECK, D. M. & KRIGER, K. M. 1999. Modeling vibrational spectra of amino acid side chains in proteins: Effects of protonation state, counterion, and solvent on arginine C–N stretch frequencies. *Journal of Physical Chemistry B,* **103,** 4744–4750.

BRATBAK, G. 1985. Bacterial biovolume and biomass estimations. *Applied And Environmental Microbiology,* **49,** 1488–1493.

BREHM, U., PASLINSKA, K. A. & KRUMBEIN, W. E. 2004. Laboratory cultures of calcifying biomicrospheres generate ooids – a contribution to the origin of oolites. *Carnets de Géologie*, **L03**, 1-6.

BRÜLL, L. P., HUANG, Z. B., THOMAS-OATES, J. E., PAULSEN, B. S., COHEN, E. H. & MICHAELSEN, T. E. 2000. Studies of polysaccharides from three edible species of *Nostoc* (cyanobacteria) with different colony morphologies: Structural characterization and effect on the complement system of polysaccharides from *Nostoc commune*. *Journal of Phycology,* **36,** 871–881.

BUNDY, J. G., DAVEY, M. P. & VIANT, M. R. 2009. Environmental metabolomics: a critical review and future perspectives. *Metabolomics,* **5,** 3–21.

BUSTIN, R.M. and GUO, Y. 1999. Abrupt changes in reflectance values and chemical compositions of artificial charcoals and inertinite in coals. *International Journal of Coal Geology*, **38**(3-4), 237-260.

CAMERON, K. A., HODSON, A. J. & OSBORN, A. M. 2011. Structure and diversity of bacterial, eukaryotic and archaeal communities in glacial cryoconite holes from the Arctic and the Antarctic. *FEMS Microbiology Ecology***,** 1–14.

CANNONE, N., WAGNER, D., HUBBERTEN, H. W. & GUGLIELMIN, M. 2008. Biotic and abiotic factors influencing soil properties across a latitudinal gradient in Victoria Land, Antarctica. *Geoderma,* **144,** 50–65.

CARPENTER, S. R., ELSER, M. M. & ELSER, J. J. 1986. Chlorophyll production, degradation, and sedimentation – implications for paleolimnology. *Limnology and Oceanography,* **31,** 112–124.

CARSON, J. K., CAMPBELL, L., ROONEY, D., CLIPSON, N. & GLEESON, D. B. 2009. Minerals in soil select distinct bacterial communities in their microhabitats. *FEMS Microbiology Ecology,* **67**(3)**,** 381–388.

CHAIGNON, V., LARTIGES, B. S., EL SAMRANI, A. & MUSTIN, C. 2002. Evolution of size distribution and transfer of mineral particles between flocs in activated sludges: an insight into floc exchange dynamics. *Water Research,* **36,** 676–684.

CHEN, M. Y., LEE, D. J. & TAY, J. H. 2007a. Distribution of extracellular polymeric substances in aerobic granules. *Applied Microbiology and Biotechnology,* **73,** 1463–1469.

CHEN, M. Y., LEE, D. J., TAY, J. H. & SHOW, K. Y. 2007b. Staining of extracellular polymeric substances and cells in bioaggregates. *Applied Microbiology and Biotechnology,* **75,** 467–474.

CHEN, M. J., LI, J., DAI, X., SUN, Y. & CHEN, F. Z. 2011. Effect of phosphorus and temperature on chlorophyll *a* contents and cell sizes of *Scenedesmus obliquus* and *Microcystis aeruginosa*. *Limnology,* **12,** 187–192.

CHENU, C. 1993. Clay polysaccharide or sand polysaccharide associations as models for the interface between microorganisms and soil – water related properties and microstructure. *Geoderma,* **56,** 143–156.

CHESHIRE, M. V., MUNDIE, C. M. & SHEPHERD, H. 1979. Transformation of carbohydrate constituents of grass during decomposition in soil. *Journal of The Science of Food and Agriculture,* **30,** 330–330.

CHINTALAPATI, S., KIRAN, M. D. & SHIVAJI, S. 2004. Role of membrane lipid fatty acids in cold adaptation. *Cellular and Molecular Biology,* **50,** 631–642.

CHRISTNER, B. C., KVITKO, B. H. & REEVE, J. N. 2003. Molecular identification of Bacteria and Eukarya inhabiting an Antarctic cryoconite hole. *Extremophiles,* **7**(3)**,** 177–183.

COLEMAN, P. B. 1993. *Practical Sampling Techniques for Infrared Analysis,* Boca Raton, FL, CRC Press.

COMTE, K., SABACKA, M., CARRE-MLOUKA, A., ELSTER, J. & KOMAREK, J. 2007. Relationships between the Arctic and the Antarctic cyanobacteria; three *Phormidium*-like strains evaluated by a polyphasic approach. *FEMS Microbiology Ecology,* **59,** 366–376.

COOK, J., HODSON, A., TELLING, J., ANESIO, A., IRVINE-FYNN, T. & BELLAS, C. 2010. The mass–area relationship within cryoconite holes and its implications for primary production. *Annals of Glaciology,* **51,** 106–110.

CULLITY, B.D. 1978. *Elements of x-ray diffraction*. Second edition. Reading, MA, Addison-Wesley.

CUYPERS, C., GROTENHUIS, T., NIEROP, K. G. J., FRANCO, E. M., DE JAGER, A. & RULKENS,

W. 2002. Amorphous and condensed organic matter domains: the effect of persulfate oxidation on the composition of soil/sediment organic matter. *Chemosphere,* **48,** 919-931.

DALLMANN, W. K. 1999. *Lithostratigraphic lexicon of Svalbard. Upper Palaeozoic to Quaternary Bedrock. Review and Recommendations for Nomenclature Use.* Tromsø, Committee on the Stratigraphy of Svalbard / Norsk Polarinstitutt.

DAVEY, M. C., DAVIDSON, H. P. B., RICHARD, K. J. & WYNN-WILLIAMS, D. D. 1991. Attachment and growth of Antarctic soil cyanobacteria and algae on natural and artificial substrata. *Soil Biology & Biochemistry,* **23,** 185–191.

DAVEY, M. E. & O'TOOLE, G. A. 2000. Microbial biofilms: from ecology to molecular genetics. *Microbiology and Molecular Biology Reviews,* **64,** 847–867.

DE BEER, D., O'FLAHARTY, V., THAVEESRI, J., LENS, P. & VERSTRAETE, W. 1996. Distribution of extracellular polysaccharides and flotation of anaerobic sludge. *Applied Microbiology and Biotechnology,* 46**,** 197–201.

DE KREUK, M. K. & VAN LOOSDRECHT, M. C. M. 2004. Selection of slow growing organisms as a means for improving aerobic granular sludge stability. *Water Science and Technology,* **49**(11-12)**,** 9–17.

DE LOS RÍOS, A., WIERZCHOS, J., SANCHO, L. G. & ASCASO, C. 2003. Acid microenvironments in microbial biofilms of Antarctic endolithic microecosystems. *Environmental Microbiology,* **5,** 231–237.

DE LOS RÍOS, A., ASCASO, C., WIERZCHOS, J., FERNANDEZ-VALIENTE, E. & QUESADA, A. 2004. Microstructural characterization of cyanobacterial mats from the McMurdo Ice Shelf, Antarctica. *Applied And Environmental Microbiology,* **70**(1)**,** 569–580.

DE PHILIPPIS, R., FARALONI, C., SILI, C. & VINCENZINI, M. 2005. Populations of exopolysaccharide-producing cyanobacteria and diatoms in the mucilaginous benthic aggregates of the Tyrrhenian Sea (Tuscan Archipelago). *Science of the Total Environment,* **353,** 360–368.

DE PHILLIPIS, R. & VINCENZINI, M. 1998. Exocellular polysaccharides from cyanobacteria and their possible applications. *FEMS Microbiology Reviews*, **22**, 151–175.

DE WINDER, B., STAATS, N., STAL, L. J. & PATERSON, D. M. 1999. Carbohydrate secretion by phototrophic communities in tidal sediments. *Journal of Sea Research,* **42**(2)**,** 131–146.

DECHO, A. W. 1990. Microbial exopolymer secretions in ocean environments: Their role(s) in food webs and marine processes. *Oceanography & Marine Biology Annual Review*, **28**, 73–154.

DECHO, A. W. 2000. Microbial biofilms in intertidal systems: an overview. *Continental Shelf Research,* **20,** 1257–1273.

DECHO, A. W. & HERNDL, G. J. 1995. Microbial activities and the transformation of organic-matter within mucilaginous material. *Science of the Total Environment,* **165,** 33–42.

DECHO, A. W. & KAWAGUCHI, T. 1999. Confocal imaging of in situ natural microbial communities and their extracellular polymeric secretions using Nanoplast® resin. *Biotechniques,* **27,** 1246–1252.

DECHO, A. W. & LOPEZ, G. R. 1993. Exopolymer microenvironments of microbial flora – multiple and interactive effects on trophic relationships. *Limnology and Oceanography,* **38**, 1633–1645.

DECHO, A. W., VISSCHER, P. T. & REID, R. P. 2005. Production and cycling of natural microbial exopolymers (EPS) within a marine stromatolite. *Palaeogeography, Palaeoclimatology, Palaeoecology,* **219,** 71–86.

DELLA VENTURA, G., BELLATRECCIA, F., MARCELLI, A., CESTELLI GUIDI, M., PICCININI, M., CAVALLO, A. & PIOCHI, M. 2010. Application of micro-FTIR imaging in the

Earth sciences. *Analytical and Bioanalytical Chemistry,* **397,** 2039–2049.

DIGNAC, M. F., URBAIN, V., RYBACKI, D., BRUCHET, A., SNIDARO, D. & SCRIBE, P. 1998. Chemical description of extracellular polymers: Implication on activated sludge floc structure. *Water Science and Technology,* **38,** 45–53.

DITTRICH, M. & LUTTGE, A. 2008. Microorganisms, mineral surfaces, and aquatic environments: Learning from the past for future progress. *Geobiology,* **6,** 201-213.

DITTRICH, M. & SIBLER, S. 2005. Cell surface groups of two picocyanobacteria strains studied by zeta potential investigations, potentiometric titration, and infrared spectroscopy. *Journal of Colloid and Interface Science,* **286,** 487–495.

DONLAN, R. M. 2002. Biofilms: Microbial life on surfaces. *Emerging Infectious Diseases,* **8,** 881–890.

DOWNING, J. A. & RATH, L. C. 1988. Spatial patchiness in the lacustrine sedimentary environment. *Limnology and Oceanography,* **33,** 447–458.

DUBOIS, M., GILLES, K., HAMILTON, J. K., REBERS, P. A. & SMITH, F. 1951. A colorimetric method for the determination of sugars. *Nature,* **168,** 167–167.

DUPRAZ, C., VISSCHER, P. T., BAUMGARTNER, L. K. & REID, R. P. 2004. Microbe-mineral interactions: early carbonate precipitation in a hypersaline lake (Eleuthera Island, Bahamas). *Sedimentology,* **51,** 745–765.

EBOIGBODIN, K. E., OJEDA, J. J. & BIGGS, C. A. 2007. Investigating the surface properties of *Escherichia coli* under glucose controlled conditions and its effect on aggregation. *Langmuir,* **23,** 6691–6697.

EDWARDS, A., ANESIO, A. M., RASSNER, S. M., SATTLER, B., HUBBARD, B., PERKINS, W. T., YOUNG, M. & GRIFFITH, G. W. 2011. Possible interactions between bacterial diversity, microbial activity and supraglacial hydrology of cryoconite holes in Svalbard. *ISME Journal,* **5,** 150–160.

EDWARDS, H. G. M., MOODY, C. A., VILLAR, S. E. J., DICKENSHEETS, D. L. & WYNN-WILLIAMS, L. D. D. 2004. Antarctic analogues for Mars exploration: A Raman spectroscopic study of biogeological signatures. *Proceedings of the III European Workshop on Exo-Astrobiology,* **545,** 33–36.

ENGLAND, R. R. & EVANS, E. H. 1983. A requirement for Ca-2+ in the extraction of O-2-evolving photosystem-2 preparations from the cyanobacterium *Anacystis nidulans*. *Biochemical Journal,* **210,** 473–476.

ESCH, P. & NEHRKORN, A. 1988. Scanning electron-microscopic examination of the microbial-population in slow sand filters. *Zentralblatt für Bakteriologie Mikrobiologie und Hygiene, Serie B,* **185,** 569–579.

ETZELMÜLLER, B., ØDEGÅRD, R. S., VATNE, G., MYSTERUD, R. S., TONNING, T. & SOLLID, J. L. 2000. Glacier characteristics and sediment transfer system of Longyearbreen and Larsbreen, western Spitsbergen. *Norwegian Journal of Geography,* **54,** 157–168.

FALCHINI, L., SPARVOLI, E. & TOMASELLI, L. 1996. Effect of *Nostoc* (cyanobacteria) inoculation on the structure and stability of clay soils. *Biology and Fertility of Soils,* **23,** 346–352.

FARMER, V.C., 1974. *The Infrared Spectra of Minerals*. Mineralogical Society, London.

FENCHEL, T. & KÜHL, M. 2000. Artificial cyanobacterial mats: growth, structure, and vertical zonation patterns. *Microbial Ecology,* **40,** 85–93.

FIERER, N., BRADFORD, M. A. & JACKSON, R. B. 2007. Toward an ecological classification of soil bacteria. *Ecology,* 88**,** 1354–1364.

FISCHER, H., MEYER, A., FISCHER, K. & KUZYAKOV, Y. 2007. Carbohydrate and amino acid composition of dissolved organic matter leached from soil. *Soil Biology and Biochemistry,* **39,** 2926–2935.

FISCHER, T., VESTE, M., SCHAAF, W., DUMIG, A., KÖGEL-KNABNER, I., WIEHE, W., BENS, O. & HUTTL, R. 2010. Initial pedogenesis in a topsoil crust 3 years after construction of an artificial catchment in Brandenburg, NE Germany. *Biogeochemistry,* **101,** 165–176.

FLETCHER, A. L., THIEL, B. L. & DONALD, A. M. 1997. Amplification measurements of alternative imaging gases in environmental SEM. *Journal of Physics D,* **30,** 2249–2257.

FOLKERSMA, R., VAN DIEMEN, A. J. G. & STEIN, H. N. 1999. Understanding the influence of gravity on perikinetic coagulation on the basis of the DLVO theory. *Advances in Colloid and Interface Science,* **83**(1-3)**,** 71–84.

FOREMAN, C. M., SATTLER, B., MIKUCKI, J. A., PORAZINSKA, D. L. & PRISCU, J. C. 2007. Metabolic activity and diversity of cryoconites in the Taylor Valley, Antarctica. *Journal of Geophysical Research – Biogeosciences,* **112**.

FORSSTRÖM, S., STRÖM, J., PEDERSEN, C. A., ISAKSSON, E. & GERLAND, S. 2009. Elemental carbon distribution in Svalbard snow. *Journal of Geophysical Research – Atmospheres,* **114**.

FORTNER, S. K., TRANTER, M., FOUNTAIN, A., LYONS, W. B. & WELCH, K. A. 2005. The geochemistry of supraglacial streams of Canada Glacier, Taylor Valley (Antarctica), and their evolution into proglacial waters. *Aquatic Geochemistry,* **11,** 391–412.

FOSTER, R. C. 1981. Polysaccharides in soil fabrics. *Science,* **214,** 665–667.

FOUNTAIN, A. G., NYLEN, T. H., TRANTER, M. & BAGSHAW, E. 2008. Temporal variations in physical and chemical features of cryoconite holes on Canada Glacier, McMurdo Dry Valleys, Antarctica. *Journal of Geophysical Research – Biogeosciences,* **113**.

FURUKI, T. 2000. Effect of stereochemistry on the anti-freeze characteristics of carbohydrates. A thermal study of aqueous monosaccharides at subzero temperatures. *Carbohydrate Research,* **323,** 185–191.

GALE, S.J. and HOARE, P.J. 1991. *Quaternary sediments*. London, Belhaven Press.

GAO, Q. & GARCIA-PICHEL, F. 2011. Microbial ultraviolet sunscreens. *Nature Reviews Microbiology,* **9,** 791–802.

GARCIA-PICHEL, F. & BELNAP, J. 1996. Microenvironments and microscale productivity of cyanobacterial desert crusts. *Journal of Phycology,* **32,** 774–782.

GEESEY, G. G., MUTCH, R., COSTERTON, J. W. & GREEN, R. B. 1978. Sessile bacteria – important component of microbial population in small mountain streams. *Limnology and Oceanography,* **23,** 1214–1223.

GEOGHEGAN, M., ANDREWS, J. S., BIGGS, C. A., EBOIGBODIN, K. E., ELLIOTT, D. R., ROLFE, S., SCHOLES, J., OJEDA, J. J., ROMERO-GONZALEZ, M. E., EDYVEAN, R. G. J., SWANSON, L., RUTKAITE, R., FERNANDO, R., PEN, Y., ZHANG, Z. Y. & BANWART, S. A. 2008. The polymer physics and chemistry of microbial cell attachment and adhesion. *Faraday Discussions,* **139,** 85–103.

GERDEL, R. W. & DROUET, F. 1960. The cryoconite of the Thule Area, Greenland. *Transactions of the American Microscopical Society,* **79,** 256–272.

GIOVANELA, M., CRESPO, J. S., ANTUNES, M., ADAMATTI, D. S., FERNANDES, A. N., BARISON, A., DA SILVA, C. W. P., GUEGAN, R., MOTELICA-HEINO, M. & SIERRA, M. M. D. 2010. Chemical and spectroscopic characterization of humic acids extracted from the bottom sediments of a Brazilian subtropical microbasin. *Journal of Molecular Structure,* **981**(1-3)**,** 111–119.

GIRALDEZ-RUIZ, N., BONILLA, I. & FERNANDEZ-PINAS, F. 1999. Role of external calcium in homeostasis of intracellular pH in the cyanobacterium *Anabaena* sp. strain PCC7120 exposed to low pH. *New Phytologist,* **141,** 225–230.

GLAZER, A. N. 1977. Structure and molecular organization of photosynthetic accessory

pigments of cyanobacteria and red algae. *Molecular and Cellular Biochemistry,* **18,** 125–140.

GLEESON, D. F., WILLIAMSON, C., GRASBY, S. E., PAPPALARDO, R. T., SPEAR, J. R. & TEMPLETON, A. S. 2011. Low temperature S(0) biomineralization at a supraglacial spring system in the Canadian High Arctic. *Geobiology,* **9,** 360–375.

GOLUBIC, S., SEONG-JOO, L. & BROWNE, K. M. 2000. Cyanobacteria: architects of sedimentary structures. *In:* RIDING, R. E. & AWRAMIK, S. M. (eds.) *Microbial Sediments.* Berlin: Springer-Verlag.

GOURAUD, H. 1971. Continuous shading of curved surfaces. *IEEE Transactions on Computers,* C **20,** 623–629.

GREGOR, J. & MARSALEK, B. 2005. A simple in vivo fluorescence method for the selective detection and quantification of freshwater cyanobacteria and eukaryotic algae. *Acta Hydrochimica et Hydrobiologica,* **33,** 142–148.

GRIBBON, P. 1979. Cryoconite holes on Sermikavasak, West Greenland. *Journal of Glaciology,* **22,** 177–181.

GROSSART, H. P., SIMON, M. & LOGAN, B. E. 1997. Formation of macroscopic organic aggregates (lake snow) in a large lake: The significance of transparent exopolymer particles, phytoplankton, and zooplankton. *Limnology and Oceanography,* **42,** 1651–1659.

GUENTHER, M. & BOZELLI, R. 2004. Factors influencing algae–clay aggregation. *Hydrobiologia,* **523,** 217–223.

HEISSENBERGER, A., LEPPARD, G. G. & HERNDL, G. J. 1996. Ultrastructure of marine snow. 2. Microbiological considerations. *Marine Ecology – Progress Series,* **135,** 299–308.

HENRIKSEN, N., HIGGINS, A. K., KALSBEEK, F. & PULVERTAFT, T. C. R. 2009. Greenland from Archaean to Quaternary. Descriptive text to the 1995 Geological map of Greenland, 1:2 500 000. 2nd edition. *Geological Survey of Denmark and Greenland Bulletin***,** 9–116.

HERAUD, P., WOOD, B. R., TOBIN, M. J., BEARDALL, J. & MCNAUGHTON, D. 2005. Mapping of nutrient-induced biochemical changes in living algal cells using synchrotron infrared microspectroscopy. *FEMS Microbiology Letters,* **249,** 219–225.

HERLORY, O., GUARINI, J. M., RICHARD, P. & BLANCHARD, G. F. 2004. Microstructure of microphytobenthic biofilm and its spatio-temporal dynamics in an intertidal mudflat (Aiguillon Bay, France). *Marine Ecology – Progress Series,* **282,** 33–44.

HERMAN, B. 1997. *Fluorescence Microscopy (2nd edition)*. Bios Scientific Publishers.

HERRICK, J. E., VAN ZEE, J. W., BELNAP, J., JOHANSEN, J. R. & REMMENGA, M. 2010. Fine gravel controls hydrologic and erodibility responses to trampling disturbance for coarse-textured soils with weak cyanobacterial crusts. *Catena*, **83**, 119–126.

HJELLE, A. 1993. *Geology of Svalbard.* Oslo, Norsk Polarinstitutt.

HODSON, A., MUMFORD, P. & LISTER, D. 2004. Suspended sediment and phosphorus in proglacial rivers: bioavailability and potential impacts upon the P status of ice-marginal receiving waters. *Hydrological Processes,* **18,** 2409–2422.

HODSON, A. J., MUMFORD, P. N., KOHLER, J. & WYNN, P. M. 2005. The High Arctic glacial ecosystem: new insights from nutrient budgets. *Biogeochemistry,* **72,** 233–256.

HODSON, A., ANESIO, A. M., TRANTER, M., FOUNTAIN, A., OSBORN, M., PRISCU, J., LAYBOURN-PARRY, J. & SATTLER, B. 2008. Glacial ecosystems. *Ecological Monographs,* **78**(1)**,** 41–67.

HODSON, A., CAMERON, K., BØGGILD, C., IRVINE-FYNN, T., LANGFORD, H., PEARCE, D. & BANWART, S. 2010. The structure, biological activity and biogeochemistry of cryoconite aggregates upon an Arctic valley glacier: Longyearbreen, Svalbard. *Journal of Glaciology,* **56**(96)**,** 349–362.

HOLM-HANSEN, O. & RIEMANN, B. 1978. Chlorophyll *a* determination – improvements in methodology. *Oikos,* **30,** 438–447.

HOPKINS, D. W., SPARROW, A. D., ELBERLING, B., GREGORICH, E. G., NOVIS, P. M., GREENFIELD, L. G. & TILSTON, E. L. 2006. Carbon, nitrogen and temperature controls on microbial activity in soils from an Antarctic dry valley. *Soil Biology & Biochemistry,* **38,** 3130–3140.

IRVINE-FYNN, T. D. L., BRIDGE, J. W. & HODSON, A. J. 2010. Rapid quantification of cryoconite: granule geometry and in situ supraglacial extents, using examples from Svalbard and Greenland. *Journal of Glaciology,* **56,** 297–308.

IRVINE-FYNN, T. D. L., BRIDGE, J. W. & HODSON, A. J. 2011. In situ quantification of supraglacial cryoconite morphodynamics using time-lapse imaging: an example from Svalbard. *Journal of Glaciology,* **57,** 651–657.

IRVINE-FYNN, T. D. L. et al. *in press*. Quantifying microbial cell export from the surface of a high-Arctic glacier using flow cytometry.

IVANOVA, E. P., ALEXEEVA, Y. V., PHAM, D. K., WRIGHT, J. P. & NICOLAU, D. V. 2006. ATP level variations in heterotrophic bacteria during attachment on hydrophilic and hydrophobic surfaces. *International Microbiology,* **9,** 37–46.

JI, J. F., GE, Y., BALSAM, W., DAMUTH, J. E. & CHEN, J. 2009. Rapid identification of dolomite using a Fourier Transform Infrared Spectrophotometer (FTIR): A fast method for identifying Heinrich events in IODP Site U1308. *Marine Geology,* **258**(1-4)**,** 60–68.

JOLLIFFE, I. 1986. *Principal component analysis*. Springer, New York.

JORAND, F., BOUE-BIGNE, F., BLOCK, J. C. & URBAIN, V. 1998. Hydrophobic/hydrophilic properties of activated sludge exopolymeric substances. *Water Science and Technology,* **37,** 307–315.

JØRGENSEN, B. B., COHEN, Y. & DESMARAIS, D. J. 1987. Photosynthetic action spectra and adaptation to spectral light distribution in a benthic cyanobacterial mat. *Applied and Environmental Microbiology,* **53,** 879–886.

JOUBERT, E. D. & PILLAY, B. 2008. Visualisation of the microbial colonisation of a slow sand filter using an Environmental Scanning Electron Microscope. *Electronic Journal of Biotechnology,* **11**.

KAÇURAKOVA, M., CAPEK, P., SASINKOVA, V., WELLNER, N. & EBRINGEROVA, A. 2000. FT-IR study of plant cell wall model compounds: pectic polysaccharides and hemicelluloses. *Carbohydrate Polymers,* **43,** 195–203.

KAISER, K. & GUGGENBERGER, G. 2003. Mineral surfaces and soil organic matter. *European Journal of Soil Science,* **54,** 219–236.

KAISER, K., GUGGENBERGER, G., HAUMAIER, L. & ZECH, W. 1997. Dissolved organic matter sorption on sub soils and minerals studied by ^{13}C-NMR and DRIFT spectroscopy. *Eur. J. Soil Sci.* **48**(2), 301-310.

KALBITZ, K., GEYER, W. & GEYER, S. 1999. Spectroscopic properties of dissolved humic substances – a reflection of land use history in a fen area. *Biogeochemistry*. **47**(2), 219-238.

KANSIZ, M., HERAUD, P., WOOD, B., BURDEN, F., BEARDALL, J. & MCNAUGHTON, D. 1999. Fourier Transform Infrared microspectroscopy and chemometrics as a tool for the discrimination of cyanobacterial strains. *Phytochemistry,* **52,** 407–417.

KAPITULÇINOVA, D., COCKELL, C. S., HALLAM, K. R. & RAGNARSDOTTIR, K. V. 2008. Effect of cyanobacterial growth on biotite surfaces under laboratory nutrient-limited conditions. *Mineralogical Magazine,* **72,** 71–75.

KAWAGUCHI, T. & DECHO, A. W. 2002. In situ microspatial imaging using two-photon and confocal laser scanning microscopy of bacteria and extracellular polymeric secretions (EPS) within marine stromatolites. *Marine Biotechnology,* **4,** 127–131.

KEURSON, G. W., MIERNYK, J. A. & BUDD, K. 1984. Evidence for the occurrence of, and possible physiological role for cyanobacterial calmodulin. *Plant Physiology,* **75,** 222–224.

KILBERTUS, G. 1980. Study of microhabitats in soil aggregates – relation to bacterial biomass and size of procaryotes. *Revue d'Ecologie et de Biologie du Sol,* **17,** 543–557.

KILBERTUS, G., PROTH, J. & VERVIER, B. 1979. Effect of dehydration on gram-negative bacteria of soil. *Soil Biology & Biochemistry,* **11,** 109–114.

KIM, C. J., JUNG, Y. H., AHN, C. Y., LEE, Y. K. & OH, H. M. 2010. Adsorption of turbid materials by the cyanobacterium *Phormidium parchydematicum*. *Journal of Applied Phycology,* **22,** 181–186.

KIORBOE, T., ANDERSEN, K. P. & DAM, H. G. 1990. Coagulation efficiency and aggregate formation in marine phytoplankton. *Marine Biology,* **107,** 235–245.

KLOCK, J. H., WIELAND, A., SEIFERT, R. & MICHAELIS, W. 2007. Extracellular polymeric substances (EPS) from cyanobacterial mats: characterisation and isolation method optimisation. *Marine Biology,* **152,** 1077–1085.

KÖGEL-KNABNER, I., GUGGENBERGER, G., KLEBER, M., KANDELER, E., KALBITZ, K., SCHEU, S., EUSTERHUES, K. & LEINWEBER, P. 2008. Organo-mineral associations in temperate soils: Integrating biology, mineralogy, and organic matter chemistry. *Journal of Plant Nutrition and Soil Science,* **171**(1)**,** 61–82.

KORBEE, N., FIGUEROA, F. L. & AGUILERA, J. 2005. Effect of light quality on the accumulation of photosynthetic pigments, proteins and mycosporine-like amino acids in the red alga *Porphyra leucosticta* (Bangiales, Rhodophyta). *Journal of Photochemistry and Photobiology B,* **80**, 71–78.

KOVAC, N., BAJT, O., FAGANELI, J., SKET, B. & OREL, B. 2002. Study of macroaggregate composition using FT-IR and H-1-NMR spectroscopy. *Marine Chemistry,* **78,** 205–215.

KRISTENSEN, E. 1990. Characterisation of biogenic organic matter by stepwise thermogravimetry (STG). *Biogeochemistry,* **9,** 135–159.

KRUSCHEL, C. & CASTENHOLZ, R. W. 1998. The effect of solar UV and visible irradiance on the vertical movements of cyanobacteria in microbial mats of hypersaline waters. *FEMS Microbiology Ecology*, **27**, 53–72.

LANGFORD, H., HODSON, A., BANWART, S. & BØGGILD, C. 2010. The microstructure and biogeochemistry of Arctic cryoconite granules. *Annals of Glaciology,* **51,** 87–94.

LANGFORD, H., HODSON, A. & BANWART, S. 2011. Using FTIR spectroscopy to characterise the soil mineralogy and geochemistry of cryoconite from Aldegondabreen glacier, Svalbard. *Applied Geochemistry,* **26,** S206–S209.

LANGFORD, H., HODSON, A. & BANWART, S. *in preparation* 2012a. Using electron and optical microscopy to study soil microaggregate structure in cryoconite from Alpine and Arctic locations.

LANGFORD, H., HODSON, A. & BANWART, S. *in preparation* 2012b. Geospatial investigation of photosynthetic pigments and carbohydrates within cryoconite on Longyearbreen glacier, Svalbard.

LARA, C., RODRIGUEZ, R. & GUERRERO, M. G. 1993. Sodium-dependent nitrate transport and energetics of cyanobacteria. *Journal of Phycology,* **29,** 389–395.

LAROSE, C., BERGER, S., FERRARI, C., NAVARRO, E., DOMMERGUE, A., SCHNEIDER, D. & VOGEL, T. M. 2010. Microbial sequences retrieved from environmental samples from seasonal Arctic snow and meltwater from Svalbard, Norway. *Extremophiles,* **14,** 205–212.

LAWRENCE, J. R., SWERHONE, G. D. W., LEPPARD, G. G., ARAKI, T., ZHANG, X., WEST, M. M.

& HITCHCOCK, A. P. 2003. Scanning transmission X-ray, laser scanning, and transmission electron microscopy mapping of the exopolymeric matrix of microbial biofilms. *Applied and Environmental Microbiology,* **69,** 5543–5554.

LAWRENZ, E., FEDEWA, E. & RICHARDSON, T. 2011. Extraction protocols for the quantification of phycobilins in aqueous phytoplankton extracts. *Journal of Applied Phycology,* **23,** 865–871.

LAYBOURN-PARRY, J. 2009. No place too cold. *Science,* **324,** 1521–1522.

LAYBOURN-PARRY, J. & MARSHALL, W. A. 2003. Photosynthesis, mixotrophy and microbial plankton dynamics in two high Arctic lakes during summer. *Polar Biology,* **26,** 517–524.

LAYBOURN-PARRY, J. & PEARCE, D. A. 2007. The biodiversity and ecology of Antarctic lakes: models for evolution. *Philosophical Transactions of the Royal Society B,* **362,** 2273–2289.

LEAPMAN, R. & ARONOVA, M. 2008. Nanoscale elemental imaging of cellular structures by electron energy loss spectroscopy in the transmission electron microscope. *Abstracts of Papers of the American Chemical Society,* **236**.

LEHMANN, J., KINYANGI, J. & SOLOMON, D. 2007. Organic matter stabilization in soil microaggregates: implications from spatial heterogeneity of organic carbon contents and carbon forms. *Biogeochemistry,* **85,** 45–57.

LEPPARD, G. G. 1992. Size, morphology and composition of particulates in aquatic ecosystems – solving speciation problems by correlative electron-microscopy. *Analyst,* **117,** 595–603.

LEPPARD, G. G. 1995. The characterisation of algal and microbial mucilages and their aggregates in aquatic ecosystems. *Science of the Total Environment,* **165,** 103–131.

LEPPARD, G. G., HEISSENBERGER, A. & HERNDL, G. J. 1996. Ultrastructure of marine snow. 1. Transmission electron microscopy methodology. *Marine Ecology – Progress Series,* **135,** 289–298.

LESLIE, J. F., GREASHAM, R. L. & HULBERT, M. H. 1984. A cyanobacterial system for consolidation of phosphate slimes. *Geomicrobiology Journal,* **3,** 343–358.

LEUNISSEN, J. L. M. & YI, H. 2009. Self-pressurized rapid freezing (SPRF): a novel cryofixation method for specimen preparation in electron microscopy. *Journal of Microscopy,* **235,** 25–35.

LEWIS, E. N., TREADO, P. J., REEDER, R. C., STORY, G. M., DOWREY, A. E., MARCOTT, C. & LEVIN, I. W. 1995. Fourier transform spectroscopic imaging using an infrared focal-plane array detector. *Analytical Chemistry,* **67,** 3377–3381.

LI, T., WU, T.-D., MAZÉAS, L., TOFFIN, L., GUERQUIN-KERN, J.-L., LEBLON, G. & BOUCHEZ, T. 2008. Simultaneous analysis of microbial identity and function using NanoSIMS. *Environmental Microbiology,* **10,** 580–588.

LI, Y., DICK, W. A. & TUOVINEN, O. H. 2004. Fluorescence microscopy for visualization of soil microorganisms – a review. *Biology and Fertility of Soils,* **39,** 301–311.

LI, Z. H., WANG, X. C., KUBA, T. & KUSUDA, T. 2011. Porous structure and spatial characteristics of aerobic granules. *International Journal of Environment and Pollution,* **45,** 25–35.

LIOTENBERG, S., CAMPBELL, D., RIPPKA, R., HOUMARD, J. & DEMARSAC, N. T. 1996. Effect of the nitrogen source on phycobiliprotein synthesis and cell reserves in a chromatically adapting filamentous cyanobacterium. *Microbiology UK,* **142,** 611–622.

LITTLE, B., WAGNER, P., RAY, R., POPE, R. & SCHEETZ, R. 1991. Biofilms – an ESEM evaluation of artifacts introduced during SEM preparation. *Journal of Industrial Microbiology,* **8,** 213–221.

LIU, H. & FANG, H. H. P. 2002. Characterization of electrostatic binding sites of extracellular polymers by linear programming analysis of titration data. *Biotechnology and Bioengineering,* **80,** 806–811.

LIU, Y., YANG, S.-F., LI, Y., XU, H., QIN, L. & TAY, J.-H. 2004. The influence of cell and substratum surface hydrophobicities on microbial attachment. *Journal of Biotechnology,* **110,** 251–256.

LUNAU, M., LEMKE, A., DELLWIG, O. & SIMON, M. 2006. Physical and biogeochemical controls of microaggregate dynamics in a tidally affected coastal ecosystem. *Limnology and Oceanography,* **51,** 847–859.

LÜNSDORF, H., ERB, R. W., ABRAHAM, W. R. & TIMMIS, K. N. 2000. 'Clay hutches': a novel interaction between bacteria and clay minerals. *Environmental Microbiology,* **2,** 161–168.

MACDONNELL, S. & FITZSIMONS, S. 2008. The formation and hydrological significance of cryoconite holes. *Progress in Physical Geography,* **32,** 595–610.

MADEJOVA, J. 2003. FTIR techniques in clay mineral studies. *Vibrational Spectroscopy,* **31**(1)**,** 1–10.

MADEJOVA, J., PENTRAK, M., PALKOVA, H., and KOMADEL, P. 2009. Near-infrared spectroscopy: A powerful tool in studies of acid-treated clay minerals, *Vibrational Spectroscopy*., **49**(2), 211-218.

MARGESIN, R., ZACKE, G. & SCHINNER, F. 2002. Characterization of heterotrophic microorganisms in alpine glacier cryoconite. *Arctic, Antarctic and Alpine Research,* **34**(1)**,** 88–93.

MARTINEZ, R. E., POKROVSKY, O. S., SCHOTT, J. & OELKERS, E. H. 2008. Surface charge and zeta-potential of metabolically active and dead cyanobacteria. *Geochimica et Cosmochimica Acta,* **72,** A597–A597.

MARX, J. G., CARPENTER, S. D. & DEMING, J. W. 2009. Production of cryoprotectant extracellular polysaccharide substances (EPS) by the marine psychrophilic bacterium *Colwellia psychrerythraea* strain 34H under extreme conditions. *Canadian Journal of Microbiology,* **55,** 63–72.

MASUKO, T., MINAMI, A., IWASAKI, N., MAJIMA, T., NISHIMURA, S. I. & LEE, Y. C. 2005. Carbohydrate analysis by a phenol–sulfuric acid method in microplate format. *Analytical Biochemistry,* **339,** 69–72.

MATTESON, A. and HERRON, M.M. 1993. Quantitative mineral analysis by Fourier Transform infrared spectroscopy, Paper No. 9308, presented at the Society of Core Analysts Conference, pp. 1–15.

MAXWELL, C. D. & NEUMAN, C. M. 1994. Photoautotrophs and the microaggregation of sand in a fresh-water beach dune complex – implications for sediment transport by wind. *Soil Biology & Biochemistry,* **26,** 221–233.

MCINTYRE, N. F. 1984. Cryoconite hole thermodynamics. *Canadian Journal Of Earth Sciences,* **21,** 152–156.

MCKNIGHT, D. M., NIYOGI, D. K., ALGER, A. S., BOMBLIES, A., CONOVITZ, P. A. & TATE, C. M. 1999. Dry valley streams in Antarctica: Ecosystems waiting for water. *Bioscience,* **49,** 985–995.

MECOZZI, M. & PIETRANTONIO, E. 2006. Carbohydrates proteins and lipids in fulvic and humic acids of sediments and its relationships with mucilaginous aggregates in the Italian seas. *Marine Chemistry,* **101,** 27–39.

MESTRES, P., PÜTZ, N. & LAUE, M. 2003. Applications of ESEM to the study of biomedical specimens. *Microscopy and Microanalysis***, 9**, pp. 490–491.

MICHELETTI, E., COLICA, G., VITI, C., TAMAGNINI, P. & DE PHILIPPIS, R. 2008. Selectivity in the heavy metal removal by exopolysaccharide-producing cyanobacteria.

Journal of Applied Microbiology, **105,** 88–94.

MINDL, B., ANESIO, A. M., MEIRER, K., HODSON, A. J., LAYBOURN-PARRY, J., SOMMARUGA, R. & SATTLER, B. 2007. Factors influencing bacterial dynamics along a transect from supraglacial runoff to proglacial lakes of a high Arctic glacier. *FEMS Microbiology Ecology,* **59,** 307–317.

MOHOLDT, G., NUTH, C., HAGEN, J. O. & KOHLER, J. 2010. Recent elevation changes of Svalbard glaciers derived from ICESat laser altimetry. *Remote Sensing of Environment,* **114**(11)**,** 2756–2767.

MORATO, J. P., ROGET, E. & LOZOVATSKY, I. 2011. Statistics of microstructure patchiness in a stratified lake. *Journal of Geophysical Research – Oceans,* **116**.

MUELLER, C. W., KOLBL, A., HOESCHEN, C., HILLION, F., HEISTER, K., HERRMANN, A. M. & KÖGEL-KNABNER, I. 2012. Submicron scale imaging of soil organic matter dynamics using NanoSIMS – from single particles to intact aggregates. *Organic Geochemistry,* **42,** 1476–1488.

MÜLLER, T., BLEISS, W., MARTIN, C. D., ROGASCHEWSKI, S. & FUHR, G. 1998. Snow algae from northwest Svalbard: their identification, distribution, pigment and nutrient content. *Polar Biology,* **20,** 14–32.

MURATA, N. & SATO, N. 1978. Studies on the absorption spectra of chlorophyll *a* in aqueous dispersions of lipids from the photosynthetic membranes. *Plant and Cell Physiology,* **19,** 401–410.

MUSCARIELLO, L., ROSSO, F., MARINO, G., GIORDANO, A., BARBARISI, M., CAFIERO, G. & BARBARISI, A. 2005. A critical overview of ESEM applications in the biological field. *Journal of Cellular Physiology,* **205,** 328–334.

MYKLESTAD, S. & HAUG, A. 1972. Production of carbohydrates by the marine diatom *Chaetoceros affinis* var *willei* (Gran) Hustedt. I. Effect of the concentration of nutrients in the culture medium. *Journal of Experimental Marine Biology and Ecology***, 9**, 125–136.

NADEAU, T. L. & CASTENHOLZ, R. W. 2000. Characterization of psychrophilic oscillatorians (cyanobacteria) from Antarctic meltwater ponds. *Journal of Phycology,* **36,** 914–923.

NAKAMOTO, K. (ed.) 2009. *Infrared Spectra of Inorganic and Coordination Compounds (9th Edition),* London: Wiley.

NAMSARAEV, Z., MANO, M. J., FERNANDEZ, R. & WILMOTTE, A. 2010. Biogeography of terrestrial cyanobacteria from Antarctic ice-free areas. *Annals of Glaciology,* **51,** 171–177.

NAUMANN, D., HELM, D. & LABISCHINSKI, H. 1991. Microbiological characterizations by FT-IR spectroscopy. *Nature,* **351,** 81–82.

NEU, T. R. & LAWRENCE, J. R. 2005. One-photon versus two-photon laser scanning microscopy and digital image analysis of microbial biofilms. *Microbial Imaging,* **34,** 89–136.

NEU, T. R., DENGLER, T., JANN, B. & PORALLA, K. 1992. Structural studies of an emulsion-stabilizing exopolysaccharide produced by an adhesive, hydrophobic *Rhodococcus* strain. *Journal of General Microbiology,* **138,** 2531–2537.

NEU, T. R., KUHLICKE, U. & LAWRENCE, J. R. 2002. Assessment of fluorochromes for two-photon laser scanning microscopy of biofilms. *Applied and Environmental Microbiology,* **68,** 901–909.

NEU, T. R., WOELFL, S. & LAWRENCE, J. R. 2004. Three-dimensional differentiation of photo-autotrophic biofilm constituents by multi-channel laser scanning microscopy (single-photon and two-photon excitation). *Journal of Microbiological Methods*, **56**, 161-172.

NEU, T. R., MANZ, B., VOLKE, F., DYNES, J. J., HITCHCOCK, A. P. & LAWRENCE, J. R. 2010. Advanced imaging techniques for assessment of structure, composition and function in biofilm systems. *FEMS Microbiology Ecology,* **72**(1)**,** 1–21.

NEWTON, A. P. W. 1982. Red-colored snow algae in Svalbard – some environmental factors determining the distribution of *Chlamydomonas nivalis* (*Chlorophyta volvocales*). *Polar Biology,* **1,** 167–172.

NIVENS, D. E., OHMAN, D. E., WILLIAMS, J. & FRANKLIN, M. J. 2001. Role of alginate and its O acetylation in formation of *Pseudomonas aeruginosa* microcolonies and biofilms. *Journal of Bacteriology,* **183,** 1047–1057.

NOFFKE, N., GERDES, G., KLENKE, T. & KRUMBEIN, W. E. 2001. Microbially induced sedimentary structures – a new category within the classification of primary sedimentary structures. *Journal of Sedimentary Research,* **71,** 649–656.

NOFFKE, N., GERDES, G. & KLENKE, T. 2003. Benthic cyanobacteria and their influence on the sedimentary dynamics of peritidal depositional systems (siliciclastic, evaporitic salty, and evaporitic carbonatic). *Earth Science Reviews,* **62,** 163–176.

O'MELIA, C. R. & TILLER, C. L. 1993. Physicochemical aggregation and deposition in aquatic environments. *In:* BUFFLE, J. & VAN LEEUWEN, H. P. (eds.) *Environmental Particles, Vol. 2.* Ann Arbor: Lewis Publishers.

OADES, J. M. 1984. Soil organic matter and structural stability – mechanisms and implications for management. *Plant And Soil,* **76,** 319–337.

OBERNOSTERER, I. & HERNDL, G. J. 1995. Phytoplankton extracellular release and bacterial growth – dependence on the inorganic N–P ratio. *Marine Ecology – Progress Series,* **116,** 247–257.

OJEDA, J. J., ROMERO-GONZALEZ, M. E., POURAN, H. M. & BANWART, S. A. 2009. Investigating the chemical interactions between *Pseudomonas putida* and hematite using in situ flow-cell ATR-FTIR with a hematite-coated Ge crystal. *Geochimica et Cosmochimica Acta,* **73,** A968–A968.

OMOIKE, A. & CHOROVER, J. 2004. Spectroscopic study of extracellular polymeric substances from *Bacillus subtilis*: Aqueous chemistry and adsorption effects. *Biomacromolecules,* **5,** 1219–1230.

OR, D., PHUTANE, S. & DECHESNE, A. 2007. Extracellular polymeric substances affecting pore-scale hydrologic conditions for bacterial activity in unsaturated soils. *Vadose Zone Journal,* **6,** 298–305.

ORTEGA-CALVO, J. J. & STAL, L. J. 1994. Sulfate-limited growth in the N-2-fixing unicellular cyanobacterium *Gloeothece* (Nageli) sp PCC-6909. *New Phytologist,* **128,** 273–281.

OWRID, G., SOCAL, G., CIVITARESE, G., LUCHETTA, A., WIKTOR, J., NOTHIG, E. M., ANDREASSEN, I., SCHAUER, U. & STRASS, V. 2000. Spatial variability of phytoplankton, nutrients and new production estimates in the waters around Svalbard. *Polar Research,* **19,** 155–171.

PAL, S., SEN, G., KARMAKAR, N. C., MAL, D. & SINGH, R. P. 2008. High performance flocculating agents based on cationic polysaccharides in relation to coal fine suspension. *Carbohydrate Polymers,* **74,** 590–596.

PAN, G., ZHANG, M.-M., CHEN, H., ZOU, H. & YAN, H. 2006. Removal of cyanobacterial blooms in Taihu Lake using local soils. I. Equilibrium and kinetic screening on the flocculation of *Microcystis aeruginosa* using commercially available clays and minerals. *Environmental Pollution,* **141,** 195–200.

PATERSON, D. M. 1997. Biological mediation of sediment erodibility: ecology and physical dynamics. *In:* BURT, N., PARKER, R. & WATTS, J. (eds.) *Cohesive Sediments.* Chichester: John Wiley & Sons.

PATERSON, D. M., ASPDEN, R. J., VISSCHER, P. T., CONSALVEY, M., ANDRES, M. S., DECHO, A. W., STOLZ, J. & REID, R. P. 2008. Light-dependant biostabilisation of sediments

by stromatolite assemblages. *PLOS One,* **3,** e3176.

PATERSON, D. M., ASPDEN, R. J. & REID, P. 2010. Biodynamics of modern marine stromatolites. *In:* SECKBACH, J. & OREN, A. (eds.) *Microbial Mats: Modern and Ancient Microorganisms in Stratified Systems: Cellular Origin, Life in Extreme Habitats and Astrobiology vol. 14.* New York: Springer.

PAWLEY, J. B. (ed.) 2006. *Handbook of Biological Confocal Microscopy (3rd edition)*: Springer.

PEARCE, D. A., BRIDGE, P. D., HUGHES, K. A., SATTLER, B., PSENNER, R. & RUSSELL, N. J. 2009. Microorganisms in the atmosphere over Antarctica. *FEMS Microbiology Ecology,* **69,** 143–157.

PEREIRA, S., ZILLE, A., MICHELETTI, E., MORADAS-FERREIRA, P., DE PHILIPPIS, R. & TAMAGNINI, P. 2009. Complexity of cyanobacterial exopolysaccharides: composition, structures, inducing factors and putative genes involved in their biosynthesis and assembly. *FEMS Microbiology Reviews,* **33,** 917–941.

PERNTHALER, A. & AMANN, R. 2004. Simultaneous fluorescence in situ hybridization of mRNA and rRNA in environmental bacteria. *Applied and Environmental Microbiology,* **70,** 5426–5433.

PETIBOIS, C., WEHBE, K., BELBACHIR, K., NOREEN, R. & DELERIS, G. 2009. Current trends in the development of FTIR imaging for the quantitative analysis of biological samples. *Acta Physica Polonica A,* **115,** 507–512.

PHOENIX, V. R., MARTINEZ, R. E., KONHAUSER, K. O. & FERRIS, F. G. 2002. Characterization and implications of the cell surface reactivity of *Calothrix* sp strain KC97. *Applied and Environmental Microbiology,* **68,** 4827–4834.

PINCKNEY, J., PAPA, R. & ZINGMARK, R. 1994. Comparison of high-performance liquid-chromatographic, spectrophotometric, and fluorimetric methods for determining chlorophyll *a* concentrations in estuarine sediments. *Journal of Microbiological Methods,* **19,** 59–66.

PISTORIUS, A. M. A., DEGRIP, W. J. & EGOROVA-ZACHERNYUK, T. A. 2009. Monitoring of biomass composition from microbiological sources by means of FT-IR spectroscopy. *Biotechnology and Bioengineering,* **103,** 123–129.

PLEE, K., ARIZTEGUI, D., MARTINI, R. & DAVAUD, E. 2008. Unravelling the microbial role in ooid formation – results of an in situ experiment in modern freshwater Lake Geneva in Switzerland. *Geobiology,* **6,** 341–350.

POKROVSKY, O. S., SHIROKOVA, L. S., BENEZETH, P., SCHOTT, J. & GOLUBEV, S. V. 2009. Effect of organic ligands and heterotrophic bacteria on wollastonite dissolution kinetics. *American Journal of Science,* **309,** 731–772.

PORAZINSKA, D. L., FOUNTAIN, A. G., NYLEN, T. H., TRANTER, M., VIRGINIA, R. A. & WALL, D. H. 2004. The biodiversity and biogeochemistry of cryoconite holes from McMurdo Dry Valley glaciers, Antarctica. *Arctic, Antarctic and Alpine Research,* **36,** 84–91.

PRICE, P. B. 2007. Microbial life in glacial ice and implications for a cold origin of life. *FEMS Microbiology Ecology,* **59,** 217–231.

PRIESTER, J. H., HORST, A. M., VAN DE WERFHORST, L. C., SALETA, J. L., MERTES, L. A. K. & HOLDEN, P. A. 2007. Enhanced visualization of microbial biofilms by staining and environmental scanning electron microscopy. *Journal of Microbiological Methods,* **68,** 577–587.

PRISCU, J. C. & CHRISTNER, B. C. 2004. Earth's icy biosphere. *In:* BULL, A. T. (ed.) *Microbial Diversity and Bioprospecting.* Washington DC: American Society for Microbiology.

PUGET, P., ANGERS, D. A. & CHENU, C. 1999. Nature of carbohydrates associated with water-stable aggregates of two cultivated soils. *Soil Biology & Biochemistry,* **31,** 55–63.

RANJARD, L. & RICHAUME, A. S. 2001. Quantitative and qualitative microscale distribution of bacteria in soil. *Research in Microbiology*, **152**(8), 707-716.

REMUSAT, L., HATTON, P.-J., NICO, P. S., ZELLER, B., KLEBER, M. & DERRIEN, D. 2012. NanoSIMS Study of Organic Matter Associated with Soil Aggregates: Advantages, Limitations, and Combination with STXM. *Environmental Science & Technology*, **46**, 3943-3949.

RICHERT, L., GOLUBIC, S., GUÉDÈS, R., RATISKOL, J., PAYRI, C. & GUEZENNEC, J. 2005. Characterization of exopolysaccharides produced by cyanobacteria isolated from Polynesian microbial mats. *Current Microbiology,* **51,** 379–384.

RIPPKA, R., DERUELLES, J., WATERBURY, J.B., HERDMAND, M. and STANIER, R.Y. 1979. Generic assignments, strain histories and properties of pure cultures of cyanobacteria. *Journal of General Microbiology*, **111**, 1–61.

ROLDAN, M. & HERNÁNDEZ-MARINÉ, M. 2009. Exploring the secrets of the three-dimensional architecture of phototrophic biofilms in caves. *International Journal of Speleology,* **38,** 41–53.

RUFFELL, A. and WILTSHIRE, P. 2004. Conjunctive use of quantitative and qualitative X-ray diffraction analysis of soils and rocks for forensic analysis. *Forensic Science International*, **145**(1), 13–23.

SABATER, S. 2000. Structure and architecture of a stromatolite from a Mediterranean stream. *Aquatic Microbial Ecology,* **21,** 161–168.

SANIN, F. D. & VESILIND, P. A. 1996. Synthetic sludge: A physical/chemical model in understanding bioflocculation. *Water Environment Research,* **68,** 927–933.

SARTONI, G., URBANI, R., SIST, P., BERTO, D., NUCCIO, C. & GIANI, M. 2008. Benthic mucilaginous aggregates in the Mediterranean Sea: Origin, chemical composition and polysaccharide characterization. *Marine Chemistry,* **111,** 184–198.

SARTORY, D. P. & GROBBELAAR, J. U. 1984. Extraction of chlorophyll *a* from fresh-water phytoplankton for spectrophotometric analysis. *Hydrobiologia,* **114,** 177–187.

SATTLER, B., STORRIE-LOMBARDI, M. C., FOREMAN, C. M., TILG, M. & PSENNER, R. 2010. Laser-induced fluorescence emission (LIFE) from Lake Fryxell (Antarctica) cryoconites. *Annals of Glaciology*, **51**, 145-152.

SÄWSTRÖM, C., MUMFORD, P., MARSHALL, W., HODSON, A. & LAYBOURN-PARRY, J. 2002. The microbial communities and primary productivity of cryoconite holes in an Arctic glacier (Svalbard 79 degrees N). *Polar Biology,* **25,** 591–596.

SCHAEFER, C. E. G. R., SIMAS, F. N. B., GILKES, R. J., MATHISON, C., DA COSTA, L. M. & ALBUQUERQUE, M. A. 2008. Micromorphology and microchemistry of selected cryosols from maritime Antarctica. *Geoderma,* **144,** 104–115.

SCHWIERZKE-WADE, L., ROELKE, D. L., BROOKS, B. W., GROVER, J. P. & VALENTI, T. W. 2011. *Prymnesium parvum* bloom termination: role of hydraulic dilution. *Journal of Plankton Research,* **33,** 309–317.

SEGAWA, T. & TAKEUCHI, N. 2010. Cyanobacterial communities on Qiyi glacier, Qilian Shan, China. *Annals of Glaciology,* **51,** 135–144.

SEKAR, R., VENUGOPALAN, V. P., SATPATHY, K. K., NAIR, K. V. K. & RAO, V. N. R. 2004. Laboratory studies on adhesion of microalgae to hard substrates. *Hydrobiologia,* **512,** 109–116.

SHENG, G. P., YU, H. Q. & YU, Z. 2005. Extraction of extracellular polymeric substances from the photosynthetic bacterium *Rhodopseudomonas acidophila*. *Applied Microbiology And Biotechnology,* **67,** 125–130.

SIEWERT, C. 2004. Rapid screening of soil properties using thermogravimetry. *Soil Science Society of America Journal,* **68**, 1656-1661.

SIGLER, W. V. & ZEYER, J. 2002. Microbial diversity and activity along the forefields of two

receding glaciers. *Microbial Ecology,* **43**(4), 397-407.

SILVA, P. G. & SILVA, H. J. 2007. Effect of mineral nutrients on cell growth and self-flocculation of *Tolypothrix tenuis* for the production of a biofertilizer. *Bioresource Technology,* **98,** 607–611.

SIMON, M., GROSSART, H. P., SCHWEITZER, B. & PLOUG, H. 2002. Microbial ecology of organic aggregates in aquatic ecosystems. *Aquatic Microbial Ecology,* **28,** 175–211.

SIX, J., ELLIOTT, E. T., PAUSTIAN, K. & DORAN, J. W. 1998. Aggregation and soil organic matter accumulation in cultivated and native grassland soils. *Soil Science Society of America Journal,* **62,** 1367–1377.

SIX, J., FREY, S. D., THIET, R. K. & BATTEN, K. M. 2006. Bacterial and fungal contributions to carbon sequestration in agroecosystems. *Soil Science Society Of America Journal,* **70**(2), 555-569.

SKOOG, D. A., HOLLER, F. J. & CROUCH, S. R. (eds.) 2007. *Principles of Instrumental Analysis.* Florence: Brooks Cole.

SMITH, B. C. (ed.) 1996. *Fundamentals of Fourier Transform Infrared Spectroscopy*: CRC Press.

SOLÉ, A., MAS, J. & ESTEVE, I. 2007. A new method based on image analysis for determining cyanobacterial biomass by CLSM in stratified benthic sediments. *Ultramicroscopy,* **107,** 669–673.

SOLÉ, A., DIESTRA, E. & ESTEVE, I. 2009. Confocal laser scanning microscopy image analysis for cyanobacterial biomass determined at microscale level in different microbial mats. *Microbial Ecology,* **57,** 649–656.

STAL, L. J., VANGEMERDEN, H. & KRUMBEIN, W. E. 1985. Structure and development of a benthic marine microbial mat. *FEMS Microbiology Ecology,* **31,** 111–125.

STANIER, R. Y., KUNISAWA, R., MANDEL, M., & COHEN-BAZIRE, G. 1971. Purification and properties of unicellular blue–green algae (order Chroococcales). *Bacteriology Reviews*, **35**, 171–205.

STANIER, R. Y. & COHEN-BAZIRE, G. 1977. Phototropic prokaryotes – cyanobacteria. *Annual Review of Microbiology,* **31,** 225–274.

STARKS, T. L., SHUBERT, L. E. & TRAINOR, F. R. 1981. Ecology of soil algae: a review. *Phycologia***, 20**, 65–80.

STEHFEST, K., TOEPEL, J. & WILHELM, C. 2005. The application of micro-FTIR spectroscopy to analyze nutrient stress-related changes in biomass composition of phytoplankton algae. *Plant Physiology and Biochemistry,* **43,** 717–726.

STEWART, D. E. & FARMER, F. H. 1984. Extraction, identification, and quantitation of phycobiliprotein pigments from phototrophic plankton. *Limnology and Oceanography,* **29,** 392–397.

STIBAL, M. & TRANTER, M. 2007. Laboratory investigation of inorganic carbon uptake by cryoconite debris from Werenskioldbreen, Svalbard. *Journal of Geophysical Research – Biogeosciences,* **112**.

STIBAL, M., SABACKA, M. & KASTOVSKA, K. 2006. Microbial communities on glacier surfaces in Svalbard: Impact of physical and chemical properties on abundance and structure of cyanobacteria and algae. *Microbial Ecology,* **52,** 644–654.

STIBAL, M., TRANTER, M., BENNING, L. G. & REHAK, J. 2008a. Microbial primary production on an Arctic glacier is insignificant in comparison with allochthonous organic carbon input. *Environmental Microbiology,* **10**(8)**,** 2172–2178.

STIBAL, M., TRANTER, M., TELLING, J. & BENNING, L. G. 2008b. Speciation, phase association and potential bioavailability of phosphorus on a Svalbard glacier. *Biogeochemistry,* **90**(1)**,** 1–13.

STIBAL, M., ANESIO, A. M., BLUES, C. J. D. & TRANTER, M. 2009. Phosphatase activity and

organic phosphorus turnover on a high Arctic glacier. *Biogeosciences,* **6,** 913–922.

STIBAL, M., LAWSON, E. C., LIS, G. P., MAK, K. M., WADHAM, J. L. & ANESIO, A. M. 2010. Organic matter content and quality in supraglacial debris across the ablation zone of the Greenland ice sheet. *Annals of Glaciology,* **51,** 1–8.

STIBAL, M., TELLING, J., COOK, J., MAK, K. M., HODSON, A. & ANESIO, A. M. 2012. Environmental controls on microbial abundance and activity on the Greenland ice sheet: a multivariate analysis approach. *Microbial Ecology,* **63,** 74–84.

STRADALOVA, V., GAPLOVSKA-KYSELA, K. & HOZAK, P. 2008. Ultrastructural and nuclear antigen preservation after high-pressure freezing/freeze-substitution and low-temperature LR White embedding of HeLa cells. *Histochemistry and Cell Biology,* **130,** 1047–1052.

SUTHERLAND, I. W. 2001. Biofilm exopolysaccharides: a strong and sticky framework. *Microbiology,* **147,** 3–9.

SUTHERLAND, T. F., AMOS, C. L. & GRANT, J. 1998a. The effect of buoyant biofilms on the erodibility of sublittoral sediments of a temperate microtidal estuary. *Limnology and Oceanography,* **43,** 225–235.

SUTHERLAND, T. F., GRANT, J. & AMOS, C. L. 1998b. The Effect of carbohydrate production by the Diatom *Nitzschia curvilineata* on the erodibility of sediment. *Limnology and Oceanography,* **43,** 65–72.

SWAIN, E. B. 1985. Measurement and interpretation of sedimentary pigments. *Freshwater Biology,* **15,** 53–75.

TAKEUCHI, N. 2002. Optical characteristics of cryoconite (surface dust) on glaciers: the relationship between light absorbency and the property of organic matter contained in the cryoconite. *Annals of Glaciology,* **34**, 409-414.

TAKEUCHI, N., KOHSHIMA, S., YOSHIMURA, Y., SEKO, K. & FUJITA, K. 2000. Characteristics of cryoconite holes on a Himalayan glacier, Yala glacier, central Nepal. *Bulletin of Glaciological Research,* **17,** 51–59.

TAKEUCHI, N., KOHSHIMA, S., SHIRAIWA, T. & KUBOTA, K. 2001a. Characteristics of cryoconite (surface dust on glaciers) and surface albedo of a Patagonian glacier, Tyndall Glacier, Southern Patagonia Icefield. *Bulletin of Glaciological Research,* **18,** 65–69.

TAKEUCHI, N., KOHSHIMA, S. & SEKO, K. 2001b. Structure, formation, and darkening process of albedo-reducing material (cryoconite) on a Himalayan glacier: A granular algal mat growing on the glacier. *Arctic, Antarctic and Alpine Research,* **33**(2)**,** 115–122.

TAKEUCHI, N., NISHIYAMA, H. & LI, Z. Q. 2010. Structure and formation process of cryoconite granules on Urumqi glacier No. 1, Tien Shan, China. *Annals of Glaciology,* **51,** 9–14.

TATON, A., GRUBISIC, S., ERTZ, D., HODGSON, D. A., PICCARDI, R., BIONDI, N., TREDICI, M. R., MAININI, M., LOSI, D., MARINELLI, F. & WILMOTTE, A. 2006. Polyphasic study of Antarctic cyanobacterial strains. *Journal of Phycology*, **42**, 1257–1270.

TELLING, J., ANESIO, A. M., HAWKINGS, J., TRANTER, M., WADHAM, J. L., HODSON, A. J., IRVINE-FYNN, T. & YALLOP, M. L. 2010. Measuring rates of gross photosynthesis and net community production in cryoconite holes: a comparison of field methods. *Annals of Glaciology*, **51**, 153–162.

TELLING, J., ANESIO, A. M., TRANTER, M., IRVINE-FYNN, T., HODSON, A., BUTLER, C. & WADHAM, J. 2011. Nitrogen fixation on Arctic glaciers, Svalbard. *Journal of Geophysical Research – Biogeosciences,* **116**.

TELLING, J., ANESIO, A. M., TRANTER, M., STIBAL, M., HAWKINGS, J., IRVINE-FYNN, T., HODSON, A., BUTLER, C., YALLOP, M. & WADHAM, J. 2012. Controls on the autochthonous production and respiration of organic matter in cryoconite holes

on high Arctic glaciers. *Journal of Geophysical Research,* **117**.

THENG, B. K. G. 1982. Clay-Polymer Interactions - Summary and Perspectives. *Clays and Clay Minerals,* **30,** 1–10.

THOMPSON, R. C., TOBIN, M. L., HAWKINS, S. J. & NORTON, T. A. 1999. Problems in extraction and spectrophotometric determination of chlorophyll from epilithic microbial biofilms: towards a standard method. *Journal of the Marine Biological Association of the United Kingdom,* **79,** 551–558.

TIESSEN, H. & STEWART, J. W. B. 1988. Light and electron-microscopy of stained microaggregates – the role of organic-matter and microbes in soil aggregation. *Biogeochemistry,* **5,** 312–322.

TISDALL, J. M. 1994. Possible role of soil microorganisms in aggregation in soils. *Plant and Soil,* **159,** 115–121.

TISDALL, J. M. & OADES, J. M. 1982. Organic matter and water-stable aggregates in soils. *Journal Of Soil Science,* **33,** 141–163.

TODA, Y., MORO, I., KOGAI, T., ASAKAWAI, H. & HAMADAI, S. 1987. Ultrastructure of extracellular polysaccharides produced by serotype c *Streptococcus mutans*. *Journal of Dental Research***, 66**, pp. 1364–1369.

TOLHURST, T. J., GUST, G. & PATERSON, D. M. 2002. The influence of an extracellular polymeric substance (EPS) on cohesive sediment stability. *Fine Sediment Dynamics in the Marine Environment,* **5,** 409–425.

TRANTER, M., FOUNTAIN, A. G., FRITSEN, C. H., LYONS, W. B., PRISCU, J. C., STATHAM, P. J. & WELCH, K. A. 2004. Extreme hydrochemical conditions in natural microcosms entombed within Antarctic ice. *Hydrological Processes,* **18,** 379–387.

TSUNEDA, S., JUNG, J., HAYASHI, H., AIKAWA, H., HIRATA, A. & SASAKI, H. 2003. Influence of extracellular polymers on electrokinetic properties of heterotrophic bacterial cells examined by soft particle electrophoresis theory. *Colloids and Surfaces B – Biointerfaces,* **29,** 181–188.

UNDERWOOD, G. J. C. & PATERSON, D. M. 1993. Seasonal changes in diatom biomass, sediment stability and biogenic stabilization in the Severn Estuary. *Journal of the Marine Biological Association of the United Kingdom,* **73,** 871–887.

VAN BOEKEL, W. H. M. 1992. Phaeocystis colony mucus components and the importance of calcium ions for colony stability. *Marine Ecology – Progress Series*, **87,** 301–350.

VARIN, T., LOVEJOY, C., JUNGBLUT, A. D., VINCENT, W. F. & CORBEIL, J. 2010. Metagenomic profiling of Arctic microbial mat communities as nutrient scavenging and recycling systems. *Limnology and Oceanography*, **55**, 1901-1911.

VINCENT, W. F. 2007. Cold tolerance in cyanobacteria and life in the cryosphere. In SECKBACH, J. eds. *Cellular Origin and Life in Extreme Habitats and Astrobiology.* Springer, Dordrecht, The Netherlands.

VINCENT, W. F. & HOWARDWILLIAMS, C. 1989. Microbial communities in Southern Victoria Land streams (Antarctica). 2. The effects of low temperature. *Hydrobiologia,* **172,** 39–49.

VISKARI, P. J. & COLYER, C. L. 2003. Rapid extraction of phycobiliproteins from cultured cyanobacteria samples. *Analytical Biochemistry,* **319,** 263–271.

VON DRYGALSKI, E. 1897. Die Kryoconitlöcher, in *Gronland-Expedition der Gesellschaft für Erdkunde zu Berlin 1891–1893*. Vol. 1. Berlin, W. H. Kuhl, 93–103.

WARREN, C. R. 2008. Rapid measurement of chlorophylls with a microplate reader. *Journal of Plant Nutrition,* **31,** 1321–1332.

WEBSTER-BROWN, J. G. & WEBSTER, K. S. 2007. Trace metals in cyanobacterial mats, phytoplankton and sediments of the Lake Vanda region, Antarctica. *Antarctic Science,* **19,** 311–319.

WHARTON, R. A., MCKAY, C. P., SIMMONS, G. M. & PARKER, B. C. 1985. Cryoconite holes on glaciers. *Bioscience,* **35,** 499–503.

WIELAND, G., NEUMANN, R. & BACKHAUS, H. 2001. Variation of microbial communities in soil, rhizosphere, and rhizoplane in response to crop species, soil type, and crop development. *Applied and Environmental Microbiology,* **67,** 5849–5854.

WILDMAN, R. B. & BOWEN, C. C. 1974. Phycobilisomes in blue-green algae. *Journal of Bacteriology,* **117,** 866–881.

WREDE, C., HELLER, C., REITNER, J. & HOPPERT, M. 2008. Correlative light/electron microscopy for the investigation of microbial mats from Black Sea cold seeps. *Journal Of Microbiological Methods,* **73,** 85–91.

XU, Y., SIMPSON, A. J., EYLES, N. & SIMPSON, M. J. 2010. Sources and molecular composition of cryoconite organic matter from the Athabasca Glacier, Canadian Rocky Mountains. *Organic Geochemistry,* **41**(2)**,** 177–186.

YALLOP, M. L. & ANESIO, A. M. 2010. Benthic diatom flora in supraglacial habitats: a generic-level comparison. *Annals of Glaciology,* **51,** 15–22.

YALLOP, M. L., DEWINDER, B., PATERSON, D. M. & STAL, L. J. 1994. Comparative structure, primary production and biogenic stabilization of cohesive and non-cohesive marine sediments inhabited by microphytobenthos. *Estuarine Coastal and Shelf Science,* **39,** 565–582.

YDE, J. C., RIGER-KUSK, M., CHRISTIANSEN, H. H., KNUDSEN, N. T. & HUMLUM, O. 2008. Hydrochemical characteristics of bulk meltwater from an entire ablation season, Longyearbreen, Svalbard. *Journal of Glaciology,* **54,** 259–272.

YEE, N., BENNING, L. G., PHOENIX, V. R. & FERRIS, F. G. 2004. Characterization of metal–cyanobacteria sorption reactions: a combined macroscopic and infrared spectroscopic investigation. *Environmental Science & Technology,* **38**(3)**,** 775–782.

YOSHIMURA, Y., KOHSHIMA, S. & OHTANI, S. 1997. A community of snow algae on Himalayan glacier: Change of algal biomass and community structure with altitude. *Arctic and Alpine Research,* **29,** 126–137.

ZAVARZIN, G.A., and ALEKSEEVA, T.V. 2009. A puddle: an ombrophilic cyanobacterial community. *Microbiology*. **78** (4), 468–473.

ZHANG, X. Q. & BISHOP, P. L. 2001. Spatial distribution of extracellular polymeric substances in biofilms. *Journal of Environmental Engineering,* **127,** 850–856.

ZHAO, X. M., BI, Y. H., CHEN, L., HU, S. & HU, Z. Y. 2008. Responses of photosynthetic activity in the drought-tolerant cyanobacterium, *Nostoc flagelliforme,* to rehydration at different temperature. *Journal of Arid Environments,* **72,** 370–377.

ZHENG, H. L., ZHU, G. C., JIANG, S. J., TSHUKUDU, T., XIANG, X. Y., ZHANG, P. & HE, Q. A. 2011. Investigations of coagulation-flocculation process by performance optimization, model prediction and fractal structure of flocs. *Desalination,* **269,** 148–156.

ZIPPEL, B. & NEU, T. R. 2005. Growth and structure off phototrophic biofilms under controlled light conditions. *Water Science and Technology,* **52,** 203–209.

ZULPA DE CAIRE, G., STORNI DE CANO, M., ZACCARO DE MULE, M. C., PALMA, R. M. & COLOMBO, K. 1997. Exopolysaccharide of *Nostoc muscorum* (cyanobacteria) in the aggregation of soil particles. *Journal of Applied Phycology,* **9,** 249–253.

APPENDIX I – LITERATURE REVIEW

1.1 - Cryoconite introduction

Cryoconite granules can be described as being aqueous microaggregates, 0.1–3mm in size and approximately 50% water, consisting largely of mineral grains, organic matter and microorganisms. Organic matter can range from microbial carbohydrates to humin and black carbon, with biological content equally diverse and including photoautotrophic filamentous cyanobacteria, heterotrophic bacteria, snow algae and fungi; as such, cryoconite granules can be considered heterogeneous. Cryoconite granules are often found within small, surface melt pools, or cryoconite holes. Regarding the formation and growth of cryoconite holes, wind-deposited sediments on the ice surface absorb greater solar radiation than the surrounding ice, warming up and melting the underlying ice, forming a generally cylindrical hole. This small cryoconite hole may then grow, by a number of processes (absorption of solar radiation transmitted obliquely through the surrounding ice, direct and diffuse radiation reaching the base of the hole, downward convection of radiation absorbed by water at the top of the hole, flow of warmer water into the hole, and through the generation of heat by microorganisms) (Gerdel & Drouet 1960; Gribbon 1979; McIntyre 1984; Wharton et al. 1985). It is believed that biological processes only contribute approximately 10% towards the growth of cryoconite holes (McIntyre 1984).

This literature review outlines the physical and structural aspects, biology, and ecosystem biogeochemistry of cryoconite; it also reviews two other areas broadly analogous to cryoconite ecosystems – the biogeochemistry of biofilms and microbial mats, and the biogeochemistry of soil and organic matter within microaggregates.

1.2 - Physical and structural aspects of cryoconite

Cryoconite holes are typically < 1 m in diameter and < 0.5 m in depth (Takeuchi et al. 2000). Indeed, Fountain et al. (2004) found that the average diameter of cryoconite holes studied within the Antarctic dry valleys is 27.1 cm. These holes are generally water-filled, with Fountain et al. (2004) noting an average water content of 14.3 cm depth, and contain cryoconite debris, either in the form of granules (e.g. Takeuchi et al. 2001a,b) or in the form of a microbial mat (e.g. Wrede et al. 2008). These holes also often become ice-lidded in winter, or for longer periods when temperatures allow – for example in the Antarctic dry valleys, where holes are 'covered with ice lids up to 30 cm in thickness, isolating the hole and creating a unique hydrochemical environment' (Porazinska et al. 2004). Although many basic measurements of the physical aspects of cryoconite ecosystems have been performed, little work has correlated these to the local environment and/or the biogeochemical composition. An example of such a study can be found in Porazinska et al. (2004), who correlate both physical and biological characteristics with location. Porazinska et al. found that, overall, physical characteristics of the cryoconite holes were not significantly affected by location on the glacier, and that hole depth was independent of hole diameter. Conversely, biological characteristics (and to an extent chemical characteristics) were more dependent on location, with cyanobacteria being more prevalent at lower and western sides of glaciers. As the prevailing winds in Antarctica are west to east katabatic winds, this suggests that allochthonous sources may provide biological inputs into the cryoconite ecosystem.

Fountain et al. (2004) also studied cryoconite holes within the Antarctic dry valleys, finding that the average surface cover by these holes is 3.5%, that the average sediment content is < 0.5 cm (thickness), and that they are invariably ice-lidded. In agreement with Fountain et al., Anesio et al. (2009) state that between 0.1–10% of glacier surface are typically covered by cryoconite holes. The

ice-lidded nature of Antarctic cryoconite promotes extremes of pH, often approaching pH 11, in an organically controlled closed system. Regarding distribution of cryoconite hole diameters on these glacier surfaces, Fountain et al. (2004) found a skewed distribution on two of the four glaciers, with patches of small holes, which they have attributed to a controlling aeolian input. On the other two glaciers, a flat distribution was observed, which they have attributed to a mixed input of aeolian- and avalanche-sourced sediments. From the above, it is clear that the physical characteristics of cryoconite holes (e.g. depth, diameter, depth of sediment layer and location) show a degree of environmental control, with local sediment sources, wind direction and aspect all noted to influence these physical characteristics. However, the information on these relationships is sparse, with no attention yet given to such environmental controls as strength of wind, solar irradiance, or type of sediment source. Further, these environmental controls may also impact on the biogeochemical characteristics of the cryoconite ecosystem, as well as just the physical characteristics of the hole.

Seminal papers concerning the structure of cryoconite granules are those of Takeuchi et al. (2001a,b). Takeuchi et al. perform ultra-structural analysis, via optical, fluorescence and electron microscopy, on whole granules, disaggregated granules and thin sections of both Himalayan and Arctic cryoconite. Results indicate that the granule is a heterogeneous agglomeration of filamentous cyanobacteria, heterotrophic bacteria, amorphous black matter and mineral particles. Structurally, filamentous cyanobacteria appear to be more prevalent towards the outer edge of the granule, whereas the inner portion of the granule appears to be more mineral-rich, with amorphous black matter often associated with these mineral grains. Heterotrophic bacteria, as indicated by fluorescence microscopy, can be found throughout the granule and can be seen to associate with both organic matter and cyanobacteria. Scanning electron microscopy (SEM) confirms that heterotrophic bacteria are often to be found attached to cyanobacterial filaments, and also show that mucus (hereafter termed extra polymeric substances [EPS]) can be seen within the granules. The cohesive effect of EPS within biofilms and microaggregates is well documented (Donlan 2002, and references therein). When other observations by Takeuchi et al. (2001a,b) are considered, namely that copper sulphate (a biological inhibitor) can inhibit the re-aggregation of disassembled granules, and that cryoconite granules show evidence of a concentric layer structure analogous to stromatolites, the likely growth mechanism is filamentous cyanobacterial growth consequent with the trapping of mineral particles on the surface.

Concerning the microstructure of cryoconite, some further work has been undertaken via electron microscopy. Foreman et al. (2007) utilized an SEM with a cryogenic stage to study cryoconite vacuum-concentrated onto a polycarbonate filter and sputter-coated with Au–Pd, whereas Stibal et al. (2008) thaw 10 mg of cryoconite onto an aluminium stub and platinum coat it before imaging via SEM, alongside elemental mapping via energy dispersive X-ray spectroscopy (EDS). Analyses by SEM clearly show a microstructure consisting of areas rich in mineral grains, areas rich in organic matter, and a network of filamentous cyanobacteria twisting between these. Elemental mapping by Stibal et al. (2008) indicated that primarily silicate mineral grains sat within a primarily carbon-rich matrix; indeed they find that organic carbon is almost exclusively associated with either microbial cells or amorphous organic matter.

Recently, attention has been given to utilizing a combination of microscopic techniques to better study the microstructure of Antarctic 'cyanobacterial mats' from within surface meltwater pools (de los Rios et al. 2004). A broad range of techniques were employed, namely optical and fluorescence microscopy, confocal laser scanning microscopy (CLSM), SEM (back-scattered electron [BSE] imaging with EDS), and low temperature SEM. The first key observation was the definite vertical stratification of the mat, as opposed to cryoconite, which has been seen to be highly heterogeneous, with some tentatively identifying stratification (Takeuchi et al. 2001a,b; Stibal et al. 2008). Low temperature SEM was found to be effective in retaining extra-cellular polymeric substances (EPS) in a natural state, allowing clear visualization; the technique also allowed the

porosity of the mat to be studied, as water occupied the pore spaces of the mat – the porosity was found to be highly homogeneous. SEM–BSE, similarly, provided excellent ultra-structural detail, identifying mineral-rich layers, cyanobacteria-rich layers and, at depth, bio-accumulations of calcium carbonate; and tentatively identified bio-alteration of clay minerals. Regarding the orientations of cyanobacterial filaments within the mat, de los Rios et al. (2004) found that within the cyanobacterial layers (and particularly near to the surface), filaments were oriented parallel to the surface, whereas within the mineral-rich layers (and particularly at depth), orientation became more random. It is clear that a combination of microscopy techniques has the potential to provide comprehensive ultra-structural details of cryoconite, as well as biological and chemical characterization *in situ*.

At the macroscale, the structure of cryoconite is generally granular, with a mean diameter of 0.5 mm, and a range of 0.1–3.0 mm (Takeuchi et al. 2001a,b). At smaller scales, the structure is broadly heterogeneous, although some suggest that the principal components of cryoconite (bacteria, mineral particles and organic matter) show a microstructure analogous to that of a stromatolite. Stromatolites are laminar domes of cyanobacteria, which grow via precipitation of calcium carbonate and accumulation of sediment; bacterial photosynthesis depletes carbon dioxide in the water surrounding the stromatolite, allowing the precipitation of calcium carbonate (Riding 2000). Although cyanobacteria clearly play a part in determining the structure of cryoconite, little is known about other, micro- and nanoscale interactions, such as those between mineral surfaces and microbial exudates or more stable organic matter, for example. The effect of hydrophobic materials in providing stimulus for aggregation is also largely unstudied.

1.3 - Biology of cryoconite granules

Original observations of cryoconite holes and the debris within them, via light microscopy, established the basic biology of cryoconite ecosystems as containing blue-green algae (now rightly termed cyanobacteria), other species of algae, bacteria, diatoms, rotifers, and fungi. Gerdel & Drouet (1960) found *Calothrix parietina* (black-pigmented, heterocystous cyanobacteria) to be particularly prevalent within the Greenland cryoconite studied. These original observations are limited by the resolving power and fluorescence capabilities of microscopes. More recently, Porazinska et al. (2004) observed a similar species assemblage (cyanobacteria, rotifers, tardigrades and ciliates) within cryoconite from Antarctica. Molecular techniques have also allowed far greater clarification of both culturable and non-culturable microorganisms within cryoconite. Margesin et al. (2002), when studying heterotrophic microorganisms, found 66 culturable bacteria, the majority gram negative, and 17 culturable yeasts to be present within Alpine cryoconite, with the dominant genera being *Pseudomonas, Sphingomonas* and *Cryptococcus*. They found that particular substrates, namely casein (protein), cellulose and lignin, allowed the cultivation of the largest numbers of microorganisms; cold-tolerance, particularly amongst the cultivable yeasts, was also noted. Margesin et al. (2002) conclude that 'the capability of culturable microbia to utilize a large variety of natural substrates at low temperatures points to the ecological significance of their roles (decomposition of organic matter, nutrient cycling and biomass production) in this cold ecosystem'. Molecular identification of both bacteria and Eukaryotes within Antarctic cryoconite has been undertaken previously (Christner et al. 2003), with 16S and 18S rDNA sequencing finding eight primary bacterial lineages (*Acidobacterium, Cyanobacteria, Cytophagales, Gemmimonas, Planctomycetes, Proteobacteria* and *Verrucomicrobia*), as well as several Eukaryotes (principally metazoans, green algae, truffle and ciliate). Christner et al. (2003) also determined a similarity between the cryoconite microbial community sampled and those of nearby lake ice and microbial mat communities, suggesting that these holes can be 'seeded' from other local environments. To summarize, cryoconite has been shown to contain a remarkably diverse microbial population considering its glacial location, and recent advances in molecular microbiology have enabled

investigators to further the understanding of cryoconite biology. No attempts have yet been made, however, to link 'form with function', in order to identify both the environmental niches in which various microbia operate and their role(s) within this ecosystem.

Cyanobacteria have been found to dominate cryoconite ecosystems (e.g. Säwstrom et al. 2002; Porazinska et al. 2004; Stibal et al. 2006, 2008), with Stibal et al. finding that the genera of *Phormidium* and *Nostoc* are particularly common within Arctic cryoconite. Cyanobacteria, gram-negative and often motile, can be defined as 'prokaryotic microorganisms that contain photosynthetic apparatus (in the form of thylakoid membranes) markedly similar to that of the eukaryotic chloroplast, and are distinguishable by their photosynthetic pigments, chlorophyll A and phycobiliproteins, and noted for the largely ubiquitous presence of inclusions (e.g. glycogen or cyanophycin), their thick peptidoglycan layer, and the excretion of polysaccharidic EPS' (Stanier & Cohen-Bazire 1977). Other distinctive features of cyanobacteria are their membrane lipids (e.g. phosphatidyl glycerol), their use of phycobiliproteins as an electron transfer chain (including the unique cyanophycin), and their production of heterocysts (specialized nitrogen fixing cells), trichomes (filament structures) and akinetes (thick, multi-layered, cell survival structures) (Stanier & Cohen-Bazire 1977). Cryoconite cyanobacteria have been found to show relatively slow rates of photosynthesis (Säwstrom et al. 2002), as well as being widely tolerant of low temperatures and pH fluctuations. Stibal et al. (2006) found a preference for low pH by cyanobacteria, which they postulate may be attributable to reduced carbon dioxide availability for photosynthesis at higher pH. Vincent (2007) found that cyanobacteria utilize a number of strategies for cold tolerance, including the production of EPS, the production of compatible solutes and macromolecules (to reduce the osmotic stress of freezing and modify ice crystal growth), and the relatively higher contents of unsaturated fatty acids and polar lipids within cell membranes (Chintalapati et al. 2004). Such chemical means of protection are only heightened by physical protection, via such means as growing beneath translucent rocks and within cracks in rocks (Cockell & Stokes 2004).

Stibal et al. (2008) ascertain, via epifluorescence microscopy using the 4,6-diamidino-2-phenylindole (DAPI) fluorescent probe, that cellular abundances of phototrophic bacteria (of which > 90% were determined to be filamentous cyanobacteria) range from $0.25 \times 10^3 - 8 \times 10^3$ cells mg^{-1} (wet weight). This is in contrast to higher abundances of heterotrophic bacteria – between $10 \times 10^3 - 50 \times 10^3$ cells mg^{-1} (wet weight). Although bacterial abundance within cryoconite has been studied, there have been limited studies into the proportion of live versus dead bacteria. Bratbak (1985) estimated that 0.2% of organic carbon within cryoconite could be accounted for by living microbial cells, with the rest pertaining to dead microbial cells and amorphous organic matter. Further, the distribution of live versus dead cells across the diameter of a cryoconite granule needs clarification – a live/dead staining protocol could be utilized to achieve this (Boulos et al. 1999).

Recently, the attachment mechanisms of microorganisms to both mineral surfaces and organic matter have received renewed research attention, thanks in part to advances in analytical techniques. This research has typically concentrated on model species found within temperate ecosystems. Kapitulçinova et al. (2008), however, study the cyanobacteria *Leptolyngbya cf. delicatula* (isolated from a tundra soil in Svalbard) and its attachment to biotite, in particular within media that is deficient in key cations present within biotite – magnesium, iron and potassium. They find that, utilizing electron and light microscopy, cyanobacteria colonized the biotite, predominantly between the mineral layers, with pits and etch marks observable on the biotite surface. This study indicates the plausibility of cyanobacterial attachment to silicate mineral surfaces and the possibility that mineral particles could be utilized as nutrient sources. However, the method of attachment still remains unclear, and further investigation is likely needed to investigate which species and minerals favour attachment. Newman (2001) reviews the 'respiration of minerals' and their use as electron acceptors, noting that the three accepted theories for mineral diffusion into bacterial cells are: the production of chelating molecules and consequent dissolution of the mineral, the use of soluble 'shuttles' (e.g. organic compounds containing

quinones) to transfer electrons between mineral and cell, and the direct electron transfer from cell surface to mineral, utilizing the mineral as a terminal electron acceptor; the third theory has been suggested by the author to be the dominant theory. Investigations into the binding of cyanobacteria and metal ions have been conducted previously (e.g. Phoenix et al. 2002; Yee et al. 2004), reporting that carboxyl, phosphoryl and amine functional groups on both the cell wall and exopolymer sheath all show affinity for and binding with metal ions, to form ligand-metal complexes. Yee et al. (2004) studied, via acid-base titration and synchrotron Fourier Transform Infra-Red (FTIR) spectroscopy, the affinity and binding of separated cells and sheath material for copper, cadmium and lead cations. Yee et al. conclude that intact cells show a higher affinity for the cations studied than separated sheath material does, with cells having the highest affinity for lead cations and the lowest for cadmium cations; they suggest metal sorption onto deprotonated carboxyl sites as the most likely binding mechanism. This study could be furthered by introducing further cations, in particular to test a) such (hydr)oxide minerals as iron and aluminium, and b) other cations present within weathered silicates, such as potassium, magnesium and sodium.

1.4 - Biogeochemistry of cryoconite ecosystems

Cryoconite holes can be thought of as distinct and individual ecosystems: microcosms with clear boundaries, energy flows, and nutrient inputs and outputs. These ecosystems, however, have true seasonality, given that energy flows and nutrient cycling are restricted during the winter, as the holes are largely ice-capped and snow-covered, whereas in the summer, the holes are open to inputs from the atmosphere and from the surrounding ice. Indeed, supraglacial meltwater often 'washes out' cryoconite holes, transporting solutes and/or cryoconite debris onto the forefield. Biogeochemical studies of cryoconite have been more prevalent than others, with the focus differing between mineralogy, biology, organic carbon content/form, and solute chemistry. The studies of Stibal et al. (2006, 2007, 2008a, 2008b) are of note, as they show an ecosystem-based methodological approach, covering key macronutrients – in particular carbon and phosphorus. Considering this literature, as well as other biogeochemical analyses of both cryoconite debris and cryoconite waters that have been undertaken in many glaciated regions globally, an idea of the generalized biogeochemistry of cryoconite holes can be determined. A summary of biogeochemical parameters and values cited within the relevant literature can be found in Appendix 1.

Within cryoconite, photoautotrophic microorganisms (namely cyanobacteria) take up inorganic carbon and fix it as organic carbon, whilst heterotrophic microorganisms largely utilize organic molecules (including carbon) to fuel respiration. The rate of soil organic carbon mineralization and carbon dioxide production by respiration is dependent on a number of factors, including: the carbon substrates present (e.g. quality and distribution), soil temperature, water content, oxygen availability and abundance of microorganisms (Elberling et al. 2004). Microbial activity in cryoconite holes is considered high given that maximum temperatures rarely exceed 0.1ºC; indeed primary production and respiration during the summer is often comparable to that found in richer soils from temperate environments (Anesio et al. 2009). Primary production can be defined as 'the production of organic compounds from atmospheric or aquatic carbon dioxide, principally via photosynthesis, with chemosynthesis also playing a part'. Total organic carbon figures indicate that between 0.8% and 4.5% of the dry weight of cryoconite is organic carbon (Takeuchi et al. 2001; Margesin et al. 2002; Elberling et al. 2004; Stibal et al. 2008a). Given the above, as well as the recorded prevalence of both heterotrophic and photoautotrophic microorganisms within cryoconite (e.g. Margesin et al. 2002), it is not surprising that many biogeochemical studies have focused on carbon fluxes within cryoconite holes. Laboratory experiments by Stibal et al. (2007), through the incubation of cryoconite slurry at 3°C & 18°C and in light or dark conditions, find inorganic carbon uptake rates of between 0.6 and 15 $\mu g\ C\ l^{-1}\ h^{-1}$. This inorganic carbon is then fixed as organic carbon, with the optimum uptake occurring at pH 7. Field measurements of both

photosynthesis rates and dissolved organic carbon (DOC) contents confirm the significance of photosynthesis within Antarctic cryoconite ecosystems (Porazinska et al. 2004; Anesio et al. 2009). Anesio et al. record average primary production rates of between 48–353 μg C g^{-1} day^{-1} for cryoconite debris, most of which was fixed as DOC. These figures contrast with respiration rates of between 15.3–42.1 μg C g^{-1} day^{-1} and, although the standard deviations on these results are high, signify that cryoconite debris can be considered net autotrophic. This is in contrast to lower primary production rates for the planktonic environment (i.e. cryoconite waters), indicating the importance of cryoconite debris as a locus for photosynthetic activity.

Stibal et al. (2008a) undertook an ecosystem-based study of Arctic cryoconite, focusing specifically on carbon fluxes. They established that c. 1.5% of the ablation area of Werenskioldbreen was covered with cryoconite holes, containing a predominantly silicate mineralogy and between 1.7 and 4.5% organic carbon (dry weight), which accounted for >95% of the total carbon content. Organic carbon was found to be almost exclusively associated with microbial cells and/or other amorphous organic matter. The seasonal ecosystem flux was found to be a decrease of c. 70% in total carbon, with the ratio of organic/inorganic remaining relatively constant, suggesting physical removal processes – i.e. washout. A similar trend was seen for EC (a proxy for solute content). Solute chemistry was highly comparable between glacier meltwater runoff and water within cryoconite holes, indicating their connectivity. The pH within the holes was found to be higher, possibly explained by active photosynthesis (Tranter et al. 2004). Chlorophyll-A abundance decreased over time, again possibly indicative of washout of bacteria and algae from the holes. Dissolved inorganic carbon uptake, measured via labelled carbonate incubations *in situ*, ranged from 0.4 to 2 μg C l^{-1} h^{-1}, with photosynthesis accounting for 82–96% of this. This concurs with earlier laboratory experiments (Stibal et al. 2007), as well as with the findings of Tranter et al. (2004), who observed depletion of dissolved inorganic carbon (DIC) and elevated pH in Antarctic cryoconite holes, suggesting photosynthesis, as well as the possibility that elevated DOC values were preventing precipitation of $CaCO_3$ and thus further preserving DIC for photosynthesis. Stibal et al. (2008a) conclude that the low annual carbon fixation relative to the total amount of organic carbon within the system cannot be explained unless allochthonous input (from nearby proglacial and coastal wetlands and soils, for example) is invoked. The above studies demonstrate a focus on the carbon fluxes of cryoconite ecosystems via the study of photosynthesis and respiration rates, both *in situ* and in the laboratory. However, little effort has been made to attempt to understand the specific forms of carbon being produced by both photoautotrophic and heterotrophic microorganisms and their utilization and storage within the cryoconite.

In relation to the wider glacial ecosystem, some studies of carbon fluxes, primary production and respiration have been considered down a transect from supraglacial to proglacial debris. Mindl et al. (2007) found that bacterial abundance and primary production increased significantly along a transect from supraglacial waters to a proglacial lake, with the main controlling factors found to be temperature and phosphorus limitation. Addition of both an organic (goose faeces) and an inorganic (rock flour) carbon source stimulated bacterial production at the proglacial lake site. Bardgett et al. (2007) found that the proglacial heterotrophic microbial community increased down a gradient from recently exposed substrate to older valley sediments, showing an increase in organic C down-gradient, with a greater humin concentration (indicating recalcitrance) in the recently exposed sediments. Hopkins et al. (2006) showed that ancient carbon and modern carbon (e.g. algal-derived carbon) sustained heterotrophic microbial in an Antarctic low carbon ecosystem. Bekku et al. (2004) analysed microbial decomposition rates (which can be understood as a function of microbial biomass, microbial respiration rate and environmental factors) along a successional gradient, finding that a) mean microbial biomass increased with successional age, as did carbon and nitrogen contents, and b) respiration rates increased exponentially with temperature but, when compared against carbon content of sediment, decreased down the successional gradient. This decrease in respiration per gram of carbon is often ascribed to a change from bacterial to fungal domination, or from algal/cyanobacterial-derived carbon to a more recalcitrant litter of vascular

plants, mosses, and humic materials. Xu et al. (2008) found that DOC production from size-fractioned Arctic tundra soils was significant, with soil leaching experiments indicating significant DOC production in the first 24 hours, falling to a more stable rate thereafter, plus that microbial decomposition of DOC was significant between 24 and 72 hours. Other controls were reported, such as low temperatures inhibiting production, acidic soils enhancing production, and more humified soils producing more DOC. Elberling et al. (2004) found that more than 95% of total ecosystem carbon was potentially bio-reactive.

Unlike traditional soil studies, little attention has been given to the organic matter content and composition of cryoconite, specifically to the humic acid, fulvic acid and humin contents. Given that Takeuchi et al. (2001) found that airborne deposits on a Himalayan glacier contained 5% less organic matter than the cryoconite upon the same glacier (1.8% versus 6.8%), it is reasonable to presume that a proportion of the cryoconite organic matter is derived from photoautotrophic production of organic carbon, followed by heterotrophic bacterial decomposition into more humic substances. Takeuchi et al. (2001) do briefly evaluate the humic content of Himalayan cryoconite using the $KMnO_4$ method of Kumada (1965, 1987), finding that it contained a significant amount of humic acid (7 ml per gram of material). The C/N ratio of the cryoconite was around 10:1, not dissimilar to well-decomposed soil organic matter. Although it is difficult to ascribe exactly how much of this humic acid is autochthonous, it is clear that cryoconite contains significant amorphous organic matter content. This content has been found to produce a low spectral albedo in the 350 to 50nm wavelength region (Takeuchi 2002), particularly in Arctic cryoconite, reducing the spectral albedo of bare ice by 20-40%. No correlation between organic matter/carbon contents and spectral reflectance was observed, indicating that it is likely that the quality of organic matter is more important than the quantity. As can be seen, the quantification of organic carbon within cryoconite has largely been performed simply and chemically, with little attention being given to the advances in spectroscopy (in particular NMR, Raman and FTIR) for organic matter analyses. Furthermore, within soil science, recent attention has been given to the effects of recalcitrant 'black carbon' on soil biogeochemistry, yet no attempt to quantify the black carbon content of cryoconite or its effect on spectral reflectance has been made.

Stibal et al. (2008b) undertook a sequential extraction protocol to gain insight into the phase association and potential bioavailability of phosphorus on an Arctic glacier. Phosphorus is a key macronutrient and, within the glacial environment, the majority is bound to sediments (Hodson et al. 2004), leaving very little (< 5 μg l^{-1}) dissolved within glacial waters. Within supraglacial and glacier runoff waters, total dissolved Phosphorus was between 5.2 and 8.5 μg l^{-1}, with soluble reactive phosphorus (SRP) being very low (< 0.5–3.6 μg l^{-1}), and dissolved organic phosphorus (DOP) being higher (2.6–8.2 μg l^{-1}). Molar ratios (DIC:SRP and DIN:SRP) exceeded their Redfield ratios, indicating a lack of biological control over dissolved phosphorus. Within the cryoconite debris itself, out of the average 2.2 mg P g^{-1}, the majority (c. 57%) was organic bound, the rest (c. 43%) being operationally inorganic, either bound within or adsorbed onto minerals. The only extract that showed significant fluctuations over the ablation season was extract 2 (Fe- and Al-bound phosphorus). Stewart & Tiessen (1987) find that microbes possessing alkaline phosphatases can consume dissolved organic phosphorus (DOP); further, adsorption of phosphorus onto minerals is shown to be largely by a reactive $-OPO_3^{2-}$ group binding to positively charged sites on minerals, mainly amorphous Fe and Al oxy-hydroxides. In a similar vain to Stibal et al. (2008a), this 'excess' phosphorus within the cryoconite debris is best explained by an allochthonous source of organic phosphorus. Further, the potentially bio-available phosphorus (extracts 1 and 2) was found to be in excess of that needed for effective primary production on the glacier. Molar ratios of C:N and N:P for the cryoconite debris, although approximated, fell within the global ratios, suggesting a degree of biological control over debris-bound phosphorus.

1.5 - Bacterial biofilms and microbial mats

Given the prevalence of cyanobacteria within it, cryoconite can be considered highly analogous to photosynthetic microbial mats, such as those found within marine tidal zones or shallow lacustrine deposits. A biofilm can be defined, based on Davey & O'Toole (2000) and Donlan (2002), as 'a simple to complex community of microbial cells attached to a surface or associated with an interface, and enclosed in a matrix of both polysaccharide-rich material and varying quantities of non-cellular material, such as mineral crystals, clay and silt particles'. A microbial mat is generally considered to be a biofilm of sufficient thickness to be visible to the naked eye; this thickness allows the development of strong vertical, chemical gradients. Watnick & Kolter (2000) liken natural biofilms to cities of microbes, where multi-species microbial communities stay and leave with purpose, form transient association with mineral surfaces for stabilization, share genetic material, and fill distinct environmental niches. Some bacteria have been shown to a) preferentially attach to a nutritive surface in nutrient-poor environments, b) have genetic coding both for EPS production and a decrease in flagella synthesis when in contact with a surface, c) communicate cell-to-cell by chemical diffusion (e.g. acyl-homoserine lactones [acyl-HSLs]), and fill niches within biofilms such as facultative anaerobic colonization of the inner layers of biofilm.

The association of a biofilm with its interface or surface of choice is incredibly complex and is affected by a number of factors, including: effects of the substratum (e.g. surface roughness or hydrophobicity), conditioning films forming on the substratum (e.g. organic respiratory secretions; Mittelman 1996), hydrodynamics of the aqueous medium (e.g. settling velocities, turbulence and mixing), characteristics of the medium (e.g. pH, ionic strength and temperature), and various properties of the cell surface (e.g. EPS production rate, hydrophobicity, and the presence of appendages) (Donlan 2002). Biofilm growth, combined with the inclusion and/or excretion of non-cellular material (e.g. mineral grains and amorphous organic deposits), leads to a highly heterogeneous biofilm with chemically and structurally different 'zones'. The chemical composition of biofilm EPS, for example, can be studied via chemical and analytical methods following extraction; however, many recent studies of biofilms *in situ* have produced high-quality, structure-specific biogeochemical information, using high-powered microscopy and staining techniques in particular.

Electron microscopy techniques have been utilized with some success in imaging biofilms and microbial mats, particularly Environmental Scanning Electron Microscopy (ESEM) and cryo-Transmission Electron Microscopy (cryo-TEM). Priester et al. (2007) utilized ESEM and a combination of heavy metal stains to produce enhanced images of microbial biofilms, in particular the EPS that encapsulates the cells. ESEM is useful in biofilm imaging as it allows imaging of hydrated samples, at variable temperatures, and external polymers are more apparent in ESEM because of this (Manero et al. 2003). Further, Chen et al. (2008) states that modern ESEM has functionality for high-quality, secondary electron imaging at high pressures (up to 30 torr), allowing the observation of hydrated species (using water vapour as the imaging gas) at realistic temperatures, whilst maintaining a suitably high relative humidity and utilizing a relatively low beam current (below 100 pA). This study utilizes ruthenium red primarily ($H_{42}Cl_6N_{14}O_2Ru_3.H_2O$), in combination with osmium tetroxide, to (as it is cationic and very electron dense) bind to the polyanionic constituents of EPS. Biofilms of *P. aeruginosa,* cultured upon Nucleopore polyester membranes, were stained by placing the membrane onto a 50µl drop of various solutions (in a clean petri dish, covered and sealed, and in a dark fridge), and were then placed onto double-sided carbon black sticky tabs attached to a standard EM stub, and imaged in wet mode at 4 Torr, 5 degrees and 10kV accelerating voltage, at both 2500x and 8000x magnification. Results indicated that changing C:N of growth media did not vary the DNA content of the resulting biofilm, but increasing C:N did increase both intracellular protein and extra-cellular uronic acid contents. Staining did improve image contrast on all occasions, with stain treatment 4 (involving ruthenium red, osmium tetroxide and lysine) producing the clearest pictures. A natural aquatic biofilm

(estuarine) also showed increased image contrast when stained, as well as exhibiting better texture and mean variety (a measure of image brightness). Beveridge (2006) utilized cryo-TEM to examine natural, hydrated biofilms. Bacteria can prove difficult to image with TEM, due to a) chemical fixatives not adequately penetrating the biofilm, b) organic solvents collapsing the EPS, and c) EPS being indistinguishable from external water. Cryo-TEM, rapidly freezing sucrose-protected biofilm to produce amorphous ice before slicing this into frozen and hydrated sections, was found to produce high quality sections that allowed visualization of finely ordered structures. Further, frozen-hydrated sections have an advantage in geomicrobiology as their 'density site: reactivity' correlation is helpful when studying bacteria and metal ion interactions. Wrede et al. (2008), in their study of Black Sea microbial mats, used resin embedding and thin-sectioning techniques to obtain two 'correlative' thin-sections (i.e. cut one after the other), of which one was subsequently stained with Con A and imaged via fluorescence microscopy, and one was stained with Con A Gold and imaged via TEM. Wrede et al. found that antigens were well preserved due to the hydrophilic nature of the resin and the low concentration of glutaraldehyde used (0.2– 0.5%), allowing carbohydrate-specific markers to bind to EPS, particularly around the outer edges of the colonies and within larger clefts, as well as showing the heterogeneity of carbohydrate content within the microbial mat. This technique shows promise, particularly as thin-sections can be stained post-section, and near-identical thin-sections can be studied via both light and electron microscopy.

Optical and laser microscopy, particularly involving fluorescent dyes, have also been shown to provide high quality imagery of biofilm material. Beveridge (2006) notes that Confocal Laser Scanning Microscopy (CLSM) with fluorescent probes is good at distinguishing molecular networks, with ratiometric dyes useful in probing chemical conditions such as pH, within biofilms. Chen et al. (2007) utilizes multiple staining and CLSM to image EPS and cells in bio-aggregates. Total and dead cells, proteins, lipids and polysaccharides were stained for using Calcofluor white, FITC, Concanavalin A conjugated with tetramethyl-rhodamine, Syto 63 Sytox blue and Nile red. Between each stain, the sample was washed twice in phosphate-buffered saline. The granule was embedded for cryosectioning and frozen at -20ºC, before sectioning to 60-micron thickness and mounting onto a microscope slide. The key to this multiple staining protocol was that the excitation spectra of all of the fluorophores did not overlap and the emission spectra did not significantly overlap, so that each could be excited and observed individually (distance between stains, in terms of wavelength, should be at least 60nm). Images were successful and highlighted structural properties well. Sandt et al. (2007) study differences between biofilms via Raman microspectroscopy, as specific biofilm properties (e.g. persistence) can often be related to structural heterogeneity (e.g. regions of dense EPS could be particularly resistant to shear stress). Using a flow cell, biofilms were cultured in artificial seawater at room temperature; EPS was separated by EDTA extraction (Sheng et al. 2005). Results indicated considerable spatial and temporal heterogeneity, with early-stage biofilm being fairly homogeneous, but late-stage biofilm showing EPS-rich and cell-rich areas, non-biological inclusions and spatial chemical differences. Very late-stage biofilm became slightly more homogeneous, but showing a different composition to the homogeneous early-stage biofilm.

In addition to the more conventional biofilms and microbial mats, stromatolites also show a degree of equivalence with cryoconite. Decho & Kawaguchi (1999) utilized CLSM to image stained and sectioned stromatolites in an attempt to better understand their ultra-structure. They note that EPS is often present as a structural matrix within a biofilm, yet is difficult to preserve in its hydrated state. To counter this, they embedded previously fixed (formaldehyde) and stained (DAPI and FITC-concanavalin A) stromatolites in Nanoplast resin, a hydrophilic resin that can be cured with minimal heating (only up to 60ºC). They utilize CLSM to image thick sections (2mm): EPS and carbonate grains being imaged by 488nm krypton-argon laser, and microbial cells being imaged by 770nm 2P titanium-sapphire laser – the two images were then merged. They found that the resin produced no detectable autofluorescence and preserved intact, hydrated EPS well. Results indicated that Con A bound well to glucose and mannose within EPS and produced fluorescence, which was heterogeneous, suggesting variable EPS composition or thickness; results also indicated

that DAPI-stained bacteria were imaged easily, even within the depths of the section, below and within sand grains. Kawaguchi & Decho (2002) also use propidium iodide to label bacterial filaments. They note that 2P-LSM reduces photo-bleaching and photo-toxicity of fluorescent probes, and so is highly useful.

1.6 - Biogeochemistry and structure of soil and organic matter within microaggregates

Though not as comprehensively studied as temperate soils, soils from Polar Regions are important in the global carbon cycle and have been shown to contain organic-rich deposits; indeed terrestrial Arctic regions hold approximately 14% of the world's organic carbon (Post et al. 1982). Elberling et al. (2004) found that Arctic soils had maximum concentrations of carbon near to the surface (as well as nitrogen) and that this concentration decreased with depth, with the exception of buried organic-rich layers. The decomposition of soil organic carbon by respiration results in soil pore CO_2 concentrations 10–100 times higher than in the atmosphere, and so diffusion into the atmosphere occurs (Welles et al. 2001).

Soil structure is greatly determined by the way in which primary soil particles (e.g. mineral grains, clays, oxides and hydroxides, organic matter and microorganisms) adhere to one another to form 'aggregates', leaving pore spaces between them. This structure of soil aggregates and the consequent pore spaces convey many of the soil's properties, such as porosity, gaseous exchange and nutrient flux. Aggregate stability, the ability of soil aggregates to resist disruption – generally by water, has been studied comprehensively within both soil and agricultural sciences, in particular the relationship between organic matter content/biological activity and aggregate stability (e.g. Puget et al. 1999; Six et al. 1998). Tisdall & Oades (1982) state that 'the water-stability of soil micro-aggregates depends on the persistent organic binding agents, and appears to be a characteristic of the soil and independent of management'. Further, they propose an aggregate hierarchy to describe soil stabilization by microorganisms and their exudates, a hierarchy upon which most of the recent research into soil structure and biogeochemistry has been based. Cryoconite can be considered analogous to soil microaggregates because, although it lacks the maturity of a typical soil, it typically contains all of the necessary primary particles and shows evidence of biological stabilization – as such, cryoconite could also be considered a glacial 'proto-soil'.

With the link between biological activity, organic matter content and soil structural stabilization becoming more evident, recent research attention has focused on exploring this, examples being the role of microbial carbohydrates and organic matter in aggregation (Six et al. 2006), bacterial microhabitats within soil aggregates (Carson et al. 2009), the location and composition of 'more humified' organic matter within soil aggregates (Lehmann et al. 2007), and organo-mineral associations within soil aggregates (Kögel-Knabner et al. 2008). Experimental procedures for the study of soil structure and biogeochemistry can be broadly described as involving chemical extraction and analysis, physical fractionation and analysis, and analytical and microscopic studies *in situ*.

Considering the presence of microbial carbohydrates (often termed bio-available organic matter) within soil microaggregates and their impact upon stabilization, much research has focused on extracting and quantifying polysaccharides from within these aggregates. Researchers have attempted to quantify and analyse the microbial carbohydrate pool using dilute-acid and hot-water extraction techniques and High Powered Liquid Chromatography (HPLC) (e.g. Puget et al. 1998). Following this, by examining the ratio of (galactose + mannose)/(arabinose + xylose), and considering that microorganisms have been found to produce polysaccharides that contain little arabinose and xylose (Cheshire 1977; Oades 1984), microbial origin can be determined; a ratio greater than 2 is said to be indicative of microbial carbohydrates. The hot-water extractable

carbohydrate pool is reportedly more akin to microbially derived carbohydrates than the dilute-acid extractable carbohydrate pool (Angers et al. 1988; Ball et al. 1996; Puget et al. 1998). Soil amino sugar concentrations have also received research attention, given that they have been proposed as a proxy of microbial organic matter content, as microorganisms have been found to produce significantly greater quantities of amino sugars (e.g. glucosamine and muramic acid) than plants (Zhang and Amelung 1996). The ratio between glucosamine and muramic acid has been found to indicate the relative contributions of fungi versus bacteria towards microbial organic matter (Chantigny et al. 1997). Given the relative abundance of microorganisms and associated exudates within cryoconite, a determination of the chemical composition of microbial carbohydrates (and possibly associated chemicals such as amino sugars and glycolipids) could prove highly useful in better characterizing carbon fluxes within cryoconite ecosystems.

Regarding bacterial microhabitats within soil aggregates, recent work by Li et al. (2004) has attempted to visualize, with the aid of fluorochromes and thin-section techniques, bacteria *in situ* within soil microaggregates. They find that a thinner section, combined with an anionic fluorochrome, such as FITC or calcofluor white, promote the staining of microorganisms while reducing autofluorescence. Soil microenvironments differ in their physical, chemical and biological properties, with microscale structural organization providing different habitats in which bacteria are heterogeneously distributed (Ranjard & Richaume 2001). Electron microscopy, both scanning (SEM) and transmission (TEM), have been utilized to visualize soil microhabitats. Chenu et al. (2001) utilize both SEM (low temperature in this case) and confocal microscopy to study the microstructure and perform direct microbial counts upon samples of both clayey and sandy soils. They find that an incubation of these soils with glucose causes bacteria to increase in number on the outside of the clay aggregates, yet both on the inside and outside of sandy aggregates. Berti et al. (2006) characterize the mineralogy and microfabric of marine sediments by TEM, including the geometry of pore spaces.

Various parameters can be found to affect the location of bacteria within microaggregates, including porosity and pore diameter, particle size, water availability and diffusion of gases, and carbon substrate availability. Kilbertus (1980) estimated a mean pore diameter of 2μm as the most likely to support bacterial colonies, whilst also noting that only about 4-10% of the pore space of an aggregate is colonized, and that no bacteria could be observed in pores below 0.8μm in size. Water availability and diffusion of gases are also linked to pore spacing, in that micropores are said to provide a more favourable environment for growth, in that they trap essential nutrients as well as protecting the bacteria from desiccation. Conversely, micropores do not provide a good environment for gas diffusion, and so micropores often support anaerobic conditions (Ranjard & Richaume 2001). Carson et al. (2009) test the hypothesis that different minerals in soil select distinct bacterial communities in their microhabitats. They incubate soil seeded with one of mica, basalt, or rock phosphate, before sieving these soils and analysing their DNA community profiles using T-RFLP. Results indicated that mineral type did significantly affect community profiles, with mica showing 25% unique ribotypes, basalt 11% and rock phosphate 10%; 53% of ribotypes were shared. These results indicate that bacterial communities are likely to be heterogeneous in composition and location within cryoconite upon glacier surfaces, given that mineralogy is usually variable and that surrounding water volume is also variable.

Considering 'more-humified' organic matter and organo-mineral interaction within soil aggregates, Lehmann et al. (2007) investigate the spatial distribution of organic matter within soil microaggregates using Synchrotron-FTIR and Near-Edge X-ray Absorption Fine Structures (NEXAFS) spectroscopy. These techniques are state-of-the-art and enable nano-scale investigation of structure and chemistry. Results indicate that carbon content showed an uneven and patchy distribution with no discernible patterns. Conversely, when aliphatic versus aromatic hydrocarbons were considered, aliphatic forms were positively correlated with the amount of O–H functional groups on kaolinite surfaces. This, combined with the fact that organic matter coatings

on mineral surfaces contained greater amounts of microbially metabolized aliphatic and carboxylic carbon than the organic matter content of the entire microaggregate, indicates that (a) organo-mineral interaction within soil microaggregates is highly important, and (b) that adsorption onto surfaces, rather than occlusion by adhering clay particles, is the dominant process of interaction in the soils tested.

Kögel-Knabner et al. (2008) review organo-mineral associations in temperate soils. Historically, an inverse correlation between grain size and organic carbon content has been ascribed to the stabilization of organic matter by association with mineral surfaces; more recently, a biological role in this stabilization has been recognized, with microorganisms adhering to mineral surfaces, excreting EPS and 'moderating the surface chemistry of the substrate'. Regarding types of mineral surface (e.g. Fe/Al (oxy)(hydr)oxides, 1:2 type clays, and 1:1 type clays) and their interaction, relationships between cation exchange capacity (CEC) and soil organic carbon (> CEC = > SOC) indicate cation exchange as a bonding mechanism; also, old (oxidation resistant) organic matter content often correlates with the content of Fe-oxides and short-order Al-silicates, with interaction and bonding likely by co-precipitation and ligand exchange. Regarding the distribution of microorganisms and microbial activity, CLSM (to study spatial arrangement *in situ*), physical fractionation (to study association with different substrates) and electron microscopy are useful tools – findings are generally that coarser OM associates with fungal activity, with small-size fractions containing the most microbial biomass, as indicated by a high abundance of bacterial-derived phospholipid fatty acids. The high affinity of bacteria to small particle size fractions suggests that mineral–organic associations in these fractions show a 'microbial fingerprint' (e.g. low C:N ratios, ^{13}C enrichment and microbial polysaccharides) (Guggenberger et al. 1994). Regarding soil surface area (SSA), while Rumpel et al. (2004) find that high organic carbon contents were associated with fine clay fractions (ascribed to having a great surface area and offering protection from degradation), Kahle et al. (2003) find that coarser clay fractions rich in Fe-oxide contain greater OC than finer clay fractions poor in Fe-oxide, suggesting a combined influence of reactive sites and surface area. Concerning the stability of organic matter, sorption to minerals often protects OM from oxidative attack (Kaiser & Guggenberger 2003) and limits their bioavailability (Kalbitz et al. 2005), particularly ligand-exchange-bound OM (Mikutta et al. 2007). The other OM fraction is the more rapid-cycling 'mineral-bound OM'; Kaiser & Guggenberger find that a greater loading of OM leads to a lower proportion of ligand bonds per molecule, making the OM more flexible and easier to degrade. In summary, organo-mineral interaction is highly complex, with several influencing parameters, although in general, soils with smaller mean particle sizes, rich in clays and iron oxides, seem to show greater interaction between organic matter and mineral surfaces, of which a proportion of this is microbially controlled.

Finally, considering briefly useful methods of organic matter analysis, Siewert (2004) utilized thermogravimetry to analyse the organic matter of several soils, as well as total N, clay and carbonate contents. Between 0.5 and 1.2g was heated on a thermo-balance, from 25ºC to 950ºC at a rate of 5 degrees per minute, with weight loss recorded every 4 seconds. Results were compared to data from more traditional methods, and indicated that losses before 200ºC correspond to water loss, thermolabile organic C (and total N) losses between 200ºC and 450ºC, stable organic C losses between 450ºC and 550ºC, and carbonate losses after 550ºC (clay losses, via coefficient of determination, were shown to be at 120ºC and 530ºC). Regression analysis indicated that for certain 10 degree temperature intervals, more than 98% of the variability of the soil properties could be predicted by thermal weight losses; for example, higher organic carbon content produced a higher thermal weight loss at 340-350ºC. It was noted that higher black carbon contents slightly altered results, giving lower reliability in statistical analysis. This method could well prove useful in the analysis of both bio-available and total organic matter contents of cryoconite debris. Considering an altogether different approach, Jehlicka & Edwards (2008) utilize Raman spectroscopy to non-destructively identify organic minerals within the geological record, a further

advantage being the microscale identification of individual organic compounds in the vicinity of minerals or even as inclusions within minerals.

To summarize, it is clear that the structure and biogeochemistry of soil and organic matter within microaggregates is a widely researched field that is also highly analogous to cryoconite ecosystems, particularly as cryoconite granules begin to grow in size and develop in complexity.

Synthesis of literature

Parameter	Data	Related comments	Reference(s)
Hole diameter	<1 m, average = 27.1 cm	• Depth is independent of diameter for Antarctic glaciers studied • Diameter may correlate with the input of Aeolian versus avalanched sediments	Fountain et al. (2004) Takeuchi et al. (2000)
Hole depth	<0.5 m	• Seasonally variable; often ice-lidded • Correlates poorly with location for Antarctic glaciers	Takeuchi et al. (2000) Porazinska et al. (2004)
Hole water level	Average = 14.3 cm	• Antarctic glaciers	Fountain et al. (2004)
Hole sediment content	<0.5 cm	• Antarctic glaciers	Fountain et al. (2004)
Granule size	0.1–3 mm, average = 0.5		Takeuchi et al. (2001)
Total organic carbon	2–4% dry weight 2.7% 1.7–4.5% dry weight 0.8–1.8%	• Organic carbon has been found to be >95% of total carbon within cryoconite	Stibal et al. (2008) Takeuchi et al. (2001) Margesin et al. (2002) Elberling et al. (2004)
pH	4.8, 5, 11	• Variable depending on e.g. presence of carbonate bedrock, perennial ice lids, and Aeolian inputs • Higher in holes than surrounding supraglacial waters, possibly due to active photosynthesis • Elevated pH and DOC can prevent carbonate precipitation	Stibal et al. (2006; 2008) Margesin et al. (2002) Tranter et al. (2004)
Total nitrogen	0.27%, 0.02–0.09%		Takeuchi et al. (2001) Margesin et al. (2002)
Inorganic carbon uptake	0.6–15 μg C L^{-1} h^{-1} 0.4–2 μg C L^{-1} h^{-1}	• Laboratory conditions, 3ºC or 18ºC, light or dark • Often low compared to TOC, suggesting allochthonous carbon input	Stibal et al. (2007) Stibal et al. (2008)
Photosynthesis	48–353 μg C g^{-1} day^{-1}	• Primary production; most carbon was fixed as DOC	Anesio et al. (2009)
Respiration	15.3–42.1 μg C g^{-1} day^{-1}	• Svalbard glaciers • Found to decrease, per gram of carbon, down a proglacial succession	Anesio et al. (2009)

			Bardgett et al. 2007
Heterotrophic microorganisms	10×10^3–50×10^3 cells mg^{-1}	• *Pseudomonas* and *Sphingomonas* are most common	Margesin et al. (2002) Stibal et al. (2008)
Photoautotrophic microorganisms	0.25×10^3–8×10^3 cells mg^{-1}	• Greater than 90% of phototrophic microorganisms present were found to be filamentous cyanobacteria, of which *Calothrix, Parietina, Phormidium* and *Nostoc* have the highest abundances	Gerdel & Drouet (1960) Stibal et al. (2006)
Percentage coverage of ice surface	1.5% of ablation area; 3.5%	• Svalbard glaciers; Antarctic glaciers	Stibal et al. (2008) Fountain et al. (2004)
Mineralogy		• Svalbard mineralogy is broadly silicates, sedimentary and meta-sedimentary rocks • Mineral heterogeneity contributes to the spatial variation in bacterial communities	Stibal et al. (2008) Carson et al. (2009)
Electrical conductivity		• Decreases, along with total carbon content, during the melt season	Stibal et al. (2008)
Chlorophyll content		• Chlorophyll-A content decreased during the melt season	Stibal et al. (2008)
Phosphorus content	Average = 2.2 mg P g^{-1} debris, 57% = organic-bound, 43% = mineral bound	• Molar ratios exceeded Redfield line – excess phosphorus in cryoconite suggests and allochthonous source • Bioavailability of debris-bound phosphorus is sufficient to sustain the prokaryotic community	Stibal et al. (2008b)
Temperature	1.5–3°C		Margesin et al. (2002)
Total $CaCO_3$	1.9–2.1°C		Margesin et al. (2002)
Organic matter	6.8% of cryoconite debris is organic matter; there are 7mL humic acids per gram cryoconite	• Given that airborne dust contains 1.8% organic matter, microbial production of organic matter seems likely • The C:N ratio of cryoconite is 10:1, and it shows high spectral reflectance, akin to well decomposed SOM • Hexose-pentose ratios are a good indicator of plant versus microbe SOM ratios.	Takeuchi (2002) von Lutzow et al. (2007)
Granule texture		• Texture has been found to account for 28.1% of microbial variability; organic C content only accounts for 12.1%	Stibal et al. (2006)
Granule water content	Approximately 50%		Stibal et al. (2008)
Cell-mineral interaction		• Svalbard-sourced cyanobacteria, grown in low- Mg, Fe and K media, shows attachment and growth on and within biotite	Kapitulcinova et al. (2008)
Cold tolerance		• Cold tolerance in cyanobacteria has been shown, via production of EPS, compatible solutes, unsaturated fatty acids and macromolecules	Vincent (2007)
EPS composition		• Polysaccharides, variable in composition and thickness, and cellular material • M. *Chthonoplastes* = dominated by glucose	Decho & Kawaguchi (1999)

		and galactose	de Winder et al. (1999)
Black carbon		• Shows low van Krevelen O:C and H:C ratios, high affinity for other hydrophobic organic compounds, a significant contribution to SOM in cold environments, and is very slowly degraded	Preston & Schmidt (2006) Liang et al. (2006)
Microstructure		• Antarctic microbial mats show strong vertical stratification, increased EPS in void spaces, and cyanobacteria-rich layers showing epicellular silica and $CaCO_3$, plus a similar orientation	de los Rios et al. (2004)
Chemical weathering		• In younger glacial sediments, carbonate dissolution, sulphide oxidation and biotite alteration dominate solute flux sources	Anderson et al. (2000)
Metal (oxy)(hydr)oxides		• Biofilms, via TEM, have been shown to contain colloidal aggregates of iron oxyhydroxide nanoparticles	Banfield et al. (2000)
Aggregation		• The addition of microbial polysaccharides of known structure allowed a degree of aggregation of disaggregated soils, as long as NaCl concentrations were not high	Chaney & Swift (1984)
Biological weathering		• Microorganisms can increase mineral weathering by removing dissolution products and ions, and by exuding protons, organic acids and siderophores	Bernasconi et al. (2008)

Literature review references:

AGBLEVOR, F. A.*, et al.* (2004) Improved method of analysis of biomass sugars using high-performance liquid chromatography. *Biotechnology Letters,* 26**,** 1207-1210.

ANDERSEN, P. & THRONDSEN, J. (2003) *Estimating Cell Numbers*, UNESCO.

ANDERSON, S. P.*, et al.* (2000) Chemical weathering in the foreland of a retreating glacier. *Geochimica Et Cosmochimica Acta,* 64**,** 1173-1189.

ANESIO, A. M.*, et al.* (2009) High microbial activity on glaciers: importance to the global carbon cycle. *Global Change Biology,* 15**,** 955-960.

ANGERS, D. A.*, et al.* (1988) Determination Of Carbohydrate-Composition Of Soil Hydrolysates By High-Performance Liquid-Chromatography. *Journal Of Chromatography,* 454**,** 444-449.

AVERY, B. W. & BASCOMB, C. L. (1974) *Soil Survey Laboratory Methods*, Soil Survey.

BALL, B. C.*, et al.* (1996) Carbohydrate composition in relation to structural stability, compactibility and plasticity of two soils in a long-term experiment. *Soil & Tillage Research,* 39**,** 143-160.

BANFIELD, J. F.*, et al.* (2000) Aggregation-Based Crystal Growth and Microstructure Development in Natural Iron Oxyhydroxide Biomineralization Products. *Science,* 289**,** 751-754.

BARDGETT, R. D.*, et al.* (2007) Heterotrophic microbial communities use ancient carbon following glacial retreat. *Biology Letters,* 3**,** 487-490.

BEKKU, Y. S.*, et al.* (2004) Soil microbial biomass, respiration rate, and temperature dependence on a successional glacier foreland in Ny-Alesund, Svalbard. *Arctic Antarctic and Alpine Research,* 36**,** 395-399.

BERNASCONI, S. M. (2008) Weathering, soil formation and initial ecosystem evolution on a glacier forefield: a case study from the Damma Glacier, Switzerland. *Mineralogical Magazine,* 72**,** 19-22.

BERTI, D.*, et al.* (2006) Characterization of Microfabric and Mineralogy of Marine Sediments by Electron Microscopy. *Microscopy and Microanalysis,* 12**,** 362-363.

BEVERIDGE, T. J. (2006) Understanding the shapes of bacteria just got more complicated. *Molecular Microbiology,* 62**,** 1-4.

BONAL, L., *et al.* (2006) Determination of the petrologic type of CV3 chondrites by Raman spectroscopy of included organic matter. *Geochimica Et Cosmochimica Acta,* 70**,** 1849-1863.

BOULOS, L., *et al.* (1999) LIVE/DEAD (R) BacLight (TM): application of a new rapid staining method for direct enumeration of viable and total bacteria in drinking water. *Journal Of Microbiological Methods,* 37**,** 77-86.

BRATBAK, G. (1985) Bacterial Biovolume And Biomass Estimations. *Applied And Environmental Microbiology,* 49**,** 1488-1493.

BUHRING, S. I., *et al.* (2009) A hypersaline microbial mat from the Pacific Atoll Kiritimati: insights into composition and carbon fixation using biomarker analyses and a C-13-labeling approach. *Geobiology,* 7**,** 308-323.

CARSON, J. K., *et al.* (2009) Minerals in soil select distinct bacterial communities in their microhabitats. *Fems Microbiology Ecology,* 67**,** 381-388.

CHANEY, K. & SWIFT, R. (1984) The influence of organic matter on aggregate stability in some British soils. *J. Soil Sci.,* 35**,** 223-230.

CHANTIGNY, M. H., *et al.* (1997) Soil aggregation and fungal and bacterial biomass under annual and perennial cropping systems. *Soil Science Society Of America Journal,* 61**,** 262-267.

CHEN, M. Y., *et al.* (2007) Staining of extracellular polymeric substances and cells in bioaggregates. *Applied Microbiology and Biotechnology,* 75**,** 467-474.

CHEN, M. Y., *et al.* (2007) Distribution of extracellular polymeric substances in aerobic granules. *Applied Microbiology and Biotechnology,* 73**,** 1463-1469.

CHEN, J., *et al.* (2008) In Situ Imaging of Hydrated Specimens at Room Temperature in ESEM. *Microscopy and Microanalysis,* 14**,** 1200-1201.

CHENU, C., *et al.* (2001) Short-term changes in the spatial distribution of microorganisms in soil aggregates as affected by glucose addition. *Biology And Fertility Of Soils,* 34**,** 349-356.

CHESHIRE, M. V., *et al.* (1977) Metal Distribution And Nature Of Some Cu, Mn And V Complexes In Humic And Fulvic-Acid Fractions Of Soil Organic-Matter. *Geochimica Et Cosmochimica Acta,* 41**,** 1131-1138.

CHESHIRE, M. V., *et al.* (1979) Transformation Of Carbohydrate Constituents Of Grass During Decomposition In Soil. *Journal Of The Science Of Food And Agriculture,* 30**,** 330-330.

CHINTALAPATI, S., *et al.* (2004) Role of membrane lipid fatty acids in cold adaptation. *Cellular And Molecular Biology,* 50**,** 631-642.

CHRISTNER, B. C., *et al.* (2003) Molecular identification of Bacteria and Eukarya inhabiting an Antarctic cryoconite hole. *Extremophiles,* 7**,** 177-183.

COCKELL, C. S. & STOKES, M. D. (2004) Ecology - Widespread colonization by polar hypoliths. *Nature,* 431**,** 414-414.

COLOMBO, C. & TORRENT, J. (1991) Relationships Between Aggregation And Iron-Oxides In Terra Rossa Soils From Southern Italy. *Catena,* 18**,** 51-59.

COOMBS, D. (1998) ATR-FTIR. *International Journal of Vibrational Spectroscopy,* 2**,** 3-4.

DAVEY, M. E. & O'TOOLE, G. A. (2000) Microbial biofilms: from ecology to molecular genetics. *Microbiology And Molecular Biology Reviews,* 64**,** 847-+.

DE LOS RIOS, A., *et al.* (2004) Microstructural characterization of cyanobacterial mats from the McMurdo Ice Shelf, Antarctica. *Applied And Environmental Microbiology,* 70**,** 569-580.

DE WINDER, B., *et al.* (1999) Carbohydrate secretion by phototrophic communities in tidal sediments. *Journal Of Sea Research,* 42**,** 131-146.

DECHO, A. W. & KAWAGUCHI, T. (1999) Confocal imaging of in situ natural microbial communities and their extracellular polymeric secretions using Nanoplast (R) resin. *Biotechniques,* 27**,** 1246-1252.

DONLAN, R. M. (2002) Biofilms: Microbial life on surfaces. *Emerging Infectious Diseases,* 8**,** 881-890.

EDWARDS, H. G. M., *et al.* (2003) Raman spectroscopic detection of biomolecular markers from Antarctic materials: evaluation for putative Martian habitats. *Spectrochimica Acta Part A-Molecular And Biomolecular Spectroscopy,* 59**,** 2277-2290.

ELBERLING, B., *et al.* (2004) Influence of vegetation, temperature, and water content on soil carbon distribution and mineralization in four high Arctic soils. *Arctic Antarctic and Alpine Research,* 36**,** 528-538.

FILSON, P. B. & DAWSON-ANDOH, B. E. (2009) Characterization of sugars from model and enzyme-mediated pulp hydrolyzates using high-performance liquid chromatography coupled to evaporative light scattering detection. *Bioresource Technology,* 100**,** 6661-6664.

FOREMAN, C. M., *et al.* (2007) Metabolic activity and diversity of cryoconites in the Taylor Valley, Antarctica. *Journal Of Geophysical Research-Biogeosciences,* 112.

FOUNTAIN, A. G., *et al.* (2004) Evolution of cryoconite holes and their contribution to meltwater runoff from glaciers in the McMurdo Dry Valleys, Antarctica. *Journal of Glaciology,* 50**,** 35-45.

GERDEL, R. W. & DROUET, F. (1960) The cryoconite of the Thule Area, Greenland. *Transactions of the American Microscopical Society,* 79**,** 256-272.

GREENSPAN, P., *et al.* (1985) Nile Red - A Selective Fluorescent Stain For Intracellular Lipid Droplets. *Journal Of Cell Biology,* 100**,** 965-973.

GRIBBON, P. (1979) Cryoconite holes on Sermikavasak, West Greenland. *Journal Of Glaciology,* 22**,** 177-181.

GROS, O. & MAURIN, L. C. (2008) Easy flat embedding of oriented samples in hydrophilic resin (LR White) under controlled atmosphere: Application allowing both nucleic acid hybridizations (CARD-FISH) and ultrastructural observations. *Acta Histochemica,* 110**,** 427-431.

GUGGENBERGER, G., *et al.* (1994) Land-Use Effects On The Composition Of Organic-Matter In Particle-Size Separates Of Soil .1. Lignin And Carbohydrate Signature. *European Journal Of Soil Science,* 45**,** 449-458.

HODSON, A., *et al.* (2004) Suspended sediment and phosphorus in proglacial rivers: bioavailability and potential impacts upon the P status of ice-marginal receiving waters. *Hydrological Processes,* 18**,** 2409-2422.

HODSON, A., *et al.* (2008) Glacial ecosystems. *Ecological Monographs,* 78**,** 41-67.

HODSON, A., *et al.* (in review) The structure, biogeochemistry and formation of cryoconite aggregates upon an Arctic valley glacier; Longyearbreen, Svalbard.

HOHENBERG, H., *et al.* (1994) Micro techniques for high pressure freezing of suspensions and tissues. IN JOUFFREY, B. & COLLIEX, C. (Eds.) *Electron Microscopy 1994, Vols 3a and 3b - Applications in Biological Sciences.* Les Ulis, Editions Physique.

HOPKINS, D. W., *et al.* (2006) Carbon, nitrogen and temperature controls on microbial activity in soils from an Antarctic dry valley. *Soil Biology & Biochemistry,* 38**,** 3130-3140.

HUANG, W. E., *et al.* (2007) Raman-FISH: combining stable-isotope Raman spectroscopy and fluorescence in situ hybridization for the single cell analysis of identity and function. *Environmental Microbiology,* 9**,** 1878-1889.

HUANG, W. E., *et al.* (2009) Resolving Genetic Functions within Microbial Populations: In Situ Analyses Using rRNA and mRNA Stable Isotope Probing Coupled with Single-Cell Raman-Fluorescence In Situ Hybridization. *Applied And Environmental Microbiology,* 75**,** 234-241.

JEHLICKA, J. & EDWARDS, H. G. M. (2008) Raman spectroscopy as a tool for the non-destructive identification of organic minerals in the geological record. *Organic Geochemistry,* 39**,** 371-386.

KAHLE, M., *et al.* (2003) Carbon storage in coarse and fine clay fractions of illitic soils. *Soil Science Society Of America Journal,* 67**,** 1732-1739.

KAISER, K. & GUGGENBERGER, G. (2003) Mineral surfaces and soil organic matter. *European Journal Of Soil Science,* 54**,** 219-236.

KALBITZ, K., *et al.* (2005) Stabilization of dissolved organic matter by sorption to the mineral soil. *Soil Biology & Biochemistry,* 37**,** 1319-1331.

KAPITULCINOVA, D., *et al.* (2008) Effect of cyanobacterial growth on biotite surfaces under laboratory nutrient-limited conditions. *Mineralogical Magazine,* 72**,** 71-75.

KAWAGUCHI, T. & DECHO, A. W. (2002) In situ microspatial imaging using two-photon and confocal laser scanning microscopy of bacteria and extracellular polymeric secretions (EPS) within marine stromatolites. *Marine Biotechnology,* 4**,** 127-131.

KILBERTUS, G. (1980) Study Of Microhabitats In Soil Aggregates - Relation To Bacterial Biomass And Size Of Procaryotes. *Revue D Ecologie Et De Biologie Du Sol,* 17**,** 543-557.

KOGEL-KNABNER, I.*, et al.* (2008) Organo-mineral associations in temperate soils: Integrating biology, mineralogy, and organic matter chemistry. *Journal of Plant Nutrition and Soil Science-Zeitschrift Fur Pflanzenernahrung Und Bodenkunde,* 171**,** 61-82.

KUMADA, K. (1965) Studies on the colour of humic acids. Part 1. On the concepts of humic substances and humification. *Soil Science and Plant Nutrition,* 11**,** 151-156.

KUMADA, K. (1987) *Chemistry of Soil Organic Matter*, Elsevier.

KUO, L.-J.*, et al.* (2008) Can levoglucosan be used to characterize and quantify char/charcoal black carbon in environmental media? *Organic Geochemistry,* 39**,** 1466-1478.

LAFRENIERE, M. J. & SHARP, M. J. (2009) The Concentration and Fluorescence of Dissolved Organic Carbon (DOC) in Glacial and Nonglacial Catchments: Interpreting Hydrological Flow Routing and DOC Sources. *Arctic, Antarctic, and Alpine Research,* 36**,** 156-165.

LAWRENCE, J. R.*, et al.* (2003) Scanning transmission X-ray, laser scanning, and transmission electron microscopy mapping of the exopolymeric matrix of microbial biofilms. *Applied and Environmental Microbiology,* 69**,** 5543-5554.

LEHMANN, J.*, et al.* (2007) Organic matter stabilization in soil microaggregates: implications from spatial heterogeneity of organic carbon contents and carbon forms. *Biogeochemistry,* 85**,** 45-57.

LI, Y.*, et al.* (2004) Fluorescence microscopy for visualization of soil microorganisms - a review. *Biology and Fertility of Soils,* 39**,** 301-311.

LIANG, B.*, et al.* (2008) Stability of biomass-derived black carbon in soils. *Geochimica Et Cosmochimica Acta,* 72**,** 6069-6078.

LOPEZ, C.*, et al.* (2005) Evaluation of microscopic techniques (epifluorescence microscopy, CLSM, TPE-LSM) as a basis for the quantitative image analysis of activated sludge. *Water Research,* 39**,** 456-468.

MANERO, J. M.*, et al.* (2003) Applications of environmental scanning electron microscopy (ESEM) in biomaterials field. *Microscopy Research and Technique,* 61**,** 469-480.

MARGESIN, R.*, et al.* (2002) Characterization of heterotrophic microorganisms in alpine glacier cryoconite. *Arctic Antarctic and Alpine Research,* 34**,** 88-93.

MCINTYRE, N. F. (1984) Cryoconite Hole Thermodynamics. *Canadian Journal Of Earth Sciences,* 21**,** 152-156.

MIKUTTA, R.*, et al.* (2007) Biodegradation of forest floor organic matter bound to minerals via different binding mechanisms. *Geochimica Et Cosmochimica Acta,* 71**,** 2569-2590.

MINDL, B.*, et al.* (2007) Factors influencing bacterial dynamics along a transect from supraglacial runoff to proglacial lakes of a high Arctic glacieri. *Fems Microbiology Ecology,* 59**,** 307-317.

MITTELMAN, M. W. (1996) *Adhesion to biomaterials, in Fletcher, M eds. Bacterial Adhesion*, Wiley.

NEU, T. R.*, et al.* (2004) Three-dimensional differentiation of photo-autotrophic biofilm constituents by multi-channel laser scanning microscopy (single-photon and two-photon excitation). *Journal of Microbiological Methods,* 56**,** 161-172.

NEWMAN, D. K. (2001) Microbiology - How bacteria respire minerals. *Science,* 292**,** 1312-1313.

NICHOLS, K. & WRIGHT, S. (2006) Carbon and nitrogen in operationally defined soil organic matter pools. *Biology and Fertility of Soils,* 43**,** 215-220.

OADES, J. M. (1984) Soil Organic-Matter And Structural Stability - Mechanisms And Implications For Management. *Plant And Soil,* 76**,** 319-337.

OBST, M.*, et al.* (2005) TEM-specimen preparation of cell/mineral interfaces by Focused Ion Beam milling. *American Mineralogist,* 90**,** 1270-1277.

PHOENIX, V. R.*, et al.* (2002) Characterization and implications of the cell surface reactivity of Calothrix sp strain KC97. *Applied And Environmental Microbiology,* 68**,** 4827-4834.

PORAZINSKA, D. L.*, et al.* (2004) The Biodiversity and biogeochemistry of cryoconite holes from McMurdo Dry Valley glaciers, Antarctica. *Arctic Antarctic and Alpine Research,* 36**,** 84-91.

POST, W. M.*, et al.* (1982) Soil Carbon Pools And World Life Zones. *Nature,* 298**,** 156-159.

PRESTON, C. M. & SCHMIDT, M. W. I. (2006) Black (pyrogenic) carbon: a synthesis of current knowledge and uncertainties with special consideration of boreal regions. *Biogeosciences,* 3**,** 397-420.

PRIESTER, J. H.*, et al.* (2007) Enhanced visualization of microbial biofilms by staining and environmental scanning electron microscopy. *Journal of Microbiological Methods,* 68**,** 577-587.

PUGET, P.*, et al.* (1999) Nature of carbohydrates associated with water-stable aggregates of two cultivated soils. *Soil Biology & Biochemistry,* 31**,** 55-63.

RANJARD, L. & RICHAUME, A. S. (2001) Quantitative and qualitative microscale distribution of bacteria in soil. *Research In Microbiology,* 152**,** 707-716.

RIDING, R. (2000) Microbial carbonates: the geological record of calcified bacterial-algal mats and biofilms. *Sedimentology,* 47**,** 179-214.

RUMPEL, C.*, et al.* (2004) Location and chemical composition of stabilized organic carbon in topsoil and subsoil horizons of two acid forest soils. *Soil Biology & Biochemistry,* 36**,** 177-190.

SANDT, C.*, et al.* (2007) Confocal Raman microspectroscopy as a tool for studying the chemical heterogeneities of biofilms in situ. *Journal of Applied Microbiology,* 103**,** 1808-1820.

SAWSTROM, C.*, et al.* (2002) The microbial communities and primary productivity of cryoconite holes in an Arctic glacier (Svalbard 79 degrees N). *Polar Biology,* 25**,** 591-596.

SHENG, G. P.*, et al.* (2005) Extraction of extracellular polymeric substances from the photosynthetic bacterium Rhodopseudomonas acidophila. *Applied Microbiology And Biotechnology,* 67**,** 125-130.

SIEWERT, C. (2004) Rapid screening of soil properties using thermogravimetry. *Soil Science Society of America Journal,* 68**,** 1656-1661.

SIX, J.*, et al.* (1998) Aggregation and soil organic matter accumulation in cultivated and native grassland soils. *Soil Science Society Of America Journal,* 62**,** 1367-1377.

SIX, J.*, et al.* (2006) Bacterial and fungal contributions to carbon sequestration in agroecosystems. *Soil Science Society Of America Journal,* 70**,** 555-569.

SPARLING, G.*, et al.* (1998) Hot-water-soluble C as a simple measure of labile soil organic matter: the relationship with microbial biomass C. *Soil Biology & Biochemistry,* 30**,** 1469-1472.

STANIER, R. Y. & COHEN-BAZIRE, G. (1977) Phototropic Prokaryotes - Cyanobacteria. *Annual Review of Microbiology,* 31**,** 225-274.

STEWART, J. W. B. & TIESSEN, H. (1987) Dynamics Of Soil Organic Phosphorus. *Biogeochemistry,* 4**,** 41-60.

STIBAL, M.*, et al.* (2006) Microbial Communities on Glacier Surfaces in Svalbard: Impact of Physical and Chemical Properties on Abundance and Structure of Cyanobacteria and Algae. *Microbial Ecology,* 52**,** 644-654.

STIBAL, M. & TRANTER, M. (2007) Laboratory investigation of inorganic carbon uptake by cryoconite debris from Werenskioldbreen, Svalbard. *Journal of Geophysical Research-Biogeosciences,* 112.

STIBAL, M.*, et al.* (2008) Microbial primary production on an Arctic glacier is insignificant in comparison with allochthonous organic carbon input. *Environmental Microbiology,* 10**,** 2172-2178.

STIBAL, M.*, et al.* (2008) Speciation, phase association and potential bioavailability of phosphorus on a Svalbard glacier. *Biogeochemistry,* 90**,** 1-13.

TAKEUCHI, N.*, et al.* (2000) Characteristics of cryoconite holes on a Himalayan glacier, Yala glacier, central Nepal. *Bulletin of Glaciological Research,* 17**,** 51-59.

TAKEUCHI, N.*, et al.* (2001) Characteristics of cryoconite (surface dust on glaciers) and surface albedo of a Patagonian glacier, Tyndall Glacier, Southern Patagonia Icefield. *Bulletin of Glaciological Research,* 18**,** 65-69.

TAKEUCHI, N.*, et al.* (2001) Structure, formation, and darkening process of albedo-reducing material (cryoconite) on a Himalayan glacier: A granular algal mat growing on the glacier. *Arctic Antarctic and Alpine Research,* 33**,** 115-122.

TAKEUCHI, N. (2002) Optical characteristics of cryoconite (surface dust) on glaciers: the relationship between light absorbency and the property of organic matter contained in the cryoconite. IN WINTHER, J. G. & SOLBERG, R. (Eds.) *Annals of Glaciology, Vol 34, 2002.* Cambridge, Int Glaciological Soc.

TISDALL, J. M. & OADES, J. M. (1982) Organic-Matter And Water-Stable Aggregates In Soils. *Journal Of Soil Science,* 33**,** 141-163.

TRANTER, M.*, et al.* (2004) Extreme hydrochemical conditions in natural microcosms entombed within Antarctic ice. *Hydrological Processes,* 18**,** 379-387.

UCAR, G. & BALABAN, M. (2003) Hydrolysis of polysaccharides with 77% sulfuric acid for quantitative saccharification. *Turkish Journal of Agriculture and Forestry,* 27**,** 361-365.

VINCENT, W. F. (2007) Cold tolerance in cyanobacteria and life in the cryosphere. *Cellular Origin and Life in Extreme Habitats and Astrobiology.* Springer.

VON LÜTZOW, M.*, et al.* (2007) SOM fractionation methods: Relevance to functional pools and to stabilization mechanisms. *Soil Biology & Biochemistry,* 39**,** 2183-2207.

VON LÜTZOW, M.*, et al.* (2008) Stabilization mechanisms of organic matter in four temperate soils: Development and application of a conceptual model. *Journal of Plant Nutrition and Soil Science,* 171**,** 111-124.

WAGNER, M.*, et al.* (2009) Combined use of confocal laser scanning microscopy (CLSM) and Raman microscopy (RM): Investigations on EPS - Matrix. *Water Research,* 43**,** 63-76.

WATNICK, P. & KOLTER, R. (2000) Biofilm, city of microbes. *Journal of Bacteriology,* 182**,** 2675-2679.

WELLES, J. M.*, et al.* (2001) Considerations for measuring ground CO2 effluxes with chambers. *Chemical Geology,* 177**,** 3-13.

WHARTON, R. A.*, et al.* (1985) Cryoconite Holes On Glaciers. *Bioscience,* 35**,** 499-503.

WREDE, C.*, et al.* (2008) Correlative light/electron microscopy for the investigation of microbial mats from Black Sea Cold Seeps. *Journal Of Microbiological Methods,* 73**,** 85-91.

XU, C.*, et al.* (2008) Potential DOC production from size-fractioned Arctic tundra soils. *Cold Regions Science and Technology,* 55**,** 141-150.

YEE, N.*, et al.* (2004) Characterization of metal-cyanobacteria sorption reactions: A combined macroscopic and infrared spectroscopic investigation. *Environmental Science & Technology,* 38**,** 775-782.

ZHANG, X. D. & AMELUNG, W. (1996) Gas chromatographic determination of muramic acid, glucosamine, mannosamine, and galactosamine in soils. *Soil Biology & Biochemistry,* 28**,** 1201-1206.

APPENDIX II – SUPPORTING MATERIAL

Supporting material for chapters 2–4:

a) Epifluorescence imagery

Epifluorescence imagery of photosynthetic microorganisms within cryoconite material

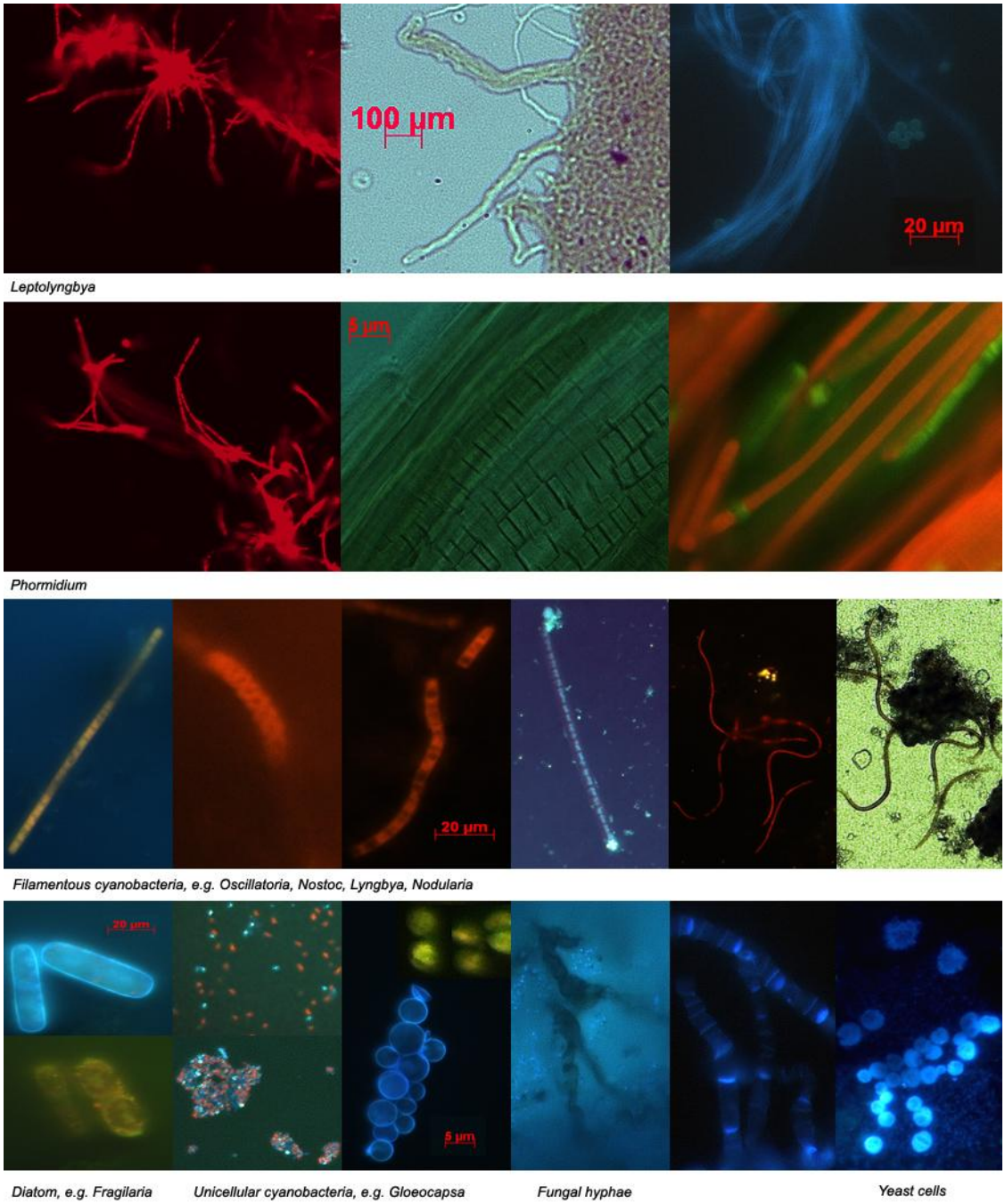

b) Energy dispersive X-ray (EDX) data

Example EDX profiles for organic and inorganic material

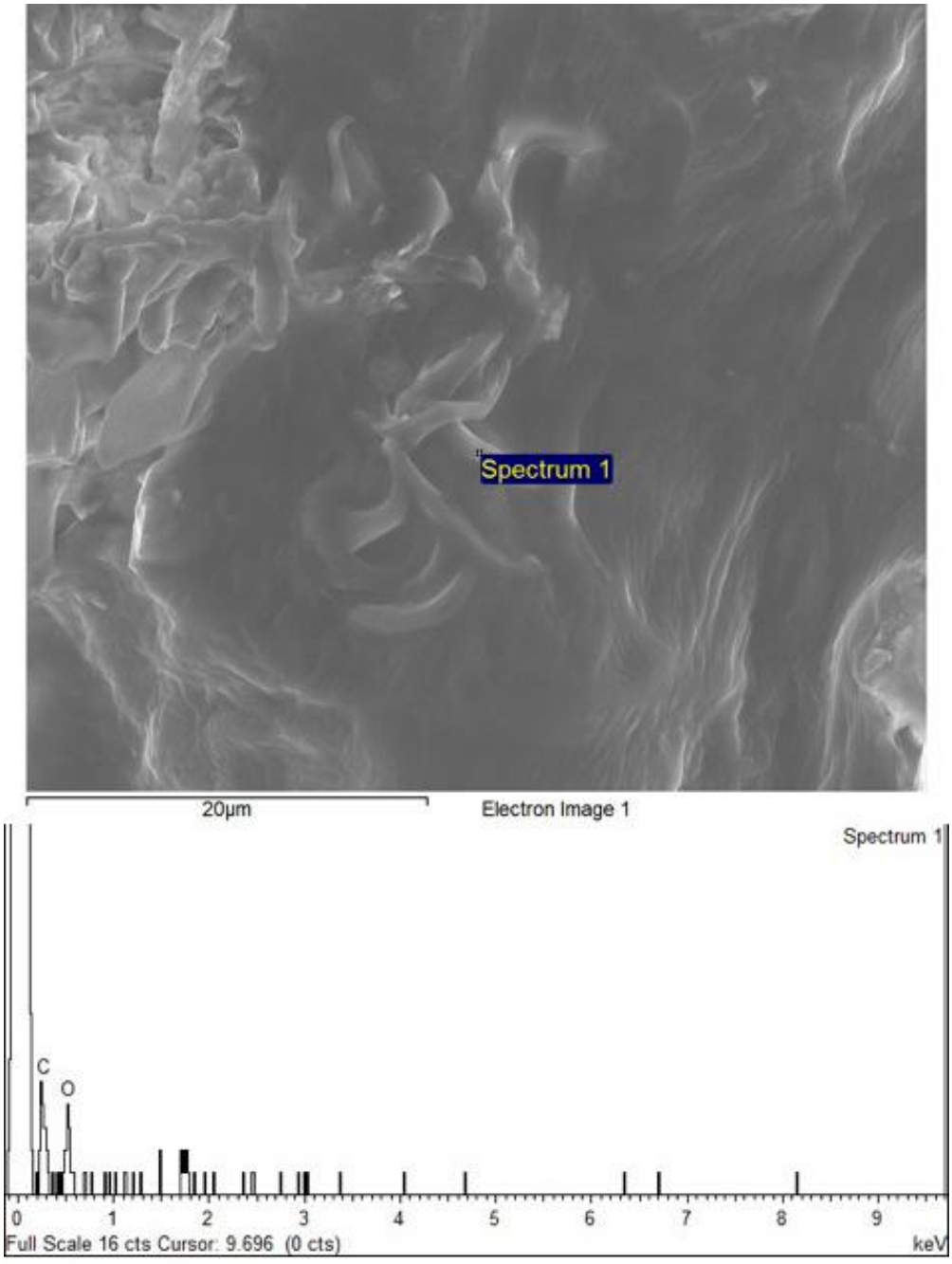

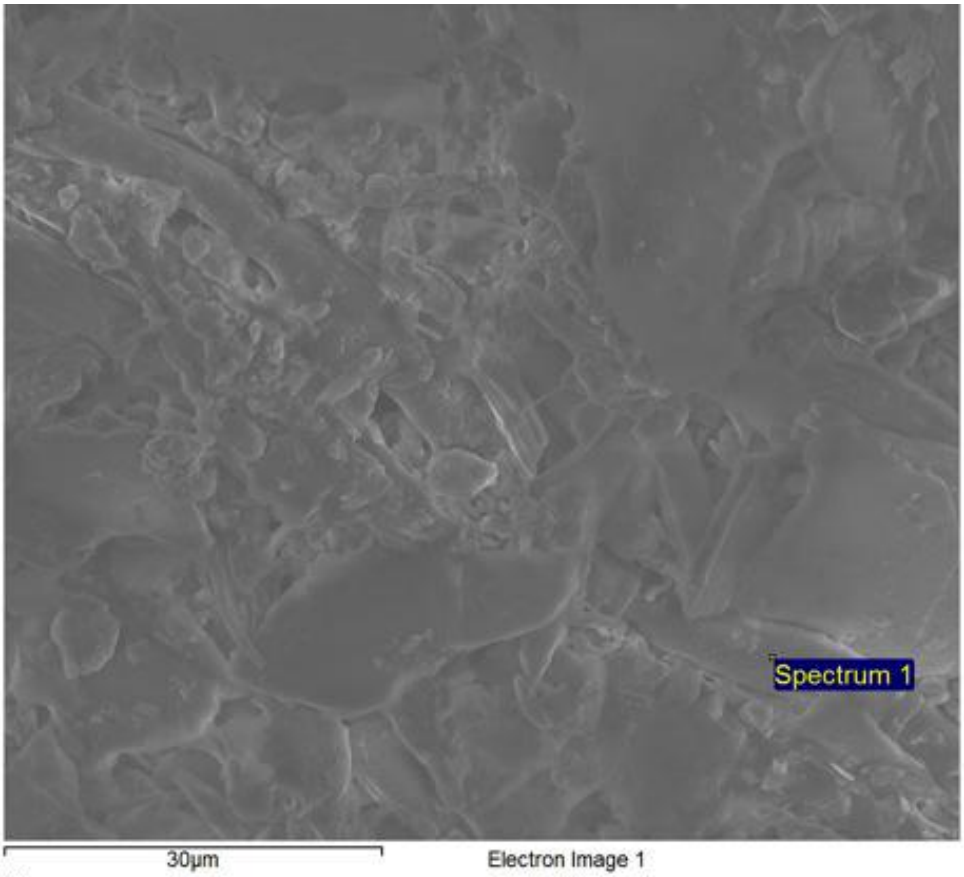
Spectrum 1
30µm
Electron Image 1

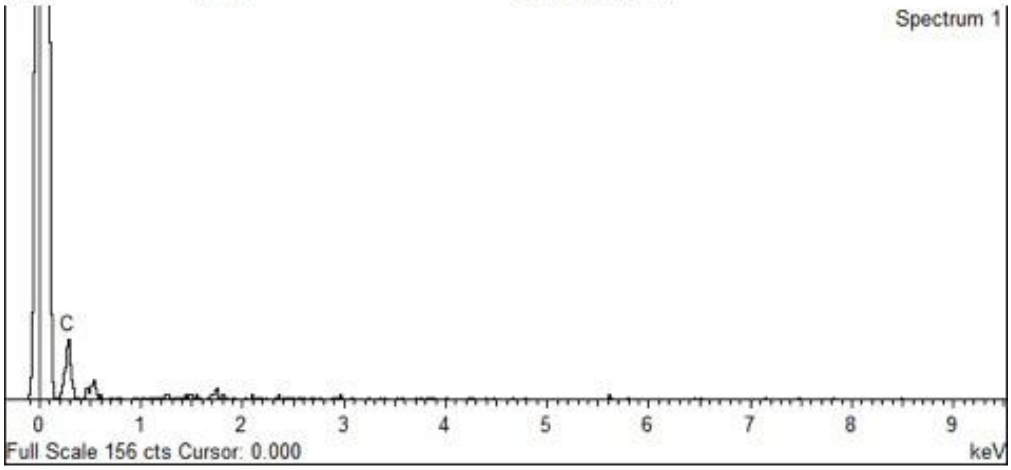
Spectrum 1
C
0
1
2
3
4
5
6
7
8
9
Full Scale 156 cts Cursor: 0.000
keV

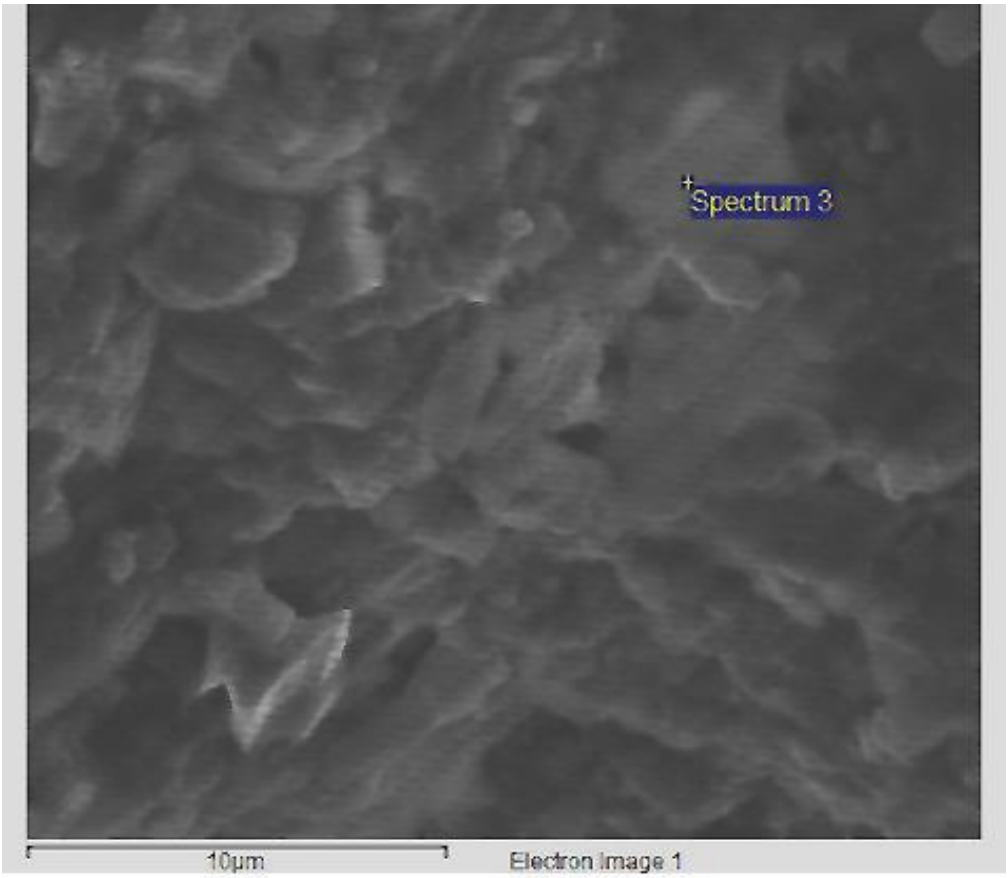
Spectrum 3
10µm
Electron Image 1

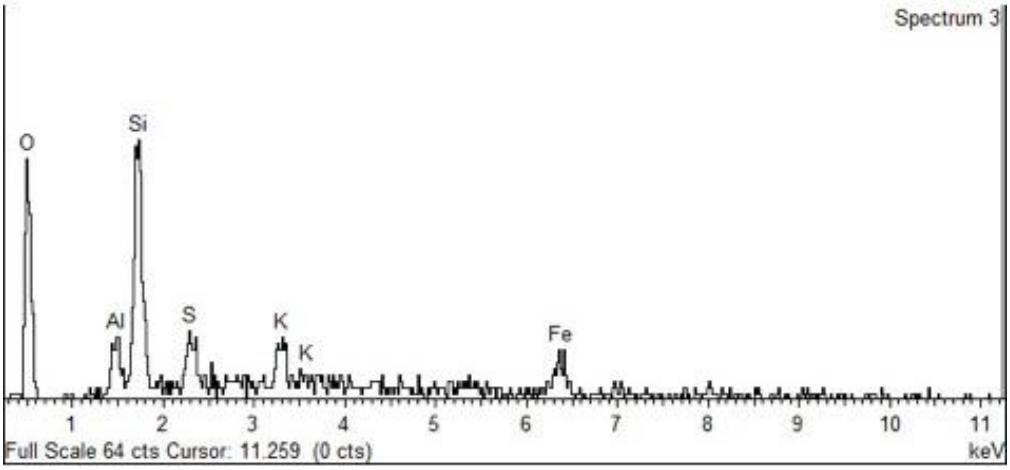
Spectrum 3
O
Si
Al
S
K
K
Fe
1
2
3
4
5
6
7
8
9
10
11
Full Scale 64 cts Cursor: 11.259 (0 cts)
keV

c) Autofluorescence spectra

Example screen shots from the Zeiss LSM 510 META software of typical autofluorescence spectra:

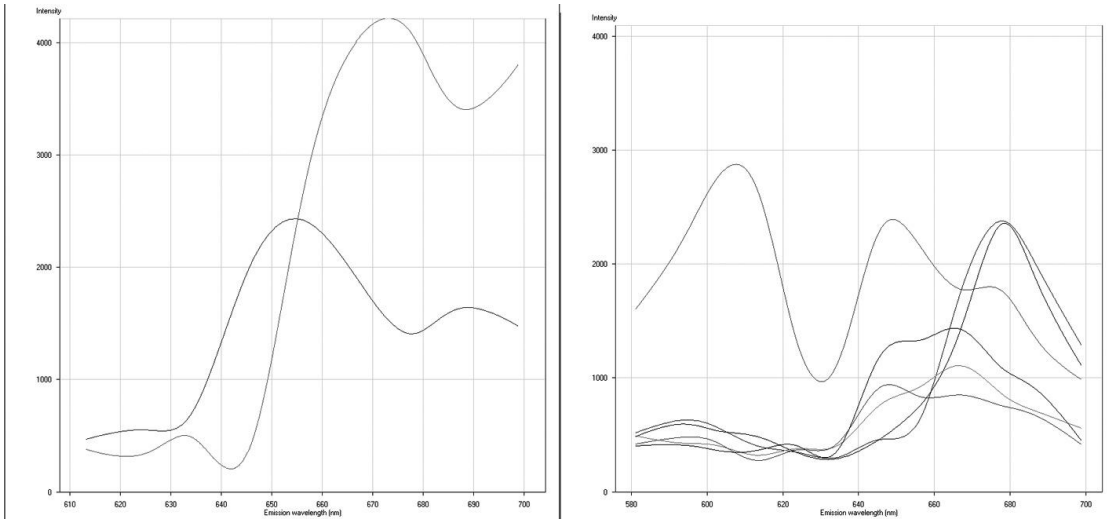

Spectra recorded in Lambda scanning mode, using META detection, induced at 532 nm and recorded between 600 and 700 nm using HFT 488,543,633 KP 725 grating:

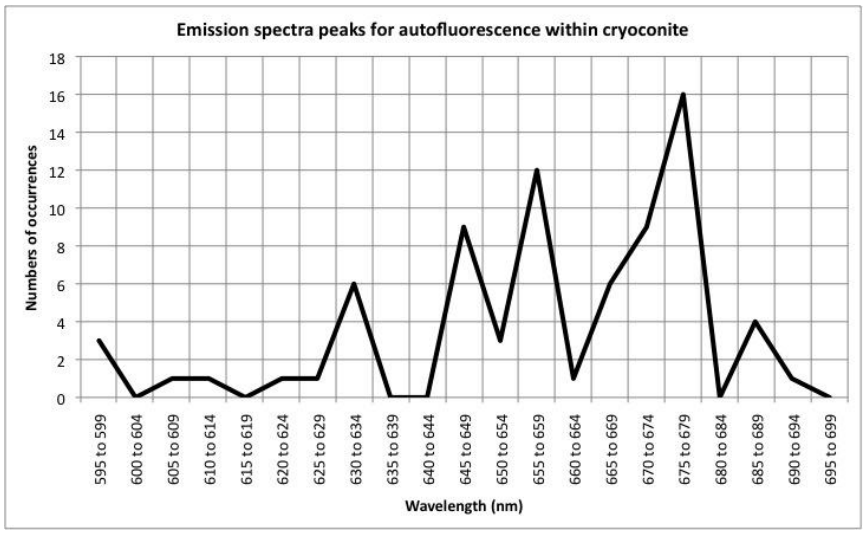

Supporting material for chapter 5:

d) UV/Vis spectrophotometry – standard curves

Standard curves for mannose, Chlorophyll a*, and phycobiliproteins*

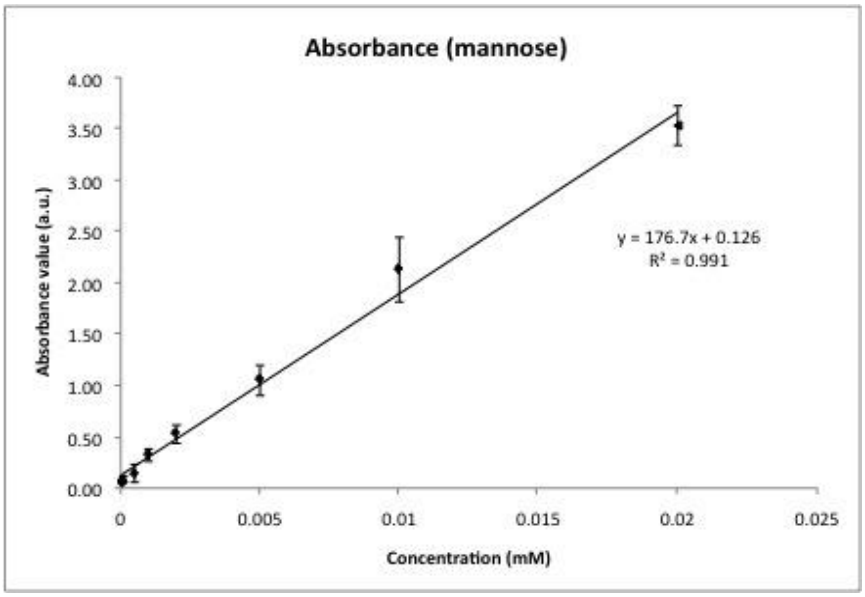

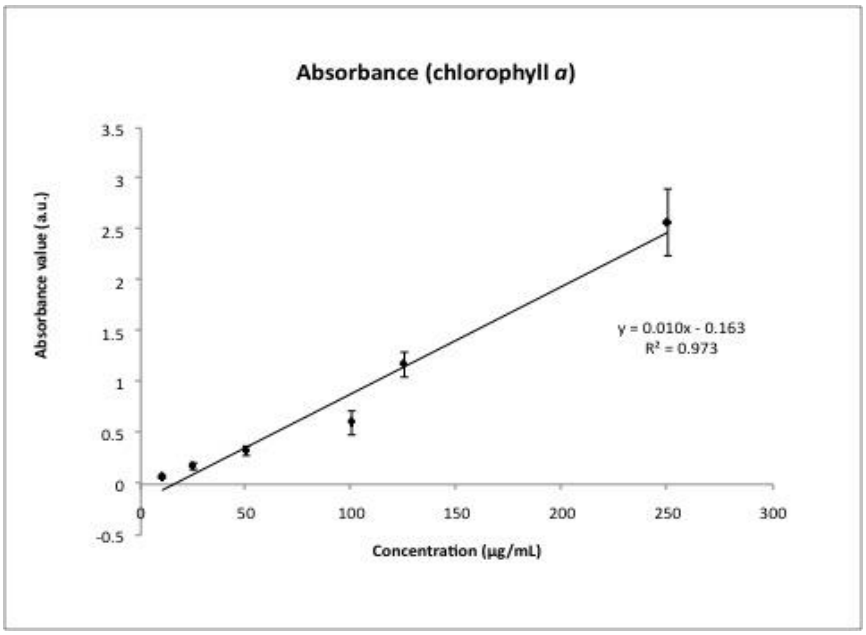

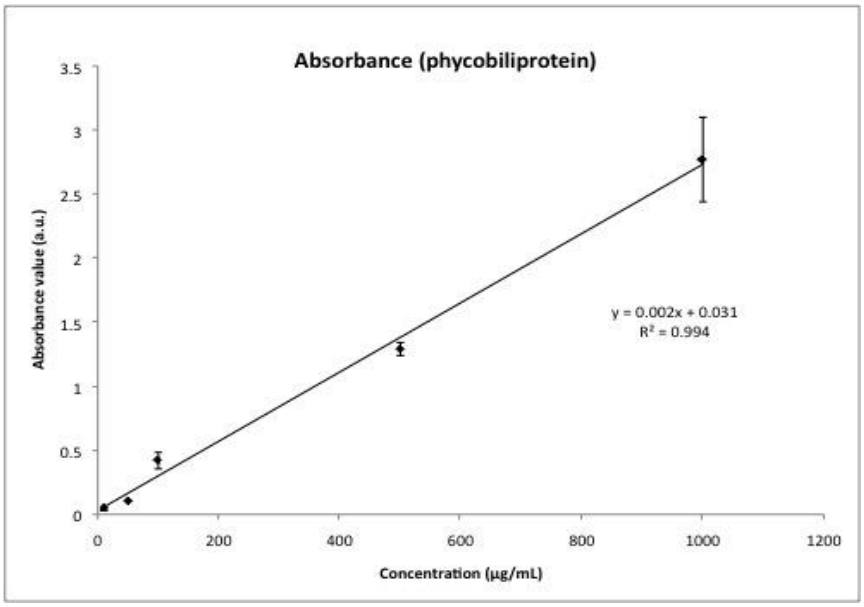
Absorbance (phycobiliprotein)
Absorbance value (a.u.)
Concentration (µg/mL)
y = 0.002x + 0.031
R² = 0.994
0
0.5
1
1.5
2
2.5
3
3.5
0
200
400
600
800
1000
1200

Supporting material for chapter 6:

e) Incubation imagery

Example images showing growth of cyanobacteria in cyanobacteria-only controls (a–b), lack of growth in mineral-only controls (c–d), and further images of aggregates (e–i), scale bar = 100 µm.

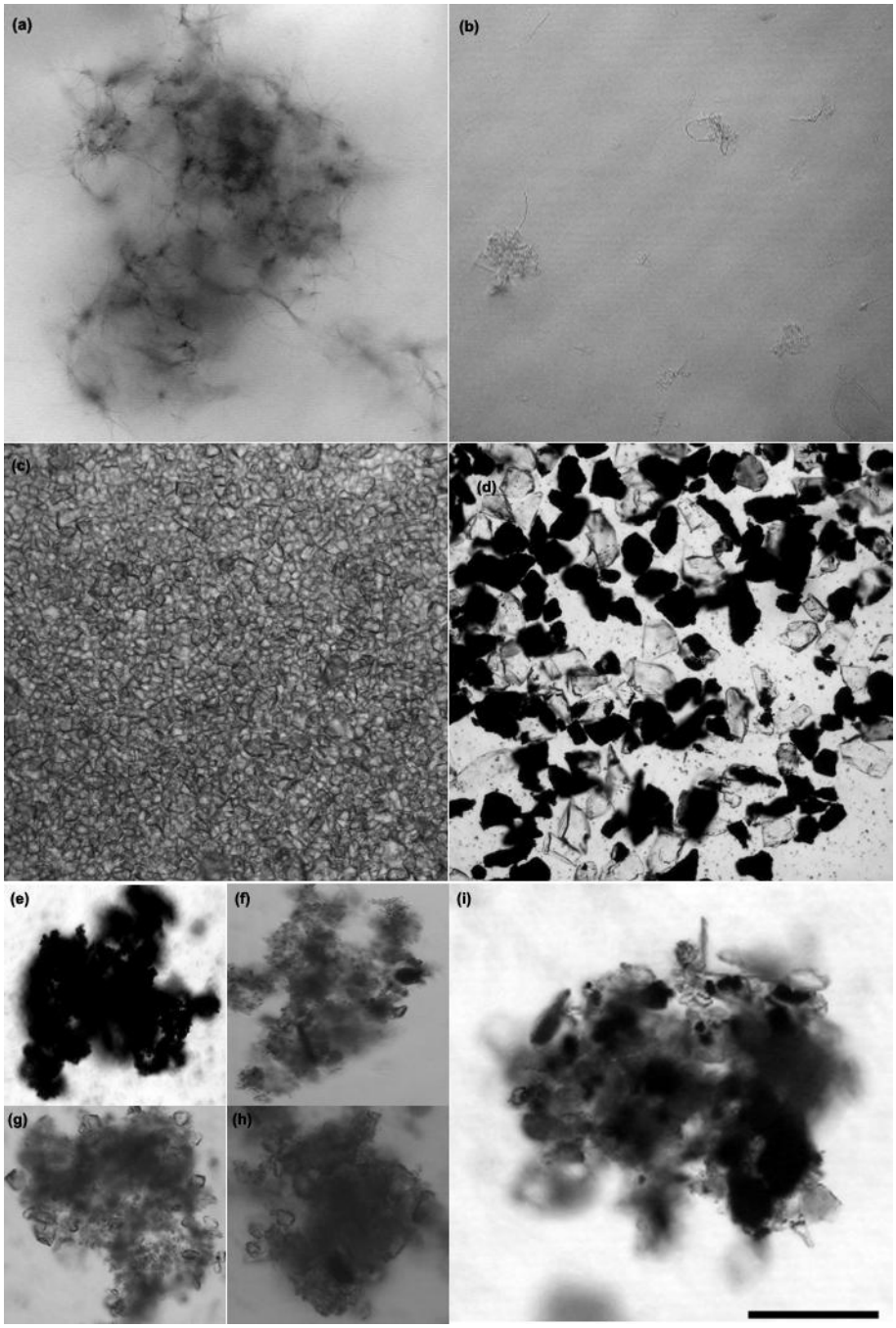

f) ImageJ macro text

Macros for determining the aggregate size and the number of pixels containing autofluorescence:

```
 <HL_thresholdandcount>
   requires("1.38o");
    dir = getDirectory("Choose a Directory");
    list = getFileList(dir);
    setBatchMode(true);
    print("File Name , Thresholded Area");
    run("Set Measurements...", "area limit redirect=None decimal=2");
    for (i=0; i<list.length; i++) {
       showProgress(i, list.length);
       open(dir+list[i]);
       mycolumn1 = getInfo("image.filename");
       getStatistics(area, mean, min, max, std);
       run("Despeckle");
       run("Enhance Contrast", "saturated=0.2");
       threshold = mean + 1.75*std;
       setThreshold(threshold, 255);
       run("Convert to Mask");
       run("Measure");
       mycolumn2 = getResult("Area", nResults-1);
       print(mycolumn1 + " , " + mycolumn2);
       close;
    }
    selectWindow("Log");


<HL_aggregatesize>
    requires("1.38o");
    dir = getDirectory("Choose a Directory");
    list = getFileList(dir);
    setBatchMode(true);
    print("File Name , Thresholded Area");
    run("Set Measurements...", "area limit redirect=None decimal=2");
    for (i=0; i<list.length; i++) {
       showProgress(i, list.length);
       open(dir+list[i]);
       mycolumn1 = getInfo("image.filename");
       getStatistics(area, mean, min, max, std);
       run("Despeckle");
       run("Remove Outliers...", "radius=5 threshold=50 which=Dark");
       run("Enhance Contrast", "saturated=0.4");
       run("Canvas Size...", "width=515 height=515 position=Center");
       setAutoThreshold("Intermodes");
       //run("Threshold...");
       setThreshold(89, 255);
       run("Convert to Mask");
       run("Dilate");
       run("Analyze Particles...", "size=100-Infinity circularity=0.00-1.00 show=Nothing display clear");
       run("Summarize");
       mycolumn2 = getResult("Area", nResults-1);
       print(mycolumn1 + " , " + mycolumn2);
       close;
    }
    selectWindow("Log");
```